Palaeodunes as archives of environmental change - A case study from the western Murray Basin (South Australia) based on optically stimulated luminescence (OSL) dating of single and multiple grains of quartz

Inaugural-Dissertation
zur
Erlangung des Doktorgrades
der Mathematisch-Naturwissenschaftlichen Fakultät
der Universität zu Köln

vorgelegt von

Johanna Lomax

aus Bergisch Gladbach

Köln, 2009

Berichterstatter: Prof. Dr. U. Radtke
Priv.-Doz. Dr. R. Zeese

Tag der mündlichen Prüfung: 9. Februar 2009

Index

List of Figures

List of Tables

1. Introduction

Deserts and desert margins react very sensitively to environmental change (Bowler 1976). Small variations in precipitation may result in large scale changes in vegetation cover and of geomorphological systems, such as rivers, dunes and lakes. Recent and future trends of global warming therefore will most likely have a huge impact on dryland areas. In order to predict future climate changes and their impact on the environment, Quaternary research aims to reconstruct past frequencies and amplitudes of environmental change. Traces of these past changes in drylands can be found in a large variety of terrestrial sediments, such as dune sands, lake shore lines and river deposits, or in organic material preserved therein. Because of their preservational nature, these are also referred to as environmental archives. Careful collection and evaluation of evidence preserved in these archives will elucidate environmental processes and events that occurred in the past. The importance of reconstructing palaeoenvironments and predicting future trends in drylands has been recognised for example in two recent IGCP (International Geological Correlation Programme) projects, namely “Understanding future dryland changes from past dynamics" (IGCP 413) and “Dryland Change: Past, Present, Future” (IGCP 500).

Major parts of the Australian continent belong to the arid and semi-arid zone (Bowler 1976). This makes Australia the driest inhabited continent of the world. The reason for this is its location within the global atmospheric circulation, with most parts lying underneath the descending limb of the southern hemisphere Hadley cell (Hesse et al. 2004). Recent and future trends of global change and the impact on geomorphological systems are thus of major importance for Australian inhabitants, with much of agricultural lands lying in dryland areas. These are highly affected by desertification and soil degradation when consecutive years of drought occur. Global warming and increase of evapotranspiration might therefore have disastrous consequences for agricultural production in Australia.

Inland dunes are considered as quintessential features for palaeoenvironmental reconstructions in arid landscapes with their formation largely controlled by climate related parameters. These are mainly sparse vegetation cover, availability of loose, sand-sized grains for aeolian transport and sufficient wind speed to carry these grains (e.g. Ash and Wasson 1983, Kocurek 1998, Lancaster 1990). Thus dunes are valuable archives to

reconstruct past aridity, wind strength and wind direction. By dating dune sands, past records of aridity and environmental change can be reconstructed.

1.1 Aim of this study

This study is concerned with the reconstruction of aeolian activity and aridity over the past ~300 ka in southeastern Australia by establishing the timing of dune formation through optically stimulated luminescence (OSL) dating. For this purpose, a study area in the western Murray Basin (South Australia) was chosen, in which linear and sub-parabolic dunes are characteristic geomorphological features. From these dunes, 97 samples from 14 palaeodune exposures were obtained.

Several luminescence dating studies on the dune fields of southeastern Australia have already been carried out (Gardner et al. 1987, Readhead 1988, Cupper and Duncan 2006, Robertson and Prescott 2006, Twidale et al. 2007). All these studies though only involved a limited number of samples, and intercomparison is hindered by the use of different methodological dating approaches, for instance OSL and thermoluminescence (TL) dating. A comprehensive study on the timing of dune formation in southeastern Australia, involving many samples dated under consistent laboratory conditions, is still lacking. However, a high number of samples, combined with a careful sampling strategy and consistent methodology is the only possibility to use this archive for palaeoenvironmental reconstruction (e.g. Fitzsimmons et al. 2007, Telfer and Thomas 2007). The reason for this is the unconsolidated nature of dune sands (Munyikwa 2005a). Once deposited, aeolian sediments can easily be eroded again and deposited elsewhere. The dune record may thus be discontinuous, and it is very likely that not all phases of dune formation will be preserved in it. Due to this, it is for example difficult to interpret gaps in a dune record, as it is not certain if they can be ascribed to lacking preservation of once deposited sands or to a dune stabilisation phase where no dune sand deposition occurred. Furthermore, it has been shown recently, that the association of dune formation with aridity might be too simplistic if wind strength or sediment supply are the major controls on dune formation (e.g. Chase and Thomas 2007). A dune record is therefore too ambiguous to be used as independent indicator of environmental change. Comparison with evidence preserved in other environmental archives is required to support the interpretation.

Two strategies were pursued in this study to overcome the problem of the discontinuous nature of the dune record. First, several dunes from a defined area were investigated, and within the individual dunes, a high sampling resolution was obtained. These samples were dated under consistent laboratory conditions. Only by this strategy, large scale regional dune formation phases can be distinguished from small events of dune reactivation on a limited local scale. Furthermore, if gaps in the dune record occur isochronously in many sections over a large area, the probability increases that these were created by dune stabilisation phases.

Second, a study area in the desert margin was chosen, in which dune sands are likely better preserved than in arid core zones (Bowler 1976). This is because small increases of precipitation will result in a more rapid transgressing of vegetational thresholds and soil formation phases which stabilise the dunes. Furthermore, the dunes contain comparatively high amounts of silt, clay and carbonates (Bowler and Magee 1978, Pell et al. 2001). They should therefore be relatively resistant to aeolian reworking and thus likely preserve multiple phases of dune formation.

The proxy potential of the western Murray Basin dune record for palaeoclimatic reconstruction will be evaluated by comparison with other palaeoenvironmental records from southeastern Australia. In this area, a large variety of well preserved environmental archives exists (e.g. Hesse et al. 2004), and good accessibility of the region has promoted their investigation. Only by this comparison it is possible to assess the degree of continuity in the record. Furthermore, it will be investigated whether dune sand deposition in the western Murray Basin is predominantly linked to aridity or to other factors controlling dune formation such as sediment availability or wind strength.

In order to reconstruct past environmental changes from any archive, a precise and accurate dating method is required to provide a chronological timeframe. The only method which allows determination of depositional ages of siliceous sediments is luminescence dating, and to a limited extent, electron spin resonance (ESR) dating. Optically stimulated luminescence (OSL) dating is particularly well suited for aeolian sediments, as they are assumed to have been well bleached during transport and deposition, which is one of the main prerequisites for sediment dating with OSL (e.g. Bray and Stokes 2003, Singarayer et al. 2005). Dependent on the environmental setting, luminescence ages up to 350 ka can be obtained (Murray and Olley 2002). However, it has been shown recently that dune sands

can be severely affected by bioturbation, resulting in mixing of dune sand layers of different age (Bateman et al. 2003a, Feathers 2003, Duller 2008). By dating very small subsamples, in best case individual grains, sediment mixing can be detected and accounted for (Duller 2008).

When sampling the dunes for this study, plenty animal burrows were observed, thus sediment mixing is to be expected. To avoid inaccuracy and imprecision of the OSL ages, the dune sands in this study were mainly dated using individual grains, the so called single grain luminescence technique. Assessment of the degree of mixing will be accomplished by comparison with ages obtained from multiple grain analysis, the luminescence measurement on subsamples consisting of some tens or hundreds of grains, and by investigation of age distributions in the samples. Techniques to extract the most relevant age component from the mixed sediments will be discussed in detail.

A further aspect of this study deals with the close vicinity of linear and sub-parabolic dunes. Dune morphology is controlled by many factors such as vegetation cover, sediment supply, wind regime or grain sizes available for aeolian transport (Lancaster 1995). By dating both dune forms, information on the main controlling factor of dune morphology can be gained. In simplified terms, if both dune types were formed at the same time, then factors other than climate would have affected the dune morphology. This could be for example a different amount of sediment supply.

Furthermore, it is estimated that dune formation in the Murray Basin reaches back as far as ~500 ka (Zhisheng et al. 1986, Bowler et al. 2006). By exposing deep sections in the dunes through backhoe trenching and dating aeolian layers close to the expected base of the dunes, possibly information can be provided on the onset of dune formation in the study area.

2. Physiographic setting of the western Murray Basin

The Murray Basin is part of the largest drainage basin in Australia, the Murray-Darling-Basin, which covers approximately a seventh of the Australian continent (Gill 1978) (Fig. 2.1(a)). The structural sedimentary Murray Basin covers an area of 300,000 km² in western New South Wales, northwestern Victoria and southeastern South Australia. It is filled with Tertiary and Quaternary deposits up to 600 m thick (Brown and Stephenson 1991) and is bordered by the southern and southeastern highlands in the south and east and the Mt Lofty and Olary Ranges in the west (Bowler et al. 2006). Most of the large river systems have their headwater catchments on the inland side of the southeastern Great Dividing Range. The main discharge of these rivers is in winter because their headwater catchments lie in sub-humid winter rainfall areas. The Darling River, a tributary of the Murray River, drains from the Great Dividing Range in northeastern Australia, and is thus fed by monsoonal summer rain, providing additional waters to the drainage system in summer. Mean discharge in the Darling River is, however, low, and in drought years flow ceases completely (Stephenson 1986).

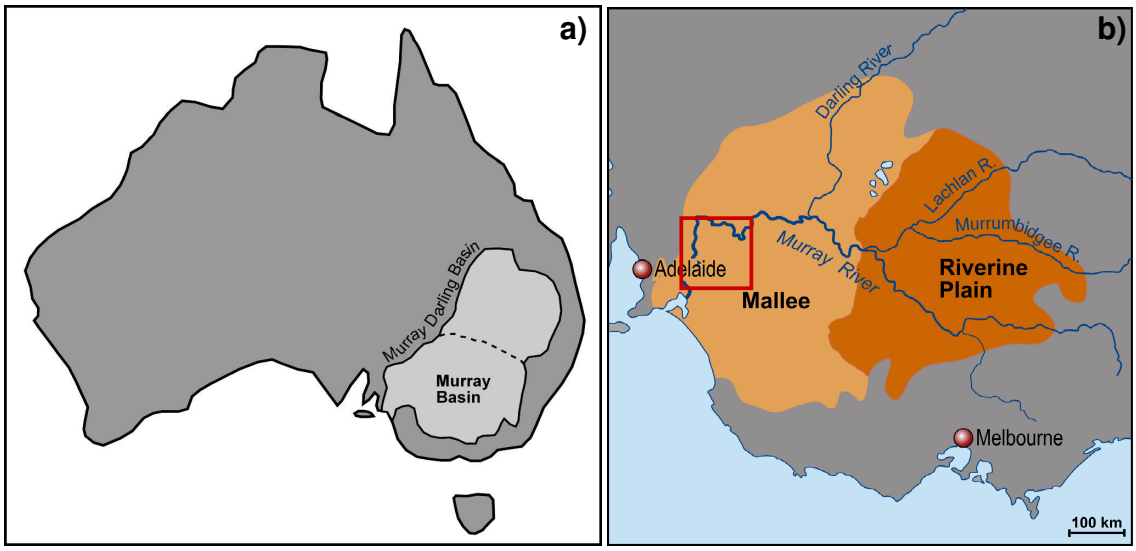

Fig. 2.1. Location maps showing (a) the extent of the Murray-Darling Basin and of the Murray Basin, (b) the location of the Riverine Plain and the Mallee and the major river systems of the Murray Basin. The red rectangle highlights the study area. (Drafts by U. Beha).

The Murray Basin can further be divided into the Riverine Plain in the east, morphologically characterised by large, meandering river systems of the Murray, Lachlan and Murrumbidgee Rivers and their fluvial deposits, and the Mallee in the west (Fig. 2.1(b)). The Mallee, where the sampling sites of this study are situated, is characterised by aeolian landforms such as linear dunes, sub-parabolic dunes, lunettes and source bordering dunes, interspersed with playas, channels and marine strandlines. The aeolian forms reflect a close interaction with fluvial and lacustrine deposits throughout the course of climate changes in the Quaternary (Pell et al. 2001). Extensive descriptions of the Mallee landforms can be found in Bowler and Magee (1978) and Bowler et al. (2006).

In the following sections, the physiographic settings of the western Murray Basin, such as climate, geology, vegetation, soils and geomorphology, are considered in more detail in order to provide an understanding of the nature of the study area, and the formation of dunes, which are the focus of this study.

2.1 Climate

Present climate in the western Murray Basin is characterised by semi-arid conditions with hot, dry summers and cool, wet winters. The seasonality is caused by the varying influence of the subtropical high pressure belt in summer and the mid-latitude westerlies in winter, bringing in cold fronts and low pressure systems (Gentilli 1986). Mean annual precipitation increases from north to south. For example, in Waikerie, in the northwestern Murray Basin, a mean annual rainfall of 250 mm was measured over the last 100 years, whereas Lameroo further to the south receives an average of 385 mm rain per year (see Fig. 2.2 and Fig. 2.3) (BOM 2006). Rain dominantly falls in the winter months between May and October. As rainfall is highly variable, drought is a very common feature over the semi-arid regions of southern Australia. The year 2006, for instance, was the driest on record since 1900 in the Murray-Darling Basin, and the severe conditions still persist (BOM 2006). The north of the Murray Basin, being closer to the arid centre, also is slightly warmer than the more southern areas. At Waikerie, the average maximum temperature in January is 31.8°C and the average minimum temperature in July 5.1°C. At Lameroo, the corresponding values are 30.9°C and 4.3°C. Annual evaporation averages ~1700 mm and greatly exceeds annual precipitation throughout the year (BOM 2006).

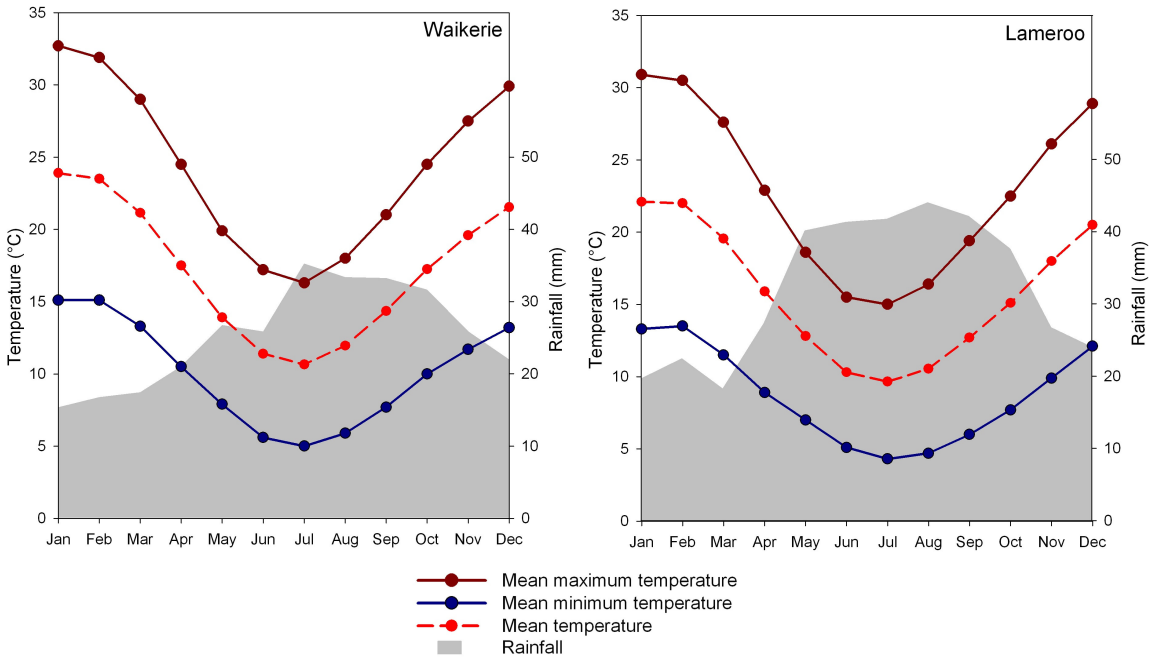

Fig. 2.2. Climate charts of Waikerie (34.18°S, 139.98°E) and Lameroo (35.33°S, 140.52°E), showing average maximum, minimum and mean temperatures and rainfall (data from BOM 2006).

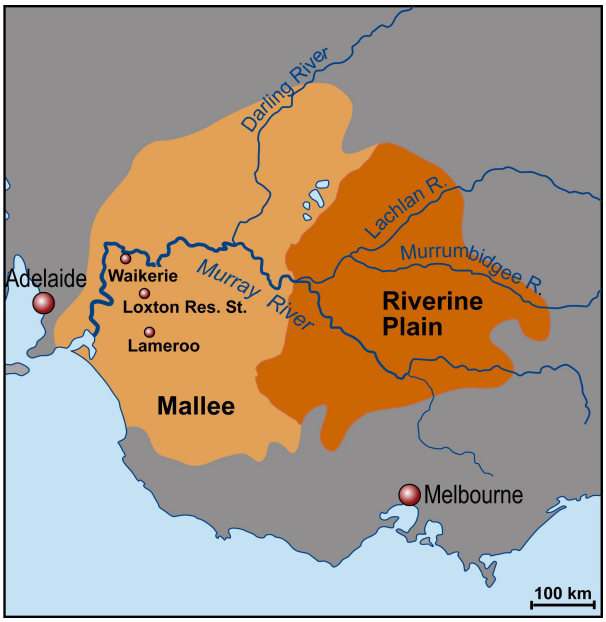

Fig. 2.3. Map of the Murray Basin showing the location of Waikerie, Lameroo and Loxton Research Station, for which climate data are presented (draft by U. Beha).

The dominant wind direction is very similar in the northern and southern part of the western Murray Basin. Over an annual period, the dominant wind direction in the western Murray Basin is from the southwest. In summer, southwesterly winds are most common. In winter, when southern Australia is strongly influenced by frontal systems brought by the westerlies, westerly and strong northwesterly winds are common besides southwesterly winds (Gentilli 1986) (Fig. 2.4). Wind strengths in the southwestern Murray Basin are higher than in the northwestern Murray Basin. At Waikerie, the average annual wind strength is 11 km/h, whereas at Lameroo, the corresponding value is 17 km/h. Winds are strongest from September to November (BOM 2006).

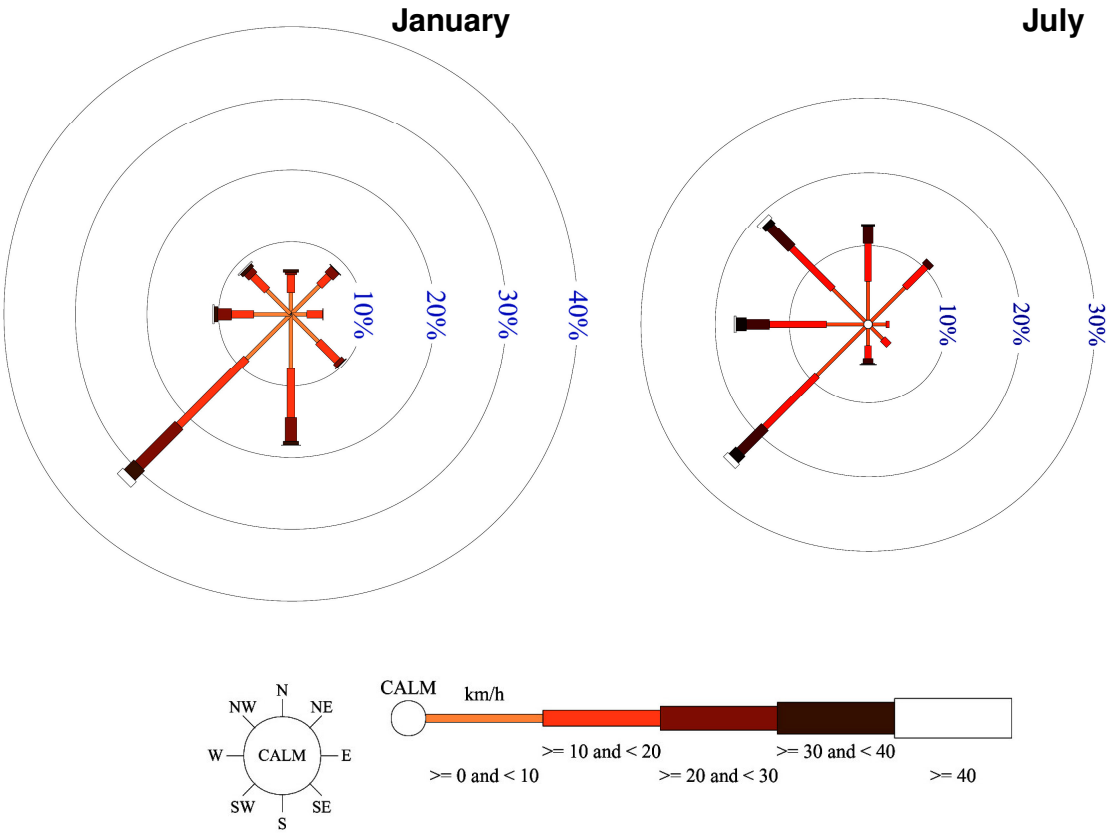

Fig. 2.4. Wind rose data for January and July measured at 3 pm at Loxton Research Station (data from BOM 2006).

2.2 Geology of the western Murray Basin

The structural Murray Basin is covered by a relatively thin veneer of Tertiary and Quaternary sediments, which have been deposited by rivers, lakes, wind, or sea water during several marine transgressions. This Cenozoic succession averages 200-300 m over much of the basin, but increases to 400-600 m in major depocentres (Brown and Stephenson 1991). Beneath these Cenozoic sediments, Mesozoic (in particular Cretaceous), Palaeozoic and Precambrian rocks form the basement of the Murray Basin (Brown and Stephenson 1991).

In the following chapter, the Tertiary and Quaternary sediments which underlie the dunes in the Murray Basin are described. A geological overview of the Murray Basin can be found in Brown and Stephenson (1991).

2.2.1 Tertiary

During the Tertiary, several marine trans- and regressions influenced the sedimentation history in the Murray Basin, documented by a thin sequence of shallow marine and estuarine deposits, intercalated with fluvial sediments.

The early Tertiary was characterised by fluvio-lacustrine environments, in which deposition of fluvial sands, intercalated by coals and peats from swamp and marsh environments, took place. These early Tertiary sequences are termed the Warina Sands and the Olney Formation (Brown and Stephenson 1991). From Oligocene to the middle Miocene large marine transgressions due to subsidence of several sub-basins occurred in the area, depositing thick sequences of calcarenites, termed the Morgan and Pata Limestone (Brown and Stephenson 1991). In the late Miocene the sea retreated, causing non-depositional or erosional conditions. In the latest Miocene and early Pliocene, a further series of marine transgressions turned the Murray Basin into a shallow epicontinental embayment of the sea which extended some 500 km inland from the present coastline (Bowler et al. 2006) (Fig. 2.5). This led to the deposition of a sequence of shallow marine, littoral and estuarine sediments. The basal units of latest Miocene-Pliocene sediments comprise the Bookpurnong Beds, which consist of calcareous clay, silt and sand and a significant fossil content and were probably deposited in low-energy marine shelf environments (Brown and Stephenson 1991). At around 6 Ma, shortly after the estimated maximum of the

transgression, the sea began to retreat (Brown and Stephenson 1991). During this time, the highly siliceous, non-calcareous Loxton-Parilla Sands were deposited, a formation combining fluvial and marine shoreline facies. Within the Loxton-Parilla Sands, over 170 strandlines, which cross the Murray Basin in northwest-southeasterly direction, give testimony of the oscillating shoreline of the retreating sea (e.g. Sprigg 1952, 1959, Blackburn 1962, Hills 1975). Fig. 2.5 shows the maximum extent of the Miocene-Pliocene transgression at around 6 Ma and subsequent retreat stages, as well as the major strandlines present in the Murray Basin as mapped by Kotsonis (1999, in Bowler et al. 2006).

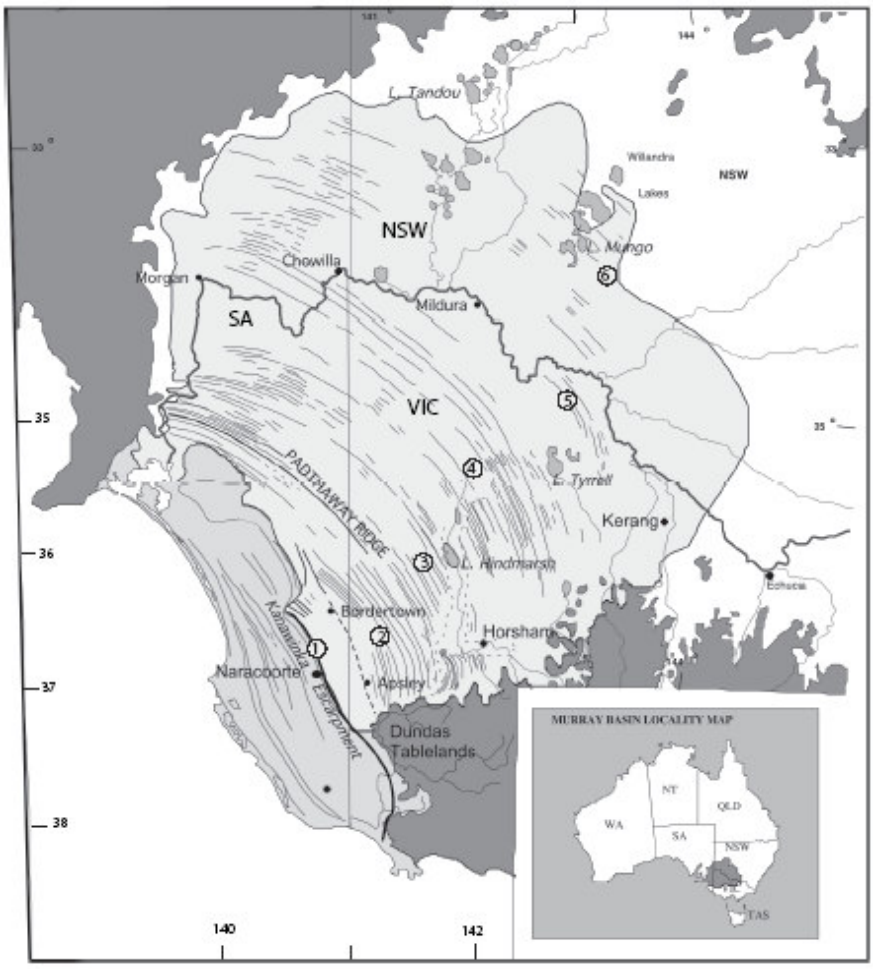

Fig. 2.5. Extent of Upper Miocene to Pliocene marine invasion of the western Murray Basin showing the patterns of strandline ridges (Loxton-Parilla Sands), the legacy of sequential shoreline retreat (modified after Kotsonis 1999). Numbered sequence 1-6 denotes shoreline positions, 1 to 6 million years ago as suggested in this interpretation (Bowler et al. 2006).

In parts, the Loxton-Parilla Sands are discordantly overlain by or merge laterally with sediments of the estuarine Norwest Bend Formation which occupies the lower Murray River valley from Tailem Bend to Overland Corner. It consists of fossiliferous sandstone and contains thick oyster beds. Near the lower course of the Murray River, the Norwest Bend Formation directly overlies the Morgan Limestone (Brown and Stephenson 1991).

The upper layers of the Loxton-Parilla Sands involve an iron- or quartz-rich horizon termed the Karoonda Surface Firman (1966a, 1973), formed under tropical or subtropical climatic conditions at the end of the Tertiary. Fig. 2.6 displays the Tertiary stratigraphy of the Murray Basin suggested by Brown and Stephenson (1991).

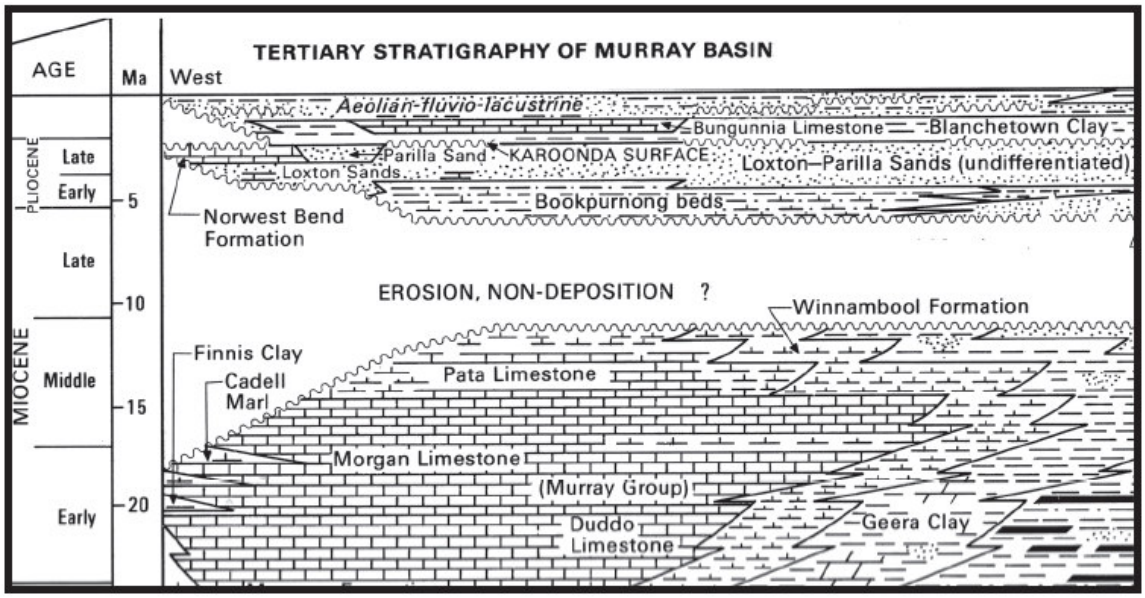

Fig. 2.6. Tertiary stratigraphy of the Murray Basin (from Bowler et al. 2006, after Brown and Stephenson 1991).

By around 4 Ma, tectonic movements resulted in the development of several fault lines trending southwest-northeast near the present course of the Murray River. Four of these, the Morgan, Hamley, Danyo and Tyrrell faults are associated with basins which developed at the same time. These are the Blanchetown, Loxton, Raak and Tyrrell basins, respectively (Bowler et al. 2006) (Fig. 2.7). The tectonic movements in the centre of the Murray Basin were succeeded by uplift of the Pinnaroo Block further to the south (Fig. 2.7). This event caused damming of the ancestral Murray River and gave rise to the formation of a huge palaeolake, Lake Bungunnia (Firman 1965). Palaeomagnetic analysis of the lake deposits

places the beginning of its formation near the Gilbert-Gauss-Boundary at around 3.5 Ma (Zhisheng et al. 1986).

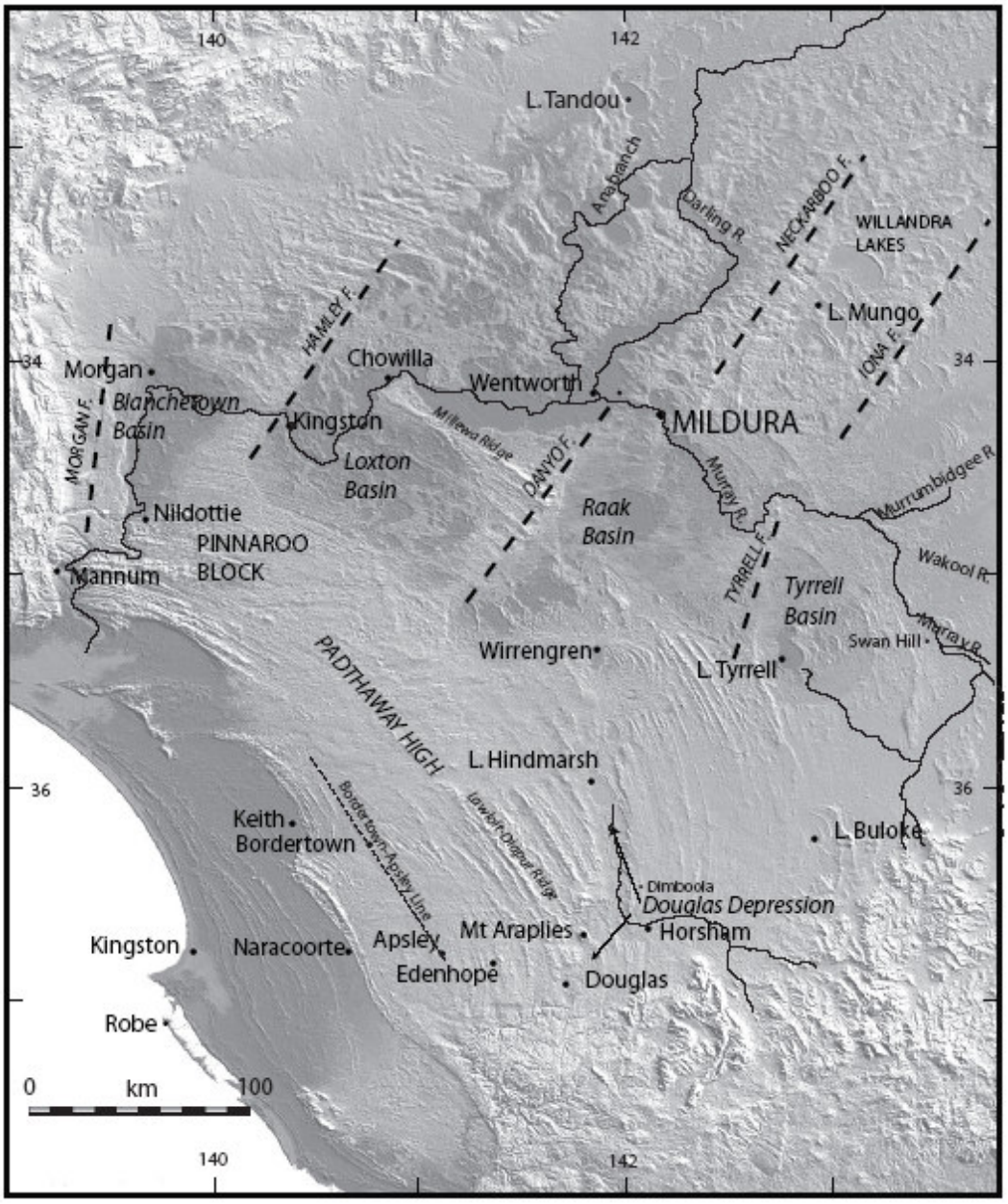

Fig. 2.7. Elevation diagram of the western Murray Basin. Dark areas indicate locations below the 60m contour, highlighting the four tectonic basins along the lower course of the Murray River (Bowler et al. 2006).

2.2.2 Quaternary

The early Quaternary in the western Murray Basin was characterised by lacustrine deposition in Lake Bungunnia. Sediments deposited during the fresh water lake phase consist mainly of up to 20 m thick micaceous sandy clay layers, the Blanchetown Clay, containing freshwater flora and fauna (McKenzie and Gill 1968). The former extent of Lake Bungunnia is estimated at ~68,000 km², covering a large area of southeastern South Australia, southwestern New South Wales and northwestern Victoria (Stephenson 1986).

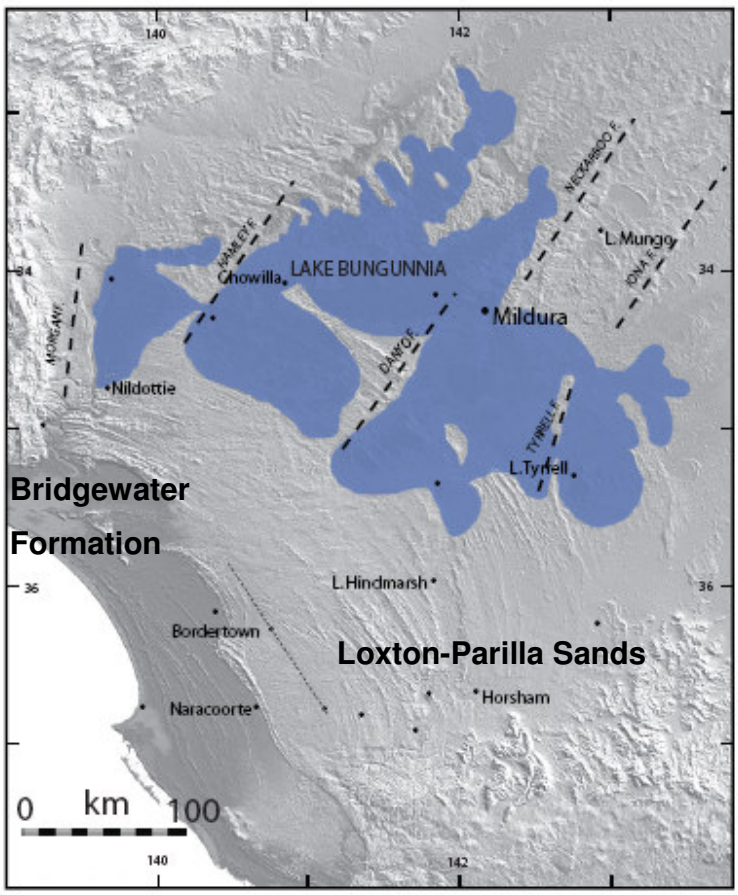

Fig. 2.8. Elevation diagram showing Lake Bungunnia near its maximum extent coincident with the 60 m contour (Bowler et al. 2006).

Deposition of the Blanchetown Clay ended with the transition to a calcareous and dolomitic facies, the Bungunnia Limestone. Its extent is restricted to the western part of the Murray Basin, mainly the Blanchetown Basin and, based on its lithology, is assumed to have been deposited in shallow lake environments (Stephenson 1986).

Palaeomagnetic measurements of the Blanchetown Clay show reversed magnetism of the Matuyama Chron in the upper part and normal magnetism (Gauss Chron) in the lower part of the sequence (Zhisheng et al. 1986). Therefore, the authors place the existence of Lake Bungunnia from the Late Pliocene (3.5 Ma) to about 0.7 Ma. The formation of a permanent outlet channel into the sea resulted in a rapid drop in lake levels and the development of separate lake basins (Bowler 1980). Subsequently, saline playa formation, soil formation (Zhisheng et al. 1986) and fluvial processes (Stephenson 1986) prevailed in the western Murray Basin. Therefore, fluvial sands, pedogenic calcretes and lacustrine sediments overlie the Lake Bungunnia sediments. The demise of Lake Bungunnia cannot be precisely dated by palaeomagnetism as the Brunhes-Matuyama boundary can be identified neither in the lake deposits nor in the overlying aeolian deposits. The palaeosols and aeolian sediments overlying the Blanchetown clay are normally magnetised (Brunhes Chron), thus their formation is placed within the last 0.7 Ma. According to Zhisheng et al. (1986), the lake phase most likely ended near or soon after the Brunhes-Matuyama boundary at around 0.7 Ma, assuming constant Pleistocene sedimentation rates. This means that the boundary used to be present in the Lake Bungunnia sediments and was subsequently obscured by pedogenic alternation of the uppermost layers of the lake deposits.

Simultaneously with the Lake Bungunnia phase, the retreating sea of the Pliocene transgression reached a line near Bordertown in the southwest of the Basin at around 1.5 Ma and near Naracoorte near 780 ka (Idnurm and Cook 1980, Huntley et al. 1993, Murray-Wallace et al. 2001). Prior to this date, the strandlines of the Loxton-Parilla Sands are characterised by non-calcareous, siliceous sediments. In contrast, the ridges deposited after around 1.5 Ma contain high amounts of carbonates (Bowler et al. 2006). These Quaternary calcarenites are termed the Bridgewater Formation (Boutakoff 1963) (Fig. 2.8). In total, 13 ridges are present, representing Pleistocene sea level high stands (Huntley et al. 1993, Belperio 1995, Murray-Wallace et al. 2001).

The demise of Lake Bungunnia and the final retreat of the sea led to the formation of modern landforms in the Murray Basin (Stephenson 1986). The western Murray Basin is today characterised by calcareous linear dunes overlying Bungunnia and post-Bungunnia sediments, and further to the south, sub-parabolic dunes overlying the Loxton-Parilla Sands. The onset of aeolian-dominated sedimentation is estimated to around 400-500 ka,

based on an assumed minimum time required to deposit the post-Bungunnia surficial sediments (Bowler 1980, Zhisheng et al. 1986).

In the following section, the dunes of the western Murrray Basin are characterised in more detail in respect to their shape, modes of formation, source sediments and age.

2.3 Dunes of the western Murray Basin: Morphology and genesis

The expansive dune fields of the Murray Basin, today well vegetated and stabilised, can be divided into two different formations. In the northwest, north of approximately 34°45'S, short and closely spaced linear dunes prevail, termed the Woorinen Formation (Lawrence 1966, 1975). Dune trend is from east to west, which, according to Sprigg (1979), does not reflect the present day sand shifting winds. Present day winds have a stronger southwesterly component, indicating that the dunes of the Murray Basin are relic forms and were generated under palaeo-wind regimes with a stronger westerly component than those prevailing in the basin today.

The linear dunes are further characterised by red-brown colours (hue 7.5 YR), and significant contents of clay and carbonates (Pell et al. 2001, Bowler et al. 2006). The dunes range in length from 0.5 to 3 km and are typically 2-6 m in height. Interdune spacing ranges from 0.2 to 1.2 km (Bowler and Magee 1978).

In the southwestern part of the basin, south of approximately 34°45'S, three lobes of sub-parabolic dunes fields, the Big Desert, the Little Desert and the Sunset Desert are present. Dune morphology ranges from irregular to sub-parabolic, and dune trend is from WSW to ENE. In South Australia, this formation is termed the Molineaux Sands (Firman 1966b), whereas in Victoria, they are called Lowan Sands (Lawrence 1966). Average dune height is 5-15 m and slopes are usually steep (Bowler and Magee 1978). The dunes are highly siliceous, and carbonate and clay contents are lower than in the linear dune field or absent. Dune colour is dominantly white to pale-yellowish (hue 10 YR) (Pell et al. 2001). Further small areas of parabolic dunes are found above the eastern edges of the Murray River gorge, a formation termed the Bunyip Sands (Firman 1967). An overview of the different dune fields in the Mallee of the Murray Basin is shown in Fig. 2.9.

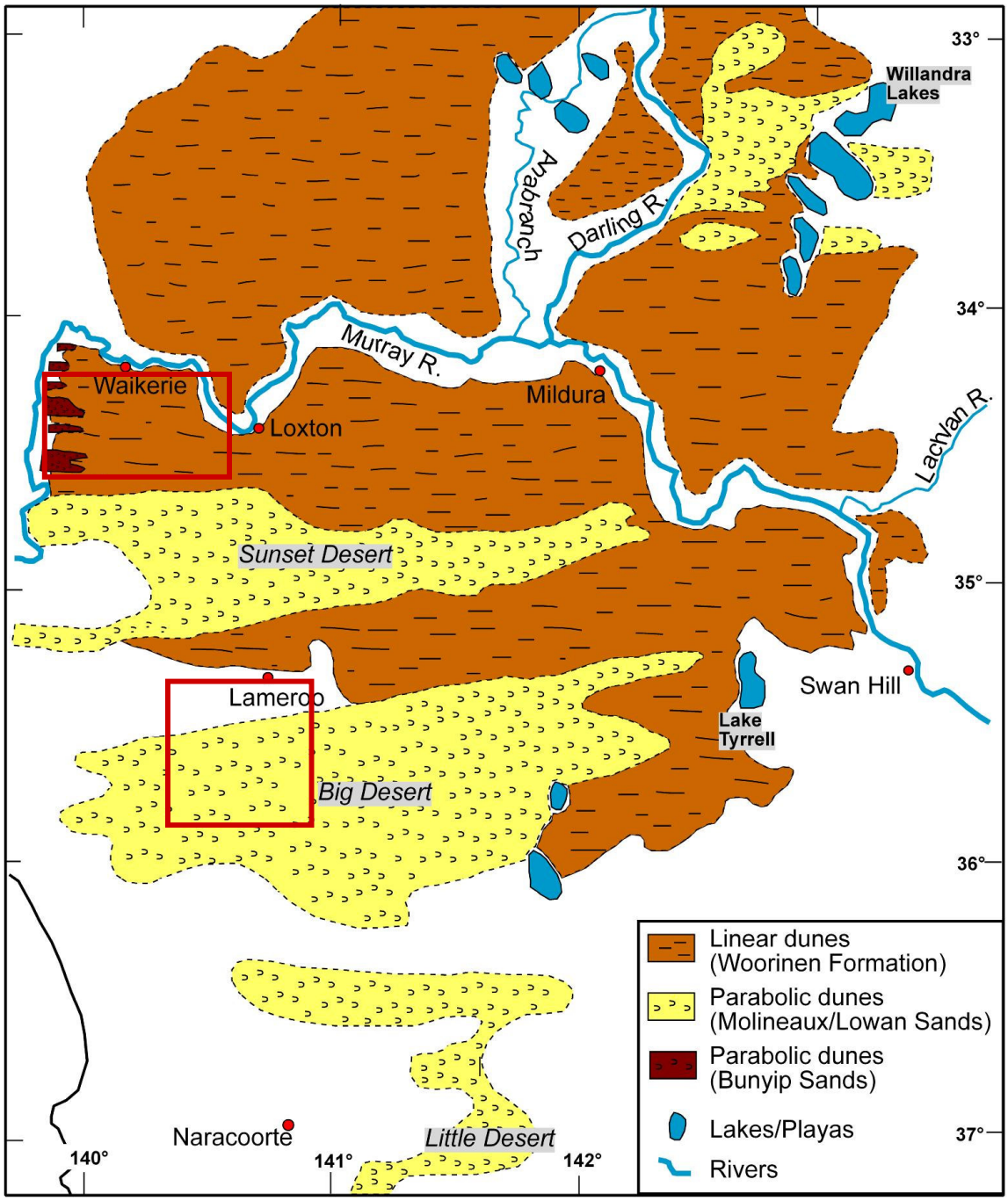

Fig. 2.9. The Mallee dune fields in southeastern Australia (modified after Pell et al. 2001). The red rectangles mark the study areas.

2.3.1 Theories of dune formation

As outlined above, two dune types with distinct morphology occur in the Mallee dune field of southeastern Australia. The question why this is the case has only found minor attention in the literature so far. In principle, the five main factors influencing dune morphology are sand supply, wind regime (variability of wind direction and wind strength), vegetation cover, grain sizes of material available for dune formation and time (Lancaster 1995).
The relation of the first three factors in respect to the dune morphology has been investigated by Hack (1941) on dunes from the semi-arid zone of Arizona (Fig. 2.10).

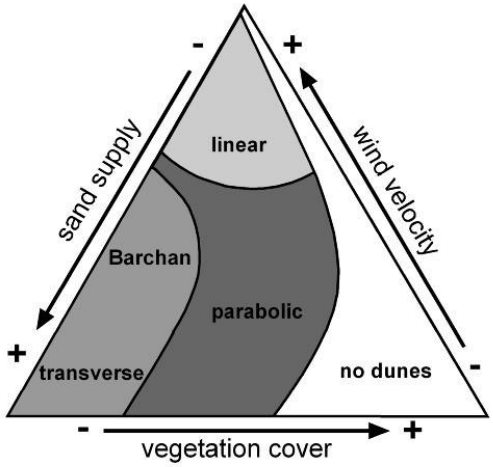

Fig. 2.10. Model showing the relation of dune types common in Arizona in respect to the controlling factors of sand supply, wind velocity and vegetation cover (modified after Hack 1941).

According to Hack (1941), linear dunes form in areas with a limited sand supply, strong winds and only sparse vegetation cover. Parabolic dunes on the other hand are restricted to areas with at least some vegetation cover, and ideally form when sand supply is also high.
For the Mallee dunes of southeastern South Australia, the different dune morphologies (that is, the linear dunes to the north and sub-parabolic dunes to the south) can be explained by two of the above mentioned controls; varying sand supply and vegetation cover. Modern precipitation rates are considerably higher further to the south (~350-400 mm/a) than in the northwestern Murray Basin (~250-300 mm/a) (see chapter 2.1). During phases of active dune formation in the past, these precipitation rates where probably lower. For the Last Glacial Maximum (LGM) palaeoclimate modelling has shown, with minor spatial exceptions, a continent-wide decrease in precipitation, but the north-south precipitation

gradient still existed (Hope 2005). This difference might have been responsible for sustaining some vegetation in the more southern areas of the Mallee whereas further to the north true arid conditions with very little vegetation cover might have prevailed, permitting linear dune formation.

The question of sand supply as a factor influencing the dune morphology of the Mallee dunes is more complex, as the exact sand sources of the dunes are not certain, and will be discussed later. In any case, a lot of the Woorinen Formation linear dunes, at least in the northwestern Murray Basin, are underlain by Lake Bungunnia clays and limestones which cannot act as source material for the dunes. In the southwest, the Loxton-Parilla Sands provide abundant sand sized material for deflation and (sub-parabolic) dune formation. Hence, the different dune morphologies most likely reflect also variations in sand supply available for aeolian transport. Bowler (1976) postulates that the increased sand supply is the main driving factor for the formation of the sub-parabolic dunes.

In the following chapters, theories on linear and sub-parabolic dune formation in general, and in the context of the Murray Basin, will be discussed.

2.3.2 Linear dune formation in the Murray Basin

The most favoured model of linear dune formation is that they develop under a bidirectional wind regime. Under this wind regime, sands are shifted in the direction of the seasonally dominant wind direction, which leads to elongation of the dune in the resultant wind direction (e.g. Bristow et al. 2000, Wiggs et al. 2001, Tsoar et al. 2004). Evidence for this theory is for instance seen in the cross-bedding of linear dunes (e.g. Tseo 1993, Bristow et al. 2000) and in the sinuous shape that many active linear dunes show (e.g. Wopfner and Twidale 2001).

However, some debate exists in the Australian literature about the sources of sand, which is strongly related to the question if sand is transported over long distances or not.

According to Twidale (1981) and Wopfner and Twidale (1988, 2001) the floodplains and channels of large river or creek systems act as major sand source for the linear dunes of the central Australian deserts. From these sources, sand is transported over long distances along the crests of dunes and deposited at their nose. This theory has been rejected by Pell et al. (2001), who found that heavy mineral assemblages in the dunes are strongly related to

the material in the adjacent corridors, and by Hollands et al. (2006) who conducted OSL measurements along a linear dune and found that ages did not get progressively younger in the downwind direction. Therefore, they state that the interdune corridors act as major source of the dunes, and sand is only swept over short distances from the corridor onto the adjoining dune flank. Wopfner and Twidale (2001) though see strong evidence for long distance transport in the fact that a lot of dunes migrate over playas or gibber plains for several tens of kilometres, where there is no sand available in the interdune corridors. Furthermore, they observed a downwind trend of reddening of dune sands, which they also view as evidence for long distance transport.

The studies mentioned above were all concerned with linear dune formation in the Simpson and Strzelecki Deserts, in the arid centre of Australia. The linear dunes of the Murray Basin are of distinctly different shape. They are much shorter, dune spacing is closer, dunes do not merge forming y-junctions, and the average clay content is higher (Bowler and Magee 1978). Thus the above mentioned models do not necessarily apply to the dunes of the Murray Basin.

The question of sand sources of the Mallee dunes has been addressed by Pell et al. (2001). They conclude that the linear dune sands have only been transported over short distances, thus dunes where formed by vertical corrosion and deflation of local sources as interdune corridors and underlying material. Evidence of this theory is seen in the absence of trend in dune colour and grain sizes in the downwind direction, and the poorly-rounded shape of the dune sands.

Bowler and Magee (1978) support the idea of vertical corrosion of dune corridors and short distance transport. Their model anticipates that during phases of high groundwater tables salts crystallise on the surfaces of interdunal swales, leading to efflorescence and formation of sand- and silt-sized clay pellets. When groundwater tables are lowered, the pellets are deflated by wind and transported onto the adjacent dunes flanks. The fact that well drained areas, where surficial salt enrichment cannot occur, are devoid of dunes, and that regularity in spacing and length of the dune persists throughout the dune field, irrespective of connection to active channels or not, supports this idea in their opinion. Further, in their view the high clay and carbonate content prevents large scale remobilisation of the linear dunes, thus no substantial downwind migration takes place and dunes remain relatively short. This model of formation appears attractive in explaining the differences between

linear dunes in arid central Australia and the Murray Basin. However, it might explain the derivation of clay pellets and carbonates in the dunes, but the sources of the sand sized quartz grains, which are the main contributors to the dunes, remain unclear in their model.
Bowler et al. (2006) pointed out that there is at least some evidence for medium scale distance transport in the western Murray Basin. The Bunyip Sands, several lobes of sub-parabolic dunes occurring in the lee of slip-off slopes of the Murray River between Morgan and Mannum (see Fig. 2.9), overlie Bungunnia Limestone and other calcretes, thus sand must derive from Murray River sediments. Part of these sands possibly functioned as sand sources for the linear dunes connecting in the downwind area (personal communication Twidale 2006).
In conclusion, the mineralogical evidence presented by Pell et al. (2001) and the morphological evidence outlined by Bowler and Magee (1978) strongly suggest that a lot of material in the linear dunes of the Woorinen Formation is provided by local sources such as interdune corridors. Nevertheless, it is also possible that some of the sand is derived from more distant sources and was transported some kilometres or some tens of kilometres downwind.

2.3.3 Sub-parabolic dune formation in the Murray Basin

According to Wasson et al. (1983), vegetation plays a major role in the formation of parabolic dunes in that it anchors the two lower sides of the dune whereas the central part advances, resulting in the U-shaped form of a parabolic dune. Bowler and Magee (1978) though suggest that during phases of sub-parabolic dune formation in the Murray Basin, a complete destruction of all vegetation and pre-existing soil layers took place due to the very high mobility of the dunes devoid of bonding clay or carbonate particles. This destruction of vegetation would then further enhance their mobility, finally leading to complete turnover of dune sands from crest to swale. Morphological evidence for this enhanced mobility is seen in the sharpened crests and steep slopes of the dunes, arguing for migration in form of avalanche sand-slip faces. The debate on the sources of sand is similar to that of the linear dunes in the Murray Basin. The irregular shape of the sand grains in the sub-parabolic dunes suggests only little downwind transport (Pell et al. 2001), implying that the underlying Loxton-Parilla Sands acted as the sand source. However Crocker (1946) and

Bowler et al. (2006) postulate a more distant source, with re-sorted material of strandline dunes of the Bridgewater Formation acting as major source material.

2.3.4 Origin of the colour of Mallee dune sands

A strong contrast in colour exists between the sub-parabolic dunes of the Molineaux Sands and the linear dunes of the Woorinen Formation. The Molineaux Sands are of yellow to whitish colour, whereas the Woorinen Formation consists of red-brown sands (Bowler and Magee 1978, Pell et al. 2001). The red colour is derived from clay cutans containing iron covering the quartz grains (Bowler and Magee 1978, Bowler et al. 2006). According to Bowler et al. (2006) these grain coatings are inherited from their parent material; that is, the coatings existed before aeolian transport and deposition as linear dunes. The development of the clay-iron cutans is considered to be a result of pedogenic processes in the Parilla Sands, producing the deeply weathered Karoonda surface at the end of the Tertiary. During aeolian transport, the red colour is retained (Bowler and Magee 1978). The white to yellow colour of the Molineaux Sands is thought to be an expression of low clay content in the sediments, and the derivation of younger parent sediments, namely the Bridgewater Formation (Bowler et al. 2006). Further, the higher degree of mobility of the sub-parabolic dunes might have prevented long term periods of stabilisation and soil formation, thus restricting post-depositional rubification (Bowler and Magee 1978, Pell et al. 2001, Bowler et al. 2006). Fig. 2.11 shows the varying colours found in samples of the Mallee dunes collected for this study. As can be seen, also the Bunyip Sands are of dark brown-red colour. This implies that either these sediments already possessed cutans when deposited by fluvial means, or that they were fluvially deposited a long time before the Bunyip Sands dune formation, allowing sufficient time for their rubification through soil formation processes. According to Bowler and Magee (1978), transport in water leads to efficient removal of iron-clay coatings, thus the latter scenario seems more likely.

Fig. 2.11. Different colours of the Mallee dune sands. (a) Molineaux Sands, (b)-(d) Woorinen Formation, (e) Bunyip Sands.

2.4 Vegetation

The characteristic vegetation of the western Murray Basin are eucalypts, which are typically of low stature and have a cluster of branches derived from an underground lignotuber (Bowler and Magee 1978) (Fig. 2.12). This special growth habit is termed 'mallee'; therefore parts of the Murray Basin in northwestern Victoria, western New South Wales and eastern South Australia, where eucalypts with mallee growth are most common, are called the Mallee.

The mallee eucalypt associations are particularly found on the well drained crests of the dunes. In the interdunal swales, consisting of finer grained material than the dunes, eucalypts are substituted by other trees such as *Callitris, Acacia, Casuarina, Hakea* and *Heterodendrum* (Bowler and Magee 1978). Furthermore, open grassland becomes more prominent in the swales. According to Ash and Wasson (1983), tall shrubs and trees cover 10-30 % of the land surface in the Mallee, and grass cover is more than 10 %. Most of the natural vegetation of the swales has been cleared for agricultural use. Besides these tree species, shrubs and grasses are found on the dunes as well as on the swales. Open areas without vegetation are also commonly found on the dunes, making them susceptible to aeolian reactivation. Drought and particularly fire are a frequent cause of death for the mallee tree associations. The eucalypts and Casuarinas though produce new shoots after fire damage, helping them to recover (Ash and Wasson 1983).

According to Ash and Wasson (1983) most of the dunes in the arid centre of Australia are inactive due to lack of strong winds, and not due to vegetation cover. This is not the case for the Mallee dunes. Despite a relatively high percentage of strong, sand-transporting winds (~25 % per year over 8 m/s) in winter-rain areas of southeastern Australia, the dense vegetation cover prevents large scale mobilisation of the dunes.

Fig. 2.12. Dune with eucalypts of typical multiple-stem mallee growth.

2.5 Soils

Soils in semiarid regions are often characterised by an enrichment of salts such as calcium carbonate, gypsum or chlorides. The western Murray Basin is one of the regions in Australia with the highest abundance of calcretes and regolith carbonates (Chen et al. 2002a). Most of the soils developed on sediments of the Woorinen Formation fall under the soil type 'Solonized Brown Soils' according to the Australian soil classification from Stace et al. (1968). This soil type is characterised by a sandy to loamy texture, a high amount of calcareous material and its brown-red colour.

For calcrete formation, three major prerequisites have to be fulfilled. First, a seasonal rainfall deficit that leads to precipitation of calcium carbonates ($CaCO_3$) from carbonate and calcium enriched soil water, mainly as a result of dehydration through evapotranspiration. As ideal climate conditions an annual rain fall between 400 and 600 mm is often quoted (Goudie 1983), combined with a high seasonality of rainfall. Second, for $CaCO_3$ to be formed, CO_2 is needed, which in soils is commonly provided by root respiration and microbial activity. Thus, calcrete formation is strongly associated with soil formation processes. Calcretes which form in the unsaturated zone of soils – typically the B-horizon – are termed pedogenic calcretes (Goudie 1983, Schaetzl and Anderson 2005). Third, an abundance of calcium is required. Thus, calcretes either form through ascending carbonate- and calcium-rich groundwater in areas with calcium-containing bedrock, or through aeolian deposition of calcareous dust and subsequent infiltration by rainwater.

Though some parts of the Woorinen Formation are underlain by calcium-rich bedrock (e.g. Bungunnia Limestone), Crocker (1946) suggested that the calcium in the Mallee calcretes was derived from the southern Australian continental shelfs during times of low eustatic sea-levels and from calcareous coastal dunes, and transported into the dunes by aeolian means. This theory was later supported by geochemical analysis providing evidence for a dominant input of marine calcium in the calcretes of southeastern Australia (Dart et al. 2005, Grevenitz 2006), brought in by either aeolian dust or by rainwater.

The most common calcretes in the study area were found to be nodules and lenses of cemented or soft calcrete, hardpan calcretes and powdery calcretes according to classifications of Goudie (1983) and Wright and Tucker (1991) (Fig. 2.13).

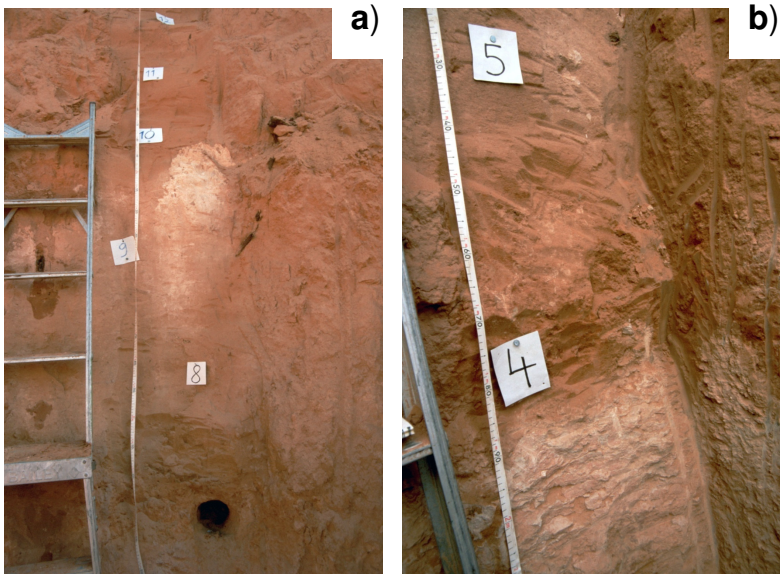

Fig. 2.13. Calcretes in the western Murray Basin. (a) Lense of cemented calcrete, (b) hardpan calcrete (Photograph A. Hilgers 2004).

Most of the calcretes in the Murray Basin are composed of $CaCO_3$, but magnesium-rich, dolomitic calcretes also occur. Dolomite is particularly found in hardpan calcretes and in lower parts of the soil profiles (Hutton and Dixon 1981, McQueen 2006). McQueen (2006) ascribed these dolomitic hardpan calcretes in low stratigraphic positions to precipitation from magnesium-rich groundwaters.

In some of the linear dunes of the Murray Basin, several generations of calcretes associated with stable soil formation have been observed, with younger calcretes overlying older ones (Churchward 1961). They are considered to have formed during more humid phases when

dunes where stabilised by vegetation (Bowler 1980). In the study area, calcareous palaeosols developed in distinct series or generations could not be observed. Some of the linear dunes investigated contained one hardpan calcrete layer and further zones with calcium carbonate enrichment. The latter though could not be identified as palaeosol horizons due to their indefinite structure and position within the dune.

A further characteristic of the soils of the Woorinen Formation is their relatively high silt and clay content (Bowler and Magee 1978, Butler and Hubble 1978). There is a general consensus that this clay component was brought into the dunes by aeolian means, i.e. as dust deposition on the dunes and subsequent infiltration by rain water (e.g. Butler 1956, Bowler and Magee 1978, Chen et al. 2002b, Hesse and McTainsh 2003).

Investigations on the Murray Basin dust deposits however concentrate on areas in New South Wales and Victoria, to the east of the area investigated in this study. There is some indication that the linear dunes in the study area contain less concentrations of clay than further east. For example, Twidale et al. (2007) reported that some of the linear dunes in the western Murray Basin lack fines and thus the trenches they produced within the dunes for sampling were quite susceptible to collapse.

In the southwestern part of the Murray Basin, where Molineaux Sands prevail, soils are non-calcareous and lack bonding clays. Whereas Pell et al. (2001) report that soil development is more or less absent on the Molineaux Sands, Bowler et al. (2006) described the soils of the Molineaux Sands as being composed of deep acidic podsol profiles.

Grain size analyses on dune sands of the Woorinen Formation and Molineaux Sands have been carried out by Pell et al. (2001). Mean grain sizes are lower in the Woorinen Formation, which is partly attributed to the high clay proportions. Furthermore, sands of the Woorinen Formation are less well sorted than Molineaux Sands, which Pell et al. (2001) ascribe to the higher stability of the linear dunes compared to the sub-parabolic dunes. This relative stability restricts aeolian sorting during transport and removal of the fine grains.

3. Quaternary climates of southeastern Australia

This chapter reviews existing studies of the Quaternary climatic and environmental change in southeastern Australia, as reconstructed from a range of terrestrial and marine archives. In Section 3.1, some aspects on the Quaternary climate before about 500 ka will be presented, although evidence of climatic change for this period and particularly the possibility to establish a chronology for this change is scarce. The second section of this chapter (Section 3.2.) reviews Quaternary climatic conditions after 500 ka, for which the palaeoenvironmental records give a more detailed picture. Section 3.3 reviews studies on changes of atmospheric circulation patterns during the last glacial and the Holocene.

3.1 The onset of Quaternary aridity in Australia

During the Pliocene, Australia experienced cooling and aridification (Bowler et al. 2006), but it was not until some time during the Early (~1.8 Ma-780 ka) or Middle (~780-130 ka) Pleistocene that arid conditions as they prevail in Australia today were established.

Little is known about the southeastern Australian Early and Middle Quaternary climates, but a few lines of evidence suggest that there was a major shift from humid to arid conditions before at least 700 ka. For example, Stephenson (1986) estimated that, to maintain the large water body of Lake Bungunnia, precipitation values around twice as much as modern values were necessary. Bowler et al. (2006) presented evidence for humid conditions prevailing until around 1.3 Ma, and full aridity developed at around 0.9 ka, with a transitional phase in between. Evidence for these estimates is seen in the change from siliceous Parilla Formation ridges to calcareous Bridgewater Formation ridges. The estimate of fully established aridity at around 0.9 Ma is in accordance with dating results from Lake Amadeus in Central Australia, where a marked change from lacustrine clay to playa sequences occurred at around this time (Chen and Barton 1991). Although the demise of Lake Bungunnia at around 700 ka was not of climatic but tectonic cause, it gave way to extensive dune building in the Murray Basin (Zhisheng et al. 1986). Bowler et al. (2006) place the onset of dune formation in the Murray Basin to around 500 ka, based on 4-5

palaeosols found in the linear dunes which are assumed to have formed in insolation-forced 100 ka cycles.

3.2 Middle to Late Quaternary climates of Australia

The Middle and Late Quaternary climate of southeastern Australia, like elsewhere in the world, is characterised by temperature oscillations of high frequency and amplitude triggered by variations in incoming insolation.

Fig. 3.1 shows Antarctic temperatures for the last 150 ka, deduced from the deuterium content in the Vostok ice core (Jouzel et al. 1987), and a stacked sea-surface temperature (SST) record from the Australasian region (Barrows et al. 2007), both expressed as deviation from present day temperatures. Both records indicate the warmest temperatures at the height of the last interglacial (Oxygen Isotope Stage (OIS) 5e) at around 125 ka, succeeded by two cycles of intermediate cooling and warming (OIS5d, 5c, 5b and 5a). The last glacial (75-12 ka) is characterised by a reduction in temperatures towards very cold conditions at around 60 ka (OIS4), followed by an interstadial (OIS3) with intermediate temperatures between around 55 and 30 ka, and succeeded by the last cold period (OIS2), including the Last Glacial Maximum (LGM) centred at around 20 ka.

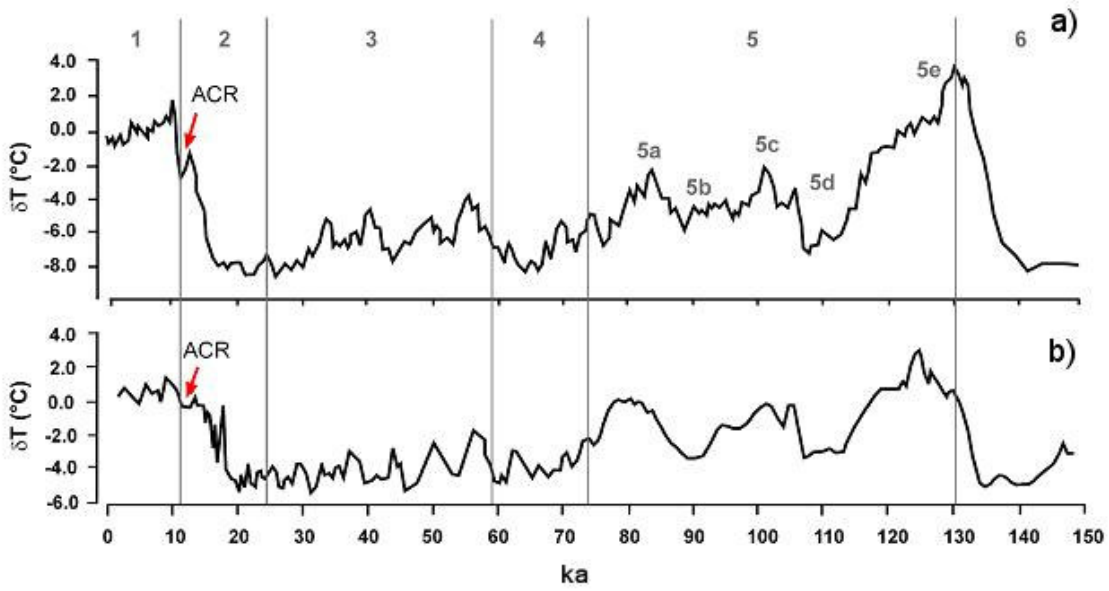

Fig. 3.1. (a) Vostok ice core (Antarctica) temperature record (Jouzel et al. 1987) and (b) stacked sea-surface temperature record (Barrows et al. 2007), shown as the difference from modern (sea) surface temperatures. ACR: Antarctic Cold Reversal. The numbers and lines denote Oxygen Isotope Stages derived from Martinson et al. (1987).

Shortly after the LGM, from around 18 ka on, Antarctic air and Australasian sea surface temperatures rose dramatically, leading into the present interglacial, the Holocene, which commenced around 12 ka ago. The isotopic composition of Antarctic ice cores shows that the last termination after the LGM however was a two step process. The warming interval was interrupted by an abrupt return to colder conditions, a period termed the Antarctic Cold Reversal (ACR, see Fig. 3.1). It lasted from around 14 to 12.5 ka (Jouzel et al. 1995), thus preceding the Younger Dryas (12.9-11.7 ka) (Lowe and Walker 1997, Rasmussen et al. 2006). Most of the Antarctic cores further show a clear Holocene temperature optimum from around 12 to 9 ka (Watanabe et al. 2003).

For the arid and semi-arid interior of Australia, temperature oscillations during glacial and interglacial times were equally dramatic, although their reconstruction is more difficult than for Antarctic and oceanic environments. Miller et al. (1997) reconstructed surface temperatures of at least 9°C colder than today for a period between 45 and 16 ka, using temperature dependent amino acid racemization of radiocarbon dated emu eggshells. Equally, sea surface temperatures in oceans surrounding Australia were lowered by 4°C in the tropics, and by up to 8°C in higher latitudes during the LGM (Barrows and Juggins 2005).

These changes in temperature resulted in major changes in global ice volume, sea levels, circulation patterns and precipitation. For example, during the LGM, sea levels were lowered significantly so that Tasmania and Papua New Guinea were linked to the Australian continent, and small valley glaciers developed in the Snowy Mountains in southeastern Australia and the Tasman Highlands (Barrows et al. 2001, 2002).

A major issue in reconstructing Quaternary climates of Australia is the uncertainty about the relationship between temperature and precipitation. In general, cooler sea surface temperatures during glacials resulted in reduced evaporation and thus a reduced atmospheric moisture level, leading to lowering of precipitation on the continents (Williams et al. 1998). Indeed, whereas the LGM was a period of more arid conditions with substantial dune building (e.g. Fitzsimmons et al. 2007, Rhodes et al. 2005) and a drying of Lake Eyre (Magee et al. 1995, 2004) in arid central Australia, most records point to interglacials being wetter than present, indicated for example through larger discharge of creeks (Croke et al. 1996, Nanson et al. 1992b) and lake level highstands (Magee et al.

1995, 2004, DeVogel et al. 2004). The next two sections consider whether this relationship between temperature and precipitation also holds for southeastern Australia.

3.3 Southeastern Australian records of palaeoenvironmental and palaeoclimatic change

The Quaternary changes of temperatures and particularly precipitation had great impact on the southeastern Australian environments. These involve, for example, changes in soil moisture and vegetation, which in turn control aeolian processes such as dune formation and dust entrainment, and changes in river discharge and lake levels. Records of these past environmental changes thus can be found in lacustrine, fluvial and aeolian deposits and in caves. By dating these deposits using techniques as luminescence, radiocarbon or uranium series dating, a chronological framework of palaeoenvironmental changes can be established. Each of these dating techniques has its own limitation though, for example considering the lower and upper dating limit or their precision. Luminescence dating, for instance, can cover a time span from a few tens of years up to about 350 ka (e.g. Murray and Olley 2002), whereas radiocarbon dating only is a reliable method for the last ~45 ka (e.g. Weninger and Jöris 2008). On the other hand, radiocarbon ages are much more precise than luminescence ages. A lot of the dating techniques have in common that their precision increases towards younger ages. Thus if Holocene records reveal greater climate variability than records of the last interglacial, this might merely be an artefact of the dating precision. Furthermore, reconstructing past environmental changes from proxy data preserved in terrestrial and marine records can be very complex. First, it has to be considered that most of the terrestrial records are discontinuous, a major disadvantage against marine records. Second, for most environmental processes, multiple causes can be found. For example, dust deposition can either be controlled by aridity or wind speed, or both, each leading to different interpretation of palaeoclimate. In the following, southeastern Australian records of palaeoenvironmental change are reviewed and problems concerning the dating, continuity, or interpretation are outlined. As reconstruction of paleoenvironments from the dune record is the major focus of this work, these issues will be explained in most detail.

A lot of the results are displayed as probability density function plots (PDF). A further description and discussion of this mode of display can be found in Section 6.5.

3.3.1 The speleothem record

In arid and semi-arid regions speleothem growth is strongly related to rainfall (Heine and Geyh 1984, Brook et al. 1990, in Ayliffe et al. 1998) and therefore has high potential for palaeoclimatic reconstructions. Furthermore, speleothems can be dated with high precision using thermal ionization mass spectrometry (TIMS) $^{230}Th/^{234}U$ dating up to about 500 ka (Edwards et al. 1987).

Ayliffe et al. (1998) dated speleothems with TIMS $^{230}Th/^{234}U$ from caves in the Naracoorte region of South Australia to establish a 500 ka record of changing effective precipitation in southeastern Australia. The location of the study site is shown in Fig. 3.3.

Fig. 3.2 displays the results of Ayliffe et al. (1998), with peaks in relative probability (y-axis) reflecting phases of enhanced effective precipitation, and their comparison with a radiolarian temperature record of the Southern Ocean (Martinson et al. 1987).

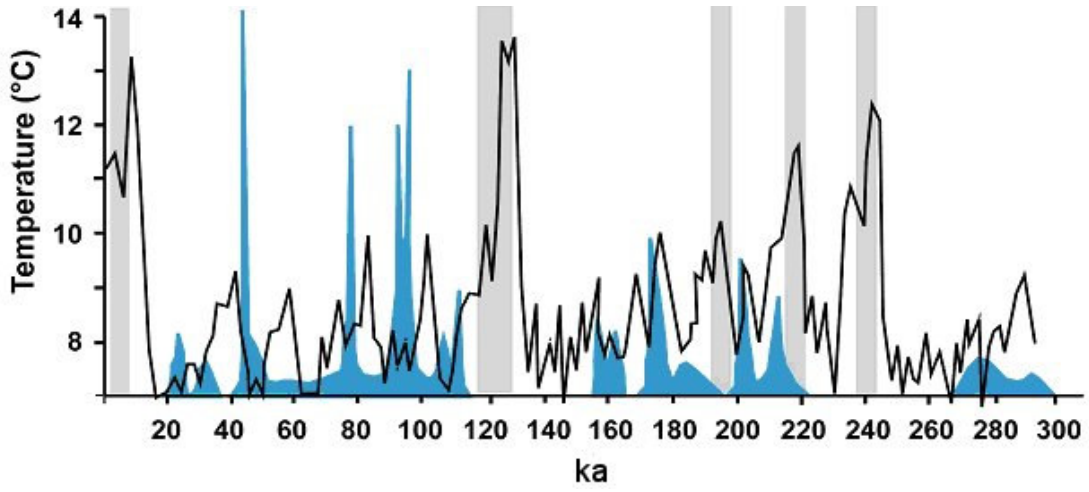

Fig.3.2. The speleothem record of the Naracoorte Caves (Ayliffe et al. 1998) (blue) and radiolarian temperatures (Southern Ocean) (Martinson et al. 1987) (black line). Grey bars highlight approximate positions of interglacials and warm interstadials (redrawn from Ayliffe et al. 1998).

From Fig. 3.2 it can be seen that the highest effective precipitation occurred during stadials and cool interstadials, whereas peak interglacials, warm interstadials and glacial maxima were comparatively arid. Speleothems of Holocene age were not found in the cave, suggesting that, like in previous interglacials, climatic conditions were too arid to permit soil moisture to enter the cave. Ayliffe et al (1998) conclude from these results that during interglacials (e.g. OIS5e, or the Holocene), very high temperatures led to high evaporation

rates, decreasing effective precipitation, whereas in the cooler stadials reduced temperatures resulted in a net water surplus. Intermediate temperatures with sea surface temperatures of ~3°C lower than today were considered ideal for the highest rates of effective precipitation (Ayliffe et al. 1998).

3.3.2 The pollen record

Past vegetation patterns can be reconstructed from pollen data deposited within terrestrial (mainly lakes and swamps) and off-shore marine sediments. Chronological assessment can be achieved by ^{14}C dating of the organic material or by dating the surrounding sediments (e.g. luminescence, varve counting, U/Th dating). Vegetation composition in arid and semi-arid regions is strongly dependent on effective precipitation and to a lesser degree, on surface temperatures, and can therefore be used to reconstruct palaeoclimates. Nevertheless, interpretation of pollen data is often not straightforward, as different dispersal mechanisms (e.g. by wind, rivers) make it difficult to differentiate between local and regional pollen (Williams et al. 1998). Furthermore, pollen sequences can include species which no longer exist today, and if their growth conditions are not known, they cannot be used for palaeoclimatic reconstructions.

In the following, all radiocarbon ages are quoted as calibrated ages (if not stated otherwise), either as given by the authors or translated from uncalibrated ages using the programme Calpal (2007) for better comparison of the results.

Harle (1997) presents palynological evidence for environmental and climate change spanning the last 125 ka from a core (E55-6) off the coast of western Victoria (Fig. 3.3), representing the past regional vegetation assembly of southeast South Australia and western Victoria. Chronology is provided by correlation with oxygen-isotope data derived from planktic foraminifera (Passlow et al. 1997).

The results of Harle (1997) imply that within the last 125 ka, OIS5 was wettest, with peak effective precipitation occurring in OIS5e. A drying trend towards the end of OIS5 is expressed in the decline of rainforest taxa and Eucalyptus, and an increase in semi-arid communities. OIS4 is associated with relatively dry conditions, evidenced by pollen from semi-arid communities and an opening up of the regional vegetation. In interstadial OIS3, there is evidence for an initial return to woodlands, hence increased effective precipitation

which gradually decreases towards the end of OIS3. In OIS2, regional vegetation appeared to be open and adapted to dry conditions, although low pollen concentration in this part of the core make interpretation difficult. High charcoal concentrations in the OIS2 part of the core, absent in the previous glacial zones, suggest aboriginal use of fire.

Two further pollen records from maar craters of western Victoria, Lake Wangoom and Lake Terang (Fig. 3.3) were investigated by Edney et al. (1990) and D'Costa and Kershaw (1995), respectively. The chronology for the Lake Wangoom record was established using radiocarbon dating, and that of Lake Terang by correlation with the Lake Wangoom record. However, the chronology for the Lake Wangoom record was later re-established by Harle et al. (1999), by using U/Th dating as a further method. The oldest ^{14}C age of 43 ka BP (Edney et al. 1990) deviated significantly from the U/Th age of around 95 ± 25 ka for the same pollen zone. From comparison with the nearby off-shore core investigated by Harle (1997), Harle et al. (1999) deduced that the zone with high rainforest taxa and Eucalyptus dominance most likely correlates with OIS5e, conflicting both the ^{14}C chronology as well as the U/Th chronology. For the younger part of the record, this would mean an increasing drying trend from OIS5d through to OIS2, with little response of vegetation to increases in precipitation during OIS3. In the Holocene part of the core, Eucalyptus increases again, indicating return to more humid conditions, consistent with the interpretation of Edney et al. (1990) and D'Costa and Kershaw (1995). The study of Harle et al. (1999) demonstrates the difficulty of establishing accurate chronologies for pollen records, especially from terrestrial lake environments.

At Tower Hill, a crater lake in southwestern Victoria (Fig. 3.3), a pollen sequence covering the period from 18 ka to the early Holocene was analysed and ^{14}C-dated by Turney et al. (2006), providing a high resolution reconstruction of palaeoenvironments. The record implies wet condition at 10-11 ka, 12.5-13.5 ka and 17-18 ka. Dry conditions are recorded at 11-12.5 ka and 13.5-17 ka.

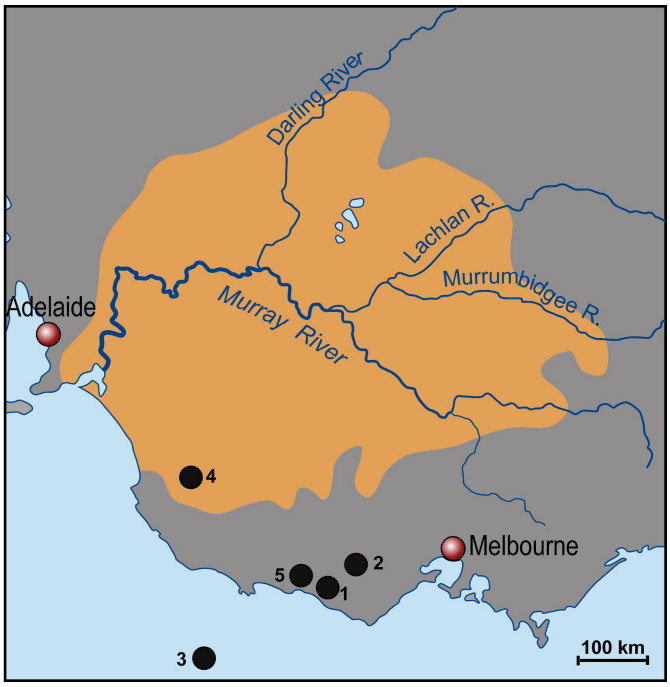

Fig.3.3. Sites of pollen and speleothem studies mentioned in the text. 1) Lake Wangoom, Edney et al. (1990), Harle et al. (1999), 2) Lake Terang, D'Costa and Kershaw (1995), 3) E55, Harle (1997), 4) Naracoorte Caves, Ayliffe et al. (1998), 5) Tower Hill, Turney et al. (2006) (draft by U. Beha).

3.3.3 The dust record

Aeolian dust is composed of silt and clay particles, which can be transported in suspension over long distances. The main requirements for dust entrainment are i) supply of fine particles readily for aeolian transport, which implies sparse stabilising vegetation cover and moisture (e.g. during phases of enhanced aridity), and ii) sufficient wind speed to lift the particles from the ground. If dust is transported off-shore and deposited in marine sediments, long and often continuous records of environmental conditions in the source area of the dust can be reconstructed, assuming that chronological control can be provided (e.g. by $\delta^{18}O$ correlation).

One of the major problems when interpreting dust records is that dust flux rates can be either dependent on wind speed or on sediment availability (or both). However, Hesse and McTainsh (1999) showed that dust flux rates in Australia depend mainly on vegetation cover in the source area and thus can provide evidence of arid conditions.

In Australia, two main dust paths exist (Bowler 1976). In central and northwestern Australia, dust is transported from source areas in the Great Sandy, Tanami and Simpson

Deserts in a northwesterly direction to the Indian Ocean. In southern and southeastern Australia, dust is transported with the westerlies to the Tasman Sea and, under high wind speeds, to New Zealand. From modern dust occurrence, Hesse and McTainsh (2003) showed that the main dust source areas of the southeast dust path are the arid and semi-arid areas of southern central and southeastern Australia, including the Mallee dune fields (Fig. 3.4).

Hesse (1994) and Kawahata (2002) calculated dust mass accumulation rates (MAR) found in marine deep sea cores in the Tasman Sea, in order to reconstruct palaeoenvironmental conditions in the source area of the dust. In both studies, chronostratigraphic control was provided by $\delta^{18}O$ measurements. The results are shown in Fig. 3.5.

The general picture deduced from the studies shows much higher MAR during glacial stages than during interglacials. Nevertheless the results from the cores investigated show some differences in dust flux rates (Fig. 3.5.). For example core E39.75 exhibits high MAR during the whole OIS6, extending well into OIS5e, whereas in core E26.1, MAR are high only in the latter part of OIS6 and decline significantly in OIS5e (Hesse 1994). A similar reduction in OIS5e is found in core NGC97 (Kawahata 2002). Another distinct difference in the cores is evident for OIS4. The two cores of Hesse (1994) show no response to this glacial period, whereas the core of Kawahata (2002) shows increased MAR at this time. Several peaks of MAR exist in OIS2 in the three cores, but the exact timing of these very high MAR is also different.

Hesse et al. (2004) ascribed the differences of MAR seen in the cores to different methodological approaches in identifying the aeolian fraction between Hesse (1994) and Kawahata (2002) and to core disturbance near the top of core E39.75.

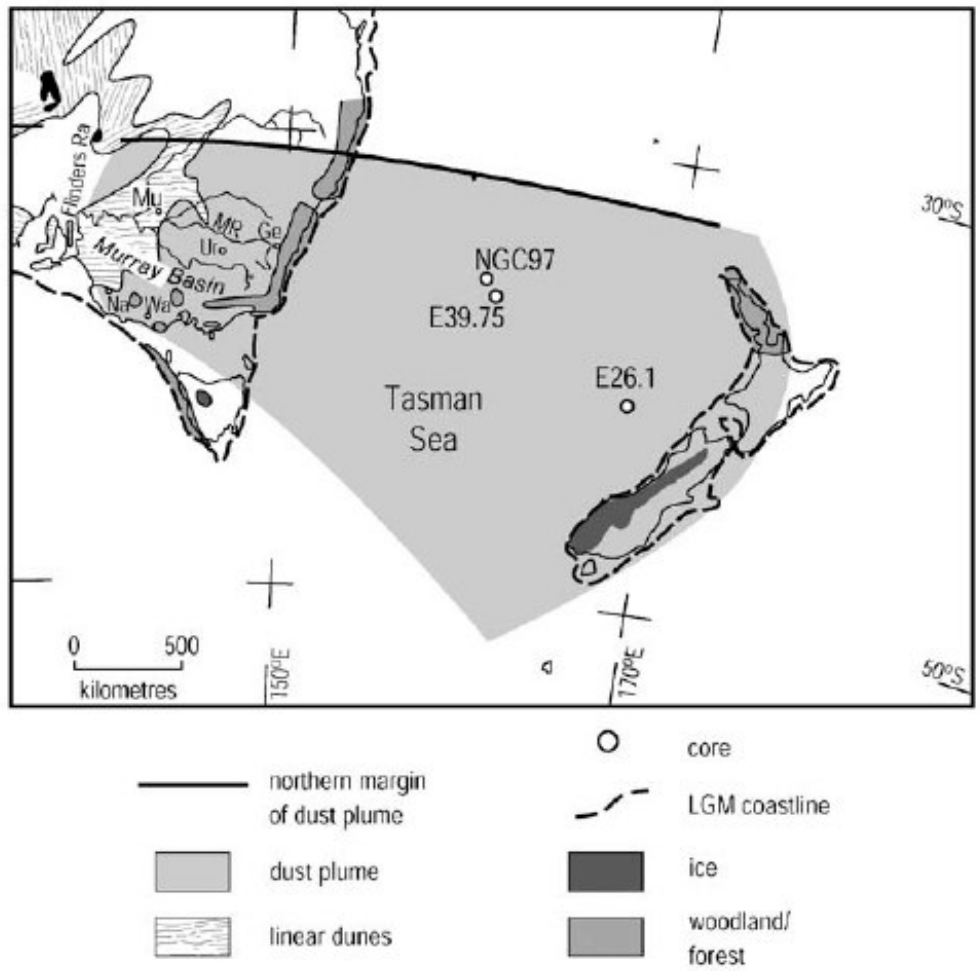

Fig. 3.4. The southeastern Australian dust path and location of the marine cores investigated by Hesse (1994) (core E39.75 and E26.1) and Kawahata (2002) (core NGC97) (from Hesse et al. 2004).

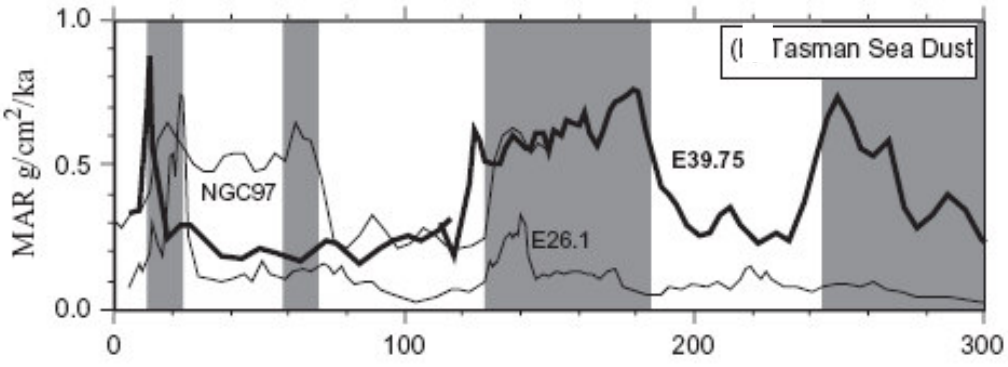

Fig. 3.5. Dust mass accumulation rates (MAR) derived from core E39.75, E26.1 (Hesse 1994) and NGC97 (Kawahata 2002). Glacial OIS are shaded in grey (from Hesse et al. 2004).

First high aeolian sedimentation rates occurred in the glacial period of OIS10, around 350 ka ago, providing evidence for the onset of Late Quaternary aeolian activity in southeastern Australia (Hesse 1994). The changes in dust fluxes observed in the cores of Hesse (1994) were found to reflect supply of erodible particles in the mainland source areas and not differences in wind speed, as shown by Hesse and McTainsh (1999). The authors also inferred that wind speed during the LGM was similar to Holocene wind speed, and that a slight increase in particle sizes found in dust deposited during the LGM was caused by different modes of dust deposition. Whereas during the LGM dry deposition was dominant, dust in the Holocene was mainly deposited by rainfall scavenging, indicating drier westerlies during glacials than during interglacials (Hesse and McTainsh 1999).

3.3.4 The fluvial record

River discharge is, among other factors as for example tectonic movements, dependent on the climate prevailing in the drainage area, and therefore fluvial deposits can provide evidence of past environmental changes. However, as many climatically driven factors influence fluvial activity, interpretation of fluvial records is a difficult task. For example, changes in effective precipitation control the water supply of rivers. Quaternary sea level changes alter the baseline of exorheic rivers, thus changing their gradient and stream length. In the upper catchments of rivers, which are often highland regions, rivers might be connected to valley glaciers during glacial times, causing discharge to be dependent on snow and ice melt, and therefore varying seasonally (e.g. Page et al. 1996). Furthermore, climatic fluctuations alter vegetation cover as well as physical and chemical weathering rates, therefore changing surficial water runoff as well as availability and grain size of transportable material. Tectonic movements can further complicate reconstruction of palaeoenvironemts from fluvial deposits.

Another problem involved when reconstructing past environmental conditions from fluvial records is the precise dating of fluvial sediments. Luminescence dating would be the method of choice to estimate fluvial sedimentation directly, but applying this method on fluvial deposits is sometimes limited due to incomplete zeroing of the luminescence signal (Section 5.5.3).

The Murray-Darling river system draining southeastern Australia exhibits many of the above mentioned problems in terms of palaeoclimatic reconstructions. It is exorheic and was therefore influenced by Quaternary sea level changes in its lower reaches, and it rises in the southeastern highlands, thus reached into the periglacial zone during glacial times, rendering its discharge dependent on snow melt processes (Page et al. 1996).

Page et al. (1996, 2001) dated palaeochannel deposits and associated source bordering dunes of the Murrumbidgee River using TL dating. According to Page et al. (1996) the fluvial and aeolian deposits represent enhanced channel activity during four major phases, named the Colleambally Phase (105-80 ka), the Kerarbury Phase (55-35 ka), the Gum Creek Phase (35-25 ka) and the Yanco Phase (20-13 ka). When displaying the TL ages presented in the studies of Page et al. (1996, 2001) as probability density function (Fig. 3.6), the four phases are centred at about 85 ka, 45 ka, 25 ka and 18 ka. The high discharge rates during the cold OIS2 are considered to reflect a highly seasonal signal through snow melting processes imprinted from periglacial environments in the upper catchment of the Murrumbidgee River (Page et al. 1996).

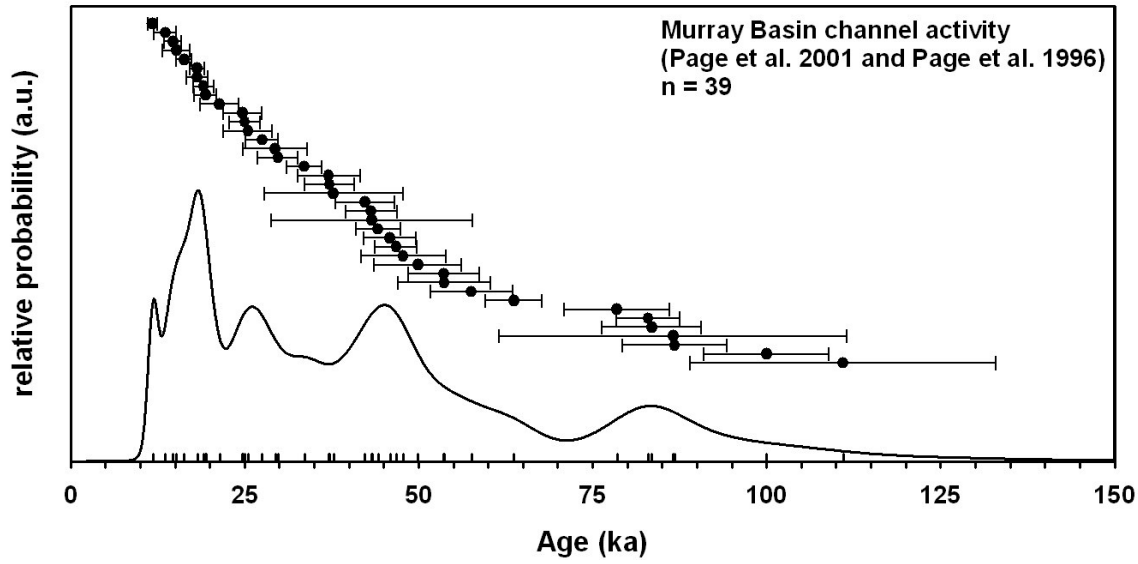

Fig. 3.6. PDF of TL ages obtained by Page et al. (2001, 2006), showing phases of increased Murray Basin channel activity. Bin width of the PDF is 0.5 ka.

3.3.5 The lake record

Lake levels in dryland regions are strongly controlled climatically. Lakes obtain water through rainfall in their catchment, through rivers and through groundwater. If precipitation

exceeds evaporation, lake levels are usually high. Therefore, former lake levels can be used to reconstruct palaeoclimate, if remains of these lake level high- and lowstands, such as shore ridges or salt crusts, are preserved and can be dated. Interpretation of lake records, however, can be complicated by a number of factors. If for example the catchment area of rivers feeding the lakes is large and expands over more than one climatic zone, lake levels may reflect climatic conditions in the source area of the river and not in the vicinity of the lake itself. This problem is exemplified by Lake Eyre, a huge internal drainage basin in arid central Australia, which is fed by river systems with source areas in northern and northeastern Queensland. Its lake levels therefore record monsoonal effectiveness in northeastern Australia, and not the climate in central Australia (Magee et al. 1995, 2004).

One of the best studied sites in Australia with respect to lake levels and their response to environmental change is the Willandra Lakes group, and within this system, Lake Mungo, in southwestern New South Wales. The Willandra Lakes are dry today, but experienced oscillating lake levels, including lake-full phases, during the Late Pleistocene. They were fed by an ancestral course of the Lachlan River, the Willandra Creek, rising in the southeastern highlands. Along the eastern shores of the Willandra Lakes, lunette dunes developed through aeolian erosion of lake shore sediments and transport with predominantly westerly winds. The lunettes in the Willandra region reflect former lake levels in the following way (Bowler 1973, Bowler 1998): When lake levels are high, quartzose beach sands are deposited by wave action at the eastern shores of the lakes. These sands are transported by wind over a short distance and are deposited as a shoreline dune composed mainly of clean quartz grains with very little clay. When the climate subsequently becomes more arid, lake levels fall. Former lake bed clays are exposed on the lake margins. Saline groundwaters directly below this zone of exposed lake beds migrate to the surface by evaporation, resulting in a crystallisation of salts on the clayey surface. The salts cause the formation of sand-sized clay pellets which can be eroded by strong winds. The former quartz shoreline dune is then covered with new sediments with a very high clay proportion.

The lunette of Lake Mungo, for instance, is composed of several layers of quartz beach sands intercalated with clay dune layers, sometimes interrupted by soils, each representing a lake full phase, a period of falling lake levels, and a period of landscape stability with

little aeolian sedimentation, respectively (Bowler 1998). These are the Golgol, the Lower Mungo, the Upper Mungo, the Arumpo, the Zanci and the Mulurulu unit (Fig. 3.7)

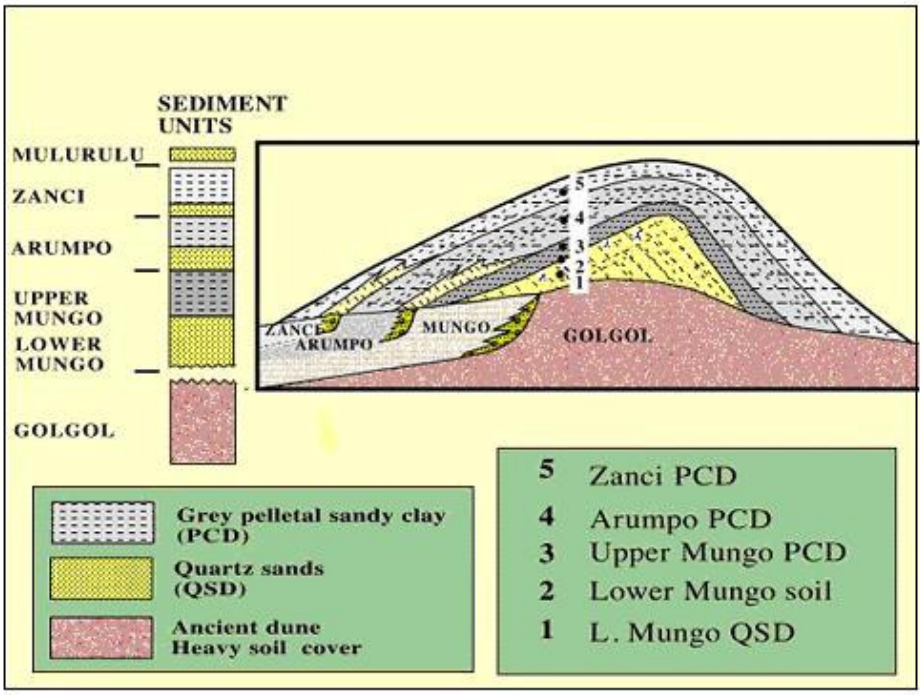

Fig. 3.7. Stratigraphy of the Lake Mungo lunette (Bowler 2002).

Radiocarbon (Bowler 1998), TL (Bowler 1998, Bowler and Price 1998) and OSL dating (Bowler et al. 2003) have been carried out on the sediments of the Lake Mungo lunette.

The Lake Mungo record indicates formation of pelletal clay units, low oscillating lake levels and thus, relatively arid conditions between 100 and 120 ka (Golgol unit) and between 40 and 19 ka (Upper Mungo, Arumpo and Zanci unit). The latter period was interrupted by a short phase of relatively high lake levels at around 30 ka (Bowler et al. 2003). A prolonged phase of lake-full conditions associated with quartose beach sand deposition was dated to 40-60 ka (Lower Mungo unit), implying more humid conditions. A further short return to high lake levels was noticed between 17 and 19 ka cal. BP (Bowler 1998), based on radiocarbon dating. After around 15 ka, no more major flooding events or lunette dune depositional events are evident in the Lake Mungo record (Bowler 1998).

3.3.6 The dune record

3.3.6.1 Dunes as palaeoenvironmental archives

For inland dunes to be formed, three requirements have to be met, similar to those needed for aeolian dust transport. First vegetation cover has to be sparse, second, sand-sized grains have to be available for aeolian transport; and third, wind speed has to be high enough to carry the sand-sized grains (e.g. Ash and Wasson 1983, Lancaster1990, Wiggs et al. 1995, Kocurek 1998). These conditions are normally found in desert regions, therefore inland dunes and palaeodunes are usually associated with (past) aridity. By dating these dunes, nowadays generally by luminescence methods, a record of past phases of arid conditions can be established.

Interpreting dune records however, is not always straightforward, for a number of reasons. Dune sands, once deposited, can be easily re-activated as long as no stabilising processes, such as soil formation and/or carbonate enrichment, take place. A gap in the dune record can thus either reflect a period in which only little aeolian sedimentation occurred, or in which constant reworking of dune sands prevented their preservation. It is thus desirable when using dunes as a palaeoenvironmental archive, that other signs of landscape stabilisation (e.g. soil formation) can be found and chronologically constrained.

It is further not evident when exactly during arid periods dunes form and are stabilised. For instance, if dune formation is strongly dependent on sediment supply through rivers, it possibly reflects the onset of arid conditions after a humid period in which source material was delivered. For instance, Chase and Thomas (2007) presented a dune record from the west coast of South Africa, which correlated very well with humid phases from a nearby fluvial record. The authors concluded that sediment supply and also wind strength were the major controls on dune formation in this area, and hence their dune record did not reflect arid phases. Removal of vegetation through human impact can further complicate the interpretation of dune records (e.g. Hilgers 2007).

If the majority of the dune sands is reactivated or recycled during the length of the arid period, and is then stabilised by a following humid phase (e.g. through soil formation processes), then the majority of the luminescence ages would date the very end of an arid period or the transition to a more humid phase. As a consequence a lot of dune record should not be considered as a measure of aeolian activity and aridity but as measure for

dune stabilisation (i.e. waning aeolian activity and aridity), a scenario proposed by e.g. Nanson et al. (1992a). Because of the high susceptibility of dunes to reactivation, Munyikwa (2005a) argued that due to the different degree of reworking, dependent on dune morphology, sediment supply, particle size distribution and wind speed, dune sand remnants of different age, but nonetheless belonging to one and the same depositional cycle, might occur in different areas, making comparison of dune records over large areas very difficult. And even on a very local scale, linear dune records might be highly variable as shown by Telfer and Thomas (2007).

If dunes are not susceptible to reworking though, perhaps due to the bonding effects of clays or carbonates, the dune record might reflect peak aridity, if vegetation cover was the major control on the dune formation.

The linear dunes of the Murray Basin indeed contain high proportions of clays and carbonates, thus are potentially relatively resistant to aeolian reworking. They are furthermore not likely to be very dependent on sediment supply through fluvial input, if very local sediments deposited before the onset of dune formation are the main contributors to the dune sands, as argued by Bowler and Magee (1978) and Pell et al. (2001). Furthermore, Hesse and McTainsh (1999) argued, that at least during the Holocene and LGM, wind strengths in southeastern Australia were similar. Therefore, varying wind strength as a major control on dune formation can possibly also be ruled out. It is thus likely that vegetation cover, and hence aridity is the main factor on dune formation in the Murray Basin. In the following, dating studies on dunes of the Murray Basin will be reviewed.

3.3.6.2 Luminescence chronologies of dunes from the Murray Basin

Despite good accessibility of the Murray Basin, only few dating studies of dunes have been carried out in this area so far. Gardner et al. (1987) took eight samples from four sections within longitudinal dunes south and east of Loxton in South Australia. TL dating yielded ages between 8.4± 1.5 and 35 ± 5 ka. Readhead (1988) established TL-chronologies of two longitudinal dunes in the eastern Mallee linear dune field, one being situated at the western margin of Lake Mungo, the other one at Nyah West in northwestern Victoria. The Lake Mungo longitudinal dune yielded ages between 6.9 ± 2.3 and 42 ± 4 ka. The dune at Nyah West can be divided into several units based on soils developed within the dune. From the

uppermost unit, the Kyalite unit, one sample was taken which yielded a TL age of 26 ± 3 ka. From the Speewa unit, which underlies the Kyalite unit, one sample gave a TL age of 90 ± 14 ka, and the other four samples ages of around 130 ka. The results indicate that a period of dune stability and soil formation must have occurred between around 90 and 26 ka. It can further be implied that dune building in this part of the Murray Basin possibly commenced a long time before 130 ka, as at least two further units of dune sands, separated by soils, underlie the Speewa unit. Twidale et al (2007) investigated three sections in longitudinal dunes in the northwestern Murray Basin. OSL-dating of the dune sands yielded ages between 157 ± 15 ka and 25 ± 2 ka. Two further samples yielded modern ages. The oldest sample was taken near the base of the dune, and is the oldest age presented for Mallee dune sands so far. Further OSL dating on a dune partly consisting of linear dune material of the Woorinen Formation and partly of lunette dune material at Lake Menindee in western New South Wales was carried out by Cupper and Duncan (2006). In the part derived from the Woorinen Formation OSL ages ranged from ~51 ± 5 to 66 ± 5 ka.

Robertson and Prescott (2006) dated a sequence with OSL at Roonka, an aboriginal burial place at the eastern bank of the Murray River. The upper part of the sequence was assigned to the Bunyip Sands formation, and dated to 4.3 ± 0.7 ka. For the lower part of the sequence, belonging to the Woorinen Formation, OSL ages between 16 ± 1 and 52 ± 4 ka were obtained. Fig. 3.8 displays all luminescence ages of the above mentioned studies as PDF (n = 41). This excludes the two modern ages obtained by Twidale et al. (2007), as the bin width of 0.5 ka does not allow display of these ages. The sites mentioned in the text are shown in Fig. 3.9.

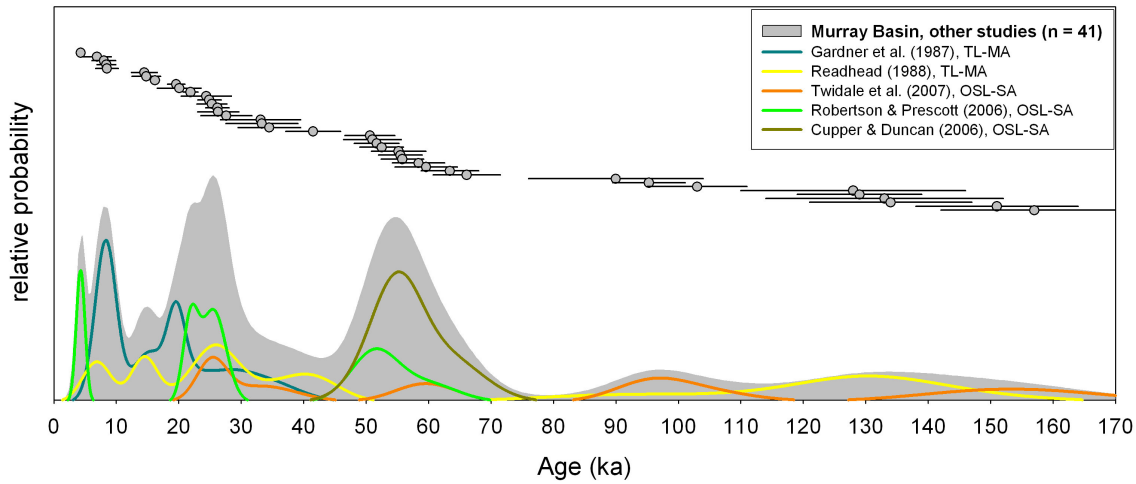

Fig.3.8. Compilation of TL and OSL ages of dune sands from the Murray Basin, obtained by Gardner et al. (1987) (n = 8), Readhead (1988) (n = 11), Cupper and Duncan (2006) (n = 8), Robertson and Prescott (2006) (n = 7) and Twidale et al. (2007) (n = 7). Bin width of the PDF is 0.5 ka. MA = Multiple Aliquot, SA = Single Aliquot.

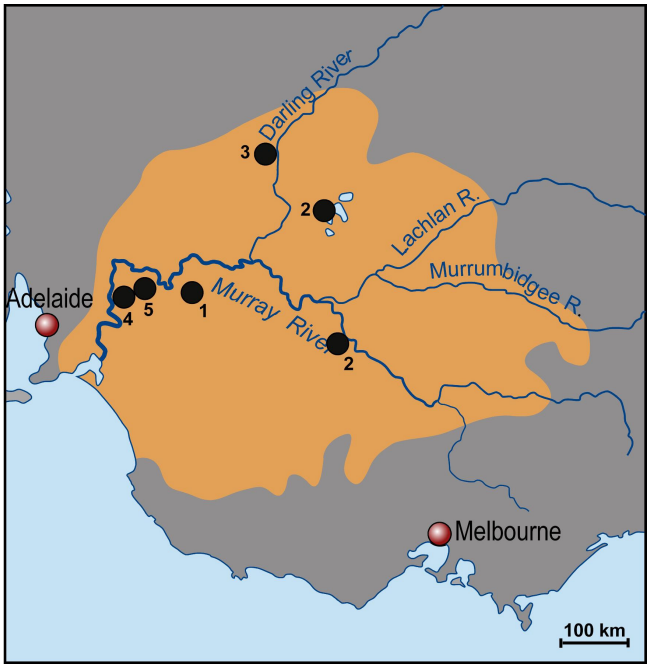

Fig.3.9. Sites of the dune studies mentioned in the text. 1) Loxton area, Gardner et al. (1987), 2) Willandra Lakes and Nyah West, Readhead (1988), 3) Lake Menindee, Cupper and Duncan (2006) 4) Roonka, Robertson and Prescott (2006) 5) Waikerie area, Twidale et al. (2007) (draft by U. Beha).

From Fig. 3.8 it can be deduced that strongest aeolian net sedimentation occurred between around 40 and 8 ka. A further peak of aeolian sedimentation is evident at around 60 ka.

Ages above 90 ka are too imprecise to discriminate further distinct phases of dune sand deposition. From the luminescence ages obtained so far, dune formation in the Mallee seems to have been initiated at least around 160 ka ago. Bowler et al (2006) estimated from assumed 100 ka cycles of soil formation phases evident as four to five palaeosols in the dunes, that dune formation in the Murray Basin was initiated at around 500 ka. Ages of >170 ka however, have not been obtained for the dunes of the Murray Basin.

Considering the complexities of interpreting dune records due to their discontinuity and the different degree of preservation from site to site, it is difficult to infer palaeoclimatic changes from the studies mentioned above. The gaps of ages seen in the compilation of luminescence ages in Fig. 3.8 for instance cannot be considered to reflect non-depositional phases. Sampling resolution is relatively low in the studies, thus gaps in the records could merely be a relict of depositional phases being missed by the sampling procedure. Also, the number of sites investigated is too low to correlate age gaps from site to site, in order to infer widespread dune stability. A further problem is that the studies use different luminescence dating approaches, such as OSL dating and TL dating, or multiple aliquot dating and single aliquot dating (see Section 6.1). This inconsistent methodology further hampers the inter-comparison of the obtained luminescence ages. Therefore, there is a clear need for a more comprehensive chronology of dune formation in the Murray Basin, established with a consistent dating methodology.

3.3.7 Synthesis

The review of southeastern Australian palaeoclimatic records most relevant for the present study reveals that on the one hand, a great variety of studies on a range of archives are available, but that on the other hand, some of the records provide conflicting evidence of palaeoclimatic conditions. In conclusion, over the last 130 ka, the much colder-than-present conditions of OIS4, the end of OIS3 and OIS2 seem to be susceptible to more arid conditions than those prevailing in southeastern Australia today, and periods with intermediate temperatures, as the early part of OIS3, to wetter conditions than today. Evidence for interglacial periods such as OIS5e and the Holocene is conflicting. The pollen records provide evidence of wet conditions (Harle 1997, Harle et al. 1999), the speleothem record of arid conditions (Ayliffe et al. 1998) and the dust record reveals some

disaccordance between the individual marine cores investigated (Hesse 1994). Some of the discrepancies might be a problem of defining dry and wet conditions. The records presented in the previous section provide only relative estimates for climatic conditions and compare past conditions with those of today. So part of the problem of the conflicting evidence is how to define the present climatic condition: Are they arid or humid? For example, the speleothem record referres to present conditions as arid, whereas the pollen records define present conditions as wet. Therefore, also the last interglacial (OIS5e), possibly with similar climatic conditions, is referred to as arid period in the speleothem record and as wet period in the pollen record of Harle (1997). With respect to the dune record, the present climate is of such conditions that it is wet enough to allow sufficient vegetation cover to stabilise the dunes. Very likely though, the dunes are close to the threshold of reactivation, as evidenced by the two modern ages of dune sands obtained by Twidale et al. (2007). Therefore, the present climate probably reflects a phase characterised by a sensitive balance between dry and wet conditions.

Further differences in the records can be explained by methodological problems, for example in precision and accuracy of the different dating methods applied, regional variations in climate, or a diffent reponse lag of the investigated environmental archives to climatic change.

3.4 Changes of circulation patterns over southeastern Australia during the last glacial

The oscillating climate of the Quaternary was not only characterised by changes in temperature and precipitation, but also by changes in atmospheric circulation. The important pressure systems with respect to present day and past southeastern Australian climate are the westerlies and the subtropical anticyclone.

At present, the southern hemisphere westerlies are located between 40/42°S and 70/75°S (Iriondo 1999), with a near-surface wind maximum at around 50° (Shulmeister et al. 2004). The interannual shift of the westerlies is estimated to around 2° (Shulmeister et al. 2004). The subtropic anticyclonic belt which causes widespread aridity in central Australia is positioned between 29-32°S in winter and 37-38°S in summer (Karelsky 1956). Compared to the other austral continents, the Australian anticyclone is very prominent, covering two-thirds of the continent and persisting throughout all seasons (Iriondo 1999) (Fig. 3.10).

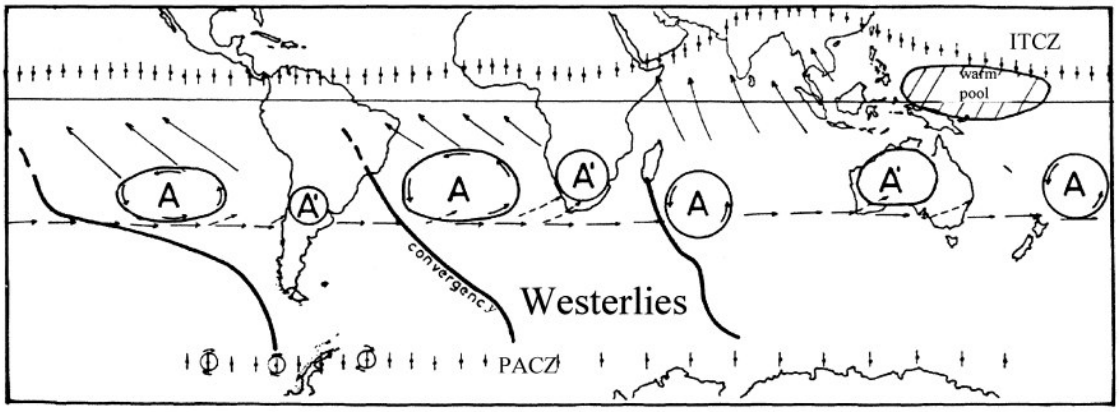

Fig. 3.10. Present position of climatic structures in winter (July). ITCZ: Intertropical Convergence Zone. PACZ: Periantarctic Convergence Zone. A: Oceanic Anticyclone. A': Continental Anticyclone (Iriondo 1999).

Several lines of proxy evidence suggest that these circulation patterns were different during the last glacial. The major changes involved in this respect are variations in latitudinal position of the pressure belt (e.g. a north- or southward shift, or their expansion or contraction) and variations in the intensity of the circulation (i.e. changes in wind strength). A further issue in respect to the westerlies is related to the amount of moisture they carry in order to induce rainfall over the southern parts of Australia.

Reconstruction of past circulation patterns is a difficult task. The major archives that can preserve both past wind directions and past wind strength are wind blown sediments like dunes or loess (Shulmeister et al. 2004). But as seen in Section 2.3.2, linear dunes form under bidirectional winds, and thus relation of dune orientation to past wind direction is not as straightforward as it may seem. And only if the aeolian sediments are dated accurately, past circulation patterns can be inferred from them. Past wind strength might be inferred from either sedimentation rates of aeolian sediment and/or their grain sizes. But grain size is not only dependent on wind strength but also on the source material available for aeolian transport. High aeolian sedimentation rates can equally reflect high wind speed, or increased sand or dust availability, e.g. due to increased aridity (e.g. Hesse and McTainsh 1999). Further, grain sizes may be altered through time by weathering.

Changes in southern hemisphere circulation patterns are mainly triggered by the extent of the Antarctic ice sheet and temperature gradient from equator to pole. A possible LGM scenario in this respect is that the extended ice sheet led to an enlargement of the Antarctic high pressure zone and a northerly shift of the Antarctic Polar Front, resulting in an

equatorward displacement of the connecting pressure belts as the westerlies and the subtropic anticyclone (STA) (e.g. Stuut et al. 2002, 2004). Further, an increased difference in air and sea surface temperatures from equator to pole might have increased the pressure gradient, which would have resulted in stronger winds. Some southeastern and central Australian terrestrial and marine proxy data indeed support this scenario. For example, a northwards displacement of the subtropic anticyclone over arid central Australia was found by Nanson et al. (1995) and Hollands et al. (2006), derived from luminescence dating of linear dunes with different trends. The inferred shift was estimated to around 150 km. A northerly shift of the westerlies was also postulated by Wasson (1986) to explain the west-east orientation of the Mallee linear dunes, which is not consistent with modern wind vector resultants (Sprigg 1979). From dust deposits found in the Tasman Sea, Hesse (1994) and Kawahata (2002) also inferred an equatorward shift of both the westerlies and the subtropical ridge during glacial times, although Hesse et al. (2004) state that the northward shift of the westerlies was only minimal. Further evidence for a northward shift of the westerlies is thought to be provided by displacement of ocean currents during the LGM off the eastern coast of Australia (Bostock et al. 2006) and by the northward shift of sea surface temperature isotherms in the Australasian region (Barrows and Juggins 2005). Based on studies on dune extent and orientation by Wasson (1986), Iriondo (1999) concludes that in western Australia, the westerlies were pushed polewards in response to the extended subtropical anticyclone. For eastern Australia, he postulate a northward displacement of the westerlies of 5-10°. He cites evidence from eastern Australia indicating more humid conditions during the LGM, although the author does not give references for these studies. An extensive review of LGM to modern (Little Ice Age, ca. 1400-1850 AD) climates of Australia and New Zealand influenced by the westerlies was presented by Shulmeister et al. (2004), including reconstructions from loess, dust, glacier advances, pollen, treerings, oceanic upwelling and ice-cores. They conclude that a lot of the evidence is ambiguous, which '*highlighted the relative lack of progress on quantifying past wind fields either in terms of areal extent or more particularly on wind intensities and tracks'* (Shulmeister et al. 2004: 45). Thus, no general trend in a latitudinal shift of the westerlies, either northwards or southwards can be inferred from the studies reviewed by Shulmeister et al. (2004). Most of the evidence presented in this study though points to an intensification of the westerlies during the LGM and the late Holocene with a peak during the Little Ice Age. The early

Holocene at around 11 ka appears to have been a period of minimum intensity of the westerlies. This however conflicts with the findings of Hesse and McTainsh (1999) who state that wind strength of the westerlies did not differ between the LGM and the Holocene, based on the observation that dust grain sizes in the Tasman Sea ocean cores did not vary between glacials and interglacials. The increased dust flux rates in glacial times were thus thought to reflect greater dust availability on the Australian continent due to increased aridity.

Another question addresses the potential of the westerlies to induce rainfall in southern Australia. On the one hand, a possible northward shift of westerlies during glacials might cause an increase in precipitation in areas affected by this shift. On the other hand, atmospheric and sea surface temperatures were greatly reduced during glacials (Jouzel et al. 1987, Barrows et al. 2007). This resulted in a globally depressed hydrological cycle which in turn could have resulted in much drier westerlies than today. Additionally, the low global sea levels resulted in exposure of great parts of the continental shelfs (Williams et al. 1998), hence the continent's interiors experienced a much higher degree of continentality, which would also result in a decrease in precipitation. According to Hesse and McTainsh (1999), the majority of dust in the Tasman sea was deposited through fallout processes and not through rainout processes during glacials. From this, they inferred drier westerlies during glacials compared to interglacial westerlies. Hesse et al. (2004: 98) further comment that '*changes in temperature and humidity of the westerly winds over Australia were probably more important in influencing the LGM environments of southern Australia than changes in either the position, strength or wave number of the zonal circulation*.'

Another possibility to deduce past climates and circulation patterns is by General Circulation Models (GCMs). These models are fed with several boundary conditions, such as sea surface temperatures, insolation, sea ice extent, land extent and topography, and from these boundary conditions they can simulate a range of climatic parameters (such as sea level pressure, wind strength, precipitation, temperatures or seasonality) for both present day and past climates. If past climates are to be reconstructed, the models rely on the reconstruction of past boundary conditions through proxy data. Hope (2005) compared LGM climate simulations using various GCMs. All models produced a southward shift of westerlies during the LGM due to an expanded subtropical anticyclone. The same finding was presented by Wyrwoll et al. (2000) through climate modelling. This scenario results in

a decrease in rainfall over southern Australia during the LGM. The models further suggest a slight reduction in mean zonal winds over southern Australia during the LGM (Fig. 3.11).

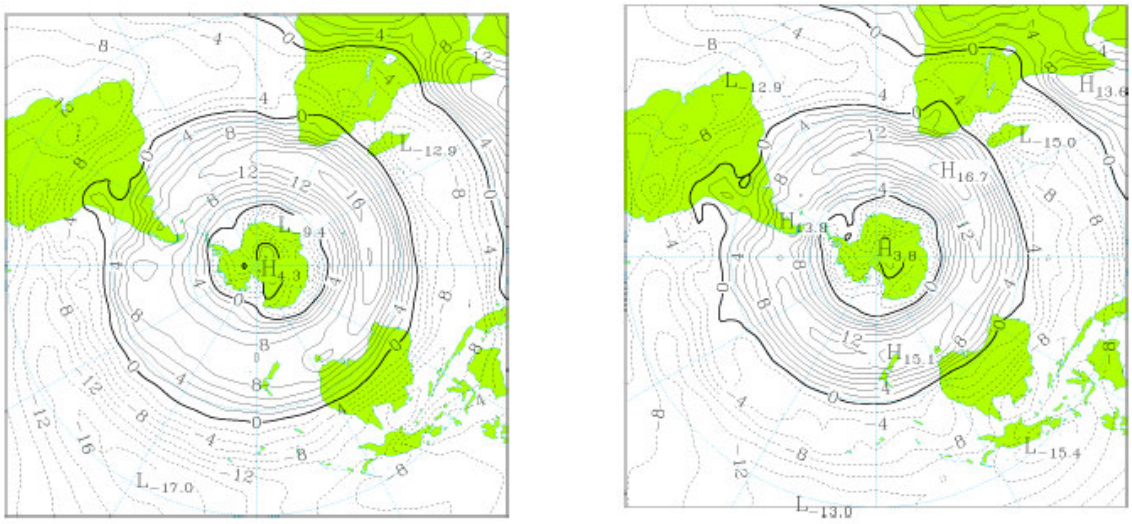

(a) PD, JJA (b) LGM, JJA

Fig. 3.11. Southern Hemisphere 850hPa winter zonal winds at (a) present day and (b) the LGM from MUGCM (Melbourne University General Circulation Model) in m/s. PD = present day, LGM = Last Glacial Maximum, JJA = June, July, August (Hope 2005).

In providing evidence that mean zonal wind strength is significantly positively correlated to winter rainfall, Hope (2005) deduces an additional decrease in rainfall for southern Australia. She also compares present day and LGM wind directions with dune orientation over the Australian continent, and concludes that annual LGM winds as simulated by the GCMs would align reasonably well with the Mallee dunes, whereas present day winds do not.

In conclusion it can be seen from this review, that proxy data and GCMs do not provide a consistent picture of southeastern and central Australian atmospheric circulation patterns during the LGM. Given the fact that LGM climates are reasonably well known based on well dated proxy data, it appears nearly impossible to reconstruct circulation patterns for earlier Quaternary periods such as the height of the last interglacial.

3.5 Conclusion

Although by Australian standards, the southeast is well investigated in terms of palaeoenvironmental and palaeoclimatic reconstructions, there are still a lot of unanswered

questions concerning the timing and nature of climate changes and circulation patterns during the middle and late Quaternary. Particulary the dune record is not investigated to its full extent. Establishing a chronology of this valuable archive can add a further piece to the jigsaw puzzle of Late Quaternary environmental change in southeastern Australia.

4. Sampling strategy and sampling sites

In Section 3.3.6, the drawbacks of using dune chronologies for palaeoenvironmental reconstructions have been outlined. The major point of concern hereby is that dune sands, once they are deposited, can easily be reactivated in later dune mobility phases due to their generally unconsolidated nature. Dune records are thus likely to be incompletely preserved (Kocurek 1998, Munyikwa 2005a, Telfer and Thomas 2007, Stone and Thomas 2008). This reactivation can be of very locally limited extent due to small scale variations in sediment composition or vegetation cover. The latter can for example be induced by aboriginal burning practices, naturally occurring bushfires or land clearance activities. Therefore, age determinations from a single site ought not to be extrapolated regionally. In order to distinguish regional dune formation phases driven by favourable environmental and climate conditions, and locally limited sand movements, possibly induced by non-climatic factors, the best strategy is to aim for a large OSL dataset with large spatial coverage (e.g. Hilgers 2007, Bateman et al. 2003b, Munyikwa 2005a). In this way, if luminescence ages are repeated in most of the investigated sections, large scale, climatically driven dune building is supported.

For this approach to be successful, a further requirement is systematic, high resolution sampling within the individual dune sections. Only if a relatively high sampling resolution is accomplished, real gaps in a dune record can be identified. If these gaps can then be ascribed to stability phases and hence be associated with wetter climate conditions, cannot be stated with certainty. The possibility remains that gaps merely represent incomplete preservation, as for instance stressed by Telfer and Thomas (2007).

Several recent studies on luminescence chronologies of southern hemisphere dune fields have been realised using this sampling approach and were able to identify periods of enhanced dune sand deposition within the last ~200 ka (Fitzsimmons et al. 2007, Telfer and Thomas 2007, Chase and Thomas 2007, Stone and Thomas 2008). Vertical sampling resolution in these studies ranges from 0.5 to 1 m with 35 to over 80 samples per study.

Interpretation of luminescence chronologies can furthermore be less ambiguous when accompanied by sedimentological or pedological findings. Palaeosols within dunes, for example, provide evidence of former dune stability phases. It therefore is advantageous to

access this information through vertical exposure faces within the dunes. If these do not occur naturally, they can be created by e.g. backhoe trenching, as recently applied by Lomax et al. (2003) and Twidale et al. (2007). Backhoe trenching though is often not possible in remote areas and furthermore very expensive, thus many studies have used augering for sampling the dune fields, which allows only limited information on the stratigraphical context (Hollands et al. 2006, Fitzsimmons et al. 2007, Chase and Thomas 2007, Telfer and Thomas 2007, Stone and Thomas 2008). Nevertheless, palaeosol units have also been successfully identified using augering as method for sampling by Fitzsimmons et al. (2007), or by ground penetrating radar (GPR) measurements (Hollands et al. 2006).

A further concern is lateral migration of linear dunes, resulting in an asymetric distribution of older dune cores within a dune. This was e.g. shown by Bristow et al. (2005, 2007) for large complex linear dunes from the Namib, in which the oldest cores were located at either the eastern or western flank of the dunes. If such dunes are vertically sampled from the crest to the base, older phases of dune sand accretion are possibly missed. This problem can be circumvented by identifying the internal sedimentary structure of a dune with GPR measurements and sampling at several positions within the flanks and the centre of the dune (Bristow et al. 2000, 2005, 2007). However, Bristow et al (2007) demonstrated that GPR measurements in central Australian linear dunes did not allow identification of sedimentary structures due to bioturbation and to high clay and silt contents. For the same reasons, GPR measurements most likely will not be effective in the western Murray Basin dunes and thus were not applied in this study.

When reconstructing palaeoenvironments from dunes, it is further advantageous to choose those dunes for sampling which are least susceptible to reworking, as they likely are able to record multiple phases of environmental change. These could be dunes which contain binding fines or palaeosols, or dunes which are located in desert margin, as suggested by e.g. Bowler (1976).

4.1 Sampling in the western Murray Basin

The western Murray Basin is a typical semi-arid desert margin zone, influenced by extensions and contractions of the arid zone in the course of Quaternary climate change (Bullard and McTainsh 2003) (Fig. 4.1). Stabilised dunes give evidence of former climatic

conditions more favourable to dune formation than today. Thus, the dunes of the western Murray Basin may record multiple phases of dune formation reaching far back in time. Furthermore, especially the linear dunes of the Woorinen Formation in the northwestern Murray Basin contain high proportions of binding fines and carbonate, rendering them quite resistant to aeolian reworking. The Murray Basin dunes are therefore considered as ideal archives for environmental reconstruction.

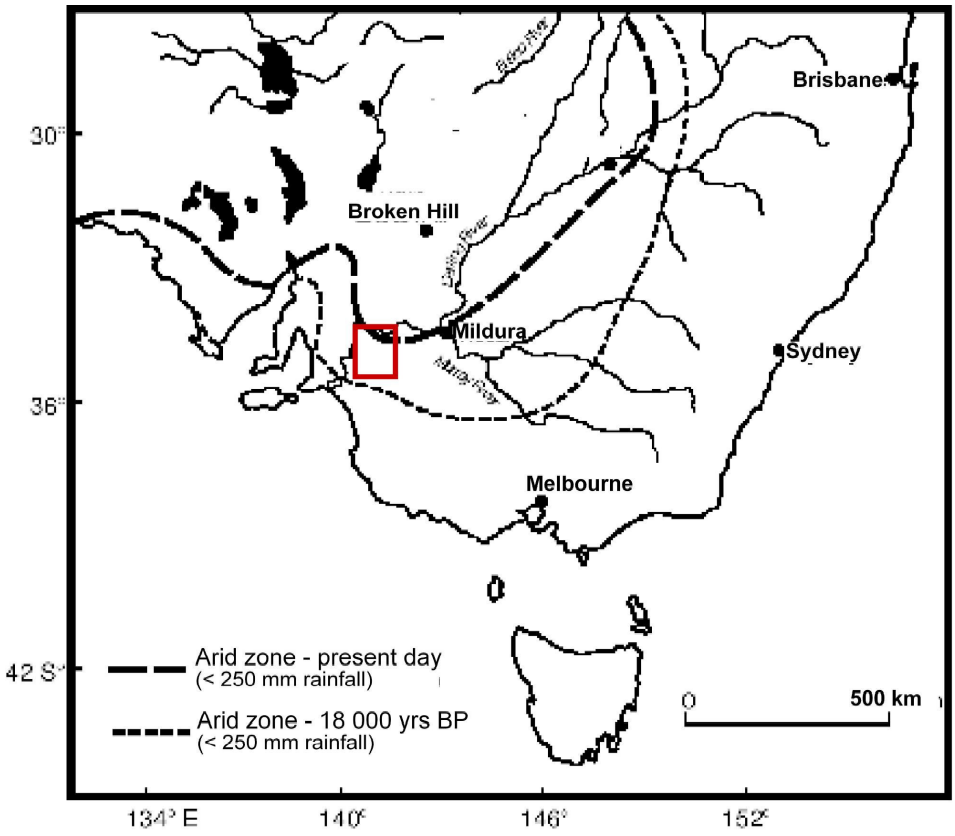

Fig. 4.1. Possible arid zone expansion in the Murray-Darling Basins during the last glacial maximum (from Bullard and McTainsh (2003)). The red square highlights the study area in the western Murray Basin.

Sampling in this study was carried out in order to achieve large spatial coverage and high resolution sampling. In total, 97 samples were taken from 13 sections, with an average sampling resolution of 0.5 m. At all sections, samples for luminescence dating were taken by driving steel tubes into cleaned exposure faces. Material at both ends of the tubes which had been exposed to light during sampling was later rejected in the laboratory. An additional 2 kg of sampling material was taken for radionuclide concentration analysis.

The sampling sites can be subdivided into two study areas within the western Murray Basin. (Fig. 4.2). Study area A is located in the northwestern Murray Basin, where linear dunes prevail. Study area B lies in the southwestern Murray Basin, where sub-parabolic dunes are more common. As outlined in Section 1.1, one of the subordinate objectives of this study is to investigate if both dune fields record aeolian sedimentation phases in the same manner and if these are of the same age. Details of sampling in the two study areas are given in the following section.

Fig. 4.2. Location of study area A and B (draft by U. Beha).

4.1.1 Study area A: linear dune field and Bunyip Sands

Study area A is located in the northwestern Murray Basin and is characterised by linear dunes belonging to the Woorinen Formation. Within this formation, seven individual dune sections were exposed by backhoe trenching. Sampling resolution was on average 0.5 m, though sometimes varied dependent on the stratigraphical context. This resulted in 70 samples from the Woorinen Formation linear dunes. A further section (BM) within study area A is located close to these linear dunes but belongs to the Bunyip Sands formation, small areas of sub-parabolic dunes in lee positions of slip-off slopes of the Murray River. A further five samples were taken from this section with a resolution of 1 m, providing a total

number of 75 samples from study area A. With these eight sections, an area of approximately 1300 km² was covered, comprising a west-east extent of ~65 km and a north-south extent of ~20 km. The locations of the sites in study area A within their geological and geomorphological context are shown in Fig. 4.3.

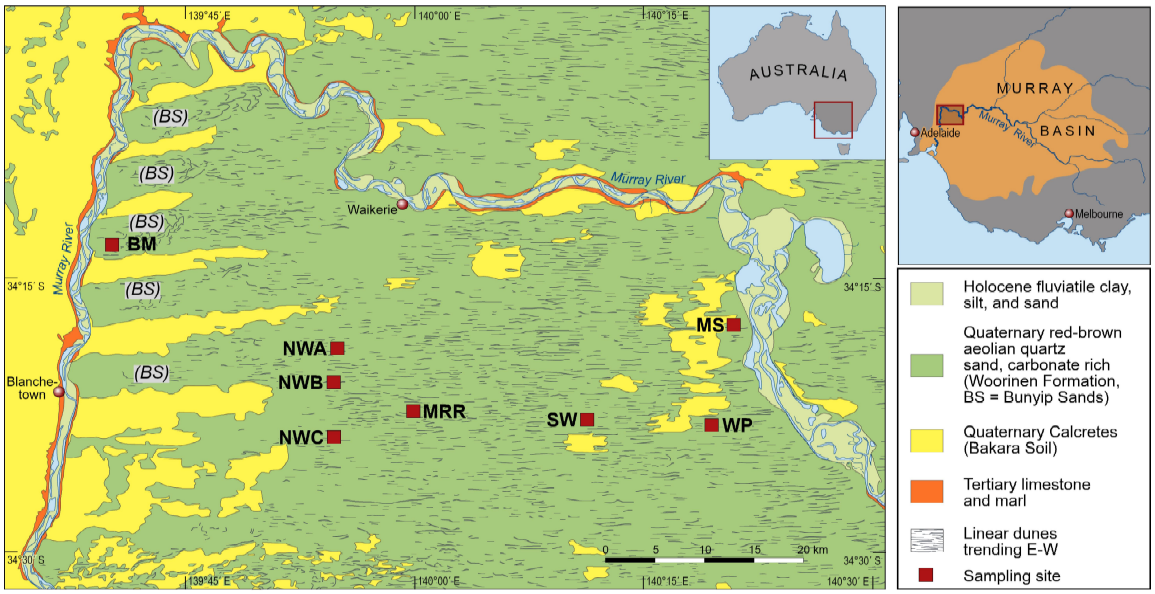

Fig. 4.3. Geology and geomorphology of study area A (Woorinen formation and Bunyip Sands (BS)) and location of the sampling sites (illustration by U. Beha, redrawn from Firman 1971).

The individual sections from the Woorinen Formations were chosen to cover a downwind west-east trending transect with a length of 40 km. Sections NWA, NWB and NWC additionally cover a north-south trending transect of ~10 km length. These three sections are located downwind of calcretes which are devoid of dunes. Pre-existing road cuttings were used to facilitate exposing a clean vertical face at most of the sites. These road cuttings traversed the dunes orthogonally at all but one site, so that exposures were produced from the approximate position of the dune's crest downwards (Fig. 4.4), either facing west or east. No roadcut existed at section NWB, therefore a trench was cut into the dune from the southern dune flank, with the exposure facing to the north. At this site, the dune crest was not exposed.

Fig. 4.4. Sampling in the linear dune field through backhoe trenching. Upper parts of the dune are already exposed through the roadcut.

In none of the sections the base of the dunes could be reached. In Fig. 4.5, the location of the sections is shown on an elevation diagram. The dashed lines mark the extent of Lake Bungunnia, as reconstructed by Bowler et al. (2006). Four of the sections are located within the Blanchetown Basin, three within the Loxton Basin, and lie in the former area of Lake Bungunnia. The base of the sections therefore is likely to consist of Lake Bungunnia lacustrine sediments (either Bungunnia Limestone or Blanchetown Clay) of Early Pleistocene age (Zhisheng et al. 1986). Bungunnia Limestone, from which Bakara Calcretes have developed as surface soils, is much more common in the Blanchetown Basin (Bowler et al. 2006). In the sections near the Murray River, Lake Bungunnia sediments were possibly eroded through post-Lake Bungunnia fluvial activity. Twidale et al. (2007) describe a dune section, also located close to the Murray River within the former Lake Bungunnia area (section MRQ at 34°12.71'S, 140°01.25'E, page 45 ff), where Tertiary Sandstone forms the base of the dune. Section MRR is located on a tectonically controlled high associated with the Hamley Fault, which separates the Blanchetown and the Loxton Basin. According to Bowler et al. (2006), the Woorinen Formation dunes at this location are underlain by Murray Group Limestone, fluviatile Loxton Sands, marine Parilla Sands, or the estuarine Northwest Bend Formation, all of Middle to Late Tertiary age.

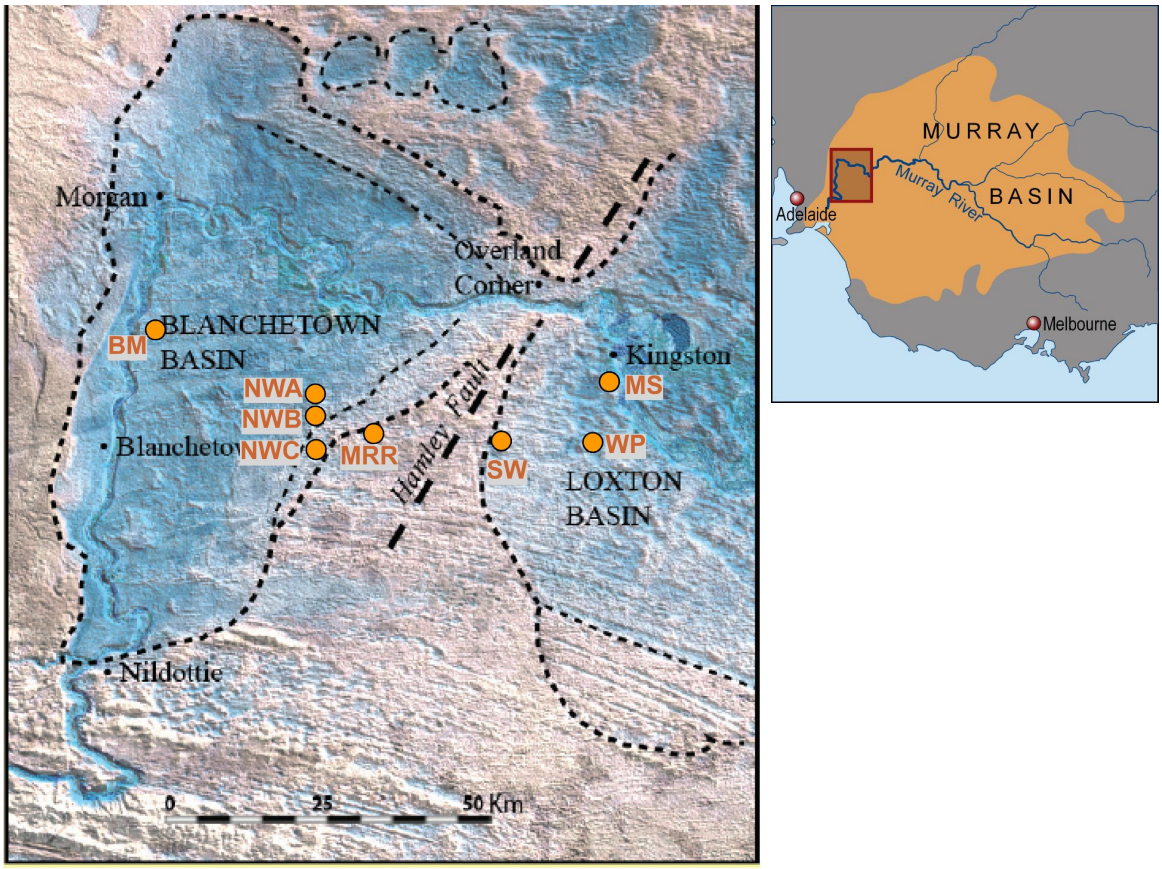

Fig. 4.5. Satellite-elevation composite diagram of Murray gorge to Hamley Fault near Kingston and location of the sampling sites of study area A. In the south, stranded beach ridges of the Loxton-Parilla Sands can be seen, continuing north along the topographic high of the Hamley Fault. Blue colours mark areas below the 60 m contour, and the extent of the palaeolake Bungunnia. Former shorelines of Lake Bungunnia are marked with dashed lines (from Bowler et al. 2006).

The internal stratigraphy of the dunes was clearly visible because vertical sections in the dunes were exposed backhoe trenching. Dune sands themselves appeared quite homogeneous with respect to colour and grain size. No bedding structures, except for some dune flank surface layers, were observed, possibly due to intensive bioturbation. Calcretes and carbonate-rich layers were clearly visible in all of the dunes, occurring at different depths below the surface. Of these, hardpan calcretes and powdery calcretes were the most common features. No palaeosol units could be clearly identified (for instance by colour changes), but the present surfaces also only show weak soil development. It is thus possible that stable phases like the present one will not be recorded in the dunes as clearly visible palaeosol units. However, the calcretes can possibly be regarded as relics of soil formation (e.g. Goudie 1983, Schaetzl and Anderson 2005). In two of the sections, MS and WP, thin

layers with abundant charcoal particles were present in the uppermost parts of the sequences. Photographs of selected sections from study area A are shown in Fig. 4.6, 4.7. and 4.8 and a summarising list of sections is given in Tab. 4.1.

Tab. 4.1. List of sections and number of samples taken in study area A.

Section	Depth of exposure (m)	Sample amount	Location	Dune type and geological formation	Latitude/Longitude
NWA (New Well Road A)	4.55	10	Blanchetown Basin, Lake Bungunnia area	Linear dune, Woorinen Formation	34°18'49''S/139°54'46''E
NWB (New Well Road B)	6.50	13	Blanchetown Basin, Lake Bungunnia area	Linear dune, Woorinen Formation	34°20'42''S/139°55'00''E
NWC (New Well Road C)	4.20	7	Blanchetown Basin, Lake Bungunnia area	Linear dune, Woorinen Formation	34°23'38''S/139°55'03''E
SW (Salt Well)	4.10	9	Loxton Basin, Lake Bungunnia area	Linear dune, Woorinen Formation	34°22'43''S/140°11'12''E
MRR (Maggea Rd. site)	4.20	8	Hamley Fault, outside Lake Bungunnia	Linear dune, Woorinen Formation	34°21'46''S/140°00'10''E
MS (Moorook South)	7.55	10	Loxton Basin, Lake Bungunnia area	Linear dune, Woorinen Formation	34°17'36''S/140°20'57''E
WP (Wappilka)	6.10	13	Loxton Basin, Lake Bungunnia area	Linear dune, Woorinen Formation	34°23'18''S/140°19'03''E
BM (Blanchetown-Morgan-Rd)	6.00	5	Blanchetown Basin, Lake Bungunnia area	Sub-parabolic dune, Bunyip Sands	34°13'36''S/139°39'21''E

Fig. 4.6. Sampling exposure of the MS section (Photograph by A. Hilgers, 2004).

Fig. 4.7. Sampling exposure of section SW section (Photograph by A. Hilgers, 2004).

Fig. 4.8. Sampling exposure of the NWC section (Photograph by A. Hilgers, 2004).

4.1.2 Study area B: sub-parabolic dune field

In study area B, sub-parabolic dunes from the Big Desert Molineaux Sands are the most common features, although at the northern margin linear dunes prevail (Fig. 4.9). Five sections were investigated; four from sub-parabolic dunes and one from a linear dune (section PSP). At the PSP site, a deep section was exposed through backhoe trenching. 14 samples were taken from this site. In the sub-parabolic dune field, backhoe trenching was not feasible, thus only small exposures were produced by hand digging. From the four sub-parabolic dune sections, 14 samples were taken. Sampling resolution averaged 0.5 to 1 m, totalling 28 samples from study area B. The study area has a west-to-east extent of 55 km and a south-to-north extent of 30 km at its eastern margin, thus covers around 1600 km². The base was not exposed in any of the sections, but Late Tertiary littoral Loxton-Parilla Sands are assumed to underlie the dunes (Bowler et al. 2006). Fig. 4.9 shows the sampling sections in their geological context.

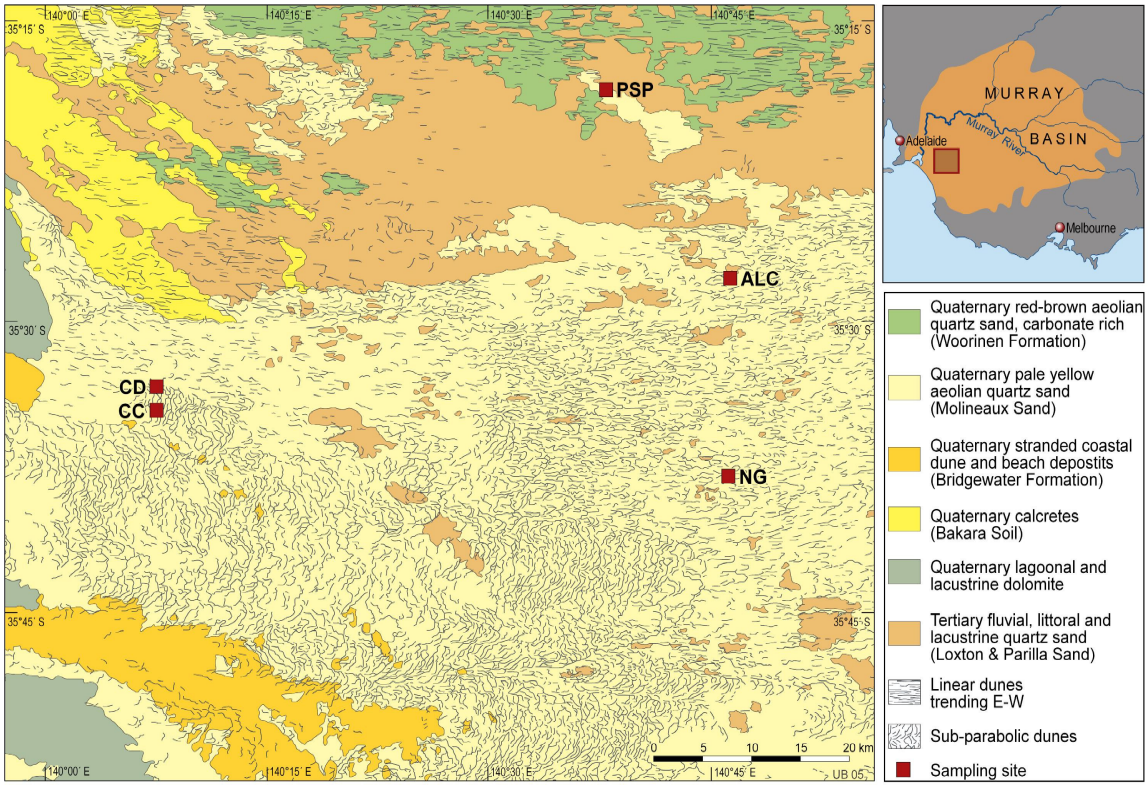

Fig. 4.9. Geology and geomorphology of study area B (Molineaux Sands) and location of sampling sites (illustration by U. Beha, redrawn from Firman 1971).

Internal stratigraphy varied from section to section. Sections CC and NG, for instance, were characterised by very homogeneous quartz sands and lack of fines and carbonates (Fig. 4.11 and 4.12). Some horizontal bedding structures were visible in the dune of section CC. Section CD, in the near vicinity of section CC also contained mainly quartz sands, but additionally several lamellae enriched with finer (and darker) material (Fig. 4.13). Mottled bleaching zones were observed in section CD and NG, possibly due to iron migration during winter waterlogging phases (Fig. 4.10). Section PSP and ALC contained significant amounts of carbonates. Only poorly developed present soil formation was observed in all sections. A list of the investigated sections is given in Tab. 4.2.

Tab. 4.2. List of sections and number of samples taken in study area B.

Section	Depth of floor (m)	Sample amount	Location	Dune type and geological formation	Latitude/Longitude
PSP (Parilla Sand Pit)	6.50	14	on Loxton-Parilla Sands	Linear dune, Woorinen Formation	35°17’57’’S/140°38’38’’E
CC (Carcuma)	3.95	4	Big Desert. on Loxton-Parilla Sands	Sub-parabolic dune, Molineaux Sands	35°34’18’’S/140°08’02’’E
CD (Carcuma Downs)	2.20	4	Big Desert. on Loxton-Parilla Sands	Sub-parabolic dune, Molineaux Sands	35°32’51’’S/140°07’57’’E
ALC (Alcharinga)	2.40	3	Big Desert. on Loxton-Parilla Sands	Sub-parabolic dune, Molineaux Sands	35°26’33’’S/140°47’20’’E
NG (Ngarkat Park)	2.70	3	Big Desert. on Loxton-Parilla Sands	Sub-parabolic dune, Molineaux Sands	35°37’09’’S/140°07’57’’E

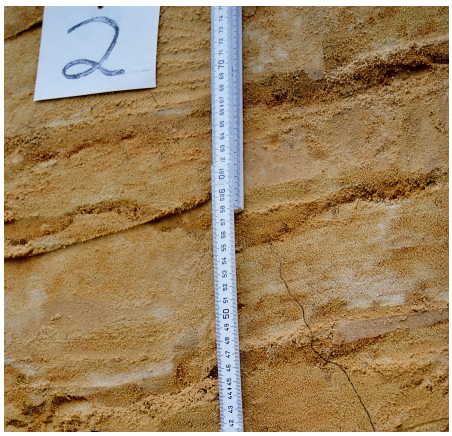

Fig. 4.10. Mottled bleaching zones in section CD. (Photograph by A. Hilgers, 2004)

Fig. 4.11. Sampling exposure of the CC section (Photograph by A. Hilgers, 2004).

Fig. 4.12. Sampling exposure of the NG section (Photograph by A. Hilgers, 2004).

Fig. 4.13. Sampling exposure of the CD section (Photograph by A. Hilgers, 2004).

5. OSL dating of sediments

5.1 Basic principle of OSL dating of sediments

Luminescence dating belongs to the group of radiation dosimetric dating methods. This group of methods makes use of the fact that certain minerals such as quartz and feldspar are able to store energy induced by ionising radiation. The necessary energy for ionisation is derived from the decay of radioactive elements such as uranium, thorium and potassium, which are omnipresent in sediments, and from cosmic radiation. The storage of energy occurs as redistribution of electrons in the crystal lattice of minerals from lower to higher energy levels, and only proceeds when the minerals are shielded from light (e.g. burial by further sediment layers). Exposure to light, for example during transport and deposition of sediments, partially releases the stored energy by of photon emission, giving rise to the phenomenon of luminescence. The intensity of the light emission, also referred to as luminescence signal, is proportional to the amount of stored energy. Thus, when the signal is monitored under laboratory conditions, it can be used as a measure of time elapsed since the last deposition of the sediment (Fig. 5.1).

For the determination of depositional ages, two parameters have to be quantified. One is the amount of stored energy per mass of mineral (1 $J*kg^{-1}$ = 1 Gy (Gray)), also referred to as palaeodose; that is, the dose of radiation received since the last exposure to sunlight. The other parameter is the rate of radiation flux interacting with the minerals used for dating, termed dose rate (Gy/ka). Calculation of the depositional age then follows the equation (5.1):

$$\text{Age (ka)} = \text{Palaeodose (Gy)} / \text{Dose rate (Gy/ka)} \qquad \text{(Eq. 5.1)}$$

However, an important complicating factor with respect to the palaeodose determination is that every single mineral grain exhibits different luminescence sensitivities in response to the natural radiation. This is even the case if mineral grains are of the same age and exposed to the same dose rate. Thus the amount of photons as a measure of the accumulated dose cannot be transferred to the palaeodose directly. Therefore, every sample needs to be exposed to known laboratory doses to assess its sensitivity to radiation. The estimate of the palaeodose determined through laboratory procedures is termed the

equivalent dose (De). The De is defined as '*the laboratory dose of nuclear radiation needed to induce luminescence equal to that acquired subsequent to the most recent bleaching event*' (Aitken 1998: 33). In the following, the term 'palaeodose' will be used when referring to the dose accumulated in nature, and the term 'equivalent dose' when referring to the estimate of the palaeodose determined in the laboratory.

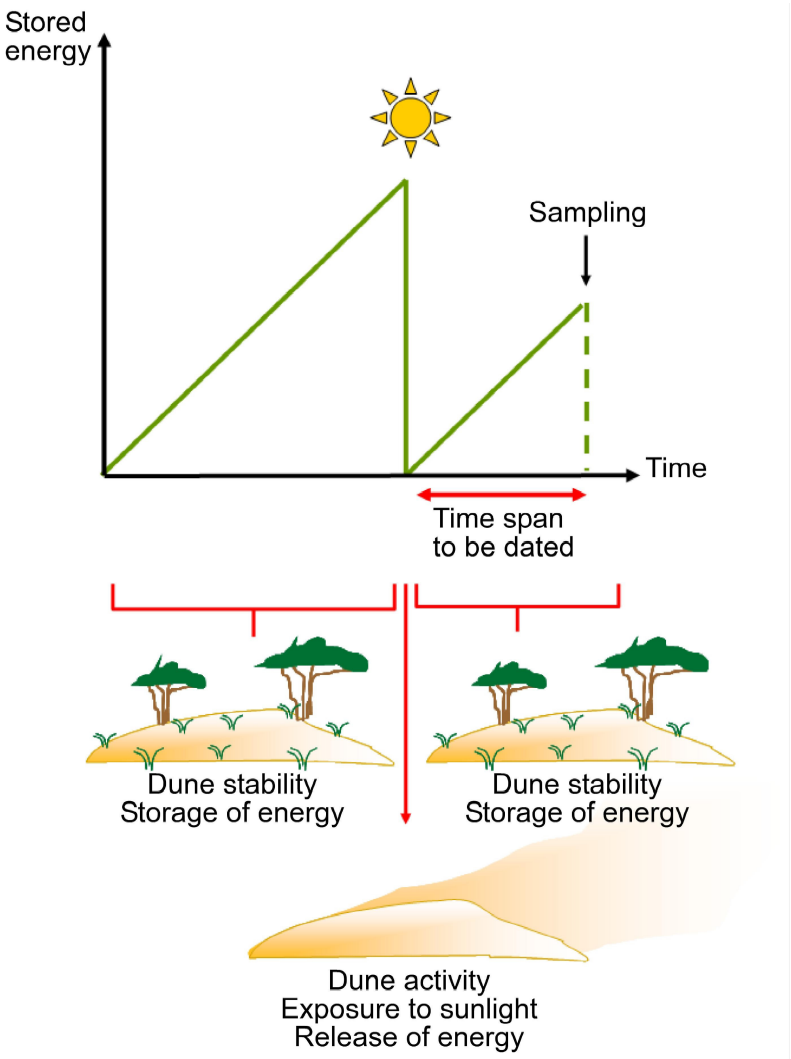

Fig. 5.1. The principle of optically stimulated luminescence (OSL) illustrated using dunes as sedimentary archive. When the dune is stabilised by vegetation and minerals such as quartz and feldspar grains are shielded from light, they store energy and build up a luminescence signal. During reactivation of the dune, the minerals to be dated are exposed to sunlight, which reduces the luminescence signal to near zero. In the following dune stability phase, the luminescence signal builds up again. When a sample of the dune sand is obtained, the luminescence signal can be detected in the laboratory, serving as measure of the time elapsed since the last exposure of the minerals to light (illustration by A. Hilgers).

5.2 Minerals used for dating

Several minerals can be used for luminescence dating. The most common minerals in this respect are feldspar and quartz, but also more exotic minerals as e.g. zircon show luminescence properties theoretically suitable for dating (Krbetschek et al. 1997).

The choice of whether to use quartz or feldspar in sediment dating is dependent on various factors, of which some are summarised in the following. One aspect is mineral abundance in sediments. Quartz is much more resistant to chemical weathering than feldspar, thus in a lot of sediments, which have undergone long periods of chemical weathering or multiple sedimentation cycles, feldspars may be scarce. One of the major disadvantages of luminescence dating of feldspars is a phenomenon called 'anomalous fading', referring to a loss of electrons from thermally stable traps at ambient temperatures which can lead to severe underestimations if not corrected for (e.g. Wintle 1973, Spooner 1992, 1994a, Lamothe et al. 2003, Auclair et al. 2003). Another advantage of quartz over feldspar is its slightly better bleachability. Sunlight bleaching experiments conducted by Godfrey-Smith et al. (1988) showed that the quartz signal is reduced to ~1 % of the initial signal after 10 s whereas for feldspars it took ~9 min to reduce the initial signal to an equal level (Fig. 5.2).

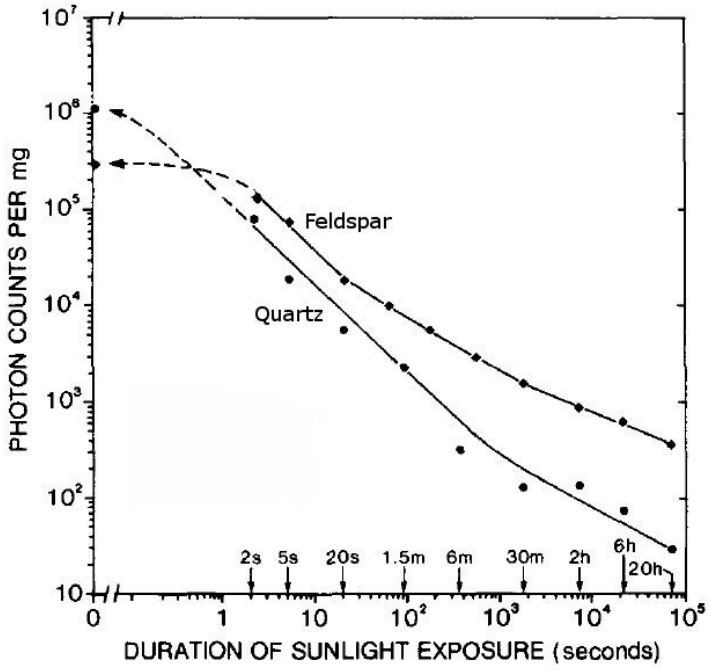

Fig. 5.2. The effect of sunlight exposure on the optical signal of a sedimentary quartz and feldspar sample. The unbleached values are shown along the vertical axis. Luminescence measurements were carried out using a 514 nm laser for stimulation (modified after Godfrey-Smith et al. 1988).

These reasons make quartz the preferable mineral for luminescence dating. There are, however, some advantages of feldspars over quartz, which in some cases can outweigh its disadvantages. These are first a higher saturation level in feldspar compared to quartz, thus dating feldspars might be preferred for old samples. The same is the case for samples containing quartz with very low luminescence sensitivity. Usually feldspars exhibit much higher luminescence intensity than quartz, thus are more suitable in some sedimentary samples. Low quartz sensitivities have been especially reported from samples from mountainous regions, a fact which has been ascribed to the young sedimentary history of the quartz grains (e.g. Duller 2006, Klasen et al. 2006, Preusser et al. 2006, Bøe et al. 2007, Lukas et al. 2007). However, the latter reason is not relevant for a lot of sediments from desert environments. These samples often exhibit high luminescence sensitivity of quartz grains due to the multiple sedimentation cycles sands in deserts have undergone (Pietsch et al. 2008). Thus, due to the many advantages quartz has over feldspar in respect to luminescence dating, in this study dating is carried out solely by using quartz as luminescence dosimeter. In the following, descriptions of the mechanism of luminescence and its relevance for dating are outlined for quartz, if not stated otherwise.

5.3 Physical background of quartz luminescence

5.3.1 The energy level model

The mechanism of luminescence is most frequently explained by the energy level model. Most minerals, such as quartz, are insulators; that is, in their crystal lattice, an energy band structure exists in which the valence band and the conduction band are separated by a "forbidden" energy gap. Usually electrons can diffuse in the valence band, and when ionised through radiation, can be transferred to the conduction band, but cannot remain in the forbidden energy gap. As every naturally grown mineral possesses defects in its crystal structure (e.g. through substitution of elements), localised energy levels within the forbidden gap are created (Wagner 1995). A very common defect in quartz for example is the substitution of a Si^{4+}-ion by an Al^{3+}-ion due to their very similar ionic radii and the high abundance of aluminium in the Earth's crust (Fig. 5.3(a)). This type of substitution provides a positive charge deficit in the crystal lattice. The crystal defects act as traps for

electrons and holes (the remnant feature of an ionised electron) being transferred between the valence and the conduction band when exposed to ionising radiation. As electrons are negatively charged and holes are positively charged, electrons require a defect with a negative charge deficit and holes a defect with a positive charge deficit to become trapped (Fig. 5.3(b)). Usually traps containing holes are located near to the valence band, while electron traps reside near the conduction band (Krbetschek et al. 1997). To release electrons from these traps, additional energy has to be introduced either through heat or light. The energy needed for eviction of electrons is dependent on the depth of the trap below the conduction band, usually given in the unit of electron Volt (eV). Traps just below the conduction band are referred to as shallow traps and require less energy for electron eviction than deep traps which are located in greater distance to the conduction band. Due to this relationship only deeper traps can store electrons for longer times and only these traps can be used for dating. According to Aitken (1998) a trap depth of at least 1.6 eV is necessary to be used by luminescence dating techniques, ensuring a residence time of electrons over several millions of years in these traps.

When electrons are released from the traps they can either be recaptured in other traps, be transferred to the valence band (via the conduction band), resulting in release of energy in form of heat, or they can recombine with trapped holes (Aitken 1998). The latter process results in the emission of photons and is referred to as luminescence (Fig. 5.3(c)).

In nature, eviction of electrons occurs every time a mineral is exposed to heat or light. When all electrons are released from traps used for dating, the mineral grain is ‘fully bleached’ or zeroed.

In the laboratory, eviction of electrons from traps and recombination is forced by exposure to artificial light (e.g. using lasers or light emitting diodes of defined wave lengths) or heat. This process is called stimulation. When light is used as stimulating agent to produce luminescence, the technique is called optically stimulated luminescence (OSL). When heat is used, the technique is termed thermoluminescence (TL), which enables dating of ceramics, volcanic materials or slags.

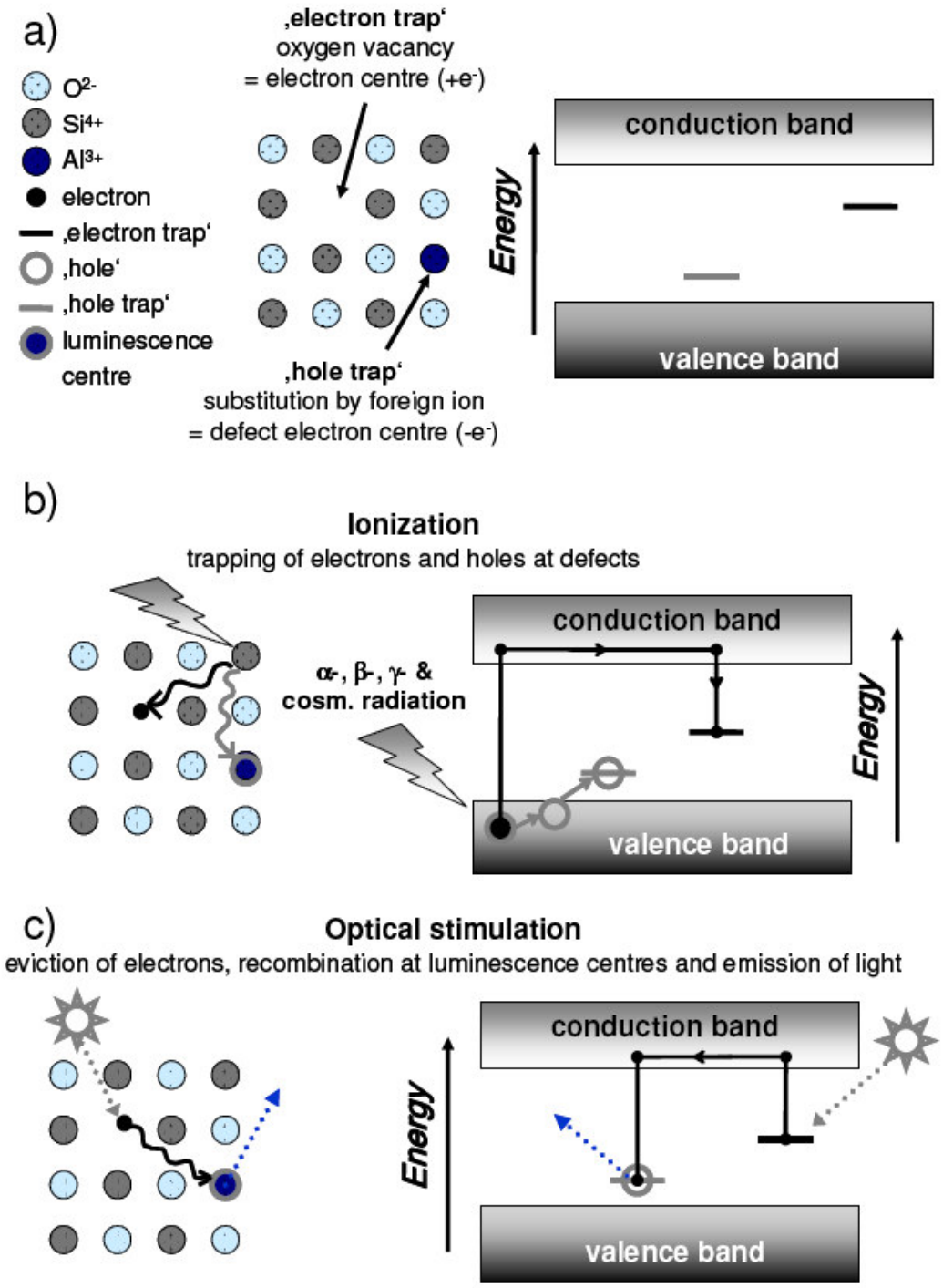

Fig. 5.3. The production of optically stimulated luminescence explained by the energy band model. (a) Structure of a naturally grown quartz crystal with negative and positive charge deficits due to atomic defects, (b) ionisation of electrons and holes through ionising radiation, and trapping of electrons and holes in defect centres, (c) the release of electrons from traps through optical stimulation and recombination at a luminescence centre, resulting in release of energy as photon emission. This light emission is referred to as optically stimulated luminescence (from Hilgers 2007).

5.3.2 Trap characteristics in luminescence dating

Thermoluminescence has not only been used for dating, but is also an important tool to derive information on the lifetime and thermal stability of electron traps in minerals. Usually when stimulating with heat, the temperature is ramped from zero to about 500°C. At lower temperatures shallow traps are emptied and followed by eviction of electrons from deeper traps. A typical TL-glow curve, displaying the stimulation temperature on the x-axis, and the luminescence signal intensity on the y-axis, shows distinctive intensity peaks at certain temperatures, indicating that traps are concentrated on discrete energy levels. Typical TL traps in quartz are located at 110°C, 150-180°C, 200-220°C, 325°C and 375°C (Fleming 1970, Wintle 1997, Wintle and Murray 1997). Traps with thermal stability of less than around 300°C are considered as thermally unstable, and deeper traps as thermally stable (Aitken 1998). The shallow and thermally unstable traps do not remain filled over geological time scales (Wintle 1997). For instance, the mean lifetime of the 110°C trap only is around 7 h at a temperature of 15°C (Aitken 1985). When artificially irradiated though, these traps are filled (Wintle 1997, Wintle and Murray 1997, 1998). This explains the need for preheat procedures (further discussed in Section 6.1.3) to overcome these differences in naturally and artificially dosed samples. The different trap types not only show differences in thermal stability, but also in bleachability. The 325°C traps bleach very rapidly when stimulated with visible light (Spooner et al. 1988). Therefore, the 325°C TL peak is often referred to as 'rapidly bleaching peak (RBP), whereas the 375°C TL peak is often termed the 'slowly bleaching peak' (Franklin and Hornyak 1990). The latter TL peak requires wavelength <400 nm (UV) for bleaching (Spooner et al. 1988).

Several studies have shown that traps associated with the 325°C TL peak are the main source from which electrons are evicted when optically stimulated (e.g. Smith et al. 1986, Spooner et al. 1988, Spooner 1994b, Scholefield et al. 1994, Smith and Rhodes 1994, Wintle and Murray 1997, Spooner and Questiaux 2000). This trap has a mean lifetime of >17 Ma at room temperature (Murray and Wintle 1999, Spooner and Questiaux 2000), thus theoretically is sufficiently stable to date Quaternary sediments up to an age of 1 Ma (Bøtter-Jensen et al. 2003a)

To avoid complex and unquantifiable interaction of luminescence signals from different trap types when determining the equivalent dose, the 325°C trap has to be isolated. As

mentioned above, charge in shallow traps is removed by preheat procedures before measurement of the luminescence signal. The 375°C TL trap also does not contribute to the luminescence signal when stimulated under laboratory conditions. This is because blue or green light is usually used for stimulation of quartz, which is not energetic enough to release charge from these traps (Spooner et al. 1988).

5.4 History and recent developments in luminescence dating

The use of the phenomenon of luminescence as a dating technique was first suggested by Daniels et al. (1953). In subsequent years, it was used as a tool to date ceramics using TL (Aitken et al. 1964, 1968, Fleming 1966, Zimmerman 1967, Mejdahl 1969). In the late 1970s and early 1980s, TL was used for the first time to date sediments (Wintle and Huntley 1979, 1980). OSL dating using light instead of heat as stimulation energy was first proposed and applied by Huntley et al. (1985). For quartz and feldspar grains, whose palaeodose has been reset by light during transport and deposition, this is the more logical approach, as the same luminescence traps are involved in nature and in laboratory measurements. It was also shown by Huntley et al. (1985) and later confirmed by Godfrey-Smith et al. (1988) that the OSL signal is more readily bleachable than the TL signal. The stimulation source used by Huntley et al. (1985) was a green argon-ion laser (514.5 nm). In 1988, Hütt et al. showed that stimulation can also be undertaken in the IR range (known as IRSL dating) when using feldspars as dosimeters. The advantage of OSL over TL in respect to signal bleachability led to wide range of applications in sediment dating. Reviews of OSL applications to sediments can be found in Prescott and Robertson (1997), Murray and Olley (2002), Lian and Roberts (2006), Preusser et al. (2008) and in Boreas, Volume 37, Issue 4 (2008). Nowadays, except for in single grain dating, light emitting diodes (LEDs) have replaced lasers as optical stimulation source (Bøtter-Jensen et al. 1999a, 1999b, 2000). The use of single aliquot protocols, initially tested on feldspars by Duller (1991, 1994a, 1995), resulted in a great increase of precision of luminescence ages (Duller 2004). The breakthrough of the single aliquot approach occurred in the year 2000, when Murray and Wintle presented a single aliquot regenerative-dose (SAR) protocol which successfully corrected for sensitivity changes involved with this technique. Murray and Wintle (2000) used the SAR protocol to date quartz, but it was soon adapted for dating feldspars

(Wallinga et al. 2000). Accuracy of luminescence ages based on SAR protocols was confirmed by numerous studies through comparison with independent age control (for a review, see Murray and Olley 2002). Today the SAR protocol forms the base for most of different luminescence dating methods, as e.g. radiofluorescence dating (Erfurt and Krbetschek 2003), red thermoluminescence dating (Fattahi and Stokes 2000), isothermal thermoluminescence dating (Choi et al. 2006c), and thermally transferred OSL dating (Wang et al. 2006). Further adjustments to the protocol are summarised in Murray and Wintle (2003).

A relatively recent development in luminescence dating is the estimation of the palaeodose using single grains, firstly applied by Lamothe et al. (1994) using feldspars and Murray and Roberts (1997) using quartz grains. Initially used to investigate luminescence properties of individual grains of quartz or feldspars, single grain dating has now become an important tool in determining the depositional age of sediments (e.g. Feathers 2003, Jacobs et al. 2003a, Olley et al. 2004a, 2004b, 2006, Duller 2006, Bøe et al. 2007). For a recent review on single grain dating, see Duller (2008). Further recent advances concentrate on improvements in instrumentation (e.g. Ballarini et al. 2005, Thomsen et al. 2006, 2008) and on extending the age range in quartz luminescence dating (e.g. Fattahi and Stokes 2000, Singarayer et al. 2000, Choi et al. 2006c, Wang et al. 2006). For reviews of recent advances in luminescence dating see Bøtter-Jensen et al. (2003a), Duller (2004) and Lian and Roberts (2006).

5.5 OSL properties of quartz

5.5.1 Stimulation and detection of the OSL signal

In luminescence measurements it is desirable to maximise the efficiency of luminescence production in order to increase the initial signal intensity. One reason for this is to enhance the signal to background noise ratio, which improves the precision of signal detection due to counting statistics. Another, more practical reason, is to efficiently zero the measured sample as quickly as possible to reduce measurement time. It has been shown that the initial luminescence signal intensity and signal bleachability in quartz samples is inversely proportional to stimulation wavelength with a broadly exponential relation (Spooner et al. 1988, Spooner 1994b, Bøtter-Jensen et al. 1994, Duller and Bøtter-Jensen 1996) (Fig. 5.4,

note the logarithmic vertical axis) This relates to the fact that the shorter the wavelength of the stimulation light, the higher the energy and thus the higher the detrapping probability. Nevertheless, it has been shown by Duller and Bøtter-Jensen (1996) that when using stimulation wavelength from 425 to 575 nm, the same charge transport processes occur and the same electron traps seem to be involved in the production of luminescence, regardless of the wavelength dependency of the luminescence production rate.

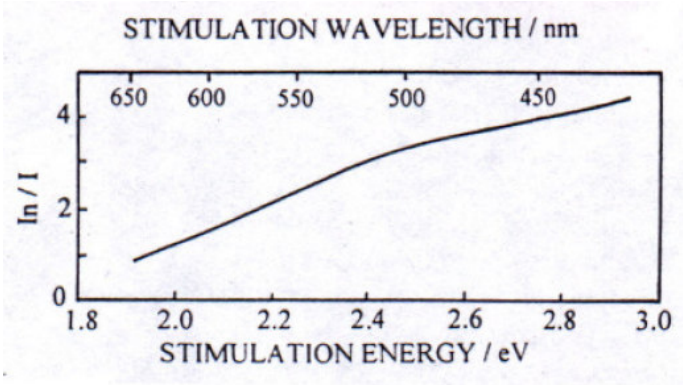

Fig. 5.4. Relationship of the stimulation wavelength, the stimulation energy and the OSL intensity (ln/I) of quartz. Note the logarithmic scale of the vertical axis (from Bøtter-Jensen et al. 1994).

Another consideration regarding the stimulation wavelength is the luminescence emission spectrum of quartz. When optically stimulated at room temperature, quartz exhibits a single peak emission centred at around 365 nm (Huntley et al. 1991) (Fig. 5.5).

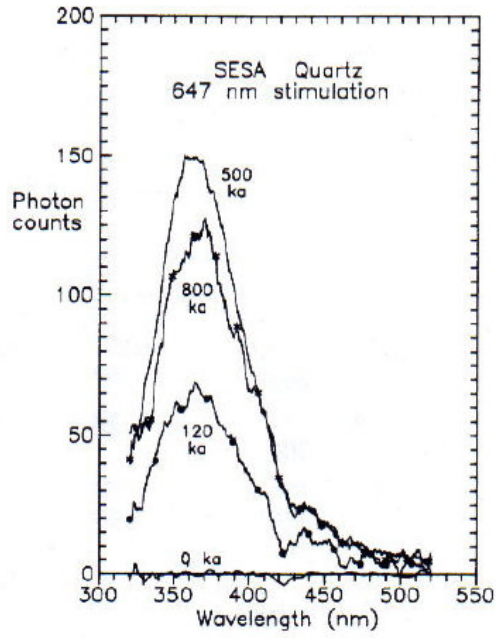

Fig. 5.5. The OSL emission spectrum of an Australian sedimentary quartz sample. Optical stimulation was carried out using a 647 nm laser (from Huntley et al. 1991).

In conventional OSL dating, stimulation and

detection of the luminescence signal are conducted simultaneously. As a consequence the stimulation light and the resulting luminescence cannot be in the same wavelength range and have to be well separated from each other. Stimulation is therefore usually carried out using blue or green light. In multiple grain dating, the most common stimulation sources nowadays are blue LEDs delivering light with wavelengths of 470 ± 30 nm (Bøtter-Jensen et al. 1999a, 1999b). In case of single grain measurements, stimulation usually is carried out using a laser with a wavelength of 532 nm (Duller et al. 1999, Bøtter-Jensen et al. 2000, 2003b).

To prevent stimulation light reaching the photomultiplier tube (see Section 6.2) and interfering with the luminescence signal, optical filters need to be placed between the sample and the photomultiplier tube. In quartz dating, both multiple grain and single grain, a Hoya U340 filter is most widely used. This filter allows peak transmission at around 340 nm and restricts transmitted wavelengths to a range between around 270 and 390 nm. In case of stimulation with blue LEDs, the tail towards the shorter wavelength reaches into the transmission band of the U340 filter. To prevent this, a cut-off filter (GG420) is additionally attached in front of the blue LED which efficiently blocks transmission of light with wavelength shorter than 410 nm from the LED (Bøtter-Jensen et al. 1999b). Fig.5.6 shows transmission and stimulation spectra for the U340 filter and the different stimulation sources. Further, the luminescence emission spectra of a natural quartz sample, stimulated at room temperature are displayed. From Fig. 5.6 it becomes evident that the U340 filter is not centred on the peak quartz emission. In case of stimulation with blue LEDs, this is unavoidable, since otherwise the detection and stimulation window would lie too close to each other. In case of the green laser stimulation though, a shift of filter transmission towards the peak luminescence emission band of quartz would be applicable and improves the light detection efficiency, but is not routinely applied in single grain OSL dating (Ballarini et al. 2005).

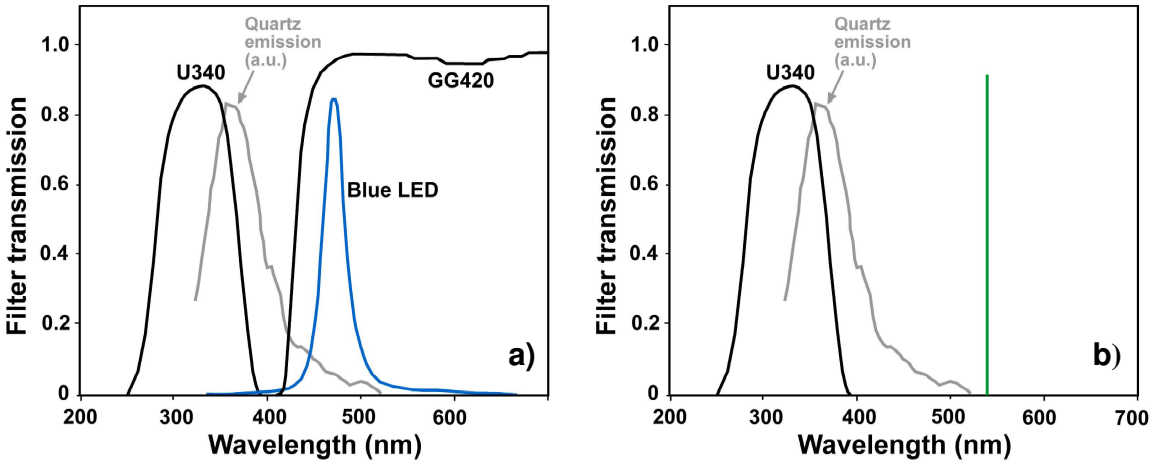

Fig. 5.6. Transmission of an U340 and a GG420 cut-off filter, the luminescence spectrum of quartz after optical laser stimulation (after Huntley et al. 1991) and (a) the emission spectrum of a blue LED (470 ± 30 nm) and (b) the emission line of a 531 nm green laser (modified from Bøtter-Jensen et al. 1999b).

The detrapping probability can further be enhanced by increasing the power of the stimulation source, and by stimulating at elevated temperatures. The latter effect is termed thermal assistance and is thought to be caused by increased vibrations of the quartz crystal lattice at elevated temperatures (Spooner 1994b, Bailey et al. 1997, Aitken 1998). If stimulation temperatures are too high though, a competing process occurs, termed thermal quenching, which is caused by a decrease of the efficiency of luminescence centres (Wintle 1975). The stimulation temperature most widely used is 125°C, which is considered the optimum temperature with respect to detrapping efficiency, thermal quenching and retrapping of electrons in the 110°C TL peak (see Section 5.5.2) (Murray and Wintle 2000).

5.5.2 The OSL decay curve

When stimulating quartz samples with a light source delivering a constant power, the OSL signal will decay with time. A typical quartz luminescence decay curve from an Australian sedimentary quartz sample is shown in Fig. 5.7.

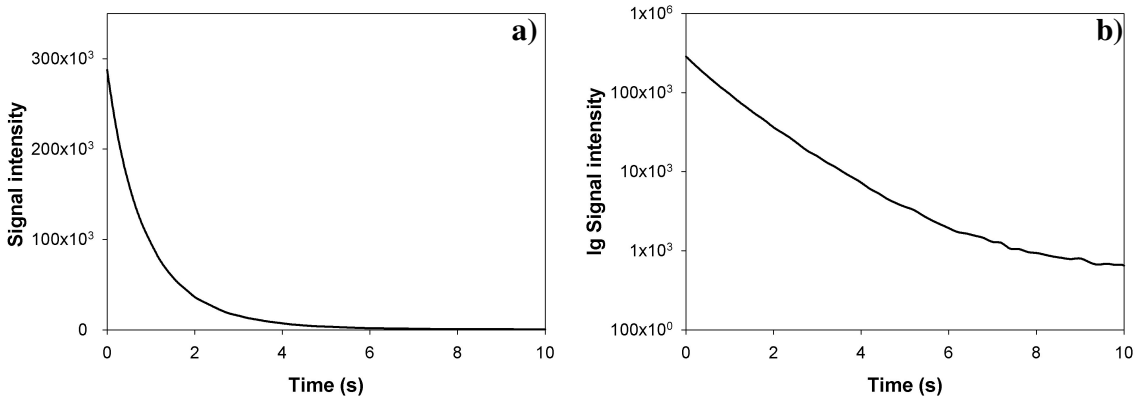

Fig. 5.7. (a) Decay curve from a naturally irradiated Australian sedimentary quartz sample stimulated using a blue LED (470 nm) at 125°C and (b) the same curve plotted using a logarithmic scale for the vertical axis.

The reason for the decrease in luminescence intensity with time is that less and less trapped electrons and recombination centres are available for the production of luminescence. If only one electron trap type was present in the quartz sample and the number of recombination centres was not limited, then one would expect an exponential decay of the luminescence intensity with time. This however is not the case, as already noticed by Huntley et al. (1985) and later confirmed by Smith and Rhodes (1994) and Bailey et al. (1997). In fact, the decay exhibits a slower-than-exponential behaviour. One of the reasons for this is retrapping of electrons in the 110° TL traps evicted from OSL traps during optical stimulation. These electrons are evicted later and contribute to the signal with a delay. The problem of retrapping can be avoided by stimulating at elevated temperatures above 100°C (Smith and Rhodes 1994). But even when stimulating at elevated temperatures, the decay curve follows a function slower than an exponential, as can be seen in Fig. 5.6b (if the decay was exponential, then the plot using a logarithmic y-axis scale would display a linear decrease in signal intensity). The reason for this is that more than one OSL trap type contribute to the OSL signal each of which are characterised by different depletion rates (Bailey et al. 1997). Smith and Rhodes (1994) found that the OSL decay curve measured at elevated stimulation temperatures can be approximated by a sum of three exponential signal components. They termed these the fast, medium and slow component according to their bleachability. Further details on the different components contributing to the OSL signal are given in the following section.

5.5.2.1 Components of the OSL signal

More detailed studies on the different OSL signal components were derived from linear modulated OSL, a stimulation method introduced by Bulur (1996). In this technique the stimulation power is ramped linearly from zero to a maximum value. As a consequence, at the beginning of stimulation only traps which are very easy bleachable are emptied by the low power, with the harder-to-bleach traps emptying later. Thus the different OSL components appear as a series of peaks in a LM-OSL curve, and can be resolved mathematically in order to separate the components. A description of how to resolve LM-OSL curves can be found in Choi et al. (2006a). Investigations on quartz luminescence signal components were carried out by e.g. Bulur et al. (2000), Kuhns et al. (2000), Singarayer and Bailey (2003, 2004), Jain et al. (2003) and Choi et al. (2003a, 2003b, 2006b). From these studies it became evident that the signal of a lot of sedimentary quartz samples comprises more than the three components identified by Smith and Rhodes (1994). Singarayer and Bailey (2003), for example, found five components in a sedimentary quartz sample, namely the fast, the medium and three different slow components (S1, S2 and S3) (Fig. 5.8), and Jain et al. (2003) identified seven signal components.

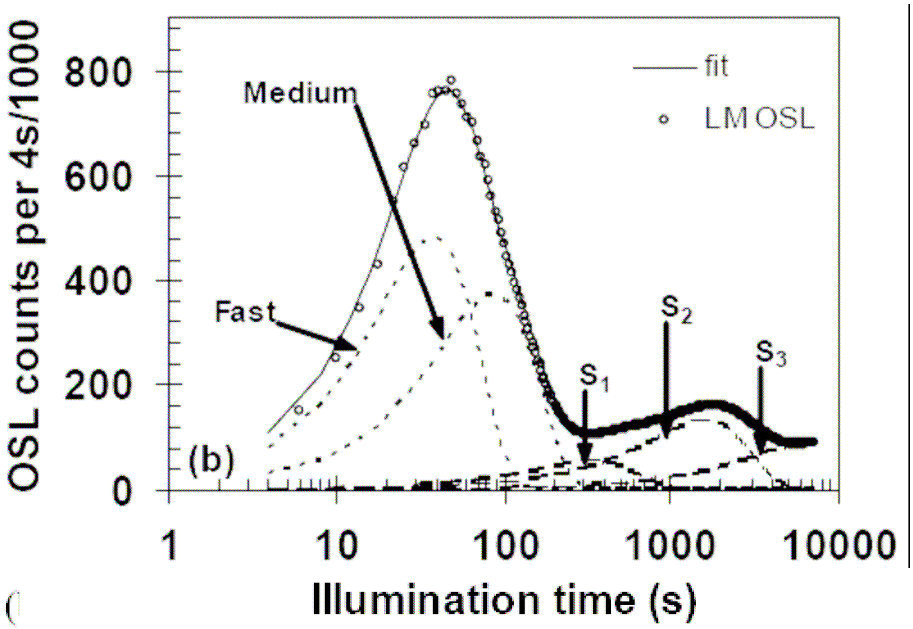

Fig. 5.8. LM-OSL curve from a sedimentary quartz sample (fitted as solid line) which has been separated into five components (fast, medium, and three slow components (S1, S2 and S3) (from Singarayer and Bailey 2003).

However, the number of luminescence signal components is sample dependent, and even varies significantly on a grain-to-grain level within one sample (Bulur et al. 2002). Further investigations using LM-OSL provided information on the saturation, trap depth and mean lifetime of the components. Trap depths of 1.74, 1.80, 2.02, 1.23 eV for the fast, medium, S1 and S2 component were determined by Singarayer and Bailey (2003). They further found that the medium and S1 component exhibit high thermal stability, followed by the fast component with an intermediate thermal stability. The S2 was shown to be thermally unstable by the authors. Lifetimes of the different components were determined by Choi et al. (2006b), confirming the studies on thermal stability from Singarayer and Bailey (2003). Lifetimes reported by Choi et al. (2006b) were 210 Ma for the fast component, 38000 Ma for the medium component, 66000 Ma for the S1 component and 0.006 Ma for the S2 component. Further, the fast, the medium and the S1 component were shown to saturate at the same order of magnitude, whereas the S2 component saturates at significantly lower doses and the S3 component at much higher doses (Singarayer and Bailey 2003). The latter component could thus be potentially used for dating samples beyond the range of conventional (i.e. fast-component-dominated) OSL dating (Singarayer et al. 2000, Rhodes et al. 2006). Due the low optical sensitivity of this component, sediment dating using the slow component might be limited though.

From several studies it has now become evident that samples with a dominant fast component are most suitable for OSL dating. Samples with a lacking fast component cannot be dated accurately using conventional OSL dating (Choi et al. 2003a, 2003b, 2006b, Jain et al. 2003). However, in ‘well behaving’ samples with a dominant fast component it follows from the above mentioned investigations that only the initial part of the signal should be used for dating which is the part of the signal with the maximum contribution of the fast component. For instance, Murray and Wintle (2000) suggest analysing the first 0.3 s of the signal.

A further aspect to consider is that the longer the wavelength used for stimulation, the higher the contribution of the fast component in the initial signal, because the slow components require light with higher energies for luminescence production (Jain et al. 2003, Singarayer and Bailey 2004). For example, Thomas et al. (2005) suggest that differences in equivalent doses estimated using single grain and multiple grain aliquots were caused by different stimulation wavelength used in the two approaches (green laser

stimulation for single grain dating, and blue LED stimulation for multiple grain dating). Thus for problematic samples with a higher than usual contribution of the medium or slow component, green light stimulation would potentially isolate the fast component more readily. This however counteracts the advantage of shorter wavelength in increasing the electron detrapping rate (i.e. producing a higher initial signal intensity) (Section 5.5.1).

5.5.3 Signal resetting at the time of deposition

The complete resetting of the OSL signal and removal of the stored energy at the time of deposition is one of the most important prerequisites for accurate luminescence dating. If sediments were not fully bleached, grains will receive a dose in addition to the residual dose inherited from the previous sedimentation cycle. Consequently, luminescence ages will be overestimated. Incomplete bleaching can be detected for instance through comparison with independent age control (e.g. Hilgers et al. 2001), by testing if modern sediments yield zero ages (e.g. Bailey et al. 2003), by analysing De distributions (e.g. Olley et al. 1998, Bailey and Arnold 2006), or by analysing quartz OSL signal components (e.g. Bailey 2000a).

It has already been mentioned in Section 5.2 that resetting of the quartz OSL signal only requires a few seconds under natural sunlight conditions (Godfrey-Smith et al. 1988). Thus, for aeolian sediments which are fully exposed to sunlight during transport and deposition, complete bleaching is very likely. Complete bleaching of aeolian sediments has been demonstrated by a range of studies. For example, Bailey et al. (2003) showed that most of the modern aeolian samples investigated in their study had De-values of less than 0.2 Gy. Further examples of well bleached aeolian sediments are given in Huntley et al. (1985), Stokes (1992), Olley et al. (1998), Hilgers et al. (2001), Murray and Clemmensen 2001, Bray and Stokes (2003), Singarayer et al. (2005) and Rhodes et al. (2006).

In waterlain sediments, the bleaching history may be different. As water significantly attenuates short wavelengths (<500 nm) of the natural sunlight spectrum (Berger 1990), bleaching of quartz grains might be slower and not as thorough as under sunlight conditions, considering the fact that quartz is most effectively bleached at short wavelength (Spooner 1994b). The most common type of incomplete bleaching is that grains from a certain sediment experienced different levels of signal resetting. Duller (1994b) termed

these sediments to be heterogeneously bleached. Examples of heterogeneously bleached fluvial samples are widespread (e.g. Olley et al. 1998, 2004b, Eitel et al. 2005, Thomas et al. 2005, Rodnight et al. 2006, Fiebig and Preusser 2007). Conversely, well bleached fluvial deposits were identified by e.g. Stokes et al. (2001) and Rittenour et al. (2003), and Jain et al. (2004) concluded that only very young fluvial samples (<1 ka) may suffer from age overestimation due to incomplete bleaching. Furthermore it has been shown by Stokes et al. (2001) that the degree of resetting is highly dependent on the transport distance, with grains transported over large distances by fluvial means likely to be better bleached than those transported over short distances.

With respect to signal resetting at the time of deposition, glaciofluvial sediments (e.g. Rhodes and Pownall 1994, Duller 2006, Klasen et al. 2007) and coastal sediments (e.g. Richardson 2001) are also problematic.

However, in a review on luminescence studies, good agreement between luminescence ages from different depositional environments (aeolian, freshwater, marine and glacial) was reported (Murray and Olley 2002). This review underlines that there is no consistent trend in overestimation of luminescence ages due to incomplete bleaching, independent on the mode of sediment transport.

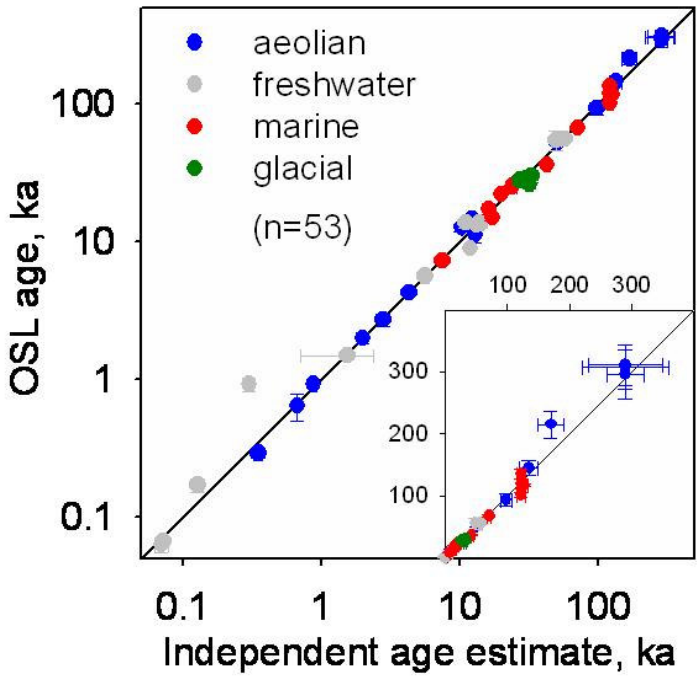

Fig. 5.9. Comparison of 53 OSL ages with independent age control (mainly ^{14}C and tephra ages), compiled by Murray and Olley (2002). Note the logarithmic scale of the axes.

5.5.4 Signal saturation and the age range covered by luminescence dating

The lower dating limit depends on the ability of the measurement devices to detect very small luminescence signals. Quartz OSL ages of less than 50 years, in agreement with independent age control were obtained by Ballarini et al. (2003) and Madsen et al. (2005).
The upper dating limit depends on the lifetime of the electron traps used for dating, the number of OSL traps present in the quartz grain, and the trap filling rate. It has been shown in Section 5.3.2 and Section 5.5.2 that the lifetime of the quartz OSL traps is large enough to potentially date material up to an age of 1 Ma (Bøtter-Jensen et al. 2003a). Thus the major limitation when dating very old samples is the finite number of OSL traps. At some point in the burial history of quartz grains, all these traps will have become filled. Further exposure to environmental (or laboratory) irradiation will not further increase the number of stored electrons and the intensity of the luminescence signal. This condition is termed signal saturation. Due to signal saturation, dose response curves follow a saturating exponential function (Singarayer and Bailey 2003) with the equation

$$I/I_0 = (1 - \exp^{-D/Do}) \qquad \text{(Eq. 5.2)}$$

where I is the OSL intensity due to dose D, I_0 is the saturation intensity and Do is the rate at which electron traps are filled (Singarayer and Bailey 2003).
Dose response and saturation level can vary considerably from sample to sample. That this is even the case on a grain-to-grain scale from one sample was shown by Roberts et al. (1999), Duller et al. (2000), Yoshida et al. (2000) and Jacobs et al. (2003a). One reason for this is the different contribution of the fast, medium and slow component to the OSL signal of individual grains (Bulur et al. 2002), with each component having a different signal saturation level (Singarayer and Bailey 2003, 2004). It is therefore impossible to give general estimates on the saturation level of quartz OSL signals. Wintle and Murray (2006) define the dose to which reliable De estimates can be obtained to be approximately 2*Do from equation 5.2. According to this definition, saturation levels for fast component dominated quartz signals range between 110 and 380 Gy (Roberts and Duller 2004, Banerjee et al. 2003, Singarayer and Bailey 2003, 2004, Jain et al. 2005). Murray et al. (2002) even demonstrated signal growth up to 1000 Gy in marine sediments from Denmark (Fig. 5.10).

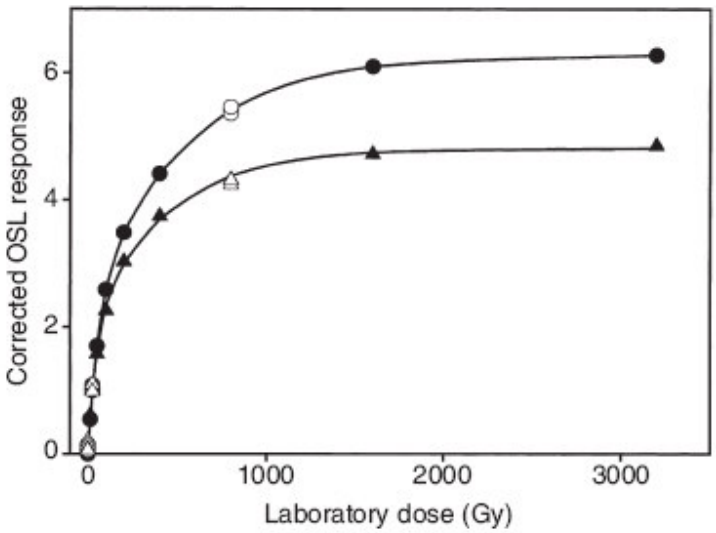

Fig. 5.10. SAR growth curves for two sedimentary quartz samples. In these samples, signal growth can be observed up to laboratory doses of at least 850 Gy (from Murray et al. 2002).

Furthermore, the environmental dose rate defines the electron trap filling rate. If dose rates are low, traps are filled relatively slowly, and the onset of signal saturation levels is late. For example, if the environmental dose rate was as low as 1 Gy/ka, and the saturation level as high as 380 Gy, ages of 380 ka could theoretically be obtained. Even older ages were reported by Watanuki et al. (2005) who obtained quartz based OSL ages from loess samples in good agreement with independent age control up to 500 ka. Rhodes et al. (2006) even obtained a quartz OSL age of 990 ± 200 ka, which was in broad agreement with age constraints provided by ESR and palaeomagnetic dating.

6. Determination of the equivalent dose

As mentioned in Section 5.1, the palaeodose of quartz cannot be determined by direct means as no absolute relation between luminescence signal intensity and palaeodose exists. Every sample from different geological environments, and even every individual grain from the same bulk sample, has different luminescence sensitivities. In other terms, even if individual grains have received exactly the same palaeodose (i.e. are of the same depositional age and were exposed to the same dose rate), luminescence signal intensities can vary considerably.

For this reason, every sub-sample needs to be calibrated for its own luminescence sensitivity. This is undertaken by comparing the natural luminescence signal induced by natural radiation to signals which are induced by known laboratory irradiation doses. The laboratory dose, which produces a signal intensity equal to the natural signal, is termed the equivalent dose (De). Furthermore, the accumulated dose and the signal intensity are not related linearly. At low doses, signal growth can be supra-linear and at higher doses, signal growth changes from linear to a saturating exponential function due to the limited amount of electron traps in the quartz grains (Bøtter-Jensen et al. 2003a) (see Section 5.3). Therefore, several artificially induced luminescence doses from different laboratory doses are necessary to characterise the function of signal growth in detail. Plots of the laboratory dose on the x-axis and the luminescence signal intensity on the y-axis are termed growth curves or dose response curves.

6.1 Measurement protocols for De determination

6.1.1 Additive- and regenerative-dose methods

There are two basic measurement approaches to determine the De, namely the additive-dose and the regenerative-dose technique. In the additive-dose technique, laboratory dosing is carried out without fully bleaching the sample before dose administration. Aliquots for determination of the natural signal receive a zero laboratory dose. The resulting growth curve intercepts with the y-axis at the height of the natural signal. For derivation of the equivalent dose, the growth curve is extrapolated to the negative part of the y-axis. This is the major disadvantage of the additive-dose technique as the growth curve function needs to be known exactly for accurate extrapolation, and hence

accurate De determination. For older samples, whose growth behaviour is non-linear, this is often a problem (Wintle 1997, Aitken 1998).

In the regenerative technique, the luminescence signal is fully reset before administering laboratory doses. In this way, a growth curve is constructed which ideally intercepts with the origin of the two axes (although it will be seen later that this is not always the case). The equivalent dose is derived by projecting the natural signal from the x-axis onto the growth curve and equating it to the dose on the y-axis. Thus, when the artificially induced signal intensities exceed the natural signal intensity, the De is determined by interpolation between two points on the growth curve. As in additive-dose techniques, the growth curve function should be accurately known, but errors induced by inadequate curve fitting are much smaller when interpolating instead of extrapolating (Wintle 1997, Aitken 1998). An additive-dose growth curve and a regenerative-dose growth curve are shown in Fig. 6.1.

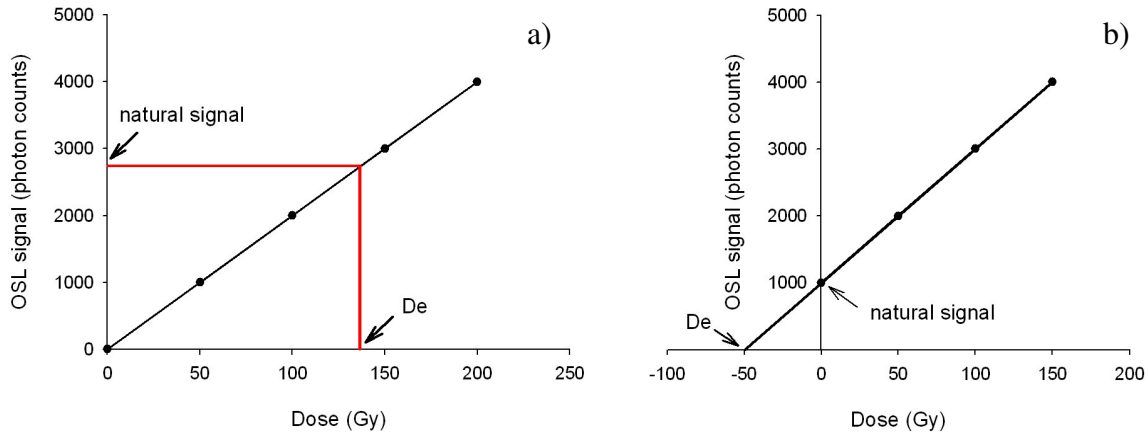

Fig. 6.1. (a) Simplified regenerative-dose growth curve. The equivalent dose (De) is derived from interpolation. (b) Simplified additive-dose growth curve. The De is derived by extending the growth curve to the y-axis, hence from extrapolation.

6.1.2 Multiple aliquot and single aliquot approaches

As explained above, constructing a growth curve requires administration of several laboratory doses and subsequent OSL measurements. These steps can either be carried out on one and the same aliquot or using several aliquots for each dose. The former is termed single aliquot dating, and the latter multiple aliquot dating. Each approach can either be combined with regenerative- or additive-dose techniques.

The major advantage of single aliquot over multiple aliquot dating is that it better accounts for variability between luminescence signals from different aliquots. This

inter-aliquot scatter has two main sources. One relates to different luminescence sensitivities of the measured grains arising from variations in the population of electron traps and/or recombination centres. As a consequence, signal intensities differ despite accumulation of the same dose (McFee and Tite 1994, Duller et al. 2000, McCoy et al. 2000). The other one is caused by different De-populations in samples due to, for instance, incomplete bleaching or bioturbation. The latter will be termed external factors of variations in the following discussion.

In multiple aliquot dating, variations in sensitivity can be corrected by normalisation procedures (Rhodes 1988, Smith et al. 1990, Stokes 1994). To minimise the effect of external variations in palaeodoses, each dose is usually administered to a group of aliquots, and a growth curve is fitted to the average signal intensity of each group. This contributes large uncertainties to the resulting De-value, on top of uncertainties derived from scatter in the natural luminescence signal and, when used in combination with additive doses, from the extrapolation procedure (e.g. Hilgers et al. 2001). A further disadvantage of multiple aliquot dating is that many aliquots and thus, a lot of material is needed for the De-determination (Duller 1994a, Lian and Roberts 2006).

In single aliquot dating, each aliquot is 'calibrated' with respect to its own sensitivity and thus differences in sensitivity are more or less accounted for. As a consequence, single aliquot De-values are much more precise than multiple aliquot De-values (Duller 1991, 1994a, Hilgers et al. 2001). Usually, several aliquots are measured in single aliquot dating, each giving an individual De-value. If these De-values differ, then these variations can mainly be ascribed to external factors. Analysis of the resulting De-distribution provides important information on the source of external variations. If for example the shape of the distribution points to incomplete bleaching, then only those De-values which are thought to have been completely bleached (i.e. the lower De-values) can be used for the determination of the burial dose (e.g. Olley et al. 1998, Galbraith et al. 1999, Lepper et al. 2000, Thomsen et al. 2003).

In conclusion, since the most precise De-values are derived from single aliquot regenerative-dose protocols, this would be the technique of choice. However, a major problem with respect to the accuracy of De-values derived from this protocol remains. Through the repeated cycles of irradiation, preheating and bleaching on one and the same aliquot, sensitivity changes throughout the measurement procedure are induced (e.g. Duller 1991, Stokes 1994). This can either be an increase or a decrease in luminescence sensitivity and is mainly dependent on the preheat temperature applied

(Armitage et al. 2000, Bailey 2000b, Jacobs et al. 2003b, 2006a, Rodnight 2006). The preheat-dependency of sensitivity changes is exemplarily shown in Fig. 6.2 from Armitage et al. (2000). Preheat temperatures >240°C result in increasing sensitivity, whereas preheat temperatures <240°C result in decreasing sensitivity.

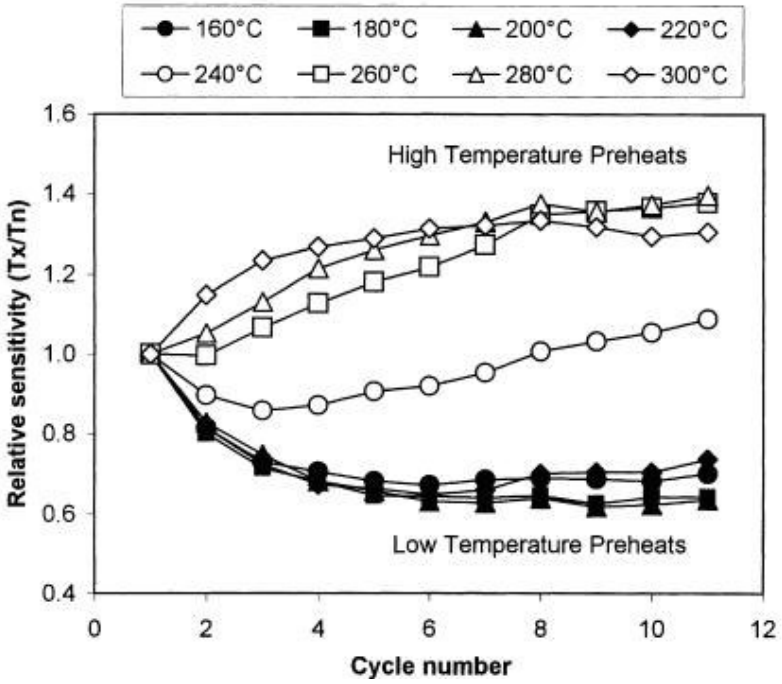

Fig. 6.2. Sensitivity changes for a sedimentary quartz sample (MAP3) in dependency of the applied preheat temperature, ranging from 160-300°C. The sensitivity was measured using the test dose response (T_x). All data were normalised to the first test dose response (T_n) obtained after measurement of the natural OSL, which was given a relative sensitivity value of 1 (Armitage et al. 2000).

These sensitivity changes can be corrected by the use of constant test doses after each measurement cycle. The test dose signals serve as a measure for the sensitivity changes and are used for the correction of the regenerative signals. The use of a SAR protocol for dating quartz including a constant test dose was first presented by Murray and Wintle (2000). Slight modifications to this protocol have later been suggested by several authors (e.g. Choi et al. 2003a, 2003b, Jacobs et al. 2006a), and are summarised in Murray and Wintle (2003) and Wintle and Murray (2006). The SAR protocol of Murray and Wintle (2000, 2003) will be described in more detail in the following section.

6.1.3 The SAR protocol of Murray and Wintle (2000, 2003)

The SAR protocol of Murray and Wintle (2000, 2003) is based on a protocol presented by Murray and Roberts (1998) who monitored changes in sensitivity using the 110°C TL response measured during the preheats following the natural and the regenerative doses. In contrast, in the protocol of Murray and Wintle (2000, 2003) the OSL response to small test doses is used as a measure for sensitivity changes. The test dose is administered after each regeneration cycle, and sensitivity changes are corrected by dividing the OSL response to the regenerative dose by the OSL response to the test dose. The basic steps of the protocol are the following:

Step 1: administration of regenerative dose
Step 2: preheat
Step 3: measurement of OSL response to regenerative dose
Step 4: administration of test dose
Step 5: preheat
Step 6: measurement of OSL response to test dose

These steps are repeated several times with four or more increasing regenerative doses to build up the growth curve. In the first cycle, the OSL response of the natural dose is measured, followed by the first test dose. The basic principle of the SAR protocol is displayed in Fig. 6.3.

The protocol furthermore consists of two additional cycles. In one of these cycles, a zero regenerative dose is given. With this procedure the origin of the growth curve is derived. Ideally, the OSL response to the zero dose would be a zero signal, but this is not always the case. Recuperation effects (re-capturing of electrons in thermally unstable, optically insensitive traps during stimulation and subsequent thermal transfer into optically sensitive traps during preheating) are responsible for this effect (Aitken and Smith 1988, Smith and Rhodes 1994, Aitken 1998). Thus, recuperation can result in a y-axis offset from zero. The zero dose cycle is conducted after the regenerative dose cycles. In a last cycle, one of the regenerative doses, usually the first, is repeated. If the correction procedure was successful, then the ratio of both corrected signals should be unity. This ratio is termed the recycling ratio (Murray and Wintle 2000). In the following, the individual steps of the protocol will be explained in more detail:

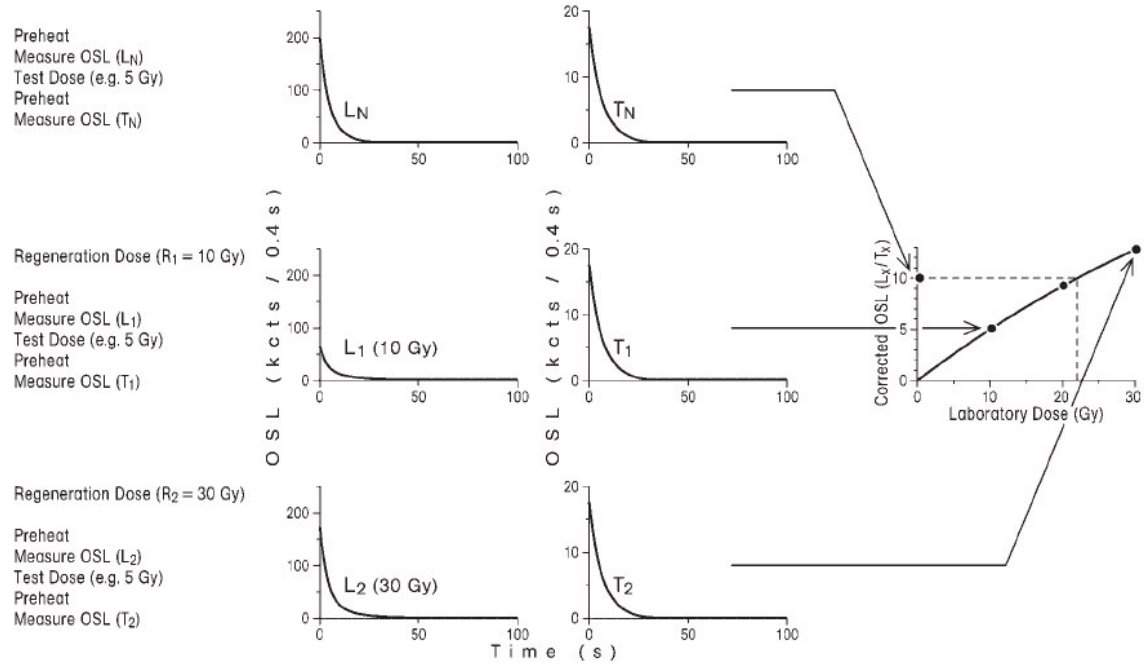

Fig. 6.3. The single aliquot regenerative dose (SAR) procedure applied to quartz. The growth of the signal with dose is characterised by administering a number of laboratory doses (regeneration doses) of different sizes (10 Gy, 30 Gy, etc.). The OSL signals resulting from these doses are measured as L1, L2, etc. After each of these measurements the luminescence sensitivity is measured by giving a fixed dose (in this case 5 Gy) and measuring the resulting OSL signal (T1, T2, etc.). The effect of changes in sensitivity can be corrected for by taking the ratio of the luminescence signal (Lx) and the response to the fixed dose (Tx). The plot of the corrected OSL (Lx/Tx) as a function of the laboratory dose (right) can be used to calculate the equivalent dose for that aliquot, in this case 22 Gy (Duller 2004).

Step 1 and 4: irradiation

Usually the laboratory doses are administered using a beta source which is included in modern luminescence readers. It has to be considered that this artificial irradiation differs considerably from natural irradiation. The latter results from a mixture of alpha, beta and gamma radiation whereas laboratory irradiation comprises only beta radiation. Furthermore, beta source dose rates are much higher than environmental dose rates. For example, a typical environmental dose rate in dune sands is 1 Gy/ka, whereas laboratory beta radiation delivers the same dose in about 5-10 seconds. Whether the process of electron trap filling and emptying of the unstable traps is the same for natural and laboratory irradiation cannot be tested experimentally, forcing a reliance on comparison with independent age control (Murray and Wintle 2000). In order to mimic natural irradiation more closely, Bailey (2004) proposed laboratory irradiation in short pulses separated by thermal treatment for redistribution of charge.

The regenerative doses should be chosen to closely bracket the palaeodose for precise interpolation of the natural signal between two artificial signals (Murray and Wintle 2000). For the test dose Murray and Wintle (2000) recommend doses of around 10-15 % of the expected palaeodose. This value though might be unpractical for very young samples or samples with a low sensitivity, because very low test dose signals would result in increased errors due to poor counting statistics (Section 6.3). This is also true for single grain measurements. Ballarini et al. (2007) therefore suggest higher test doses when analysing young samples using single grains. They also note that bracketing the palaeodose with the regenerative doses is inappropriate for very young samples and presented a protocol which uses only one regenerative dose above the expected natural one (Ballarini et al. 2007). A linear function was forced through this point and the origin to construct the growth curve, which is only feasible for samples with equivalent doses in the linear part of the growth curve.

Step 2 and 5: preheat

Preheating after laboratory doses is essential in order to empty and redistribute charge from thermally unstable traps, which are filled after laboratory irradiation but usually are empty in naturally dosed samples. According to Murray and Wintle (2000), preheats after the regenerative dose can range from 160 to 300°C, held for 10 s. Above that temperature, the main OSL trap at 325°C is progressively eroded. The most appropriate preheat temperature can be derived from preheat plateau tests. In this test, the De of different groups of aliquots is determined using different preheats for each group. Murray and Wintle (2000) state that consistent De-values over a range of temperatures indicate successful isolation of the stable components and that any temperature that lies within the plateau may then be chosen for preheating. Bailey (2000b) though demonstrated that this is not necessarily the case.

In the protocol of 2000, Murray and Wintle propose that the preheat following the test dose should be less aggressive than that following the regenerative dose. The reason for this is to not additionally alter the sensitivity by this procedure. They therefore suggest a ramping of the temperature from 0 to 160°C, followed by immediate cooling. This treatment is referred to as cutheat. It has been shown that it does not induce further sensitivity changes and removes charge from the unstable trap associated with the 110°C TL peak. For some samples, this low cutheat temperature was shown to be inadequate. This is especially true for samples with a high contribution of the slow

component to the luminescence signal (e.g. Choi et al. 2003a, 2003b, Jacobs et al. 2006a). These authors demonstrated that a higher cutheat temperature results in a better isolation of the fast component. It has also been suggested to chose a cutheat temperature which is 20°C lower than the preheat temperature following the regenerative dose, as outlined in Murray and Wintle (2003, 2006). This was shown to be the best preheat-cutheat combination in loess samples from northern America (Roberts 2006).

Step 3 and 6: OSL measurement

In multiple grain quartz dating the OSL signal nowadays is usually produced by stimulation with blue LEDs (470 ± 30 nm) (Bøtter-Jensen et al. 1999a, 1999b, 2000). Murray and Wintle (2000) suggest stimulation for 40 s at an elevated temperature of 125°C to keep the 110°C TL trap charge free. This efficiently zeroes the OSL signal to negligible values. The signal is derived by integrating over parts of the OSL decay curve. In order to use the part of the signal with the highest proportion of the fast component, only the initial part of the decay curve is used for the determination of the signal intensity. Murray and Wintle (2000) suggest integration intervals of 0.3 or 0.8 s. In the final part of the decay curve a small proportion of luminescence remains, referred to as the background. The background signal results from some photons reaching the photomultiplier from the stimulation source despite optical filters, and from a contribution from the slow component. The latter is dose dependent and can accumulate over several measurement cycles (Wintle and Murray 1997), and thus has to be accounted for by a correction. This is realised by integrating over the final part of the decay curve and subtracting this background signal from the initial signal.

In single grain dating of quartz, stimulation is carried out with green lasers (Bøtter-Jensen et al. 2000). As their power is much higher than the power of blue LEDs, only short stimulation times of about 1 s are necessary (Bøtter-Jensen et al. 2000, Wintle and Murray 2006). It consequently follows that integration limits are also much smaller. The sensitivity corrected OSL signal which is used to construct the growth curve is derived by dividing the background corrected regenerative dose signal by the background corrected test dose signal.

The SAR protocol of Murray and Wintle (2000, 2003) was originally designed for dating of coarse grain quartz. It has been adopted for feldspar dating by Wallinga et al.

(2000), although some parameters, such as stimulation temperatures, stimulation wavelength or signal integration intervals, are different.

6.1.3.1 Testing the robustness of the SAR protocol

Murray and Wintle (2000) suggest three tests to evaluate if the SAR protocol is appropriate to determine the De of a sample. Two of these have already been mentioned above, namely the recuperation test and the recycling ratio test. The former is conducted by monitoring the OSL response to a zero dose, and the latter by repeating one of the regenerative doses to check if the sensitivity corrected signals are equal. The recycling ratio thus is a measure of the effectiveness of the sensitivity correction. Thresholds for an appropriate performance of the SAR protocol given in Murray and Wintle (2000) are <5 % for the recuperation, expressed as the corrected zero dose signal in percent from the corrected natural signal, and 0.9-1.1 for the recycling ratio.

A further test is the dose recovery test (DRT). This test aims to recover a known laboratory dose and should be performed to verify that the first test dose adequately corrects for sensitivity changes of the natural signal, induced by the first preheat (Murray and Wintle 2003). Further details on DRTs are given in Section 6.8.4.3.

Rodnight (2006) and Klasen (2008) further recommend conducting LM-OSL measurements (Section 5.5.2.1) before running a SAR protocol in order to test if the signal is dominated by the fast component (Singarayer and Bailey 2003, Jain et al. 2003). This is because samples with a non-dominant fast component can pose problems when using the SAR protocol (e.g. Choi et al. 2003a, 2003b, Jacobs et al. 2006a, Klasen 2008).

6.2 Instrumentation

The modern luminescence readers produced by Risø National Laboratory (Roskilde, Denmark) (e.g. Bøtter-Jensen et al. 2000) are designed to carry out all the steps required for the SAR protocol of Murray and Wintle (2000, 2003). For measurement, aliquots are placed onto a carousel, which can usually hold 48 aliquots. These aliquots consist of small amounts of sample material placed onto steel or aluminium discs. The carousel is turned by a motor and thus each aliquot can be moved to different positions within the reader. First, the sample is irradiated with the $^{90}Sr/^{90}Y$ beta source, and then is moved to a position under the photomultiplier. At this position a heater plate lifts the disc and the

sample is preheated. Stimulation is undertaken at the same position, either using blue LEDs for quartz multiple grain, IR LEDs for feldspar multiple grain, a green laser for quartz single grain or an IR laser for feldspar single grain. Simultaneously, the luminescence signal is detected with the photomultiplier. Between the sample and the photomultiplier, appropriate detection filters need to be placed (see Section 5.5.1). Fig. 6.4 shows a schematic drawing of a Risø TL/OSL reader.

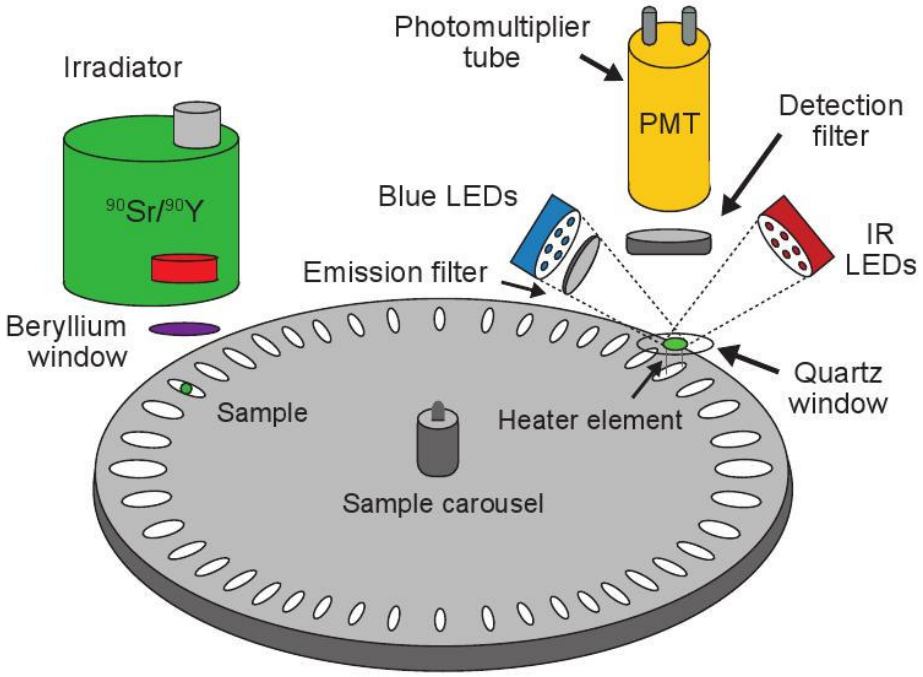

Fig. 6.4. Schematic drawing of a Risø TL/OSL reader (Risø 2008).

In single grain dating, the individual quartz grains are mounted onto special discs containing 100 wholes with a diameter of 300 µm, arranged in a 10x10 array (Bøtter-Jensen et al. 2003b) (see Fig. 6.5).

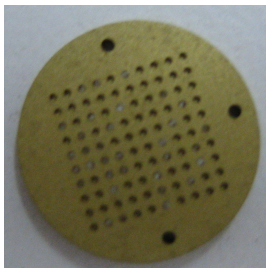

Fig. 6.5. Photograph of a single grain disc (Photograph by J. Lomax, 2006).

It is thus theoretically possible to produce 100 growth curves and 100 De-values with one disc (this is not the case as not every grain gives a detectable luminescence signal or a determinable De-value). Irradiation is carried out simultaneously on the 100 grains, as are the preheating procedures. For the OSL measurement, each quartz grain needs to be

stimulated separately. For this purpose, the green laser is aimed at the exact position of each grain with two mirrors (Duller et al. 1999, Bøtter-Jensen et al. 2000, 2003b).

6.3 Error estimation for individual De-values

When using the programme Analyst (Duller 2005) for De-calculation, the uncertainty calculated for each De-value consists of the error of the curve fitting procedure, the instrumental error, and the error induced by counting statistics. The latter combines the number of counts in the signal and the magnitude of the background signal (Galbraith 2002, Duller 2007). Grains or aliquots with low luminescence sensitivity, thus with a low signal intensity, result in high uncertainties and vice versa. The instrumental error considers the ability of a luminescence reader to reproduce results from repeated measurements. Differences in measurement reproducibility are mainly caused by variations in the power of the stimulation source and by a heterogeneous dose rate of the beta source in the reader (Thomsen et al. 2005). The latter is a particular problem when measuring single grains as with non-uniform dose rates of the beta source, every single grain will receive different dose rates in laboratory irradiation. Ballarini et al. (2006) have shown that one of the beta sources used in their laboratory delivered dose rates varying by a factor of two from one margin to another. This problem can be overcome by estimating the dose rate of the beta source for every single position on the single grain disc using a calibration sample and then, when measuring natural samples, using individual dose rates for every grain. The variations induced by the stimulation source cannot be corrected for, but they can be estimated by reproducibility checks. These tests can be conducted by measuring the luminescence signal of a constant laboratory dose repeatedly and correcting for sensitivity changes. In recent studies, measurement reproducibility was estimated to around 1.5 % or 2.1 % for single grain measurements, dependent on the initial integral of the shine down curve used for calculation (Thomsen et al. 2005, Jacobs et al. 2006b). The fact that larger integrals resulted in a reduction of the instrumental error gives rise to the assumption that fluctuations in laser power are a significant factor for measurement reproducibility in single grain devices. For multiple grain measurements the reproducibility due to instrumental variations is around 1.5 % (Galbraith et al. 2005). An exact description of how to calculate and combine these errors is given in Duller (2007).

The magnitude of the De-error is further dependent on the shape of the growth curve. In the linear part of the growth curve, the uncertainty on the measured natural signal due to

counting statistics results in the same uncertainty of the De-value (if no additional uncertainties from the curve fitting procedure and from instrumental fluctuations are incorporated in the error calculation). Thus, if the signal can be determined with an uncertainty of 2 %, the resulting De-value will also have an error of 2 %. In the non-linear part of the growth curve, errors on the signal determination will result in comparatively larger errors on the De-estimate, as illustrated in Fig. 6.6.

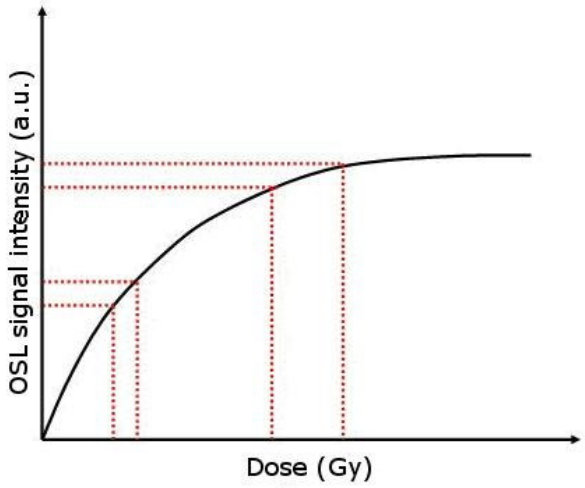

Fig. 6.6. Illustration of the relation between errors on the OSL signal intensity, the resulting error on the equivalent dose and the shape of the growth curve.

It is crucial, for several reasons, to correctly estimate errors of each individual De-value. First, some modes of calculating mean De-values are based on error weighting, such as the central age model or the minimum age model (Galbraith et al. 1999) (see Section 6.7). Hence, if individual uncertainties on De-values are not correctly assessed, the mean values will also be affected.

6.4 Sources of equivalent dose variations

In single aliquot dating of sedimentary quartz, it is possible to determine the De of multiple replicates of multiple grain aliquots (tens to thousands of grains), or of single grains. When comparing De-values of a sediment sample it will be noticed that these values scatter to a certain degree. These variations have many sources, which can be divided into three main groups: external sources of variations, instrumental sources of variation and intrinsic sources of variation.

The first group (external sources of variations) is associated with the environmental setting of the sedimentary sample. Deviating palaeodoses can be caused by, for instance, incomplete bleaching, post-depositional mixing or microdosimetric effects.

The latter are probably found in all sediments, and have shown to be present even in a relatively homogeneous loess sample (Kalchgruber et al. 2003). Incomplete bleaching can be a problem in fluvial or glacio-fluvial sediments, but is unlikely to be a problem in aeolian sediments (e.g. Singarayer et al. 2005) (Section 5.5.3). Post-depositional mixing might occur in environments where roots or burrowing animals are present. If not accounted for, for example by analysing the De-distribution and selecting the De-population with the true burial dose, then these sources of variations may lead to erroneous De-determination. A more detailed description of external sources of variations will be given in Section 6.8.7.3.

The second group (instrumental sources of variations) is related to random uncertainties of the luminescence measurement itself. The main factors hereby are instrumental fluctuations and counting statistics, as already explained in Section 6.3. They are unavoidable in any laboratory measurement. If enough sample replicates are measured, they will not result in erroneous De-determination, but it is important to know the precision with which a De-value can be obtained. The relation between luminescence sensitivity and variations in De-values has been shown by e.g. Duller et al. (2000) (Fig. 6.7). The 'dark' grains in the left part of the diagram scatter to a much greater extent around the known dose of 29 Gy as the 'bright' grains in the right part of the diagram.

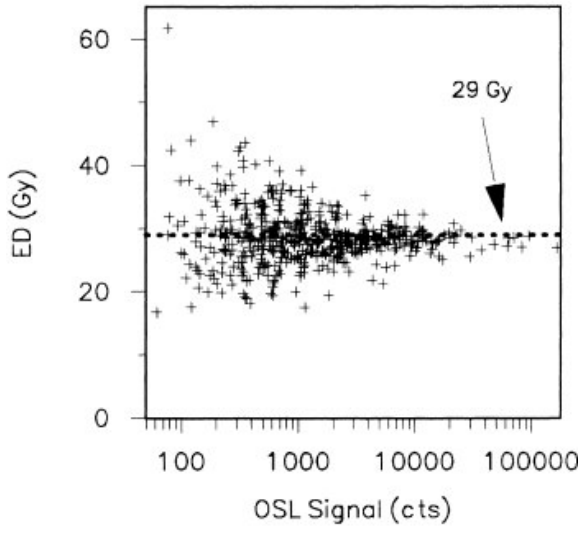

Fig. 6.7. Relation between the signal intensity and the accuracy of equivalent doses for a sedimentary quartz sample from Tasmania. All grains were given a known dose of 29 Gy (Duller et al. 2000).

A final group is related to the different intrinsic luminescence properties of every quartz sample, even on a grain-to-grain scale. Each sample might show different recuperation, different sensitivity changes or their luminescence signal can be composed of different

proportions of the fast, medium and slow component (e.g. Roberts et al. 2000, Jacobs et al. 2003a, 2006a, 2008). The SAR protocol of Murray and Wintle (2000, 2003) takes these problems into account to a certain degree, and subsamples which do not fulfil certain criteria can be rejected. Yet, if such problems stay unnoticed, they can result in erroneous De-determination.

Furthermore, similar to the dependency of the error of individual De-errors and the shape of the growth curve, the spread in De-values will also increase with increasing non-linearity of the growth curve. This relation is shown in Fig. 6.8 by Murray and Funder (2003). They calculated that a relative standard deviation of sensitivity corrected OSL signal of 10 % (expressed by the Gaussian curve (a)) would result in a relative standard deviation of the De-values of 12 % (expressed by the Gaussian curve (a')) in the linear part of the growth curve. In the non linear part of the growth curve, the same standard deviation of the sensitivity corrected OSL signals (10 %, as expressed by the Gaussian curve (b)) would result in a relative standard deviation of De-values of 23 % (expressed by the Gaussian curve (b')).

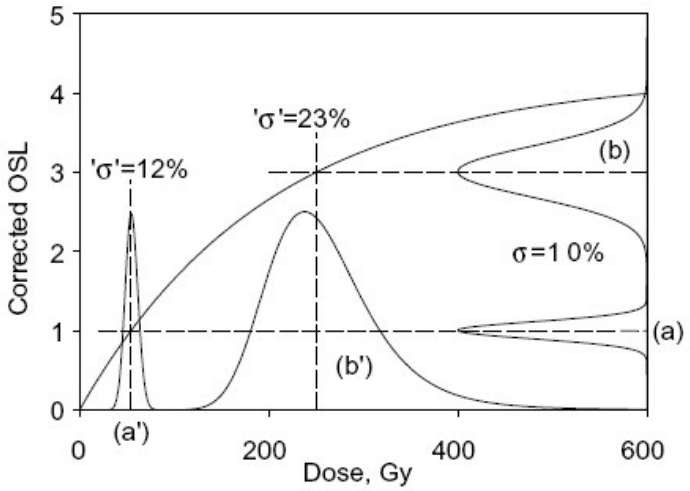

Fig. 6.8. The effect of a non-linear growth curve on the distribution of measured doses. Two normalised Gaussian OSL distributions are shown on the right hand axis, each with a relative standard deviation of 10 %. When these are interpolated onto the growth curve (dashed lines interpolate the centre of each distribution) they result in the two dose distributions on the horizontal axis. The relative intensities and shapes of the interpolated dose distributions change significantly as the growth curve approaches saturation (Murray and Funder 2003).

6.5 Display of De-distributions

There are several ways to display De-distributions. The most common ones are histograms, probability density functions and radial plots (Bøtter-Jensen et al. (2003a). Fig. 6.9 shows these three modes of display for a sample analysed in this study.

Histograms do not incorporate the individual uncertainty on each De-value. This is typically not a problem in multiple grain dating using large aliquots, where the De-values usually have similar uncertainties. In single grain dating though, individual uncertainties on the De-values might vary considerably. This is mainly due to different signal intensities and thus different counting statistics. Histograms can therefore be misleading as one cannot assess if outliers occur because they were measured imprecisely (e.g. due to a weak signal intensity) or because they belong to a different De-population (e.g. due to incomplete bleaching or post-sedimentary mixing). Plotting ranked individual De-estimates including error bars in the histogram circumvents this problem to a certain degree. A further problem is that their shape is dependent on the bin width, and bin width selection often does not follow any particular rule (Bøtter-Jensen et al. 2003a). Nevertheless, histograms can provide easy assessment of the shape of a distribution, with respect to, for instance, skewness or multi-modality.

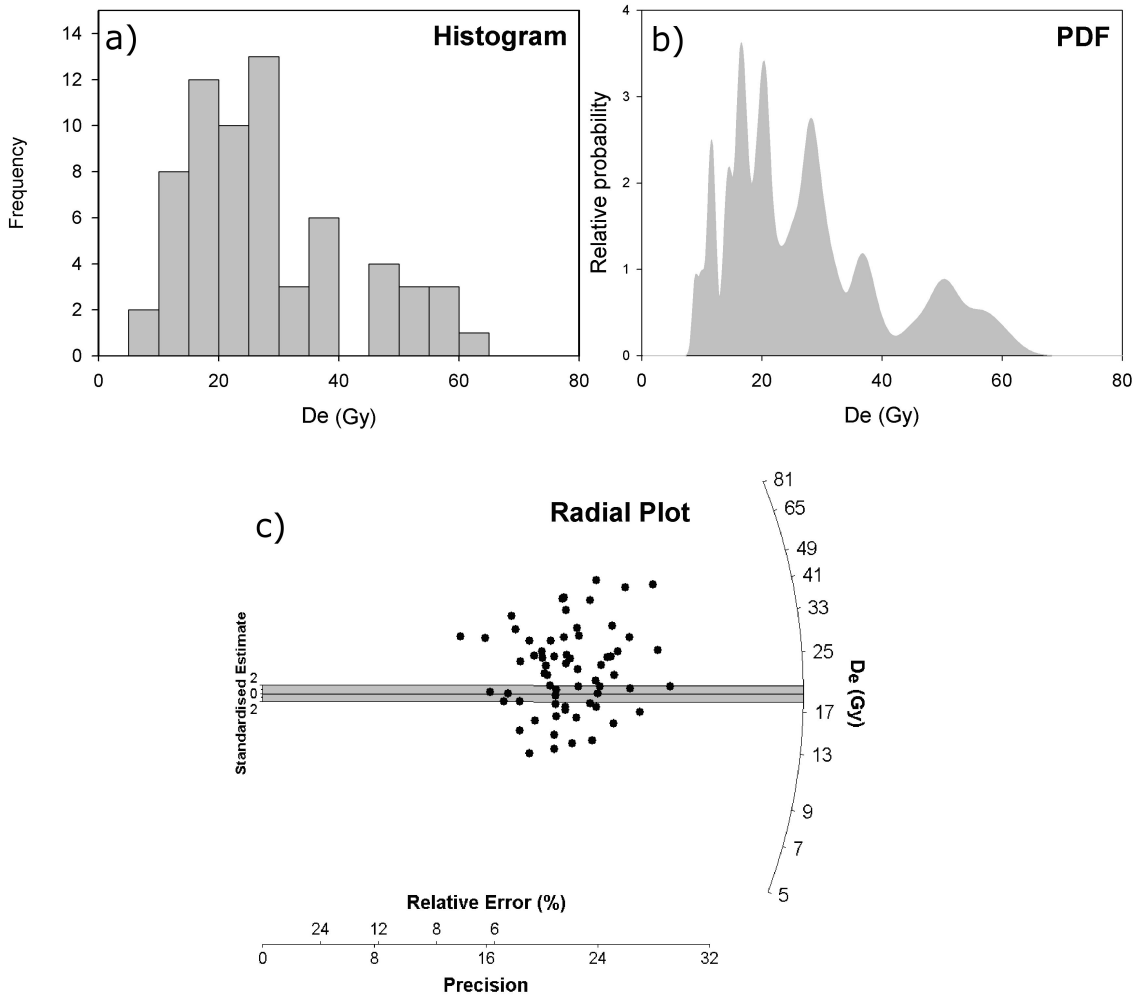

Fig. 6.9. Different modes of displaying De-values exemplarily shown for multiple grain analysis of sample SW8 from the western Murray Basin. (a) Histogram (n = 65, bin width 5 ka), (b) probability density function (PDF) (n = 65, bin width 0.2 ka),

(c) radial plot (n = 65, centred to the central age mean De of 19.2 Gy. The overdispersion for this sample is 31 %).

Probability density functions are constructed by displaying each individual De-value as a Gaussian curve, with the individual De-error serving as standard deviation of the curve. A precise De-value thus will give a narrow Gaussian curve, and an imprecise one a broad Gaussian curve (Fig. 6.10). A description of how to construct PDFs can be found in Singhvi et al. (2001).

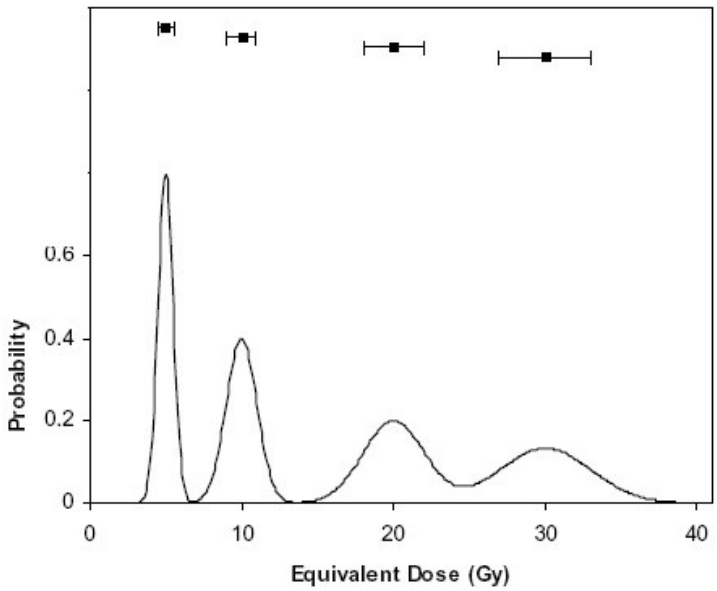

Fig. 6.10. Probability density functions (PDFs) are constructed by summing Gaussian curves each representing one De-value with its error. The less precise a value is known, the broader the Gaussian curve. The standard deviation of the Gaussian curve is expressed by the absolute error on the individual De-value. In this hypothetical dataset, all De-values have the same relative error (10 %) but different absolute errors (from Duller 2005).

For the total distribution, all the Gaussian curves are summed to give a continuous probability density function. This way of displaying the De-distribution therefore incorporates the individual error, and is furthermore less bin width dependent than a histogram. Nevertheless, probability density functions have been heavily criticised by Galbraith (1998). His major points of objection were that the modes in a PDF do not necessarily represent discrete De-populations and that information from precise De-values is concealed by combining them with imprecise De-values.

Radial plots were originally developed for fission track ages by Galbraith (1990), and were suggested for displaying single grain De-values by Galbraith et al. (1999). In a radial plot, each De-value is plotted individually as a point using three axes. The left hand y-axis is a standardised estimate and determines the number of standard deviations

a De-value deviates from the mean De (or some other reference value). The right hand y-axis is of radial shape, of logarithmic scale and displays De-values in Gy. The De-value of each point can be read off by extending a line from the origin on the left hand y-axis to the right hand y-axis passing through the data point in question. The x-axis measures the relative error of an individual De-value (and its precision, which is the reciprocal individual De-error). Well known De-values with a low relative standard error and a high precision value fall in the right part of the graph. Often, a 2 sigma band (the two sigma standard deviation of the standardised estimate) is also indicated on the left hand axis of a radial plot. In a homogeneous dataset (in which the scatter of De-values does not exceed the scatter expected from the individual error on each De-value, cf. Galbraith 2003), 95 % of the values will fall into this 2 sigma band. The distribution shown in the radial plot in Fig. 6.9(c) is highly inhomogeneous, with only 18 % of all De-values falling into the 2 sigma band. Radial plots do not show the symmetry of a distribution as clearly as histograms or PDFs. In some studies thus radial plots and one of the other forms of display are given to present De-data (e.g. Duller et al. 2000, Jacobs et al. 2003a).

6.6 Analysis of De-distributions

De-distributions, whether displayed as histograms, PDFs or radial plots allow some assessment of how many De-populations are present in a sample. Their analysis is a powerful tool to detect sources of external De-variations such as incomplete bleaching.

A certain amount of scatter of De-values is to be expected in any sample due to instrumental variations (see Section 6.3 and 6.4). When De-data vary within the expected range of instrumental variations, the dataset is termed ‘homogeneous’ according to Galbraith (2003). If the observed variation exceeds the expected variation, the distribution is termed overdispersed (Galbraith et al. 1999). Assessment of whether a distribution is homogenous or not can be undertaken by either an homogeneity test after Galbraith (2003), visualisation of data through radial plots (in an homogeneous dataset 95 % of the De-values should fall into the 2 sigma band), or by calculating the overdispersion value following Galbraith et al. (1999) (a homogeneous dataset has a overdispersion of zero, hence the central age model reduces to the common age model). If individual uncertainties on De-values are underestimated (e.g. through underestimation of the instrumental error) overdispersion is incorrectly calculated, and,

conversely, homogeneity might be assumed in case of overestimation of errors (see Section 6.3).

In a sample that is well-bleached and not affected by post-sedimentary mixing or by microdosimetric effects (note that this will never be found in sedimentary samples), one would expect a normal Gaussian or log-normal distribution of De-values. Whether the distribution is normal or log-normal mainly depends on the shape of the growth curve. When the majority of De-values is in the linear part of the growth curve (i.e. young samples), a normal distribution results, and when the majority of De-values is in the non-linear part of the growth curve (i.e. old samples), a log-normal distribution is produced (Murray et al. 2002, Murray and Funder 2003, see also Fig. 6.8 in Section 6.4). The distribution will be slightly overdispersed (due to different intrinsic luminescence properties of the quartz grains), thus less than 95 % of De-values will fall into the 2 sigma band of a radial plot.

A sample affected by microdosimetry and/or different intrinsic luminescence properties will show a broader than normal or log normal, but still unimodal, distribution. In a radial plot, less than 95 % of the values will lie in the 2 sigma error band, indicating that the observed scatter is broader than that expected from instrumental uncertainties and counting statistics alone.

A sample which has been incompletely bleached will be strongly positively skewed, displaying a tail towards high De-values (e.g. Olley et al. 1998, 1999, Duller et al. 2000). In a radial plot, the unbleached De-populations will be recognised as data points above the 2 sigma band. These De-values may still have a high precision (see Fig. 6.11). It is further noted at this point that there are other ways to detect incomplete bleaching in samples besides through De-distribution methods. These methods assess the degree of bleaching of the different components that contribute to the OSL signal (namely, the fast, medium and slow component). Using this approach to identify incomplete bleaching is described in Bailey (2000a) and Bailey et al. (2003).

Samples affected by bioturbation may show a multimodal distribution (Bateman et al. 2003a) which will show in histograms, PDFs and radial plots.

Assessing the sources of variations through distribution methods is much more complex than described above. In a lot of sedimentary samples more than one source of variation occurs, thus identification of different De-populations can be complicated, if not impossible.

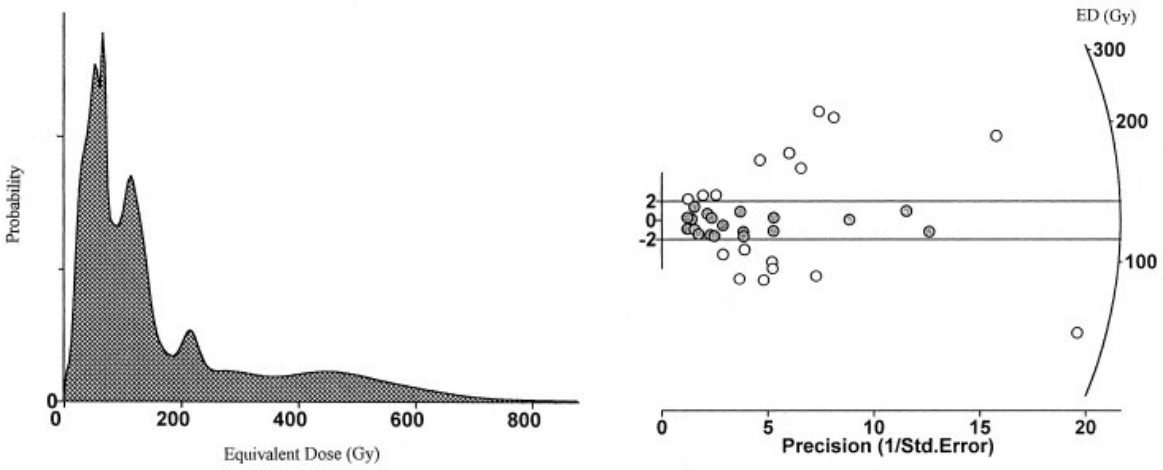

Fig. 6.11. De-distribution of a sample that was heterogeneously bleached at deposition, displayed as PDF and as radial plot (from Duller et al. 2000).

6.6.1 The scale of analysis

The importance of the aliquot size on the De-distribution and their analysis has been outlined by Olley et al. (1998), Wallinga (2002) and Duller (2008). The larger the number of grains on an aliquot, the less variations in De-values will be seen, as the measured OSL signals consist of the sum of many OSL signals from individual grains. How many grains on a multiple grain aliquot contribute to the signal is sample dependent, but in sedimentary samples, an average of only 5-10 % of the grains contribute 90-95 % of the total luminescence signal, as confirmed by single grain measurements (Duller et al. 2000, Jacobs et al. 2003a). Therefore, small multiple grain aliquots, consisting of some tens of grains, will only carry very few luminescent grains.
If a sedimentary sample consists of two or more De-populations, then it is very likely that grains with high equivalent doses (incompletely bleached grains) will dominate the total signal in multiple grain De-determinations. This can lead to severe De-overestimations (e.g. Duller 2006). The most detailed De-distributions will be derived from single grain measurements.

6.7 Mean De calculation

Usually, the equivalent dose of a sample is determined on many replicates of subsamples; that is, either on many aliquots in multiple grain dating or on many individual grains in single grain dating. There are several ways to combine these multiple De-values to form a mean equivalent dose. Which of these is the most appropriate is, for instance, dependent on the De-distribution. Mean De-calculations can

be divided into two groups; one that accounts for the errors on each individual De-value, and one that does not.

Mean values which do not incorporate individual errors on De-values are only appropriate for samples in which the individual errors do not vary significantly. This is only the case when large multiple grain aliquots are measured, thus when the summed OSL signal of each aliquot is of similar brightness and errors induced by curve fitting are similar from aliquot to aliquot. The arithmetic mean is only appropriate when De-values derive from a single De-population and when the distribution is symmetrical. Murray and Funder (2003) have demonstrated that the saturating exponential function of the growth curve results in non-symmetric, log-normal De-distributions especially in older samples (see Fig. 6.7 in Section 6.4). They advocate the use of the median to account for the log-normality of the distribution. Even better suited for log-normally distributions is the geometric mean, which is the exponentiated arithmetic mean of logged values ($x = \exp(n^{-1}\sum\log(x))$).

The geometric mean thus relies on the assumption that logged values of a log-normal distribution are normally distributed in which case the arithmetic mean is justified. It is not as robust towards outliers though as the median (Schönwiese 2000).

In small aliquot multiple grain dating, and particularly in single grain dating, errors might vary considerably (for instance, bright grains can be measured with high precision and dim grains with low precision due to counting statistics). Therefore, it is important to account for these variations in De-errors by giving precise values more weight than imprecise ones. The common age model (Galbraith et al. 1999) is a weighted geometric mean. It thus accounts for the log-normal distribution of De-values and for varying errors. According to Galbraith et al. (1999) the common age model is to be used when De datasets are homogeneous, thus when measurement uncertainties fully account for the observed spread of the De-values (Galbraith 2003). This is most likely not the case when measuring naturally dosed samples as some further variation is caused by microdosimetric effects in most samples. For overdispersed datasets, in which the observed spread exceeds the expected variation, the central age model is the most appropriate way to calculate the mean value (Galbraith et al. 1999). The central age model first estimates the overdispersion, that is the total spread in De-values less the expected spread due to measurement uncertainties. Overdispersion hence is produced by external factors of variation such as incomplete bleaching, bioturbation of microdosimetric effects. After estimation of the overdispersion, a weighted geometric

mean is calculated, but unlike for the common age model, the central age mean is weighted by the individual uncertainties on each De-value and the overdispersion. When the overdispersion is zero, the central age model reduces to the common age model. Both age models are designed for datasets, which consist of De-values from a single population.

Yet, in incompletely bleached samples and in samples affected by bioturbation, more than one De-population may be present. A lot of models have been presented in the past to calculate a mean De for incompletely bleached samples (e.g. Olley et al. 1998, Galbraith et al. 1999, Lepper et al. 2000, Fuchs and Lang 2001, Thomsen et al. 2003). All of these models concentrate on the lowest De-values, and therefore are often termed minimum age models. For samples affected by post-sedimentary mixing the most appropriate model for De-calculation is a finite mixture model, such as that presented by Galbraith and Green (1990). This model distinguishes between different De-populations, and for each population calculates a mean De based on the central age model. Rodnight et al. (2006) compared ages based on the minimum age model and the finite mixture model for incomplete bleached fluvial samples. From comparison with independent age control they concluded that the finite mixture model gave the more accurate results.

6.8 De-determination of the western Murray Basin samples

6.8.1 Sample preparation

The 100-250 µm quartz fraction of the bulk sample was extracted by dry sieving and then treated with hydrochloric acid (HCl, 10 %) and hydrogen peroxide (H_2O_2, 10 %) to remove carbonates and organic material. Density separation using sodium polytungstate was carried out to extract the quartz rich fraction (2.58-2.68 g/cm³). The remaining grains were subjected to hydrofluoric acid (HF, 40 %) for 40 minutes for removal of remaining feldspars and of the outer alpha-irradiated layer, and subsequently rinsed in HCl (10 %) to remove fluorides. The etched quartz grains were divided into three grain-size classes, 100-150 µm, 150-200 µm and 200-250 µm, by dry sieving.

Four different sizes of aliquots were prepared. For large multiple grain aliquots, quartz grains were attached to the central 8 mm Ø of a 9 mm Ø stainless steel disc using silicon spray. One large aliquot thus consists of >1000 quartz grains. For

medium and small multiple grain aliquots the same procedure was used but only covering the central 2 or 1 mm of the disc with quartz grains. This resulted in a total number of grains of ~200 ± 100 and ~50 ± 25, respectively. For the multiple grain aliquots, the grain-size class 100-150 µm was used. For preparation of single grain aliquots, a generous pile of quartz grains was mounted on the single grain aluminium disc. The disc was shaken on a piece of paper until all 100 holes of 300 µm diameter were filled with a grain each. The surface of the disc was then cleaned with a brush. For single grain aliquots, the grain-size class 200-250 µm was used to ensure that only one grain fitted in in each hole of the disc. For the age calculation, the different grain sizes used were accounted for by using different beta-attenuation factors (Mejdahl 1979, Brennan 2003).

6.8.2 Instrumentation

Two Risø TL-DA-15 luminescence readers were used for the OSL measurements. Both are equipped with blue LEDs (470 ± 30 nm) for stimulation of multiple grain quartz aliquots and $^{90}Sr/^{90}Y$ beta source for irradiation (Bøtter-Jensen et al. 1999a, 1999b). Dose rates of the beta sources are ~0.10 Gy/s in Reader B and ~0.19 Gy/s in Reader C. Reader C is additionally equipped with a green Nd:YVO_4 diode-pumped laser (532 nm) delivering a power density of ~50W/cm² for stimulation of single grains (Bøtter-Jensen et al. 2000, 2003). OSL signals were detected with an EMI 9235 photomultiplier tube after passing through a Hoya U340 optical filter (7.5 mm).

6.8.3 SAR protocol parameters

6.8.3.1 Preheat and cutheat temperatures

For routine SAR measurements, several parameters have to be chosen, dependent on the intrinsic luminescence properties of the samples. Two of these parameters are the preheat and cutheat temperature. In order to find the appropriate preheat temperature, preheat plateau tests were carried out on selected samples. These samples were chosen to cover samples from each dune field, and to approximately represent the range of equivalent doses expected from all western Murray Basin samples. For the tests, a SAR sequence was run on medium or large multiple grain aliquots, using four regenerative

doses at 40, 80, 120 and 160 % of the expected equivalent dose, a zero dose point and a repeat of the first regenerative dose. Stimulation was carried out for 50 s at 125°C, using blue LEDs. Each subset of samples, either consisting of six medium aliquots or three large aliquots, was measured with a different preheat temperature, ranging from 200 to 300°C hold for ten seconds, and two different cutheat temperatures of 160 and 220°C, followed by immediate cooling.

No significant change of De with preheat-cutheat combination was noticed in the samples with equivalent doses up to about 100 Gy. For samples with higher De-values, preheat-cutheat combinations of 200-220 and 220-220°C appear inappropriate, resulting in above average De-values. Fig. 6.12 visualises the results of the preheat plateau tests.

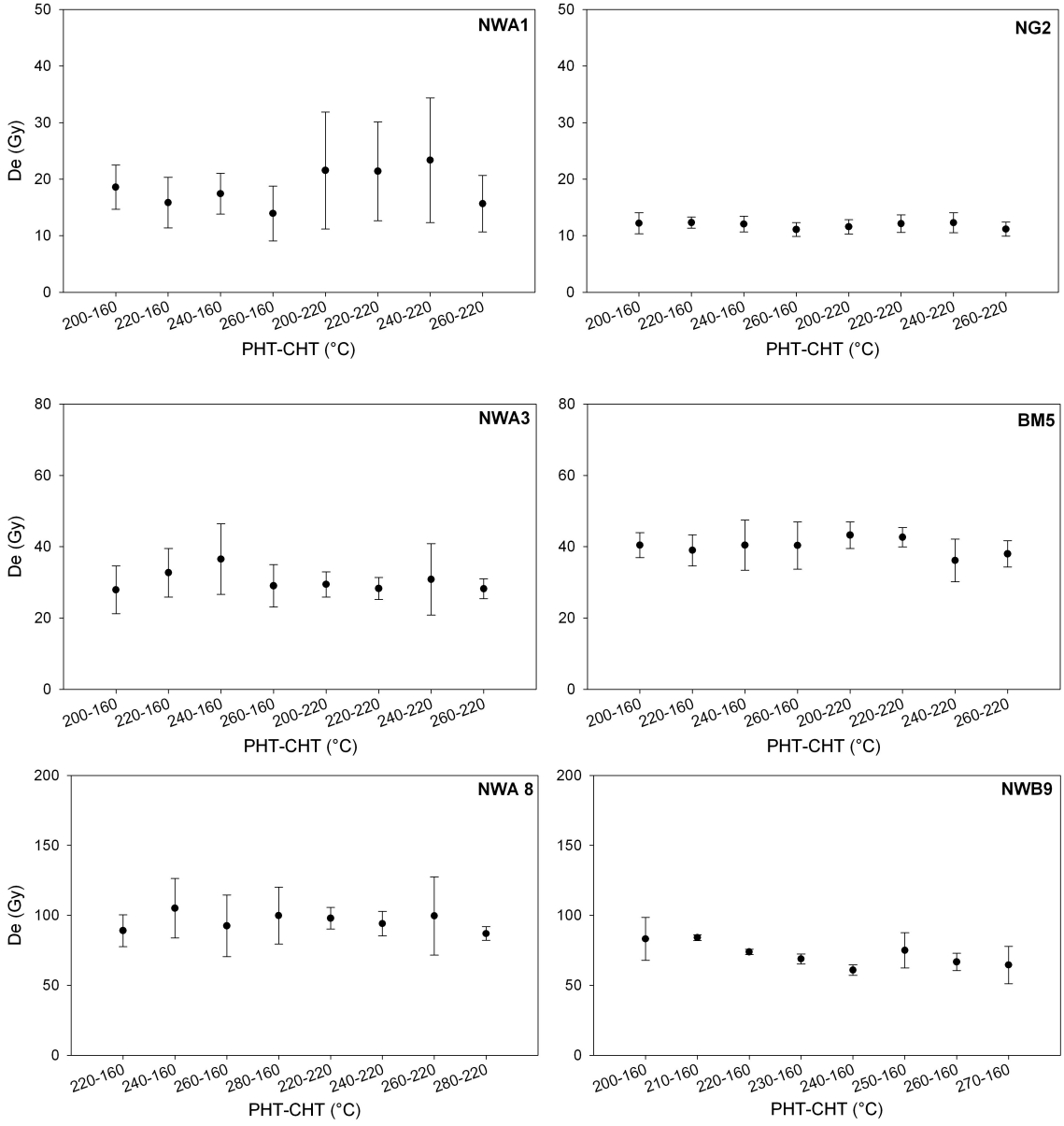

continued on the next page

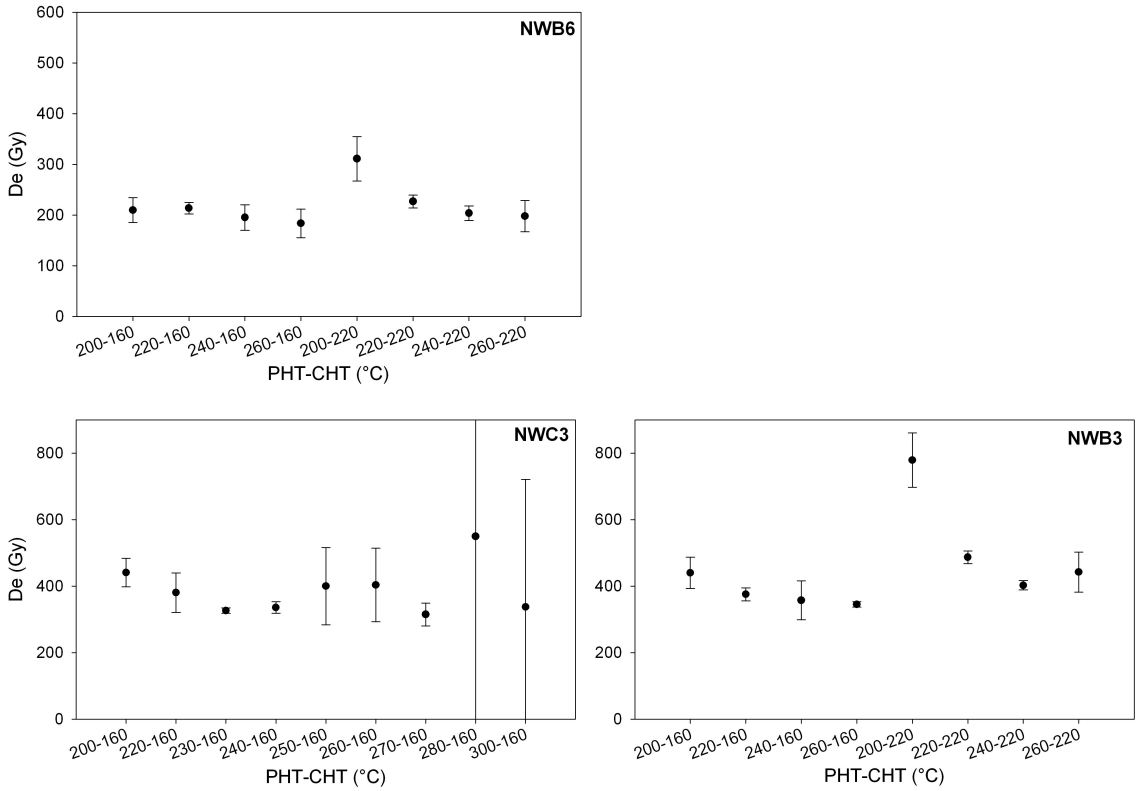

Fig. 6.12. Preheat plateau tests for selected samples from the western Murray Basin. Samples NWA1, NWA3, NWA8, NWB3, NWB6, NWB9 and NWC3 are from the linear dune field, sample NG2 is from the sub-parabolic dune field and sample BM5 from the Bunyip Sands formation. Note that samples NWB9 and NWC3 were measured with only one cutheat temperature (160°C). All other samples were measured with two different cutheat temperature (160 and 220°C). The error bars show the standard deviation of either three large or six medium aliquots.

In order to select the best preheat-cutheat temperature combination from these tests, three parameters were investigated. These were the the Δ_{Median}-value, the relative standard deviation (RSD) and the Recycling Ratio. The Δ_{Median}-value was derived by calculating the median value of all De-values (consisting of the arithmetic mean of either three or six individual De-values) from each preheat test. The De-value from each preheat-cutheat temperature combination was then divided by the median value. Values with above average equivalent doses thus yield Δ_{Median} values above 1. The relative standard deviation was calculated from the three or six individual De-values derived for each preheat temperature (also expressed as error bars in Fig. 6.12). The recycling ratio is expressed as the arithmetic mean of recycling ratios from either three or six measurements per preheat temperature. The three parameters are summarised in Tab. 6.1.

Tab. 6.1. Parameters for selection of the best preheat-cutheat temperature combination. All values are mean values derived from preheat plateau tests of nine samples, shown in Fig. 6.12.

PHT-CHT (°C)	Δ_{Median}	RSD	Recycling Ratio
200-160	1.08	0.15	0.99
220-160	0.97	0.11	1.02
240-160	0.96	0.15	1.02
260-160	0.93	0.16	1.00
280-160	1.15	0.49	0.99
300-160	0.83	0.70	0.98
200-220	1.40	0.21	0.96
220-220	1.08	0.14	1.01
240-220	1.06	0.17	1.02
260-220	0.96	0.21	1.00

The best Δ_{Median}-values closest to unity were found for preheat-cutheat combinations of 220-160, 240-160 and 260-220°C. Preheat-cutheat combinations of 300-160, 280-160 and 200-220°C resulted in the poorest Δ_{Median}-values. The smallest average RSD values was produced when using a preheat-cutheat temperature combination of 220-160°C, and largest for combinations of 280-160 and 300-160°C. The recycling ratios were within 2 % of unity for all preheat-cutheat combinations used, implying appropriate correction of sensitivity changes independent of the preheat-cutheat combination. Following these criteria, preheat temperatures of 220°C in samples with De-values <200 Gy and of 240°C in samples above 200 Gy were chosen, and combined with a cutheat temperature of 160°C.

The results from these preheat plateau tests were also applied for the single grain measurements, although the test were only carried out on multiple grain aliquots. Preheat plateau tests for the single grain measurements were considered impracticable, due to the large scatter in De-values associated with this method. It has to be considered though that individual grains from one and the same sample might react differently to preheat and cutheat temperatures (Ballarini et al. 2007).

6.8.3.2 Signal integration limits and illumination time

Another important parameter to be set in the SAR protocol is the signal integration limits in which the photon counts are collected. Integration limits are dependent on the brightness of the signal. For aliquots or grains with high luminescence sensitivities it is desirable to limit the integration interval to a small proportion of the initial signal. This ensures analysis of signal components derived from easy to bleach traps, namely the fast component (Murray and Wintle 2000) (see Section 5.5.2.1). For very dim grains, the initial integration interval should be larger, to reduce uncertainties from counting statistics. However, this bears the risk that the signal contains significant contributions from other components, which may be not fully bleached in nature and thus would lead to a De-overestimation (Bailey et al. 2003, Singarayer et al. 2005), or are thermally unstable, such as the S2 component (Singarayer and Bailey 2003) which could result in a De-underestimation. On the other hand, with longer integration intervals, measurement uncertainties derived from small-scale laser fluctuations can be decreased (Thomsen et al. 2005, Jacobs et al. 2006b).

Fig. 6.13 shows OSL decay curves of two single grains and of one multiple grain aliquot of sample NWA2. Signals of the single grains are reduced to background levels after ~0.6 s, and the multiple grain signal is reset after ~10 s of stimulation. Nevertheless, longer stimulation times of 2 s in case of the single grain measurements and 50 s in case of the multiple grain measurements were used. The different decay rate between single and multiple grain measurements results from the higher power density of the green laser (10 W/cm²) compared to the blue LEDs (~30 mW/cm²) (Bøtter-Jensen et al. 2000). In case of the two single grain decay curves, it can be seen that both grains have distinctively different signal intensities, although they have the same equivalent dose of around 16 Gy. The different signal intensities also result in different error estimates of 10 % for the dim grain and 1.5 % for the bright grain based on counting statistics.

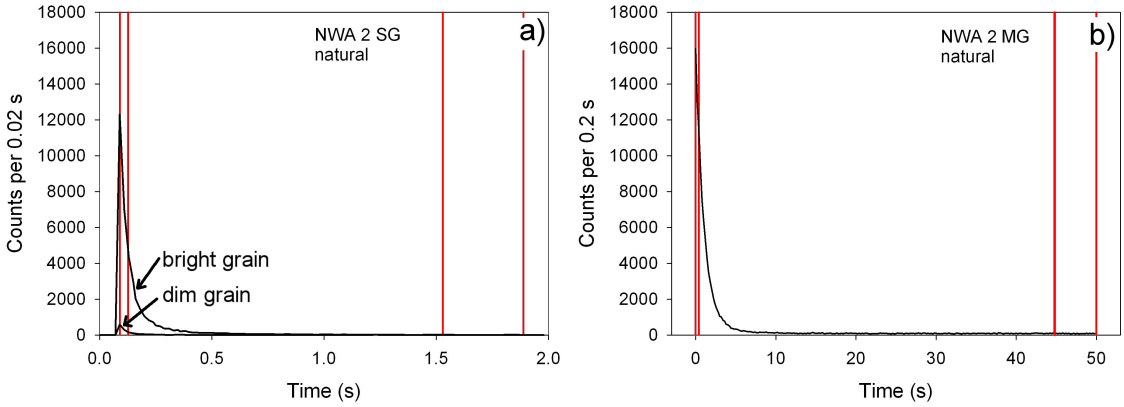

Fig. 6.13. OSL decay curves of the natural signals of (a) two single grains (SG) of quartz and (b) a small multiple grain aliquot (MG), and integration limits set for the western Murray Basin samples. Note that the signal intensities of the two single grains vary significantly, although both have the same equivalent dose.

Single grain signals were integrated over the first 0.04 s of the shine down curve subtracted by a background signal integrated over an interval from 1.5 to 1.9 s. For very bright grains, this interval is relatively large, but as it is not feasible to choose different integration limits for each grain dependent on its sensitivity, this interval was chosen to also account for weak signals of dim grains and reduce their uncertainties derived from counting statistics. In the multiple grain measurements, the signals were integrated over the first 0.6 s, subtracted by the signal integral of the last 5 s. By visual inspection of the single grain and the multiple grain decay curves and the chosen integration limits in Fig. 6.13 it can be seen that a much smaller part of the signal is analysed in case of multiple grain OSL measurements compared to the single grain measurements. While in case of the single grain measurements the signal is reduced to 35 % in the bright grain and 24 % in the dim grain within the integration interval, it is only reduced to 70 % in the multiple grain measurement. It is thus likely that the risk of measuring significant proportions of the medium or slow component is higher in case of the single grain measurements. On the other hand it has been demonstrated that the longer stimulation wavelength of the green laser compared to the blue LED results in a better isolation of the fast component (Singarayer and Bailey 2004, Thomas et al. 2005). Negative effects through larger integration intervals in the single grain measurements are thus possibly compensated for by the use of longer stimulation wavelength. Investigations on the components of the OSL signals using LM-OSL measurements on the western Murray Basin will be discussed in Section 6.8.4.1 and it will be seen that the samples analysed are dominated by the fast component.

6.8.3.3 Regenerative doses and test doses

In all multiple grain and single grain measurements, four regenerative doses were applied, followed by a zero dose to monitor recuperation effects and a repetition of the first regenerative dose to calculate the recycling ratio as a measure of sensitivity change correction. For most of the samples, regenerative doses of 40, 80, 120 and 160 % of the expected equivalent dose were chosen. The constant test doses were set to around 15 % of the expected equivalent dose as suggested in Murray and Wintle (2000). In all single grain measurements, a test dose of at least 4 Gy was applied, in order to reduce measurement uncertainties through poor counting statistics. In case of some younger samples, this means that test doses sometimes even exceeded the expected equivalent doses. However, Ballarini et al. (2007) have shown that test doses which are higher than the natural dose do not have a negative effect on the De-determination.

6.8.4 Tests on the suitability of the Murray Basin samples for a De-determination using the SAR protocol

6.8.4.1 LM-OSL measurements

As stressed by Wintle and Murray (2006), the SAR protocol is only appropriate for samples in which the OSL signal is dominated by the fast component. In order to investigate if the OSL signals of the western Murray Basin samples show a dominance of the fast component, LM-OSL measurements were carried out on selected samples. The samples analysed with this approach cover the three different geological formations (MS8, NWB2 and NWA2 from the linear dune field of the Woorinen Formation, NG2 from sub-parabolic dune field of the Molineaux Sands, and BM2 from the Bunyip Sands). Furthermore, four samples with comparatively low De-values and one with a high equivalent dose were chosen for analysing differences in signal composition in differently dosed samples. LM-OSL measurements of the natural signals were carried out on small multiple grain aliquots by linearly ramping the blue LED power from 0 to 90 % over a period of 3600 s at a stimulation temperature of 125°C. Before LM-OSL stimulation, samples were preheated at 220°C or 240°C for 10 s. Photon counts were collected in intervals of 4 s. The resulting LM-OSL curves were resolved into the components following the description of Choi et al. (2006a).

Total LM-OSL curves and the resulting components produced by the mathematical fitting procedure are shown in Fig. 6.14. Three of the investigated samples show only three components, which are the fast, the medium and one slow component. In other studies, for most samples at least five components, made up by the fast, medium and three slow components were identified (Choi et al. 2006b, Jain et al. 2003, Singarayer and Bailey 2003). However, Choi et al. (2006b) also found only three components in a sedimentary quartz sample from western Australia. Two other samples investigated here are composed of four components, due to the identification of two slow components. All samples investigated, whether comparatively young or old, show a strong dominance of the fast component, and only minimal contribution by the medium and slow components. It is thus concluded that the choice of integration intervals, especially the relatively large one in case of the single grain measurements, as discussed in Section 6.8.3.2, is not a problem for the samples investigated in this study. It has to be noted though that the number of components and contribution of the components to the initial signal might vary on a grain-to-grain scale (Bulur et al. 2002, Yoshida et al. 2003, Jacobs et al. 2008). Thus the multiple grain LM-OSL analyses might not be directly transferable to the single grain measurements.

Also investigated was the component composition of OSL signals induced by artificial beta doses. Fig. 6.15(a) shows the LM-OSL curve and resulting components induced by a regenerative dose of 150 Gy and a subsequent preheat of 240°C. LM-OSL measurement conditions were the same as for the natural signals described above. The total LM-OSL and the contribution of the different components are very similar to those of the natural signal of sample NWB2 shown in Fig. 6.14. Fig. 6.15(b) shows the LM-OSL which followed a test dose of 4 Gy and a subsequent cutheat of 160°C. Here, contributions of the medium and slow components are much higher. This behaviour is most likely a relic of the relatively low cutheat temperature of 160°C applied (Jain et al. 2003, Choi et al. 2003a, 2003b). However, as shown in the preheat plateau tests in Section 6.8.3.1, SAR measurements using 160°C cutheats yield the same results as SAR measurements with 220°C cutheats. The relatively strong contribution of the slow components to the test-dose induced OSL signals does not seem to have any significant effects on the resulting equivalent dose.

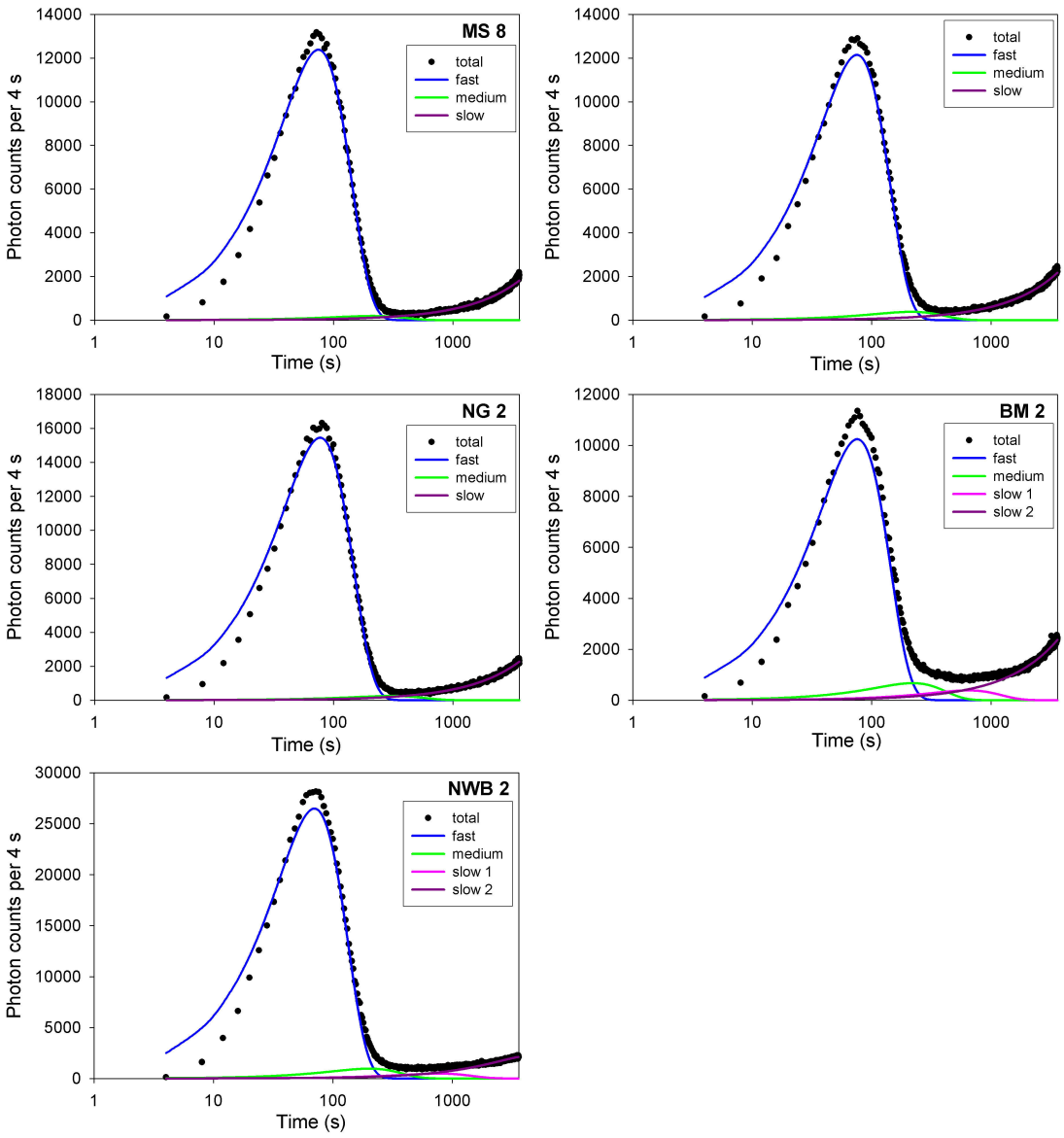

Fig. 6.14. LM-OSL curves and separation into several components through mathematical fitting of five naturally dosed samples from the western Murray Basin.

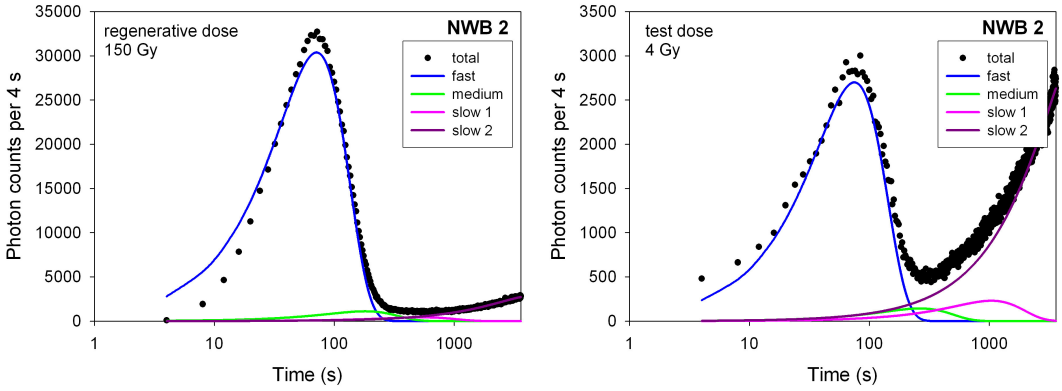

Fig. 6.15. LM-OSL curves and separation into several components through mathematical fitting of a laboratory dosed sample from the western Murray Basin. (a) The LM-OSL curve following a laboratory beta dose of 150 Gy and a subsequent preheat of 240°C for 10s, (b) the LM-OSL curve following a laboratory dose of 4 Gy and a subsequent cutheat of 160°C.

6.8.4.2 Test for feldspar contamination

In both single grain and multiple grain measurements, a test on potential feldspar contamination was carried out. The basic principle of this test is to administer a further beta dose to the aliquots after each SAR run, followed by a preheat and stimulation with IR diodes. A sample solely consisting of quartz grains should show no response to stimulation in the wavelength range of IR, whereas a contaminated sample would produce a clear IRSL signal and subsequent decay with stimulation time.
None of the samples measured using the multiple grains showed a response to IR stimulation. It is thus concluded that feldspar contamination is not a problem in the western Murray Basin samples. In single grain measurements the IRSL test procedure is slightly more complicated, as the single grain reader used does not contain an IR laser. As a consequence, the response of individual grains to IR stimulation cannot be tested directly. The IRSL test on single grains was carried out by repeating the last test dose cycle of the SAR run, with the only difference of intercalating an IR stimulation between the cutheat and the single grain OSL measurement, similar to the approach described in Duller (2003) and Jacobs et al. (2003a). The last seven steps of the SAR cycle are thus the following:

1. test dose
2. cutheat (160°C)
3. SG-OSL measurement (2 s at 125°C)
4. test dose
5. cutheat (160°C)
6. IR stimulation (20 s at 50°C)
7. SG-OSL measurement (2 s at 125°C)

If the SG-OSL signal of an individual grain measured in Step 7 is significantly lower than that measured in Step 3, than this grain is very likely a feldspar or a quartz grain with a feldspar inclusion. In Fig. 6.16, such a case is shown exemplarily for a SG-OSL measurement on sample MS4. It has to be noted that other possibilities for the signal reduction exist. These could be for example that the laser in the last SG-OSL measurement did not fully hit the grain, or that the differences in signal intensity merely represent measurement uncertainties. A further explanation is that sensitivity changes occurred between the measurement cycles used for the test on feldspar contamination.

The latter is considered relatively unlikely though as at the end of the SAR cycle the quartz grains should be sufficiently sensitised to not be seriously affected by sensitivity changes any more. However, in all samples, only a maximum of one or two grains showed a signal reduction after IR light exposure, implying that feldspar contamination is not of major importance in the samples investigated in this study.

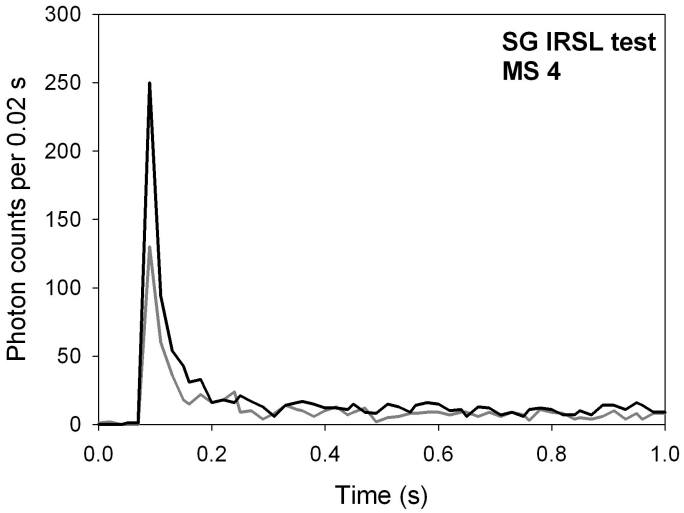

Fig. 6.16. IRSL depletion test to analyse feldspar contamination in single grains of quartz. The black line shows the OSL response to a test dose of 4 Gy, the grey line the OSL response to a test dose of 4 Gy followed by stimulation with an IR diode for 20 s.

6.8.4.3 Dose recovery tests and recycling ratios

Dose recovery tests were proposed by Murray and Wintle (2003) in order to check if the first test dose appropriately corrects sensitivity changes of the natural signal, which measurement is preceded by a preheat. For a dose recovery test, the palaeodose accumulated under natural conditions is reset, a known laboratory beta dose is administered and subsequently the administered dose is measured using the SAR protocol. If sensitivity changes which have occurred in the first measurement cycle (the measurement of the natural OSL signal) are correctly accounted for, then the ratio of the known beta dose and the measured dose will be unity. Furthermore, a dose recovery test provides information on the spread of a De-dataset in the absence of external sources of variation, such as incomplete bleaching, microdosimetric effects or post-sedimentary mixing (Wintle and Murray 2006). As samples measured in a dose recovery test are fully bleached through the LED exposure and irradiated homogeneously through exposure to the beta source, the spread observed in a dose recovery test will be of

intrinsic nature, hence derived from instrumental fluctuations and internal luminescence properties of the quartz grains.

For the dose recovery tests carried out in this study, the natural OSL was zeroed by exposure to blue LEDs for 100 s at 125°C. In case of the single grain dose recovery tests, green laser exposure for 5 s at 125°C was used for signal resetting. The tests were conducted on a wide range of samples with different equivalent doses. The beta doses administered were designed to closely match the equivalent doses obtained through OSL measurements on the naturally dosed samples. Tab. 6.2 summarises the results of the dose recovery tests. Administered beta doses ranged from 4 to 385 Gy. For a lot of samples, small aliquots or single grain aliquots were used to gain detailed information on the spread in data (the RSD in Tab. 6.2).

Tab. 6.2. Dose recovery tests carried out on the western Murray Basin samples. The table displays the size of the given dose, the preheat-cutheat-temperature combination used in the SAR protocol, the aliquot size (SG: single grain), the number of valid measured De-values, the ratio of the measured dose and the given dose (D_{rec}/D_{giv}) and the relative standard deviation (RSD).

Sample	Given dose (Gy)	PHT-CHT (°C)	Aliquot size (mm)	n	Ratio D_{rec}/D_{giv}	RSD (%)
NG2	4	220-160	SG	18	1.02	9.8
PSP14	10	220-160	SG	39	1.02	8.8
CC4	10	220-160	1	16	1.00	2.6
NWC7	10	220-160	1	18	1.01	3.0
SW6	25	220-160	1	23	1.00	6.7
SW7	25	220-160	1	24	0.98	3.6
SW4	30	220-160	1	24	1.00	4.6
SW5	30	220-160	1	20	1.00	7.2
MRR1	90	220-160	1	15	0.96	4.6
NWB7	114	220-160	1	9	1.00	3.3
NWB7	114	220-160	SG	48	1.01	18.5
SW2	120	220-160	1	24	0.99	10.4
SW1	150	220-160	1	24	1.00	7.1
WP13	160	220-160	2	6	1.02	5.4
NWC1	200	240-160	2	6	0.94	5.4
NWB6	257	240-160	2	6	0.87	6.5
NWC3	320	240-160	SG	29	1.02	25.1
NWC3	334	240-160	1	11	0.97	11.5
MS0	350	240-160	1	17	0.85	30.5
NWB1	385	240-160	2	6	1.12	18.5

The results of the dose recovery tests were excellent for samples which were given a dose <200 Gy. All samples yielded dose recovery ratios within 4 % of unity, the majority of the samples even within 2 % of unity. This clearly demonstrates the suitability of the western Murray Basin samples (with equivalent doses from ~0-200 Gy) for OSL measurements using the SAR protocol of Murray and Wintle (2000, 2003). The relative standard deviation in samples <200 Gy, measured with small aliquots, ranged from 2.6 to 10.4 %. Samples that were given beta doses >200 Gy yielded dose recovery ratios within 15 % of unity. The reason for the increased discrepancy between the given dose and the measured dose is most likely not caused by inappropriate correction of sensitivity changes in the first measurement cycle, but by the OSL signal approaching saturation (see Section 6.8.5). This is also confirmed by the increased RSD values. The increased spread in data also results in increased (relative) standard errors, and even when considering these errors, the given dose and the measured dose differ significantly from each other (except for sample NWC3). The severest discrepancies occur in samples NWB6 and MS0, which are underestimated by at least 10 % and 8 %, respectively, when considering their standard errors. Sample NWC1 is underestimated by at least 4 % and sample NWB1 is overestimated by at least 4 %. Together with the evidence of signal saturation occurring on average at around 200 Gy, the dose recovery tests further underline that reliable equivalent doses above 200 Gy are difficult to obtain.

The RSDs of the single grain measurements are higher than those of the multiple grain measurements. This was expected, as variations of De-values on a single grain scale are averaged out in multiple grain measurements, as long as the samples contain many luminescent grains. This is the case for the western Murray Basin samples, as will be seen in Section 6.8.6.

All recycling ratios measured were within 10 % of unity, thus sensitivity changes were appropriately corrected. This further demonstrates the suitability of the SAR protocol and the chosen measurement parameters for determining the equivalent doses on the western Murray Basin samples.

6.8.5 The resulting growth curves and signal saturation

The applied SAR protocol resulted in growth curves with six dose-response data points, consisting of four regenerative dose-response points, one zero dose-response point, and

a repetition of the first dose-response point. Most of the aliquots measured showed saturating exponential plus linear growth. Further functions observed were linear growth in very young samples and saturating exponential growth in very old samples approaching saturation.

The origin of each growth curve results from the zero dose signal, included in the SAR protocol to monitor recuperation. If significant recuperation effects occur, then the growth curve will not pass through the origin but will intercept with the y-axis in height of the sensitivity corrected zero-dose signal. A growth curve for a grain which exhibits some recuperation (14 % of the natural signal) from the western Murray Basin is shown in Fig. 6.17. However, less than 5 % of all single grains which passed the rejection criteria (Section 6.8.7.2) exhibited significant recuperation >7 % and these grains were removed from the data sets. In the multiple grain measurements, no significant recuperation was detected at all.

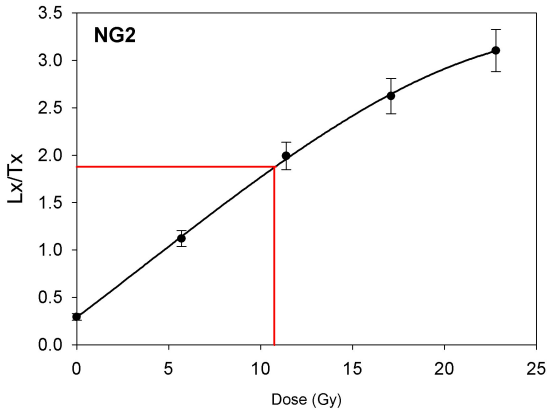

Fig. 6.17. Growth curve of a single grain with high (14 %) recuperation.

Fig. 6.18 shows growth curves from single grains for a young sample (PSP 1, ~2 Gy) and a medium aged sample (NWB9, ~80 Gy). In the young sample (PSP1), growth behaviour of the single grains is relatively uniform. The majority of the grains show linear growth up to the highest dose administered (38 Gy), although two grains already show clear exponential plus linear growth. In the older sample (NWB9), growth behaviour is more variable from grain to grain. Some grains still show clear signal growth with doses up to 180 Gy, whereas other grains already approach saturation at about 90 Gy. It was also investigated whether growth behaviour of individual grains in these two samples was related to their luminescence sensitivity. In Fig. 6.18, different sensitivity of the grains is expressed by four different colours of the growth curves, with yellow curves representing very bright grains, red curves bright grains, green curves

grains with medium sensitivity, and blue curves dim grains. The first test dose response was taken as the measure for the sensitivity. No clear dependency of sensitivity and signal growth could be observed. By inspecting the growth curves of sample NWB9 though, it appears that some of the dim grains saturate at much higher levels than brighter grains. Possibly this implies that in dim grains it is not the amount of electron traps that limits their sensitivity, but the rate of electron ionisation and trapping and/or of recombination of electrons at luminescence centres.

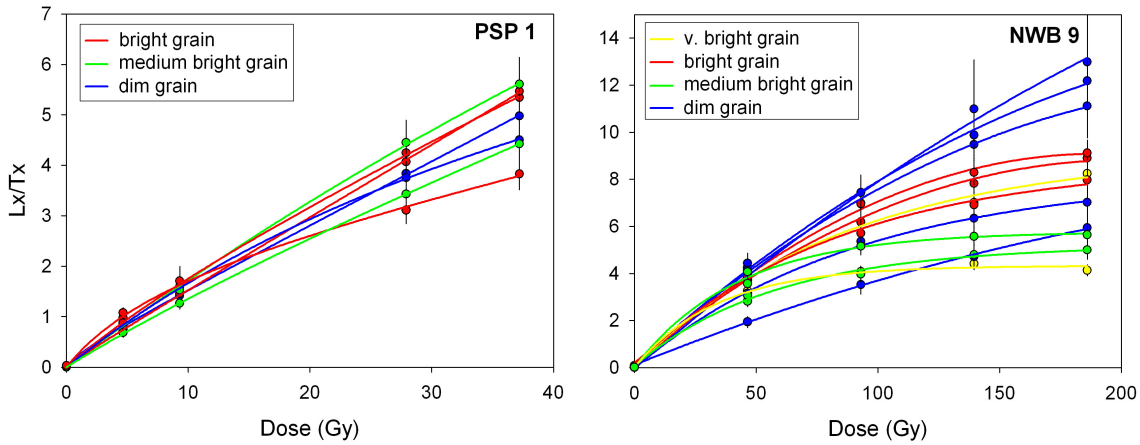

Fig. 6.18. Single grain growth curves of samples PSP1 with a De of ~2 Gy and of sample NWB9 with a De of ~80 Gy. Different luminescence sensitivity of the grains is indicated through different colours of the growth curves.

As the amount of electron traps is limited in natural dosimeters such as quartz, at some point signal intensities will not increase with higher doses. The dose at which saturation occurs might be different from sample to sample, or even from grain to grain within one sample, as already shown in the further above. For example, Roberts et al. (1999) and Yoshida et al. (2000) presented single grain measurements on Australian quartz samples and showed that for the majority of grains, OSL signal saturation occurred between 100 and 200 Gy, but that in some grains it was not reached even at 400 Gy.

Wintle and Murray (2006) suggested calculating saturation levels as 2*Do, with Do being a parameter of the saturating exponential growth curve function (see Section 5.5.4). In Tab. 6.3, average (median) Do and 2*Do values are given for three of the western Murray Basin samples with the highest palaeodoses, as derived from multiple grain growth curves. For further two samples, 2*Do values from single grain growth curves are given. Also, the range of 2*Do values is indicated.

Tab. 6.3. Average (median) and range of Do and 2*Do values of the four oldest samples from the western Murray Basin.

Sample	Do (Gy)	2*Do (Gy)	Range of 2*Do (Gy)
MS0 (MG)	108	216	194-252
NWB1 (MG)	98	196	128-330
NWC1 (MG)	92	184	130-242
NWC 1 (SG)	109	218	88-746
PSP3 (SG)	96	192	60-552

From the average 2*Do values it follows that equivalent doses above 200 Gy are difficult to obtain. One multiple grain growth curve of sample NWB1 had a 2*Do value of ~330 Gy, allowing De determination up to this value.

The single grain growth curves showed similar average 2*Do values, but the range of the 2*Do is much greater. Potentially, for some individual grains, equivalent doses of up to ~750 Gy in sample NWC1 would be determinable. As it is difficult though to measure enough grains with growth curves exhibiting high Do-values in order to obtain a statistically sound dataset, all ages calculated from equivalent doses >200 Gy for the western Murray Basin samples are considered unreliable.

6.8.6 Multiple grain De-distributions

In order to achieve reliable De-estimates it is important to investigate if individual De-values from one sample are from a single population. If this is not the case, then the reason for multiple populations, such as incomplete bleaching or bioturbation have to be assessed, and the population that most likely reflects the true burial dose has to be selected for the mean De-determination.

Fig. 6.19 shows De-distributions from small-aliquot multiple grain measurements from Section SW, displayed as radial plots.

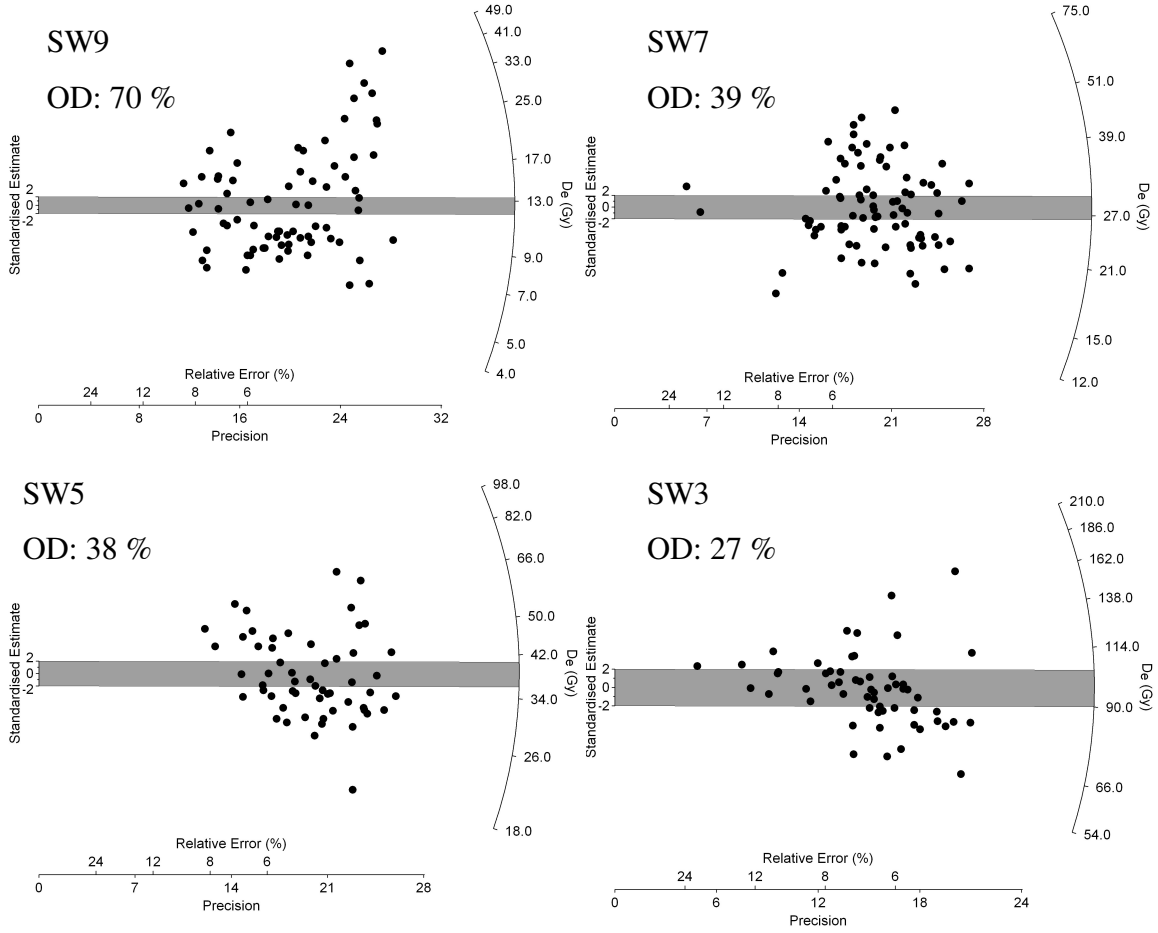

Fig. 6.19. Radial plots showing the De-distributions of four samples from section SW, located in the linear dune field of the western Murray Basin.

It can be seen from Fig. 6.19 that all samples are highly overdispersed. Overdispersion is highest in the youngest sample (SW9). In order to evaluate the degree of the observed spread it is important to know how many grains on a multiple grain aliquot produce a detectable luminescence signal. For example, in several single grain studies it was demonstrated that 95 % of the total light sum originated from only 5 to 10 % of grains (Duller et al. 2000, Jacobs et al. 2003a, Duller 2006). When such a sample is measured using small multiple grain aliquots consisting of around 50 grains, then only two or three grains would dominate the total luminescence signal. In such samples, a high scatter of De-values is not surprising. However, the western Murray Basin samples show a marked difference in sensitivity to the samples presented by Duller et al. (2000), Jacobs et al. (2003a) and Duller (2006). In Fig. 6.20, the sensitivity of 200 grains from selected samples of the western Murray Basin is shown. As can be seen, an average of about 50 % of the grains give detectable luminescence signals >50 counts per 0.04 s. The sensitivity and amount of luminescent grains of some samples is even comparable

to that of a calibration quartz sample (Risø) which has been deliberately sensitised by annealing it to 1000°C.

Thus, when small multiple grain aliquots of the western Murray Basin samples are measured, the total luminescence signal of one aliquot will reflect the sum of luminescence signals from about 25 grains, provided the small aliquot contains about 50 grains. Considering this, the high overdispersion already observed on a multiple grain scale should be even more pronounced when analysing single grains. Furthermore, the usefulness of De-distribution methods on multiple grain measurements has to be questioned for the western Murray Basin samples, bearing in mind that De-values derived from mixed luminescence signals from multiple grains are compared to each other. Therefore, in the following chapter, De-distributions from single grain analysis will be used to infer possible reasons for the high degree of scatter in the De-values of the Murray Basin samples.

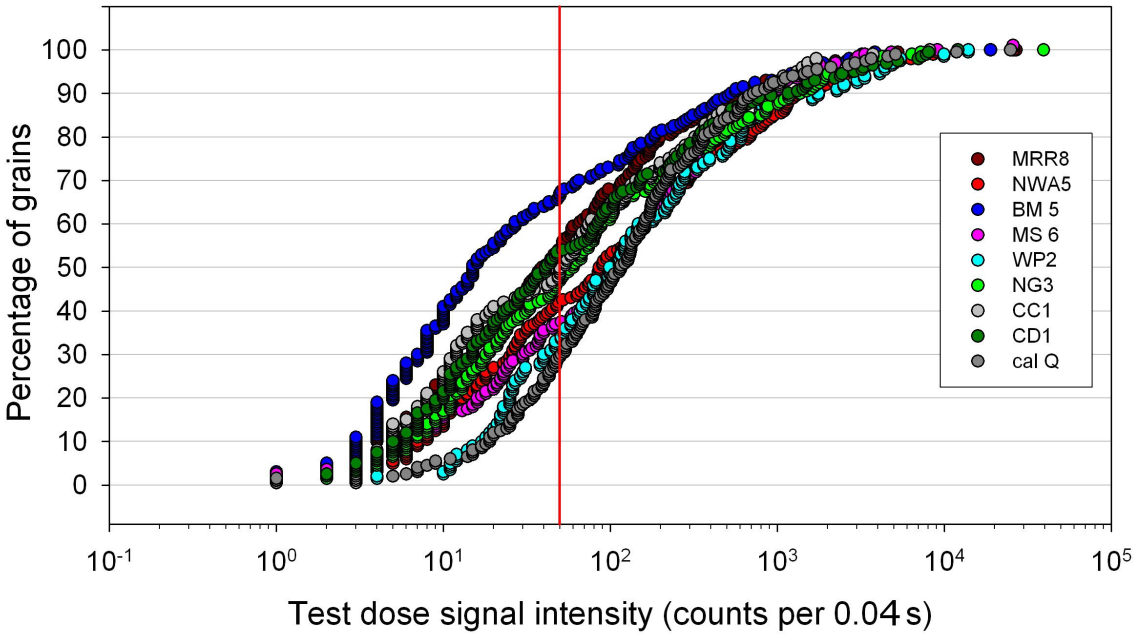

Fig. 6.20. OSL response to the first test dose (5.7 Gy) of selected samples from the Murray Basin and of the Risø calibration quartz. Note the logarithmic scale of the x-axis. The red line highlights the threshold of 50 counts, above which OSL signals are high enough to produce meaningful growth curves.

6.8.7 Single grain De-distributions

When interpreting single grain De-distributions, a careful assessment of the degree of scatter induced by the measurement itself needs to be carried out (Duller et al. 2000, Thomsen et al. 2005, Jacobs et al. 2006b). Single grains can have very low signal intensities compared to multiple grain aliquots, thus variations of De-values due to poor

counting statistics are much more common than in multiple grain dating. A further problem is associated with instrumental fluctuations. For example, when the beta source of a luminescence reader does not deliver a uniform dose to the sample, this will be particularly noticed in single grain dating as every grain will receive a different dose according to its position beneath the beta source. In multiple grain measurements, the effects of a non-uniform beta dose rate will be averaged out. In the following, the uniformity of the beta dose rate in the luminescence reader used for western Murray Basin samples will be tested and the influence of counting statistics on the De-distribution will be assessed. Subsequently, external sources of variations on the De-values of the samples investigated in this study will be discussed.

6.8.7.1 Assessment of the homogeneity of the beta source

Before analysing the single grain De-distributions for information on external sources of variations, some aspects on the reproducibility of the single grain luminescence reader used in this study will be discussed. Errors induced by instrumental variations might be different for each luminescence reader and need to be estimated from De-measurements of calibration samples which have received a known and uniform dose. Such a calibration sample, provided by Risø, was used to test the dose rate uniformity of the beta-source in the single grain reader, and to estimate the amount of uncertainties induced by instrumental variation. Studies on the instrumental reproducibility of single grain readers were carried out by Truscott et al. (2000), Thomsen et al. (2005) and Jacobs et al. (2006b). Truscott et al. (2000) found an instrumental uncertainty of 3.5 % in the reader they used. Values from Thomsen et al. (2005) and Jacobs et al. (2006b) are lower with 2.5 and 2.1 % respectively. The better reproducibility in the more recent studies was ascribed to technical improvement of the measurement devices (Jacobs et al. 2006b).

In this study, eight single grain aliquots were prepared using the Risø calibration quartz. The De of the quartz grains was determined by running a SAR sequence with three regenerative doses of 4.8, 9.5 and 14.3 Gy, and test doses of 5.7 Gy, a preheat of 220°C for 10 s and a cutheat of 160°C. Signals were retrieved by green laser stimulation for 2 s at 125°C. De-values could be determined for 307 grains, and the data set had a relative standard deviation of 17 %. From these 307 De-values, the weighted mean De for each of the 100 positions on the single grain disc was calculated, usually consisting of three

individual De-values. Subsequently, the dose rate for every individual position on the single grain disc was determined by dividing the equivalent dose (in s) by the known calibration dose of 5 Gy. When displayed as a 3D-plot, it becomes very obvious that the dose rate delivered by the beta source of the single grain reader is not uniformly distributed (Fig. 6.21).

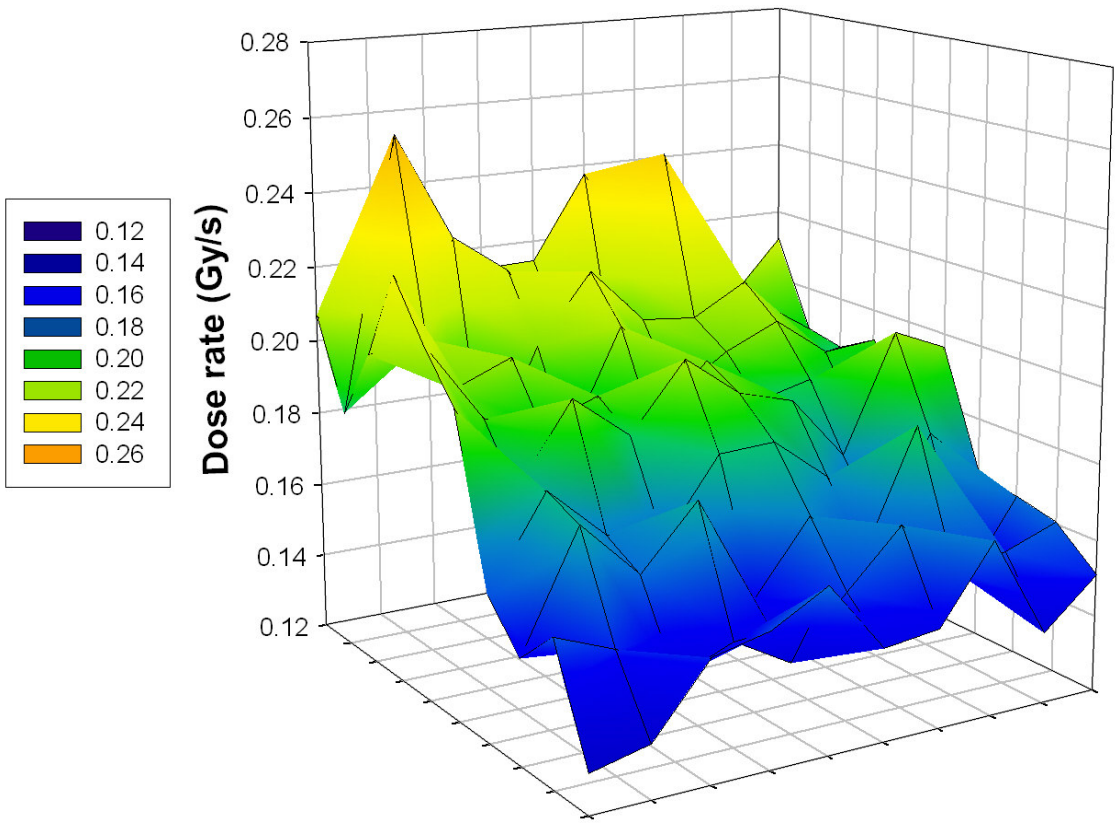

Fig. 6.21. Dose rate distribution of the beta source of the single grain luminescence reader used for the single grain De-determination of the western Murray Basin samples.

Dose rates from one margin of the disc to the other vary by about a factor of two. A possible reason for this is that the beta source is tilted to a certain degree. A very similar dose rate distribution was found by Ballarini et al. (2006), with the same variation by an order of two. The non-uniform distribution can be corrected by using individual beta source dose rates for each position on the disc. For this correction the rather rough surface seen in Fig. 6.20 was smoothed by assuming that the beta source was installed in the reader with a certain tilt, and that the dose rate was uniform if the source was arranged in a planar way. A certain degree of uncertainty by this modelled dose-rate distribution thus has to be expected.

When the De-dataset of the calibration quartz is corrected for position specific dose rates, the relative standard deviation reduced from 17 % to 12 %. None the less, even

after this correction, the observed spread is relatively large, considering that the calibration quartz sample was thermally annealed and homogeneously irradiated. This is also expressed in an overdispersion value of 10 %. Only when incorporating an instrumental error of 3.5 % in the total error calculation of individual De-values, the data set becomes approximately homogeneous, when using the homogeneity test described by Galbraith (2003). The instrumental error of 3.5 % is relatively large compared to values of 2.1 and 2.5 % recently determined by Jacobs et al. (2006b) and Thomsen et al. (2005). Most likely the non-uniform dose rate, and uncertainties related to the dose rate correction for individual positions on the disc contributes to this additional instrumental uncertainty. For the following De-determinations on the naturally dosed samples from the western Murray Basin, an instrumental error of 3.5 % was incorporated in the De-uncertainty estimation.

6.8.7.2 The influence of counting statistics on the De-distribution and the choice of rejection criteria

In single grain De-determination, it is crucial to set some threshold values in order to decide if a signal and a De-value present reliable estimates and whether they should be included into the total data set. To assess the influence of the rejection criteria on the samples used in this study, the single grain data set of sample NG2 was analysed using different rejection criteria, in order to determine which rejection criteria have the greatest influence on the distribution and the mean De-value, and to assess the influence of SAR performance and intrinsic luminescence properties on the De-distribution of a natural sample.

The most important rejection criterion was found to be the test dose error. This error reflects the uncertainty of the first test dose response due to counting statistics and thus provides a good measure of the brightness of a grain (Duller 2005). When analysing two single grain aliquots of sample NG2, De-values of 81 grains could be obtained, when no rejection criteria were applied. The relative standard deviation of this data set is 32 % and the overdispersion is 18 %. The data set has a central age mean De of 10.9 ± 0.3 Gy. When all grains with a test dose error >10 % are removed from the data set, the number of valid De-values reduces to 44. Despite this significant reduction of De-values, the spread in De-values decreases from 32 to 21 %. The overdispersion of this data set is 17% and the central age mean De 10.9 ± 0.4 Gy. The influence of the test

dose error on the spread of the data set highlights the importance to exclude dim grains from a data set, as the signal of grains with low luminescence sensitivity is measured with a high uncertainty. Therefore dim grains contribute significantly to the spread in single grain De-datasets, as already pointed out by Duller et al. (2000). Fig. 6.22 shows the total data set of sample NG2 (where no rejection criteria were applied), in which the De is plotted on the y-axis and the test dose signal intensity on the y-axis. Bright grains with a test dose error <10 % are highlighted with red circles. It is obvious that the De-values of dark grains in the left part of the diagram exhibit a greater spread than those of bright grains in the right part of the diagram.

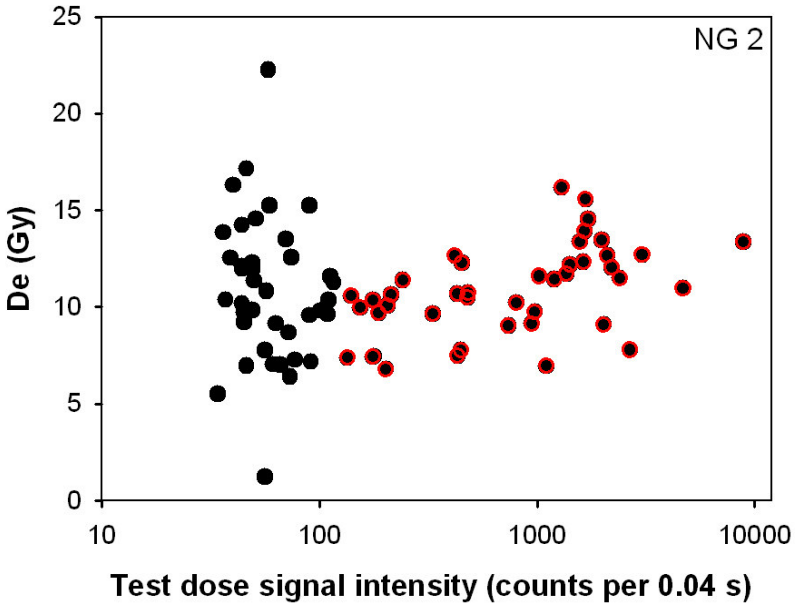

Fig. 6.22. De-values plotted against the signal intensity of the first test dose response of a naturally dosed sample from the western Murray Basin (NG2). The total data set (black dots, n = 81) is obtained, when no rejection criteria are applied. By setting the rejection criterion 'test dose error' to 10%, dark grains with a low test dose response are removed from the data set. Bright grains, which passed the 'test dose error' rejection criterion are highlighted with red circles.

As can be seen in the example discussed above, the rejection criterion 'test dose error' does not influence the mean De-value. This is because dim grains have a high uncertainty and their contribution to a weighted mean De-value, such as the central age mean, is low. Furthermore, grains with low De-values as well as grains with high De-values are removed from the data set when applying the rejection criterion 'test dose error'. When analysing De-distributions in order to gain information on external sources of variations in De-values, such as incomplete bleaching or bioturbation, it is recommended to reduce variations in De-values induced by counting statistics to a minimum. The rejection criterion 'test dose error' was therefore set relatively strict for the western Murray Basin samples. For young samples with a test dose of 4-6 Gy, the

threshold was set to 10 % and for older samples, where test doses of >6 Gy were used, the threshold was set to 5 %. By the application of this rejection criterion the number of valid De-values reduces significantly, as can be seen by the example discussed above. When a test dose of 5.7 Gy is used, grains with a test dose response <140 counts (in the first 0.04 s) are rejected. In Fig. 6.20 it can be seen, that from hundred grains, an average of 30 grains have a test dose signal >140 counts. The average number of valid grains per single grain aliquot correspondingly ranges from 20-30 grains in the western Murray Basin samples.

Although selecting only relatively bright grains for determination of the De, a certain scatter induced by counting statistics remains in the De-datasets of the naturally dosed samples. For example for sample NG2 the average scatter induced by counting statistics alone is around 4 % when grains with a test dose error > 10% are rejected and this has to be considered when analysing the external factors of variation. However, the central age mean allows calculating the overdispersion, which is the spread in data exceeding the spread induced by counting statistics, the instrumental error and the curve fitting procedure. Assessment on the degree of scatter induced by external factors is thus nonetheless possible.

The rejection criteria recycling ratio (10 %) and recuperation (7 %) had no effect on the total data set of sample NG2. None of the grains hat a recycling ratio exceeding 10 % from unity and only two grains had a recuperation of >7 %. Removal of these grains did not change the central age mean De or the relative standard deviation. Furthermore, no grains of this sample showed a significant (>30 %) reduction of the OSL after IR exposure (see Section 6.8.4), thus no feldspar contamination was present in this sample. In all subsequent measurements of other samples, grains with a recycling ratio exceeding 10 % of unity, a recuperation of >7 % and a signal reduction of >30 % after IR exposure were rejected.

6.8.7.3 External factors of equivalent dose variation in the western Murray Basin samples

After considering causes of variations through the luminescence measurements alone (counting statistics and instrumental variations), the further spread in the natural samples can be mainly ascribed to external factors such as microdosimetry, bioturbation, and incomplete bleaching.

With one exception, all the samples from the linear dune field in the western Murray Basin yielded overdispersion values of over 30 %. The maximum overdispersion in these samples was 84 % (a radial plot of the De-distribution of this sample is shown Fig. 6.23(a)). In the sub-parabolic dune field overdispersion was much lower in the majority of samples, averaging around 20 % (Fig. 6.23(b)). An exception from this behaviour was found in section CD, where overdispersion ranged from 44 to 71 %. Average (median) overdispersion values for the linear and the sub-parabolic dune field are shown in Tab. 6.4. The values are further grouped according to the mean De, in order to investigate if a relationship exists between the amount of external scatter and the size of the equivalent dose. From this grouping it can be seen that samples with low De-values yield highest overdispersion values.

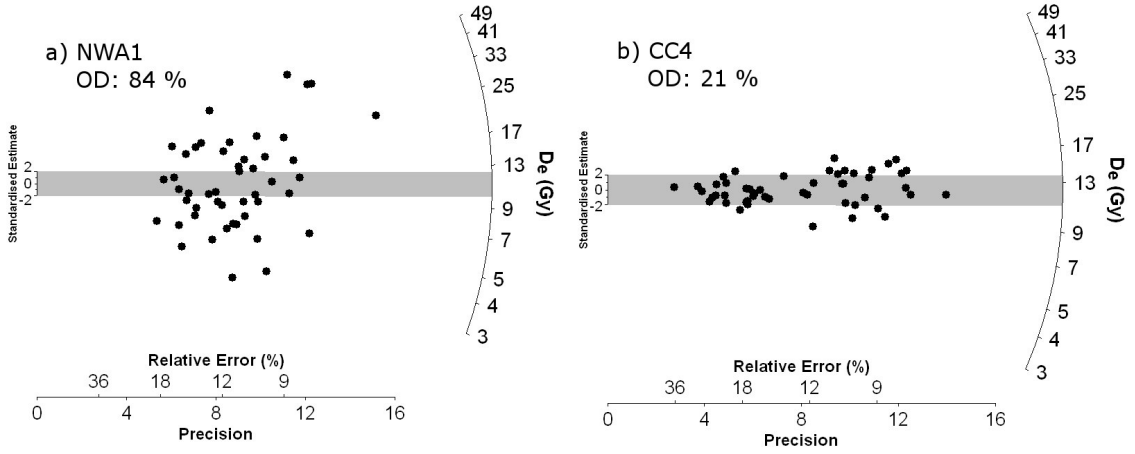

Fig. 6.23. Radial plots of single grain De-values from (a) sample NWA1 from the linear dune field, with the highest overdispersion value observed of all samples investigated and (b) sample CC4 from the parabolic dune field with one of the lowest overdispersion values of all samples investigated.

Tab. 6.4. Average (median) overdispersion values of single grain De-values grouped according to the dune field and to the size of the equivalent dose.

Dune field	0-5 Gy	5-13 Gy	13-20 Gy	20-30 Gy	30-50 Gy	50-100 Gy	100-190 Gy	>190 Gy
linear	0.72	0.56	0.69	0.44	0.52	0.40	0.40	0.41
sub-parabolic		0.22				0.19		

From these average overdispersion values, their dependence on the size of the equivalent dose, and the distinct difference in scatter from the two dune fields, some conclusions can already be drawn in respect to the sources of this wide variation in

equivalent doses. The fact that overdispersion values are higher for samples with low equivalent doses argues against microdosimetry as main source of variation, otherwise the observed spread would be independent of the size of the equivalent dose. Factors like incomplete bleaching and bioturbation, on the other hand, are much more likely to have a larger effect on low dosed samples. If, for example, a sample contains a few incompletely bleached grains with a residual dose of 5 Gy, these grains will deviate significantly from the mean De of a young sample, whereas in an old sample of 100 Gy, a 5 Gy deviation from the mean De will not be noticed as it will be masked by the measurement uncertainties. The same applies to post-sedimentary mixing. A sample mixture from a 2 Gy and a 4 Gy sand layer will have a higher relative standard deviation (and overdispersion) than a sample mixture from a 22 Gy and 24 Gy sand layer. In the following, the three possible external factors of variation will be investigated in more detail, in order to detect the major source of variation and account for it by the most appropriate mean De-calculation.

6.8.7.3.1 Incomplete Bleaching

Aeolian samples are usually assumed to be completely bleached due to the thorough and direct exposure to daylight during aeolian transport and deposition (Bailey et al. 2003, Bray and Stokes 2003, Singarayer et al. 2005). Nevertheless, incomplete bleaching of Australian dune sands due to rapid deposition has also been reported in the past (e.g. Twidale et al. 2001).

It has been shown in the previous section that especially the sands from the linear dune field show especially high overdispersion values. This creates the suspicion that the intense iron/clay crusting could have prevented the complete bleaching of the quartz grains. This theory of course only holds under the assumption that the iron/clay-coatings are a pre-depositional feature, and not a product of post-depositional weathering. It has been shown by Bowler et al. (2006) that the linear dune sands inherited their coating from their source material; they are pre-depositional. Evidence for this theory can also be observed in the field by the fact that modern sands have the same intense red colour as older dune sands, arguing against the red colour being a product of weathering.

Several approaches to detect incomplete bleaching in luminescence methods are discussed in the literature, the most common being analysis of De-distributions (e.g. Bailey and Arnold 2006), analysis of the different components of the OSL signal (e.g. Bailey 2000a) or age determination of modern samples (e.g. Fiebig and Preusser 2007).

Recently, Bailey and Arnold (2006) presented threshold statistic parameters of De-distributions in order to assess if a sample was incompletely bleached. The parameters used by the authors were overdispersion, weighted skewness and weighted kurtosis. When applying these criteria on the western Murray Basin samples all of the samples with equivalent doses <20 Gy from the linear dune field would fall into the category of incompletely bleached samples. However, the threshold values of Bailey and Arnold (2006) should be treated with caution, as distributions from samples affected by post-sedimentary mixing were not considered in their model. Positive skewness however is also common in samples where older grains intruded into younger layers by bioturbation. Therefore, other tests to investigate the degree of bleaching in the samples from the linear dune field of the western Murray Basin were carried out.

LM-OSL curves

In Fig. 6.14 (Section 6.8.4), LM-OSL curves of several samples and were shown. Three of these investigated samples (MS8, NWA2, BM2) exhibit an extraordinary wide spread in equivalent doses. None of these samples showed significant contributions of the medium or slow components. This argues for the fact that bleaching times during transport and deposition were long enough to reduce the slowly bleachable components to negligible values. It follows that under these circumstances, the fast component will also be bleached during transport and deposition.

Equivalent doses of modern samples

Some of the linear and parabolic dunes in the western Murray Basin contain massive caps of modern dune sands which are possibly the product of land clearance and/or bush fires. These modern sand caps provide an excellent opportunity to investigate if they were fully bleached during transport and deposition by testing if they yield zero luminescence ages. In this study, two modern samples were analysed to test the zero-age assumption. Sample MS9 is derived from a linear dune near Loxton in the eastern margin of the study area, and sample BM1 is derived from a Bunyip Sands parabolic dune. Sampling depth is 1.10 m for sample BM1 and 1.55 m for sample MS9, and both samples exhibit intense red or brown-red colour due to iron/clay-coatings.

For sample BM1, three discs (~300 grains), and for sample MS9, one disc (~100 grains) were measured using the SAR protocol. After applying the rejection criteria described in Section 6.8.7.2, 79 De- values could be obtained for sample BM1 and 52 for sample

MS9. In Fig. 6.24, histograms for sample BM1 and MS9 are shown, also displaying individual De-values and their errors (it is not possible to show the distributions of these samples as radial plots as they do not permit the display of zero and negative De-values).

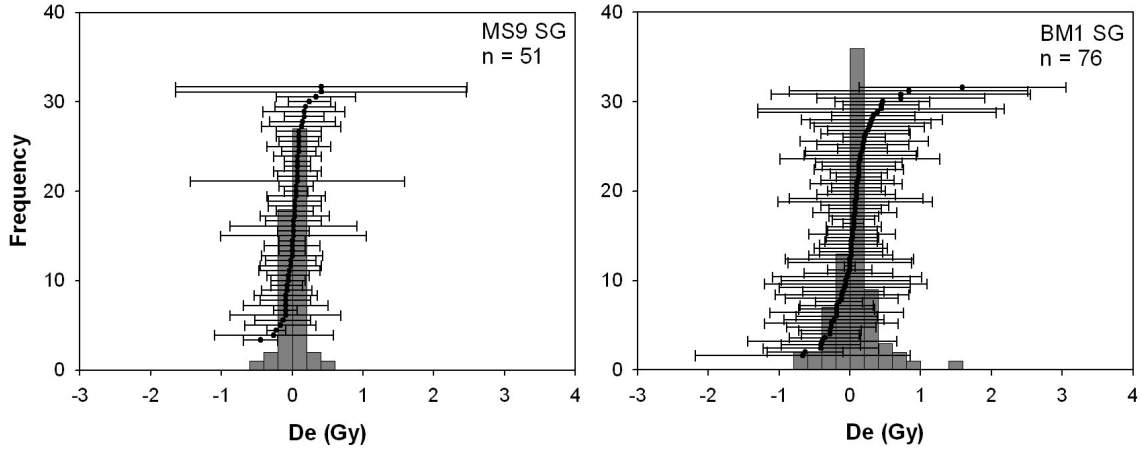

Fig. 6.24. Histograms of single grain De-values from two modern samples from the western Murray Basin.

The distributions of both samples are narrow, non-skewed and cluster around a zero De. Furthermore, within errors, sample MS9 yielded one (negative) De-value out of 52 distinguishable from zero, and sample BM1 two De-values out of 76 distinguishable from zero (the outlier at 1.59 Gy and one negative value).

Therefore, in principle, both samples yield zero mean equivalent doses and zero ages, which suggests that the sands of the linear dune field and of the Bunyip Sands parabolic dunes in the western Murray Basin are completely bleached during transport and deposition.

Laboratory bleaching experiments

To investigate the bleachability of iron- and/or clay-coated quartz grains in more detail, two experiments were carried out using a sample which had undergone the standard laboratory treatment without the HF etching procedure, which usually removes the iron/clay coatings. For extraction of the quartz fraction, a heavy density liquid of 2.62 g/cm³ was used instead of the 2.58 g/cm³ routinely used for the samples investigated in this study, in order to get rid of as many feldspars as possible. It has to be pointed out though that by exposing the sample to HCl and H_2O_2 to remove carbonates and organic matter, some of the iron/clay coatings might have been removed by these acids. Nevertheless, the treated and un-etched sample still exhibited an overall red colour and

was made up of a mixture of coated and un-coated grains, which is also the case for an untreated, natural sample.

In the first experiment, the signal resetting in natural sunlight of the un-etched sample was compared to the resetting of an etched sample, with the iron/clay-coatings removed. The etched and un-etched sample, containing a natural dose of ~17 Gy, were fixed to 8mm discs, and subsequently exposed to sunlight for 10 s, 30 s, 60 s, 120 s and 240 s. After each period of sunlight exposure, the remaining equivalent dose was measured using blue light emitting diodes (70 % diode power) for 0.1 s at 40°C for stimulation. No feldspar contamination was present in the grains used for the bleaching experiment, which was tested by IRSL-measurements on the same aliquots.

The resetting of the OSL signal by sunlight exposure is shown in Fig. 6.25. Although resetting of the OSL signal of the grains with iron/clay-coatings is slower than for grains without coatings, the coated quartz grains are bleached to negligible levels (0.1 % of the initial signal) after 120 s. This ought to be sufficient to bleach the quartz OSL signal during transport and deposition. Incomplete bleaching as an external source of scatter is therefore not likely.

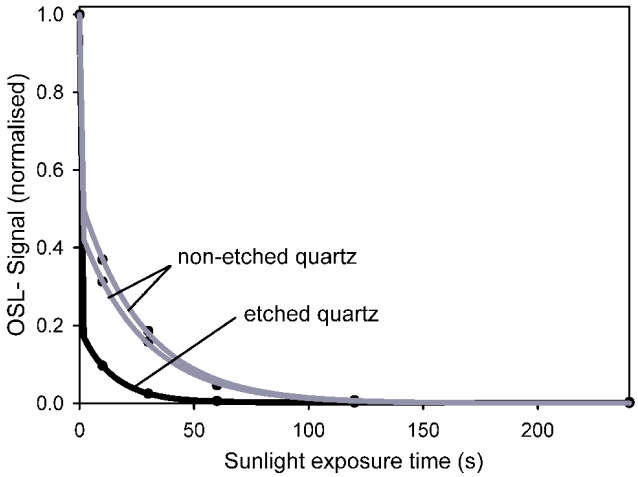

Fig. 6.25. Decrease of signal intensity of an etched and non-etched quartz with different sunlight exposure times (10, 30, 60, 120 and 240 s). Each curve represents one large aliquot (8mm diameter covered with quartz grains). Measurements were carried out using blue light-emitting diodes(70% diode power) for 0.1 s at 40 1C for stimulation. No feldspar contamination was present in the grains used for the bleaching experiment, which was tested by IRSL-measurements on the same aliquots (artificially irradiated after the bleaching experiment).

In a further experiment to compare the bleachability of coated and non-coated quartz grains, the natural dose of the same un-etched quartz sample (consisting of a mixture of coated and uncoated quartz grains) was measured using single grain analysis. After the

measurement, the colour of the grains in the single grain disc was determined with a microscope to test if the red, coated grains yielded different De-values as the un-coated grains. If the coated grains were not as well bleached as the un-coated grains, they should yield higher De-values.

Fig. 6.26 shows a weighted histogram of the white, uncoated quartz grains and the red, coated quartz grains. Both distributions show a peak in the same region at around 17 Gy. Two outliers at ~120 Gy were produced by 'white' grains. The median value of the 'red' grains is 15.7 ± 2.7 Gy, and the median of the 'white' grains, excluding the two outliers, is 17.8 ± 3.1 Gy. Thus no significant difference in the mean equivalent doses of 'white' and 'red' grains exists, which again argues against the hypothesis that the coated quartz grains are not well bleached.

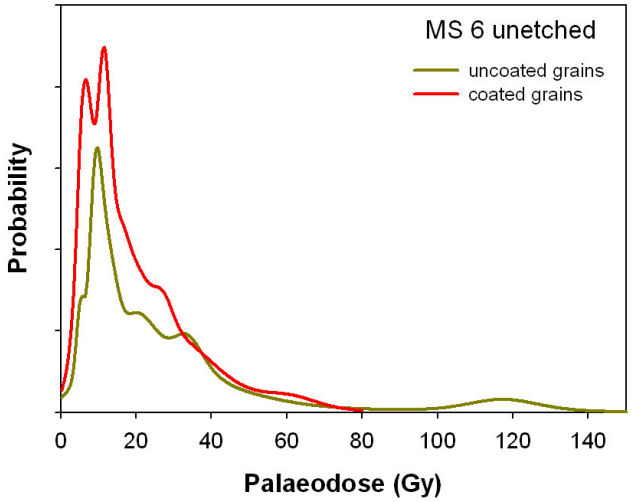

Fig. 6.26. Single grain De-values of red grains with iron coatings and of white grains without iron coatings of a non-etched sample from the western Murray Basin.

On the whole, multiple lines of evidence show that incomplete bleaching is not a problem for the samples investigated. This is even the case for the heavily iron-coated dune sands from the linear dune field. It is suggested that broad and positively skewed distributions do not necessarily indicate incomplete bleaching of a sample (cf. Bailey and Arnold 2006).

6.8.7.3.2 Microdosimetry

In any sediment, radionuclides that are responsible for dose build up in natural dosimeters as quartz grains, are unevenly distributed. This is caused by the fact that some minerals contain very little or no radionuclide concentrations such as quartz, and others very high concentrations, such as potassium-rich feldspars (high potassium

content) and zircons (high uranium content). Thus, a quartz grain located next to a feldspar grain will receive a much higher beta dose than a quartz grain surrounded by other quartz grains with no or very little internal radionuclide concentrations (see Section 7.2.2.4). Other explanations for beta dose rate heterogeneity could be unevenly distributed pore water or unevenly distributed carbonates in a sediment. (e.g. Murray and Roberts 1997, Olley et al. 1997, Kalchgruber et al. 2003).

This heterogeneity poses problems especially for the beta dose rate in luminescence dating, as the 2mm range of beta particles is comparably small. The fact that the beta dose rate contributes to around 50% of the total dose rate underlines the relevancy of beta radiation heterogeneity. For the remaining ~ 50% of the total dose rate, delivered through gamma – including cosmic - radiation, unevenly distributed radionuclides are not a problem because the range of gamma particles of ~30 cm is high enough to produce a homogeneous gamma radiation field.

Further problems with respect to microdosimetry are caused by iron coatings of quartz grains as they can increase the attenuation of incoming radiation (Vandenberghe et al. 2003, personal communication B. Mauz, 2007). The amount of variability in palaeodoses due to different thickness of coatings has so far not been investigated, and is a difficult task.

As a consequence of the uneven distribution of radionuclides, individual quartz grains receive different amounts of beta doses over a period of time. Therefore, some percentage of variations in palaeodose distributions has always to be ascribed to microdosimetric effects.

Several approaches have been undertaken in the past to assess the amount of variability in palaeodose distributions caused by heterogeneity in the sediments dose rate. Vandenberghe et al. (2003) determined radionuclide concentrations on small amounts (1g) of subsamples through NAA. The U and Th concentrations of the small subsamples indeed showed a considerable spread, which led them to the conclusion that the overdispersion in their samples was caused by microdosimetric effects. Kalchgruber et al. (2003) buried sand sized grains of aluminiumoxide in a loess sediment for six months and subsequently measured the dose of these grains. They found that even in a relatively homogenous material such as loess, beta dose rate variations caused a spread in data (relative standard deviation) of 18%. Murray and Roberts (1997) also mainly ascribed the overdispersion observed in an aeolian sedimentary sample from Australia to variations in beta dosimetry. In this sample, the heterogeneity was caused by

unevenly distributed carbonates in their sediment, thus quartz grains surrounded by carbonates receiving a substantially lower beta dose than quartz grains surrounded by aeolian material. The variations of the dose rate for this particular site were calculated by Olley et al. (1997) and were found to be in the same order of magnitude as the overdispersion of their De-distribution.

Another way to assess the relation of dose rate heterogeneity and palaeodose distributions is through modelling, which was undertaken by Nathan et al. (2003) and Mayya et al. (2006). In both studies it was observed that dose rate heterogeneity can cause positively skewed palaeodose distributions, which may mimic incomplete bleaching. In their model, Mayya et al. (2006) computed the amount of variability in palaeodoses induced by varying K-contents in a sediment, based on the assumption that few potassium-rich feldspars in a sediment are the main trigger of dose rate heterogeneity. They found that the higher the potassium concentration of a sample, the lower the beta dose rate heterogeneity and the lower the RSD of the modelled De-distribution. They displayed the relation of the RSD of De-values as a function of the K concentration, which can be seen in Fig. 6.27. This function in principle would allow a user to determine the proportion of variability in each De-distribution caused by beta dose heterogeneity based on the K-concentration of a sample. The drawback of this model however is that the U and Th concentrations of a sample are not considered. Therefore, the net RSD will always be lower than predicted in their model (Mayya et al. 2006). For instance, the loess sample investigated by Kalchgruber et al. (2003) had a K-concentration of 1.1 %. The predicted RSD_{beta} according to Mayya et al. (2006) would be ~27.5 %, whereas the measured RSD_{beta} only yielded a value of ~18 %.

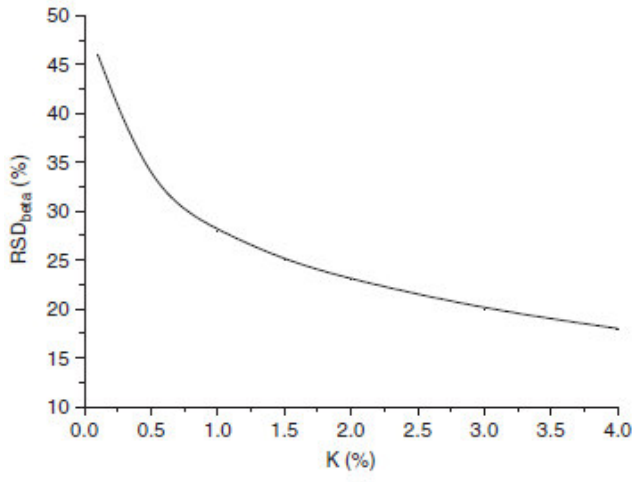

Fig. 6.27. Variation of the relative standard deviation (RSD_{beta} (%)) of the dose distribution due to the ^{40}K beta dose with increasing K concentration (from Mayya et al. 2006).

The average K-concentrations of the western Murray Basin samples are 0.59 % in the linear dune field, 0.85 % in section BM (Bunyip Sands) and 0.33 % in the sub-parabolic dune field (including section PSP) (see Section 7.3.2 and Tab. 7.3). According to the model of Mayya et al. (2006), De-values of the samples from the sub-parabolic dune field should yield the highest overdispersion. This is not the case; on the contrary, overdispersion of the De-distribution is much lower in the sub-parabolic dune field than in the linear dune field and in the Bunyip Sands. From this it is concluded that microdosimetry is not the only source of variation producing the large spread in De-values in the samples from the linear dune field and the Bunyip Sands. When predicting overdispersion values according to the model of Mayya et al. (2006), the De-values of the linear dune field samples should yield RSD_{beta} values of ~32 %, those of the Bunyip Sands RSD_{beta} values of ~28 % and those of the sub-parabolic dune field (including section PSP) RSD_{beta} values of ~ 38 %. When a similar reduction of the net RSD_{beta} as for the sample investigated by Kalchgruber et al. (2003) is assumed, the corresponding RSD_{beta} values of the western Murray Basin samples would be 21 % in the linear dune, 18 % in the Bunyip Sands and 25 % in the sub-parabolic dune field. The latter value appears slightly overestimated, as external variation (overdispersion) in the samples from the sub-parabolic dune field is only around 19-22 % (see Tab. 6.4). However, it appears plausible that microdosimetric effects produce a spread of De-values of around 20 %. A similar maximum overdispersion value of 22 % was reported by Olley et al. (2004a) for well-bleached, non-disturbed samples when analysed on a single grain scale. It follows that in the sub-parabolic dune field the observed scatter of De-values might be caused by a heterogeneous beta radiation field alone. In the linear dune field and the Bunyip Sands formation, an additional source of variation seems to be present. It is not thought that beta dose heterogeneity is even more pronounced in the carbonate-rich layers than in the sandy layers. First, the carbonate-rich samples have similar dose rates as the non-carbonate-rich samples, and furthermore, the carbonate-rich samples do not exhibit higher overdispersion values than non-carbonate-rich samples.

6.8.7.3.3 Bioturbation

Bioturbation is a very common process in sediments and soils from arid and semi-arid environments (Bateman et al. 2007). Evidence of sediment mixing due to bioturbation caused by roots and animals could be observed in the field at every site investigated the western Murray Basin (Fig. 6.28).

Fig. 6.28. The work of ants at the linear dune section PSP.

Samples from the linear dune field exhibit clear multi-modality of the De-distributions (Fig. 6.29(a)-(c)), a potential indicator for bioturbation (Bateman et al. 2003a, 2007). Samples from the sub-parabolic dune field have uni-modal De-distributions (Fig. 6.29(d)).

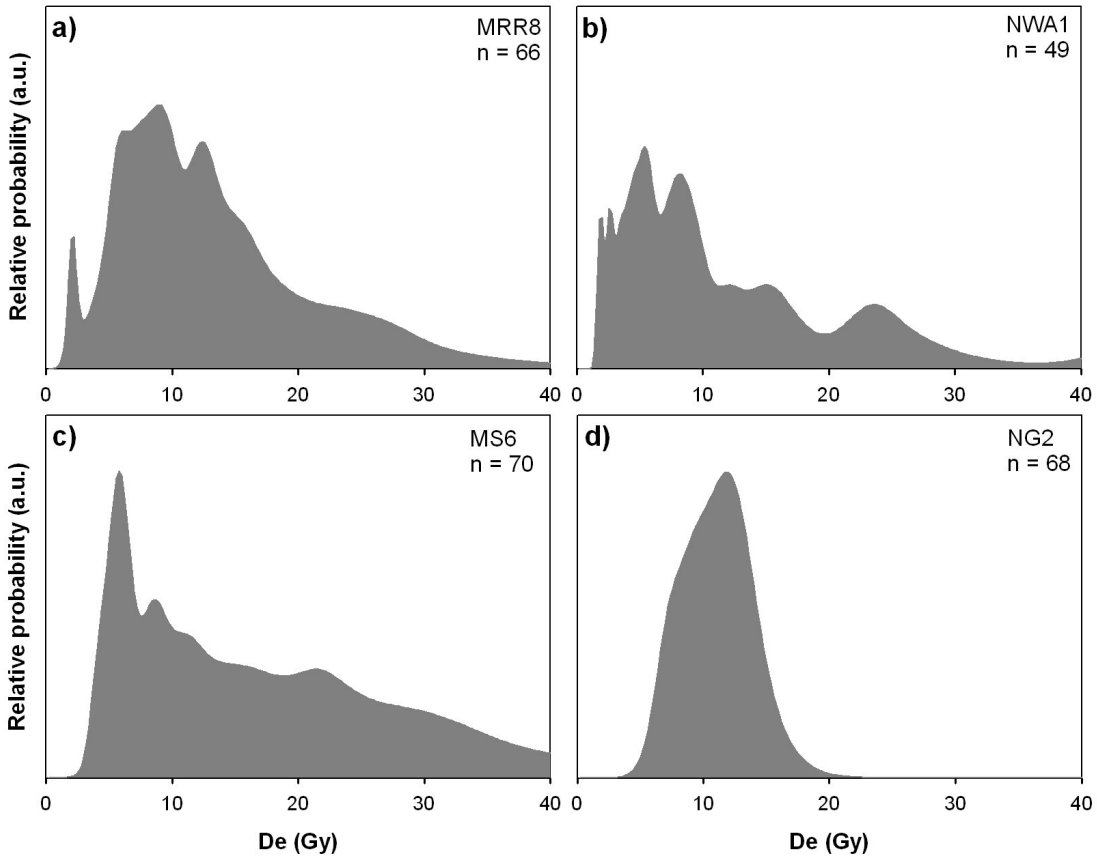

Fig. 6.29. Single grain De-distributions displayed as PDFs. (a)-(c) Samples from the linear dune field (MRR8, NWA2, MS6) have a multi-modal distribution, implying bioturbation. (d) The sample from the sub-parabolic dune field (NG2) has a uni-modal distribution.

Nevertheless, signs for bioturbation were clearly evident in both the sub-parabolic dune field and the linear dune field. It is thus not immediately obvious why the spread in equivalent doses is significantly higher in the linear dune field than in the sub-parabolic dune field. If bioturbation was the major factor of equivalent dose variations, then a similar spread should be expected in sands from both dune fields. The answer to this problem is very simple though. Sections with the lowest overdispersion values were those which had similar equivalent doses throughout the sampled profile. Section CC has similar equivalent doses of 11 and 12 Gy within 1.5 m of sampled profile, section NG consistent doses of 10 to 12 Gy within 1.1 m of sampled profile and section ALC consistent equivalent doses of ~55 Gy within 1 m of sampled profile. These three sections, all from the sub-parabolic dune field, had the lowest overdispersion values of all samples investigated. All other sections from the linear dune field, the sub-parabolic dune from the Bunyip Sands, and one section from the sub-parabolic dune field (section CD) had significantly different equivalent doses of neighbouring samples, within the sampling resolution of approximately 0.5 m. The reasons for these different net sedimentation rates will be discussed in Section 9.1. The fact that those sections with lowest net sedimentation rates, and hence different equivalent doses in adjacent samples, exhibit the highest spread in De-values, together with observations made in the field, is considered as strong evidence that bioturbation is a major source of variation in the sample investigated.

6.8.7.3.4 Conclusion about the external sources of variation

In conclusion, it is believed that microdosimetry and bioturbation are responsible for the large scatter of equivalent doses in the western Murray Basin samples. In the sections with the lowest overdispersion values (~20 % in samples from the sub-parabolic dune field), microdosimetry is probably the only source of equivalent dose variation. Bioturbation affected these dune sands too, but it has no effect on the spread of De-values, as grains with the same burial dose were mixed. A minimum of 20 % overdispersion due to microdosimetry can thus be expected in all sections investigated. The observed overdispersion exceeding 20 % in most of the samples of the linear dune field can be ascribed to post-sedimentary mixing through bioturbation. For older samples with De-values above ~100 Gy, approaching luminescence signal saturation is most likely another source of variation in equivalent doses. Incomplete bleaching as a

cause of spread in De-values can be ruled out, as confirmed by measurements of modern samples, bleaching experiments and LM-OSL measurements.

6.8.8 Calculation of De-values

For samples affected by post-sedimentary mixing, the most appropriate way to determine a mean equivalent dose would be a model which enables to separate different De-populations within in a mixed distribution. This can be accomplished by finite mixture models (FMMs) (Roberts et al. 2000, Rodnight et al. 2006). Furthermore, it has become evident in the previous section that the multiple grain analysis might not be appropriate to resolve the complex distribution and to separate individual De-components, as a high proportion of grains is luminescent and thus variations of De-values will be averaged out. Therefore, in the following, only the single grain analyses will be considered for the determination of a mean De and will be used for the age calculation.

For the samples investigated in this study the finite mixture model of Galbraith and Green (1990) was applied. This model requires the definition of a sigma value which accounts for the expected overdispersion in each De-population. The most appropriate way of setting this sigma value is to use the average or minimum overdispersion value of samples from the same study area which are thought to consist of a single De-population. Thus, for the samples investigated in this study, the sigma value was set to 20 %, the average overdispersion from the sections in the sub-parabolic dune field where microdosimetry is considered to be the only source of variation in equivalent doses (see Section 6.8.7.3.2 and 6.8.7.3.3). This sigma value is consistent with an estimate of Olley et al. (2004a) who concluded that single grain De-distributions <20 % are most likely from a single De-population. The number of De-components was assessed on the base of the Bayesian Information Criterion (BIC), with the lowest BIC value indicating the correct number of components. The programme used for calculation of the finite mixture model (Freeware R and Tinn-R, with the algorithm described in Galbraith (1988), programmed and kindly provided by R. Galbraith) also calculates the proportion of grains within each De-population. The population with the highest proportion of grains was used for age calculation as it is assumed that it represents the palaeodose of the host sediment into which younger and/or older grains intruded through bioturbation.

In Fig. 6.30, the application of the finite mixture model with the above mentioned settings is shown exemplarily for sample MS6, also indicating the proportion of grains of each De-component.

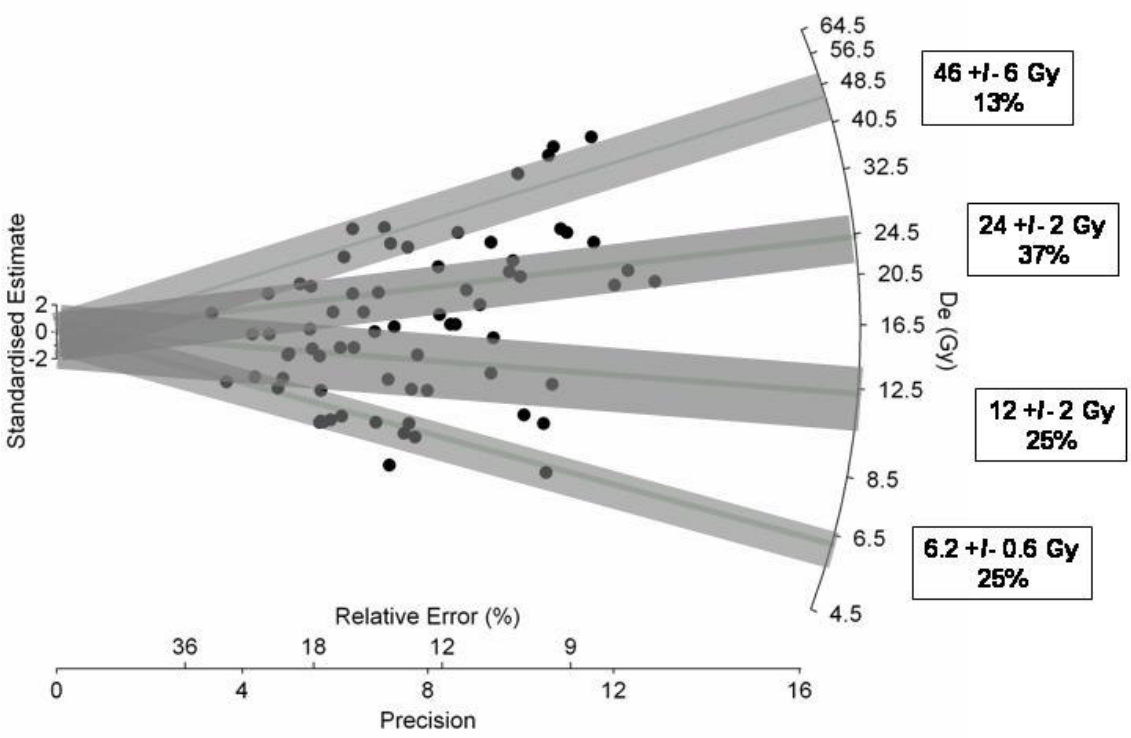

Fig. 6.30. Based on the Bayesian Information Criterion (BIC) and a sigma value of 20 %, the De-distribution of sample MS6 was separated into four De-components using the finite mixture model of Galbraith and Green (1990). The component which incorporates the highest number of De-values is the one at 24 ± 2 Gy, with a proportion of grains of 37%. This component is later used for the age calculation.

The finite mixture model with a sigma value of 20 % was only used for samples with De-values <85 Gy. Until at least 60 Gy, the use of the 20 % sigma value is justified as confirmed by the overdispersion value (~19 %) of samples ALC1-3 from the sub-parabolic dune field. For samples with higher doses, the effects of approaching signal saturation will increase the spread of the De-components. To account for this problem, a sigma value of 27 % was used in the finite mixture model for samples >85 Gy, which was the lowest overdispersion value of all samples with a De >85 Gy in the linear dune field. Another reason for this sigma value was the result of a single grain dose recovery test using sample NWB7. This sample was given a known dose of 114 Gy, and the 48 recovered De-values yielded a RSD of 18.5 % (see Section 6.8.4.3 and Tab. 6.2). This spread will have its source in instrumental variations, counting statistics, varying internal properties of the quartz grains and the shape of the growth curve. Combined with the 20 % spread due to microdosimetry, the two sources of variation add up to a spread of 27 % by Gaussian error propagation ($\sqrt{(18.5^2 + 20^2)} = 27$). Due to this

relatively high sigma value, a lot of samples consisted of only one De-component. For these samples, the central age model (Galbraith et al. 1999) was used for calculation of a mean De. A maximum of four De-components was identified in the samples investigated. The number of components for each sample, and the De-value of the main component are given in Table 2 in the Appendix.

A comparison of De-values derived from the FMM main component and of the central age model (incorporating all De-values of a dataset) is shown in Fig. 6.31. It can be seen from this figure that for De-values <50 Gy, the FMM yields lower De-values than the central age mean for the majority of samples. In a lot of samples >85 Gy, a small population of low dosed grains was identified and removed from the data set. As a consequence, a lot of samples yielded higher De-values when using the mixture model, compared to the central age De of the total data set.

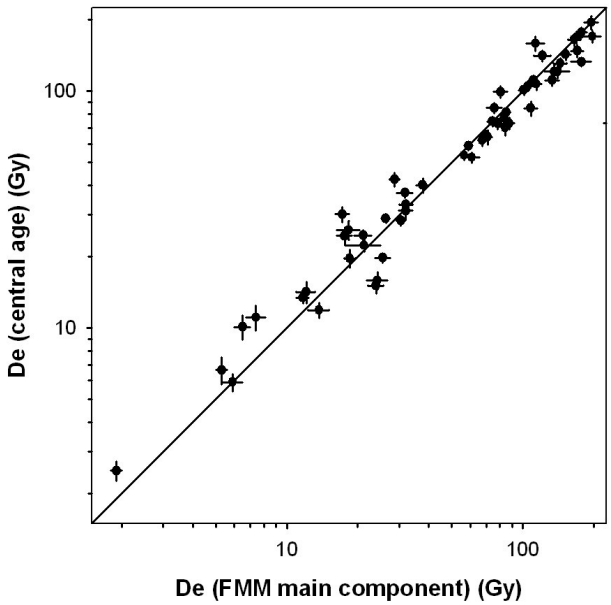

Fig. 6.31. Comparison of De-values derived from the main component identified by the finite mixture model (FMM) and of De-values calculated from the central age model including all De-values from a dataset.

For some of the very young samples with near zero ages (WP1, MS9 and BM1), median De-values were calculated. The reason for this is that in these samples, some individual De-values yielded negative values. Neither the finite mixture model nor the central age model is able to deal with negative values, as they use exponentiations of logarithmic De-values for the mean calculation. Furthermore, for samples with De-values >200 Gy, the finite mixture model was not applied due to the proximity of these De-values to signal saturation. For these samples, the central age model was used for mean De-

calculation. As discussed in Section 6.8.4.3 and 6.8.5, De-values of >200 Gy are considered unreliable.

6.8.9 Validity of multiple grain measurements from the western Murray Basin

All luminescence studies previously carried out on dune sands from the western Murray Basin were conducted using (differently sized) multiple grain aliquots of quartz (Gardner et al. 1987, Readhead 1988, Cupper and Duncan 2006, Robertson and Prescott 2006, Twidale et al. 2007). It has been shown in the previous sections that
a) dune sands from the Murray Basin can be severely affected by bioturbation and
b) the dune sands from the western Murray Basin contain a high proportion of luminescent grains.
Thus, the use of multiple grain luminescence dating has to be questioned, as signal averaging of differently dosed grains, even when using small aliquots, will most likely occur. In order to assess the validity of multiple grain analysis in the western Murray Basin, comparative measurements using both small (1 mm) multiple grain aliquots and single grains were carried out on section MS and SW, both from the linear dune field.
Fig. 6.32 shows the comparison of central age mean De-values for single grains and small multiple grain aliquots from both sections, ranked in order of the multiple grain De. It can be seen that for samples with equivalent doses <25 Gy, the single grain analysis yield significantly lower De-values than the multiple grain estimates. The reason for this significant deviation is most likely the very high overdispersion observed in the single grain measurements of these samples. In multiple grain aliquot dating, even small proportions of older grains possibly dominate the total luminescence signal. Signals of younger grains on the other hand will be concealed by those of older grains, as shown e.g. by Bateman et al. (2003a). Severe overestimation of De-values of multiple grain analysis compared to single grain analysis can also occur in incompletely bleached samples (Duller 2006). In the range of 25-140 Gy, single grain and multiple grain De-values are consistent within errors. Above 150 Gy, two single grain De-values are again significantly lower than the corresponding multiple grain De-values. If this is a consistent trend cannot be said from the two samples alone. It is thought that the underestimation of single grain De-values in high dose ranges (>150 Gy) is caused by a few low dosed grains, which, due to their relatively high precision, are over-weighted in weighted means such as the central age model. Application of the finite mixture model

removes these low dosed grains and results in equivalent doses consistent with the multiple grain mean De-values.

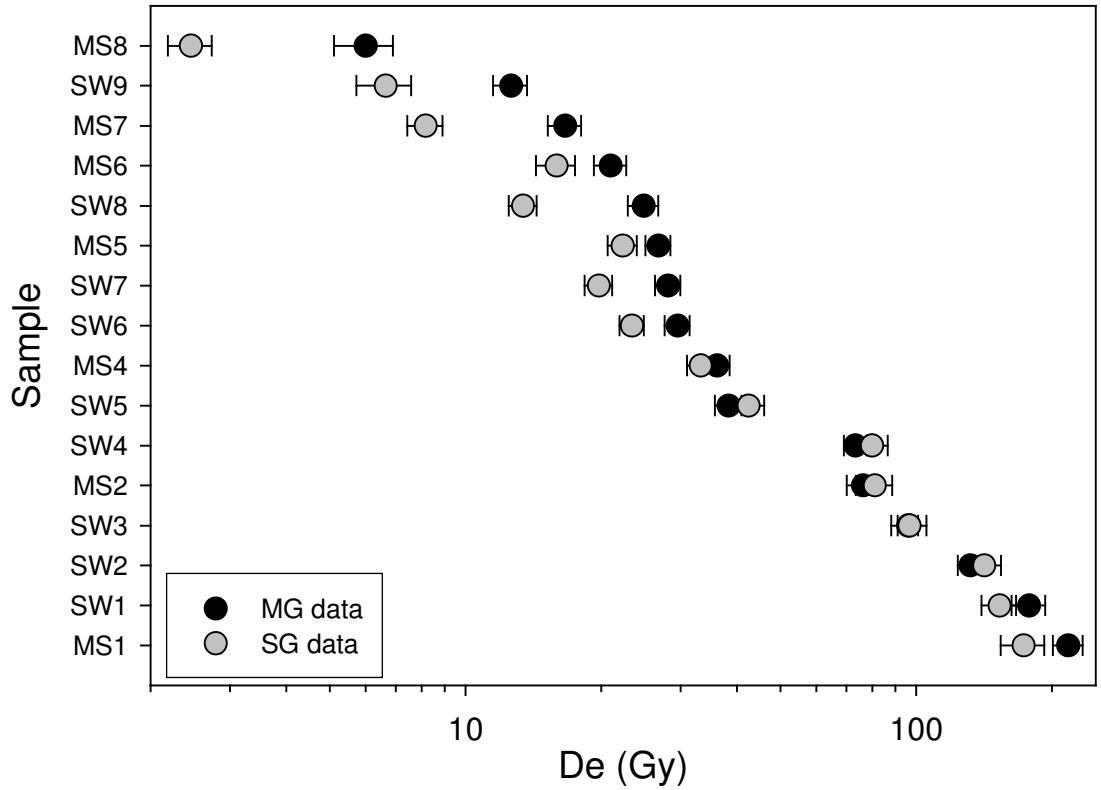

Fig. 6.32. Comparison of single grain and small (1 mm) multiple grain mean De-values, both calculated from the central age model of Galbraith et al. (1999).

Especially for lower De-values (<25 Gy), single grain analysis are most likely to yield more reliable results than multiple grain analysis for the samples investigated in this study. It has been shown in Section 6.8.8 that for the single grain datasets, multiple De-populations with different proportions of grains could be identified using a finite mixture model. Possibly, the De-values from the mixed signals when using multiple grain analysis do not reflect the De-population with the highest proportion of grains, but a higher De-population. To test this assumption, for sections SW, the finite mixture model was applied on both the single grain and multiple grain data sets, though only for samples <60 Gy. For the multiple grain data, a sigma value of 15 % for each De-population was assumed. The results are displayed in Fig. 6.33 and Fig. 6.34. For better comparability, luminescence ages instead of De-values are compared. The reason for this is that for single grains, dose rates are slightly lower (by about 2 %) than for multiple grain analysis, because of the different grain sizes used for De-determination (which leads to different beta attenuation values). Furthermore, dose rates vary slightly from layer to layer.

In the single grain data set of sample SW9 (Fig. 6.33), four components were identified, as well as in the multiple grain data set. The main proportions yield luminescence ages of 6.7 ± 0.7 ka and 11.1 ± 1.3 ka for the single grain and multiple grain data respectively. The multiple grain age (main component FMM) overestimates the single grain age significantly. However, the multiple grain age is statistically indistinguishable from the single grain main component age for the underlying sample, SW8. Here, the main De-population results in an age of 11.8 ± 1.0 ka. Furthermore, the lowest De-population in the multiple grain data of SW9 yields a luminescence age of 7.1 ± 1.4 ka, which is consistent with the main proportion single grain age of the same sample. A similar relation is found for sample SW8. The main proportion luminescence ages of the single grain and multiple grain data (11.8 ± 1.0 and 27 ± 3 ka) vary significantly by a factor of more than two. The main proportion luminescence age of the multiple grain data of sample SW8 is indistinguishable though from the main proportion luminescence age of the single grain data of the underlying sample, SW7 (27 ± 3 ka). In sample SW8 however, the lowest De-population age from the multiple grain data (15.6 ± 1.6 ka) does not coincide with the main proportion single grain age of 11.8 ± 1.0 ka.

For samples SW7, SW6 and SW5, the main proportion ages of the single grain and multiple grain data are indistinguishable from each other within errors. This supports the findings mentioned further above that for samples with De-values >25 Gy, single grain and multiple grain De-values are very similar.

All in all, components derived from the finite mixture model are quite similar for the single grain and multiple grain data set. This also can be seen in the PDF of Fig. 6.33, in which all component ages are included, regardless of the proportion of grains. The probability density curves of the multiple grain and single grain components are strikingly similar, although the youngest component of around 2 ka was not detected using multiple grain analysis.

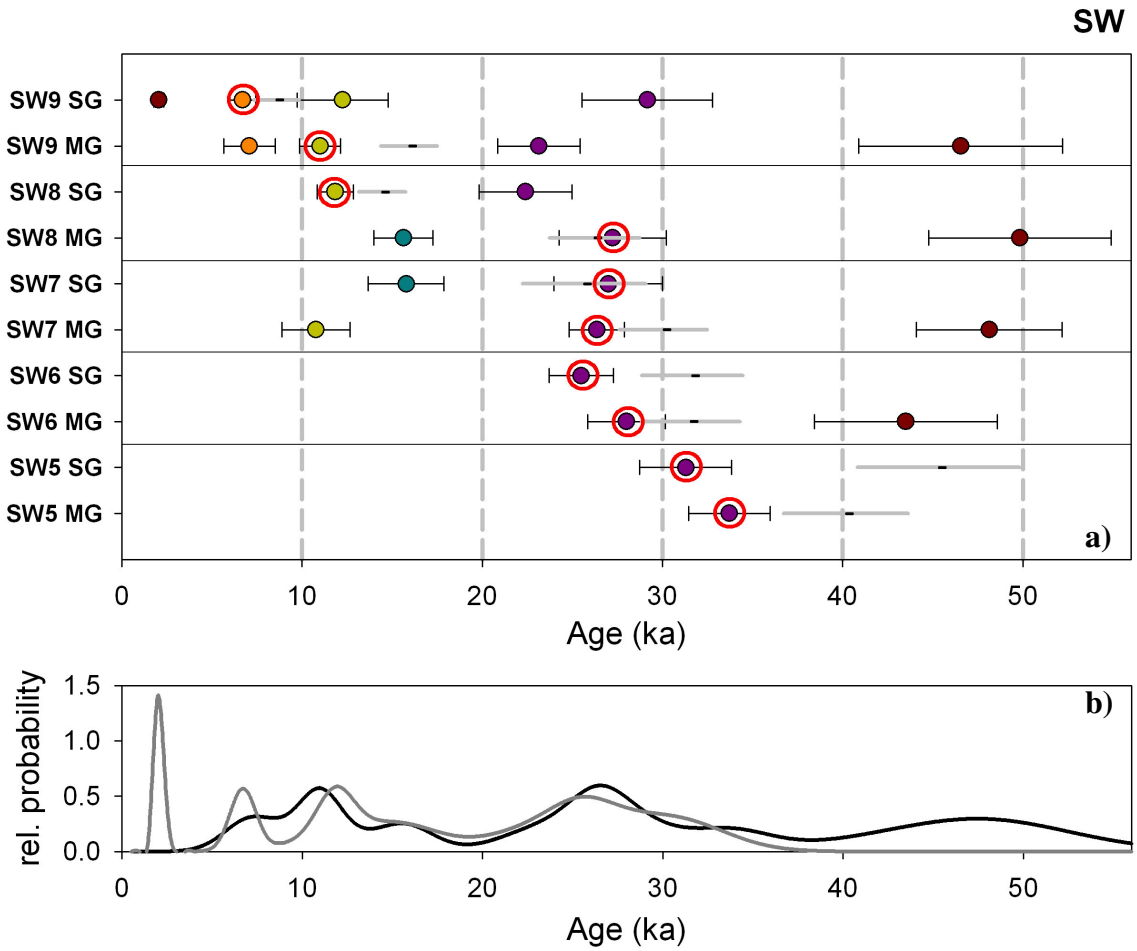

Fig. 6.33. (a) OSL ages < 55 ka from section SW, derived from all De-components identified by the finite mixture model, both for single grain and for small aliquot multiple grain analyses. The age derived from the main component is highlighted with a red circle. The age based on the central age mean is shown as grey line. (b) PDF of luminescence ages using all components identified by the finite mixture model. The grey line shows the single grain ages, the black line the multiple grain ages.

It is concluded that from small multiple grain analysis, similar De-populations can be identified as when using single grains for De-determination. However, young age populations might be concealed on a multiple grain scale. Even central ages from the multiple grain data are sometimes not entirely different from one of the FMM components, but this is not the case in younger age ranges. These statements may not be valid if larger (>1 mm diameter) multiple grain aliquots are analysed. In conclusion, applying the finite mixture model on samples affected by post-sedimentary mixing is the most appropriate way to deal with this problem.

7. The environmental dose rate

7.1 Nature and derivation of the environmental dose rate

As mentioned in Section 5.1, the luminescence age is derived by dividing the palaeodose by the dose rate. The latter is defined by the flux of ionising radiation (per unit time) interacting with the mineral grains to be dated and is expressed in Gy/ka. Ionising radiation is mainly caused by the decay of radioactive isotopes in the surrounding sediment and within the minerals to be dated. The main contributors to naturally occurring radiation are the radioactive decay of ^{40}K into stable ^{40}Ca and stable ^{40}Ar and the decay of ^{232}Th, ^{235}U and ^{238}U, which disintegrate over a series of unstable isotopes to stable lead isotopes (Fig. 7.1). The contribution of ^{235}U hereby is very minor due to its very low abundance. Several minerals occurring abundantly in most sediments contain high concentrations of the above mentioned radionuclides. Potassium, for instance, is abundant in some feldspars, micas and clay minerals, and uranium and thorium can occur in high concentrations in the heavy mineral zirconium. Calcretes, common features in soils of the semi-arid zone, can also contain concentrations of these three radioisotopes (Singhvi et al. 1996, Grevenitz 2006). Further radiation is contributed by cosmic rays and to a very limited extent by the decay of ^{87}Rb.

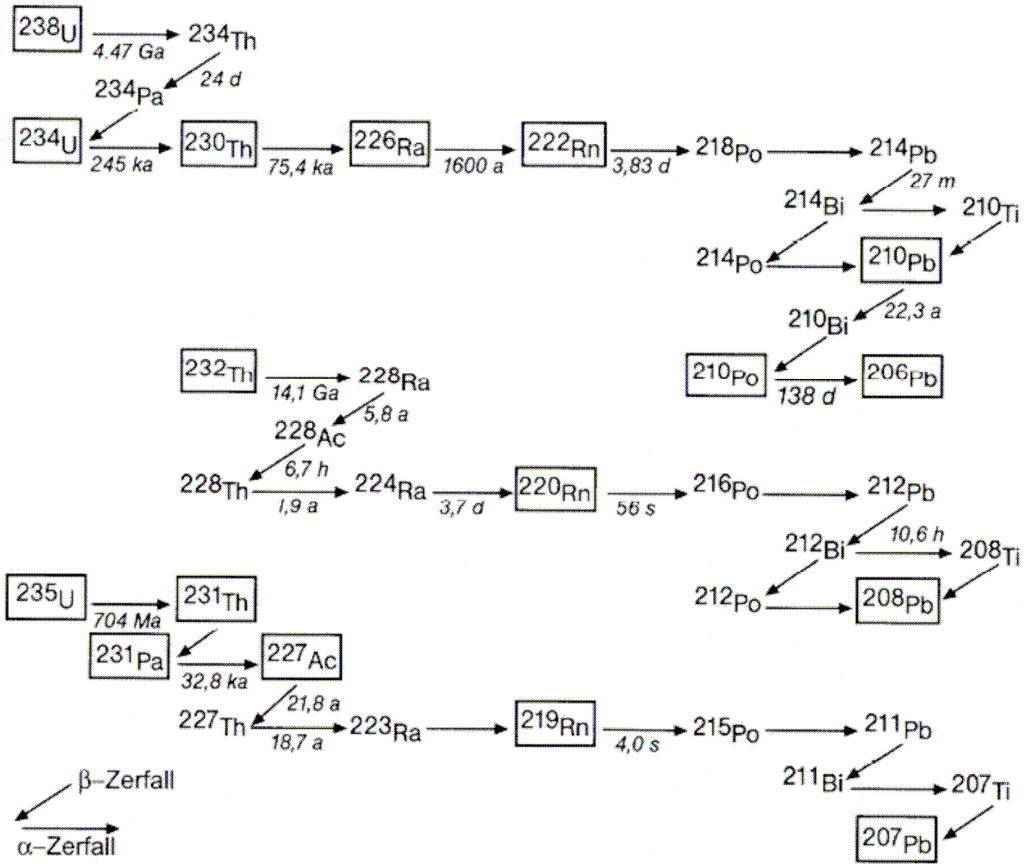

Fig. 7.1. Radioactive decay series and half-lives of ^{238}U, ^{232}Th, and ^{235}U (Geyh 2005).

Radioactive decay results in the emission of alpha and beta particles and gamma rays, whereas alpha particles are only emitted with the decay of U and Th. Cosmic radiation produces gamma rays. The emission products exhibit different penetration depth when interacting with solid matter such as minerals, which has several important implications for the determination of the dose rate.

Alpha particles consist of He^{2+} nuclei, which have a limited range in silicates of about 20 µm (Grün 1989). As a consequence, when source-free sand sized grains (such as those used in this study, with a grain size of 100-250 µm) are used for luminescence dating, only the outer rind of these grains is affected by alpha radiation. On their way through the rind of the mineral grain, alpha particles have a very high ionisation density and produce tracks along which electron traps are filled and saturated very rapidly. As a consequence, the production rate of ionised and trapped electrons is decreased compared to the ionisation efficiency of an equivalent dose of beta particles and gamma rays (Aitken 1998). Alpha radiation and its decrease in efficiency, however, is not relevant when dating coarse (>100 µm) grains of quartz for two reasons. First, it is usually assumed that quartz does not contain isotopes of the uranium and thorium decay

series, thus is free of internal alpha emitters (Aitken 1998). Furthermore, the outer rind of quartz grains which has been affected by external alpha radiation is removed by treatment with concentrated hydrofluoric (HF) acid. Thus, the alpha dose rate in quartz and problems associated with the low alpha efficiency are negligible when calculating the total dose rate (Folz et al. 2001).

Beta particles, consisting of electrons, have a penetration depth of around 2 mm in silicates (Grün 1989). Quartz grains with a size of a few hundredth of microns usually used for coarse grain luminescence dating are fully penetrated. However, when beta-particles diffuse through sand-size quartz grains, they experience progressive attenuation. In quartz grains with a diameter of 100-200 µm this beta attenuation is taken into account by multiplying the beta dose rate with a beta-attenuation factor of around 0.9 (Mejdahl 1979, Brennan 2003).

Gamma rays are an accompaniment of beta and alpha decay. They are produced when an atomic nucleus falls back to a low energetic ground state after being set to an excited state by alpha or beta decay. Gamma rays can be described as electromagnetic waves or, alternatively, as flux of photons with very high energies ranging from 10^2 to 10^4 keV, equivalent to wavelengths of 10^{-11} to 10^{-13} nm (Debertin and Helmer 1988). Photons resulting from gamma radiation are thus more energetic than visible light by around four orders of magnitude. Compared to alpha and beta particles, gamma rays have the lowest ionising energy. Due to this, their range in sediments is large, averaging 30 cm (Aitken 1985, 1998). They do not experience attenuation when penetrating sand sized mineral grains.

Cosmic radiation is primarily derived through particle bombardment from outer space. Primary cosmic radiation consists of protons, electrons, and heavy atomic nuclei. These particles are deflected to a certain degree by the Earth's magnetic field which explains why cosmic radiation is dependent on the geomagnetic latitude (particle flux deflection is higher at the equator than at geomagnetic poles, thus the particle flux density is higher at the poles). When entering the Earth's atmosphere, cosmic particles collide with atmospheric molecules or nuclei, to form new particles, of which some reach the Earth's surface. This so called secondary cosmic radiation mainly consists of electrons and muons, amongst other particles. Whereas the electrons are absorbed within the first few decimetres of soils or sediments, muons penetrate the Earth's surface to considerable depths but get more and more attenuated through absorption with increasing depth below surface (Prescott and Stephan 1982, Prescott and Hutton 1988,

1994). From this it follows that the cosmic dose rate depends on the geomagnetic latitude, the altitude (the higher, the more secondary cosmic particles are available) and on the depth of a sample below surface. The latitudinal dependency hereby is relatively small at sea level, so that the dose rate at sea surface is practically the same from the pole to a geomagnetic latitude of 35° (Prescott and Hutton 1994). From 35° on towards lower latitudes, the cosmic dose constantly decreases and reaches minimum values at the equator. Here, the cosmic dose is ~7 % lower than at a latitude of 35° (Aitken 1998). Usually, the contribution of the cosmic dose rate to the total dose rate is relatively small, but can rise to considerable proportions in sediments with low dose rates or at altitudes above 1 km (Aitken 1998, Munyikwa 2000).

7.2 Determination of the dose rate

As mentioned above, it is usually assumed that quartz grains possess negligible levels of radioactive isotopes (Aitken 1998). Thus internal dose rate contributions (i.e. from within the quartz grains themselves) are not be expected, and only external dose rate contributions, derived from radionuclides in the surrounding sediments and from cosmic radiation, have to be considered. Furthermore, as explained before, the influence of alpha radiation on the quartz grains can be removed by appropriate laboratory treatment. Therefore, the total dose rate (D_0) for coarse grains of quartz can be calculated as the sum of the beta dose rate (multiplied by a beta attenuation factor of ~0.9) (D_{beta}), the gamma dose rate (D_{gamma}) and the cosmic dose rate (D_c). Usually, D_{beta} and D_{gamma} are determined by laboratory measurement on dried samples. Therefore, further corrections concerning the natural water content of sediment samples need to be taken into account as water in interstices of sediments attenuate radiation more readily than air. For example, a water content of 10 % decreases the beta and gamma dose rate by around 11 % (Aitken 1998), based on attenuation factors of Zimmerman (1971).

7.2.1 Methods for dose rate determination

In general, there are two ways to determine the external beta and gamma dose rate. One approach is to measure element concentrations of the relevant radionuclides (U, Th, K) in the surrounding sediment, and then transfer these concentrations into dose rates via conversion factors. Element concentrations can be determined using for example neutron activation analysis (NAA), inductively coupled plasma mass spectrometry

(ICP-MS), or gamma-spectrometry. NAA and ICP-MS hereby measure the concentrations of the mother nuclides of the uranium and thorium series, whereas gamma-spectrometry mainly determines the activity of some U- and Th-series daughter nuclides. Gamma spectrometry can either be carried out in the laboratory or directly in the field (in situ gamma spectrometry). The latter method quite elegantly circumvents errors in dose rate determination induced by sediment inhomogeneities; see Section 7.2.2.4), but on the other hand may be impracticable, because long measurement intervals are often necessary. As laboratory gamma-spectrometry is used for the determination of the dose rate in the present study, this method is explained in more detail in Section 7.2.1.1.

The most recent dose rate conversion factors were reported by Adamiec and Aitken (1998). Dose rates resulting from these conversion factors are listed in Tab. 7.1.

Tab. 7.1. Beta (D_{beta}), gamma (D_{gamma}) and total (D_0) dose rate conversion factors as determined by Adamiec and Aitken (1998).

Radionuclide content	D_{beta} µGy/a[a]	D_{gamma} µGy/a	Total D_0 µGy/a
1 ppm U	131	113	224
1 ppm Th	25	48	73
1 % K	704	243	947

[a] including a beta attenuation factor of 0.9.

The other approach for determining the external dose rate is to use a detector system (e.g. a beta counter or gamma scintillometer) to count gamma and beta emissions, from which dose rates can directly be calculated, though without deriving information on discrete radionuclide concentrations.

The cosmic dose is not measured directly but calculated through equations incorporating its dependency on the sampling depth below surface, geographic latitude and altitude. Prescott and Hutton (1988, 1994) give the following equations to calculate the dose rate. First, the cosmic dose is estimated solely based on the sampling depth below surface, using Equation 7.1:

$$D_c = \frac{6072}{((x + 11.6)^{1.68} + 75)\,(x + 212)} \exp(-0.00055\,x) \qquad \text{(Eq. 7.1)}$$

where D_c is in Gy/ka and x is the depth below surface (in m) multiplied with the average overburden density (in g/cm³).

If necessary, hence when samples are near to the equator (<35° geomagnetic latitude), or located in significant altitudes (<1 km), the cosmic dose derived from Equation 7.1 is corrected using Equation 7.2:

$$D_{c,\,corrected} = D_c\left[F + J \exp \frac{h}{H}\right] \qquad \text{(Eq. 7.2)}$$

where h is the altitude in km, and the values for F, J, and H are taken from the graph in Fig. 7.2. For the samples from the western Murray Basin analysed in this study this correction is not necessary as the sample locations are far below 1 km altitude and are positioned at a geomagnetic latitude of 45°S.

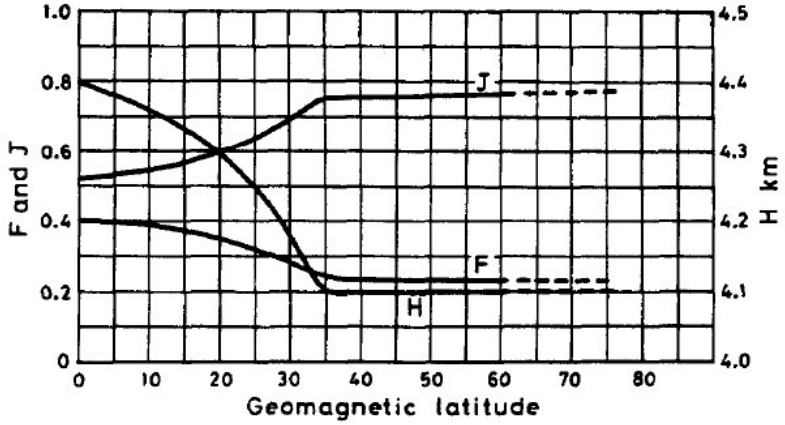

Fig. 7.2. Parameters F, J and H for finding the cosmic ray dose rate as a function of altitude and geomagnetic latitude (from Prescott and Hutton 1994).

7.2.1.1 Gamma spectrometry

In the following, the basic principles of gamma spectrometry will be outlined. A detailed description of the method can be found in Debertin and Helmer (1988) and all information given in the following is taken from this source.

Gamma spectrometry makes use of the fact that during radioactive decay different radioisotopes release gamma rays with different and specific energies. ^{226}Ra, a daughter isotope from ^{238}U emits for example gamma rays with an energy of 186 keV. At the lower end of this series, ^{214}Pb decay releases gamma rays with energies of 242, 295, and 352 keV. When these energies are measured, they provide the possibility to qualify and quantify a given radionuclide within the sediment to be analysed. Measurement of the released energy by gamma radiation is carried out in a gamma spectrometer in the following way: A gamma photon emitted in the process of radioactive decay in a sample enters the gamma ray detector, which commonly consists of a high purity

germanium (HPGe) crystal. In this crystal, the photon interacts with the atoms of the detector crystal by ejecting a bound electron from the shell of the crystal atoms. This secondary electron migrates through the detector crystal, ionising other electrons, hence generating electron-hole-pairs. As detector crystals such as high purity germanium are semi-conductors, the ionised electrons and holes are transferred from the valence band to the conduction band. The quantity of charge produced in this process can be measured by inducing an electric field in the detector using high voltage. As a consequence, the charge pairs in the conduction band shift to electrodes where they induce electric pulses. These pulses are amplified passing through a preamplifier and amplifier, after which they can be collected and sorted in a multi-channel analyser (MCA). The gamma spectrometry measurement process is illustrated in Fig. 7.3. In order to convert the measured charge quantity to the equivalent energy released by the initial photon, an energy calibration of the gamma spectrometer has to be carried out using samples with known energy lines. Hereby, the measured charge quantity is linearly related to the initial energy of the gamma photon, thus only two energy lines are needed for calibration. After the energy calibration, a gamma spectrometry measurement of a given sediment sample produces a gamma spectrum where the gamma photon energy is shown on the x-axis and the intensity of each energy line on the y-axis. To relate the intensity of the energy peaks to radionuclide concentrations in the sample, any gamma ray detector needs to be calibrated for its efficiency with standard samples of known radionuclide concentrations or activities.

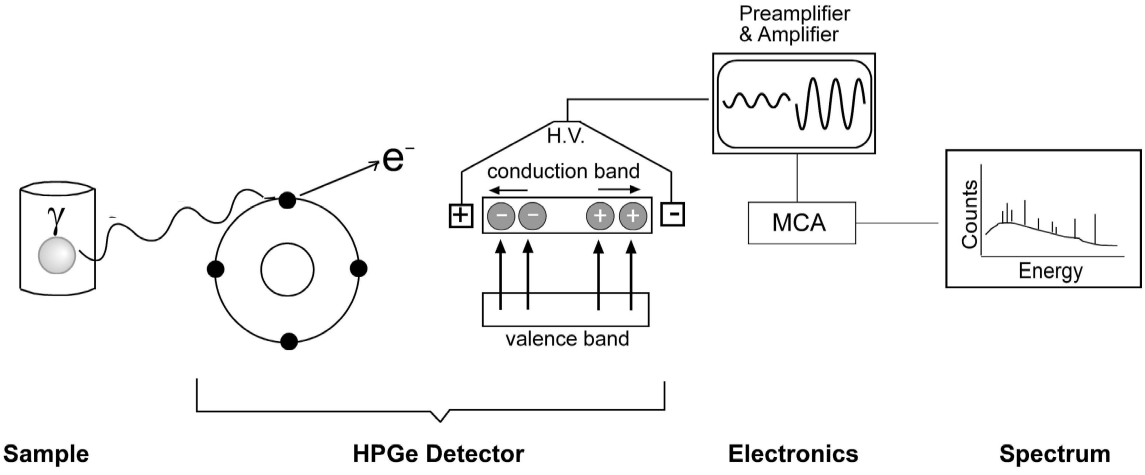

Fig. 7.3. Basic principle of a gamma spectrometry measurement. From the sample, containing radionuclides, gamma photons are emitted, producing free electrons in the detector, which again allow multiple electron-hole-pairs to migrate to the conduction band. Charge from the conduction band is collected by inducing an electric field on the detector using high voltage. The pulses are amplified, sorted in a Multi Channel Analyser (MCA) and converted into a gamma spectrum.

In order to prevent interaction within the detector from gamma rays derived from cosmic radiation or radionuclides in the building, the detector and the sample need to be shielded by a lead castle of appropriate thickness. Furthermore, germanium detectors need to be cooled with liquid nitrogen to prevent thermally induced ionisation process in the detector crystal. An example of a gamma spectrometer is shown in Fig. 7.4.

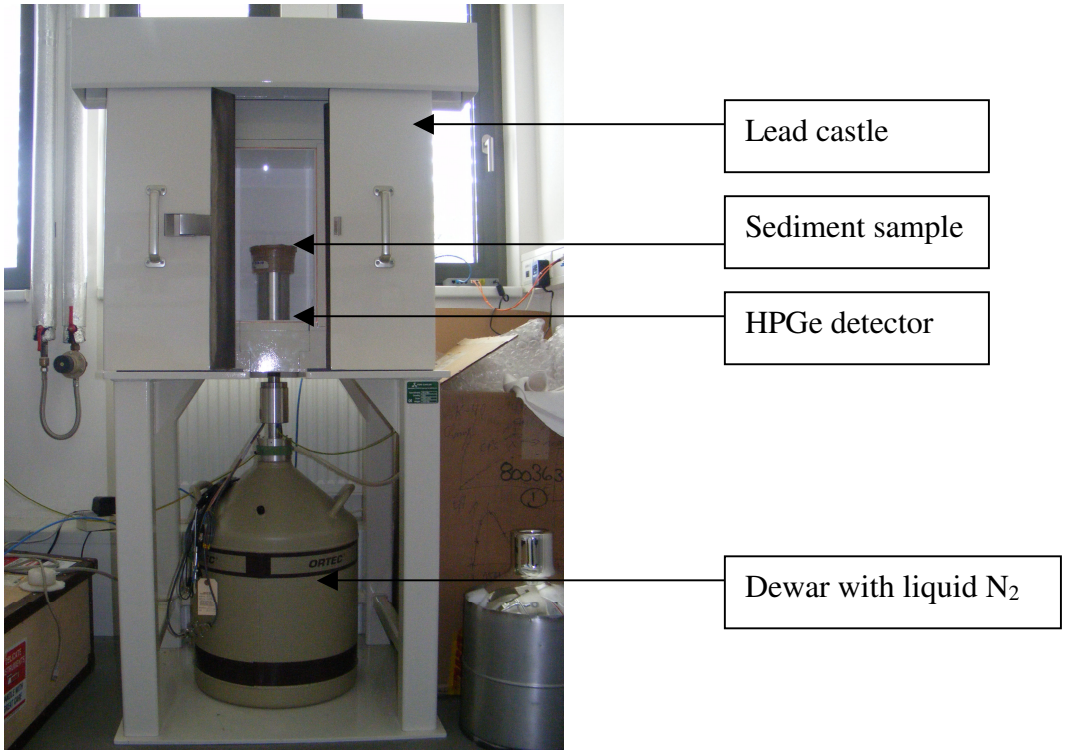

Fig. 7.4. Ortec gamma spectrometer of the Cologne Luminescence Laboratory (Photograph by J. Lomax, 2008).

In order to interpret the resulting gamma spectrum, further details on the interaction of gamma radiation and the detector crystal need to be outlined. Basically, there are two main interaction processes that need to be considered when analysing sedimentary samples; the photo effect and the Compton effect. The photo effect occurrs when a gamma photon with a discrete energy or wavelength released from an atomic nucleus passes its entire energy onto the ejected electron and produces an equivalent quantity of charge through further ionisation processes. The Compton effect is produced when a gamma photon hits an electron at a certain angle, loses part of its energy to the ejected electron and subsequently migrates – with lower energy and higher wavelength – through the detector crystal (Fig. 7.5).

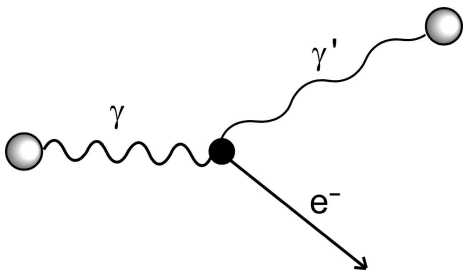

Fig. 7.5. Schematic display of the Compton effect. A photon (γ) only imparts some of its energy onto the electron (e^-), and further migrates through the detector with lower energy (i.e. larger wavelength) (γ') (redrawn from Debertin and Helmer (1988)).

If the Compton-scattered photon is absorbed in the detector by the photo effect, possibly involving several Compton scattering incidents, then the total energy of the initial photon is recorded in the detector. In this process, two or more electrons are ejected and the sum of their energies is equal to that of the initial photon. If the photon escapes the detector before being absorbed by the photo effect, then the resulting charge measured will not be equivalent to the energy of the initial photon, but lower. Due to this latter process, the gamma spectrum displays a continuous background (the Compton background). Superimposed on the Compton background are narrow, Gaussian-shaped peaks, which are induced by photo effects. These peaks are also referred to as full energy peaks or photo-peaks. A typical gamma spectrum of a sedimentary sample is shown in Fig. 7.6.

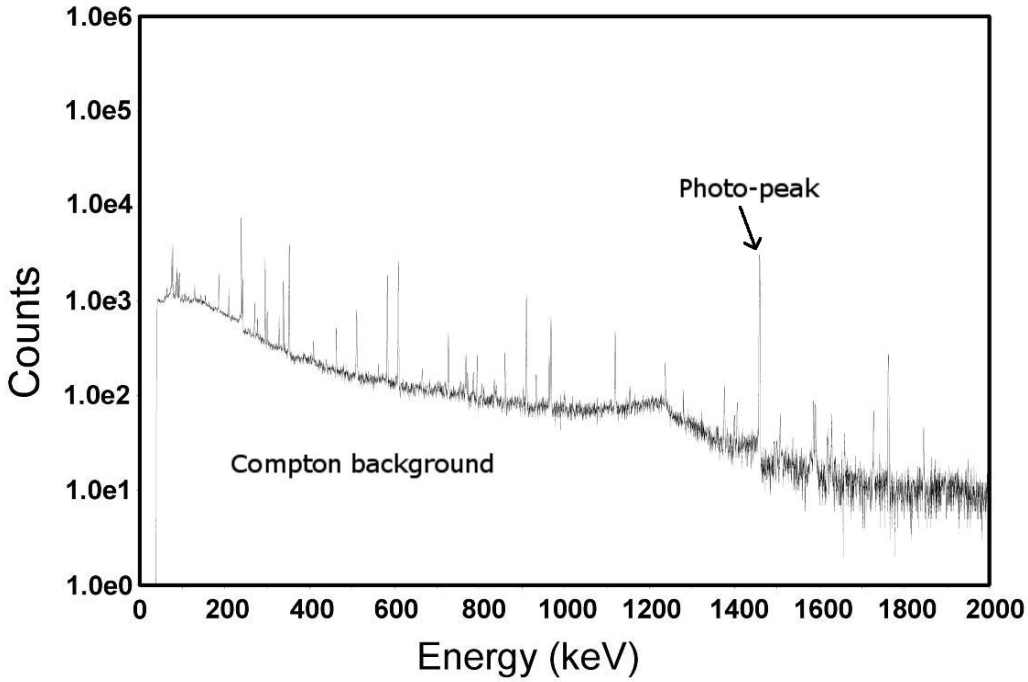

Fig. 7.6. Typical gamma-spectrum of a sedimentary sample (Nussi-Loess) showing photo-peaks and the Compton background.

7.2.2 Sources of errors in the determination of the dose rate

In the literature, possible sources of errors on dose rate estimates and their potential correction have received little attention compared to those of the palaeodose. This is despite the fact that multiple complicating factors affect the determination of the dose rate.

One of the major sources of error is that dose rates are often calculated from 'as found' parameters (e.g. the modern concentrations of U, Th, K, or presently occurring sampling depth, water content and level of cosmic radiation). It is then often presumed that these 'as found' conditions persisted over the time span to be dated, but this assumption might not always be valid. Another problem is associated with the sample amount on which radionuclide concentrations are determined as small sub-samples may not be representative for the total environmental radiation affecting the quartz grains to be dated.

7.2.2.1 Cosmic dose variations

As outlined in Section 7.2.1, the cosmic dose is mainly calculated from equation (7.1), in which the sampling depth below surface is the variable parameter. Usually, the depth below surface is derived from measuring the distance between the surface and the sampling position, and then taken as having remained constant since the deposition of the sediment layer, from which the sample was taken from. This is most likely not the case, unless this sediment layer was covered immediately to the present surface level. In dunes, the sedimentary history often consists of multiple depositional cycles, interrupted by stable phases with soil formation (e.g. Lomax et al. 2003, Munyikwa 2005a, 2005b, Fitzsimmons et al. 2007). Thus, after its deposition a sediment layer might have functioned as dune surface for a long period, before being covered by new sands in a further depositional phase. As a consequence, the cosmic dose received from grains in this layer might be higher than calculated from the present depth below surface. Usually, this problem is treated as having minor importance due to the low contribution of the cosmic dose to the total dose rate (often lower than 10 % (Aitken 1998, Munyikwa 2000)). In the samples investigated in this study though, the contribution of the cosmic dose is higher, averaging some 15 % and exceeding 40 % in some of the samples near the surface (see Section 7.4). However, variations in cosmic dose rates in these surface samples are not significant when it is assumed that they were located near

the surface since they were deposited. The possibility remains though that they were covered by further sediment layers which were eroded later. Hilgers (2007) simulated sedimentation history scenarios for dunes in northeastern Germany to account for variations in cosmic dose rates, and found that the corrected ages only differed by ~3 % on average from uncorrected ages, a difference well within the total error of luminescence ages.

Long term variations of the cosmic radiation due to migration of the geomagnetic poles and geomagnetic latitudes or changes in the production of primary galactic cosmic radiation also occurred during the Quaternary inducing long term changes in cosmic dose rates. The effect on luminescence ages was calculated to be insignificant though (Prescott and Hutton 1994).

However, due to non-quantifiable sediment overburden during the time span to be dated and possible minor variation of incoming cosmic radiation, relatively large errors on the cosmic dose rate should be considered to account for these problems.

7.2.2.2 Radioactive disequilibria

Dose rates are usually calculated or measured from presently occurring radionuclide concentrations in sediments, under the assumption that these element concentrations remained constant over the time span to be dated. For the mother nuclides ^{40}K, ^{235}U, ^{238}U and ^{232}Th, this assumption is quasi correct as due to their long half-lives in orders of 10^9-10^{10} a, their concentrations will not be significantly reduced through radioactive decay during time spans relevant for luminescence dating (several 10^5 a). If the sedimentary system is closed, hence no radionuclides are added or removed, these mother nuclides decay via a series of daughter isotopes, each of them exhibiting the same activity (disintegration per time unit). In such a case, the decay chain is termed to be in secular equilibrium. However, from the U and Th decay chains several isotopes might be removed or added, for example radon due to gaseous emanation, radium due to its mobility (Aitken 1985) or ^{234}U caused by fractionation due to a weaker binding in minerals compared to its mother ^{238}U (Krbetschek et al. 1994). In the ^{232}Th decay chain, disequilibria were shown to be of very minor importance because of the short half lives of the mobile daughter products (Olley et al. 1996, 1997, Krbetschek et al. 1994). Disequilibria in the ^{235}U decay series are also negligible due to the low abundance of ^{235}U. In contrast, radioactive disequilibria can persist over many decades in the ^{238}U

decay chain, because of longer half-lives of the relevant daughters. In various studies it has been demonstrated that disequilibrium of the ^{238}U decay chain most likely occurs in water lain sediments, but not in aeolian sediments (Krbetschek et al. 1994, Prescott and Hutton 1995, Vandenberghe 2003). Nevertheless, the possible occurrence of radioactive disequilibria will be investigated in Section 7.3.3.

7.2.2.3 Variations in sediment properties and water content

Usually, in luminescence dating the 'as found' water content at the time of sampling is measured by laboratory methods. It is obvious though that the measured water content is not representative for the whole time span since the sediment was deposited, for example due to climate change and/or groundwater fluctuations. As it is nearly impossible to estimate the degree of water content fluctuations during the time span to be dated, the water content is considered as one of the major sources of errors in dose rate determination (Aitken 1998). This problem should be allowed for by assuming an appropriate range of possible water contents when calculating the attenuation of the dose rate induced by pore water.

Further changes in the dose rate during the time span to be dated may arise from changes of sediment properties. For example, calcretes may form within sediments that have been deposited a long time before the calcrete formation itself. If the calcretes have different radionuclide concentrations than the sediment they formed in, the dose rate will have changed since the time the calcrete formed. The same is possibly true for downward movement of clay particles in a sediment body with infiltrating rain water or for compaction of sediment layers through increasing overburden through time. This will not only change the radionuclide concentrations, but also the ability to store moisture, both having an effect on the resulting dose rate.

7.2.2.4 Sediment heterogeneities

In many sediments, radionuclides are not distributed homogenously. These heterogeneities occur on a grain-to-grain level, and on a larger scale level, if layers or areas of different sediment composition exist.

Layers of different sediment composition will induce variations in the flux of gamma-radiation with its typical range of around 30 cm in sediments. For example, when sandy layers alternate with clayey layers, then the clayey layer will probably have much higher

radionuclide concentrations than the sandy layer. Quartz grains within the sandy layer less than 30 cm away from the clayey layer will receive some of the increased gamma dose from the clayey layer. Similar problems arise when large blocks with different radionuclide concentrations are distributed in the sediment Fig. 7.7(a). There are several ways to account for these large-scale gamma dose heterogeneities. One way is to take samples for dose rate determination as representative as possible. In the case of strong sedimentary heterogeneity, this would mean large amounts of sample material with a representative distribution of the various sediment components. Another possibility would be to take several samples from layers with markedly different composition and then model the varying influence on the dose rate the sample to be dated is exposed to. Modern luminescence age calculation programmes such as ADELE (Degering et al. (submitted)) include such modelling of dose rates in the case of different sediment layers. A further way to circumvent heterogeneity problems are in-situ measurements of the dose rate, e.g. through field gamma spectrometers or field gamma scintillometers.

Radionuclide variations on a grain-to-grain level, also referred to as microdosimetric effects, are only relevant for the flux of beta radiation with its typical range of 2 mm in silicates. For example, a quartz grain which is located next to a potassium-rich feldspar grain will be exposed to a higher beta dose rate than a quartz grain surrounded only by other quartz grains (Fig. 7.7(b)). As it is impossible to measure dose rates on a grain to grain level in the original sediment matrix, microdosimetric effects will be noticed in variations of the palaeodose of individual quartz grains, but cannot be accounted for. This case of heterogeneous radionuclide distribution will therefore be discussed in Section 6.8.7.3.2.

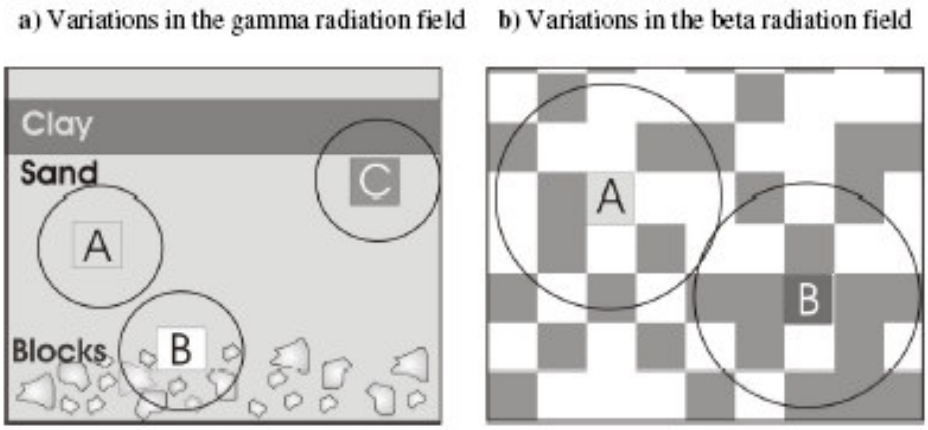

Fig. 7.7. Variations in the environmental radiation field due to sedimentary heterogeneity. (a) The gamma radiation field at sampling position 'A' is homogeneous. Provided that the blocks at the bottom of the section contain very low concentrations of radionuclides, the gamma dose at position 'B' is lower compared to the homogeneous radiation field at position 'A'. Higher radionuclide concentrations in the clay layer compared to the sand unit result in an increased gamma dose rate at sampling position 'C'. The circle indicates the range of gamma radiation. (b) Grey shaded areas represent grains with a higher content of radionuclides (e.g. zircons, K-rich feldspars), thus representing stronger radioactive sources than the grains represented by white areas (e.g. quartz grains). A grain sampled from position 'A' would have accumulated less radiation dose compared to the grain at position 'B'. The circle indicates the range of betaparticles (from Hilgers 2007).

7.3 Gamma spectrometry measurements of the western Murray Basin samples

7.3.1 Instrumentation and sample preparation

All laboratory gamma spectrometry measurements were carried out in the luminescence laboratory of the University of Cologne, using a Canberra 20 % p-type HPGe detector. Further details of apparatus and calibration of this gamma spectrometer can be found in Preusser and Kasper (2001). Approximately 1700 g of sampling material were dried at 105°C for 24 h, and filled into airtight Marinelli beakers. To allow re-establishment of secular equilibrium which might have been disrupted during preparation due to radon loss, the samples were stored for at least 28 days before the measurement (Debertin and Helmer 1988). Measurements were carried out for 20 h on each sample. The energy lines used for determination of U-, Th-, and K-concentrations, and their source nuclides are shown in Tab. 7.2. The line at 186 keV is a superposition of ^{226}Ra and ^{235}U, and has been used by e.g. Zander et al. (2007) and Preusser and Degering (2007) to infer radioactive disequilibria between ^{238}U and ^{226}Ra in the ^{238}U decay chain (see Section 7.3.3).

Tab. 7.2. Radionuclides and their energy lines used for determination of U, Th, and K concentrations from laboratory gamma-spectrometry.

Uranium series		Thorium series		Potassium	
Energy (keV)	Source Nuclide	Energy (keV)	Source Nuclide	Energy (keV)	Source Nuclide
186	$^{226}Ra/^{235}U$	239	^{212}Pb	1461	^{40}K
295	^{214}Pb	300	^{212}Pb		
352	^{214}Pb	338	^{228}Ac		
609	^{214}Bi	583	^{208}Tl		
1120	^{214}Bi	727	^{212}Bi		
		911	^{228}Ac		
		2615	^{208}Tl		

The mean instrumental error for the gamma spectrometer used in this study, resulting from uncertainties in peak matching and background variability, was determined to 3.4 % for U, 4.6 % for Th and 2.1 % for K by Preusser and Kasper (2001). Additionally, the standard deviation between the results of the different energy lines used for U and Th determination, was considered in the total error calculation.

7.3.2 Radionuclide concentrations of the western Murray Basin samples

The results of the radionuclide measurements of the western Murray Basin samples are given in Table 1 in the Appendix. Median values of the U-, Th and K-concentrations for the different dune fields and geological formations are given in Table 7.3.

Tab. 7.3. Median U-, Th- and K-concentrations of the Murray Basin samples for the different dune fields and geological formations.

Dune field or section, geological formation	Uranium (ppm) (median)	Thorium (ppm) (median)	Potassium (%) (median)
Linear dune field, Woorinen Formation	0.45	2.23	0.59
Section BM, Bunyip Sands	0.82	3.98	0.85
Sub-parabolic dune field, Molineaux Sands	0.33	1.63	0.26
Section PSP, (Woorinen F. and Molineaux S.)	0.33	1.66	0.35

In general, the measured radionuclide concentrations are comparatively low, which is probably due to low clay, feldspar and heavy mineral concentrations in the dune sands. Radionuclide concentrations in the sub-parabolic dune field are significantly lower than in the linear dune field. This was expected considering the lower clay concentrations in the sub-parabolic dune field described by Pell et al. (2001) and Bowler and Magee (1978). Radionuclide concentrations of the samples from the Bunyip Sands (section BM) are very high compared to the samples from the linear dune field, although grain sizes were similar to the linear dune field. An explanation would be a distinctly different sand source for the parabolic dunes of the Bunyip Sands and the linear dunes of the Woorinen Formation. This would argue for very local sources and against long distance transport of the dune sands, as already stated by Pell et al. (2001). Section PSP from a linear dune is located in a transitional zone of the Woorinen Formation and the Molineaux Sands. Due to its morphology, the dune is assigned to the Woorinen Formation, which is characterised by linear dunes. The low radionuclide concentrations though, which are very similar to those of the sub-parabolic dune sands of the Molineaux Sands argue for a similar source of the dune sands from section PSP and the sub-parabolic dune field.

In the linear dune field, the carbonate-rich samples have similar radionuclide concentrations as samples with little carbonate content (see Table 1, Appendix). It is thus concluded that the carbonate rich layers within the dune sequences will not pose any serious problems concerning heterogeneous distribution of radionuclides referred to in Section 7.2.2.4.

7.3.3 Assessment of radioactive disequilibrium

Zander et al. (2007) and Preusser and Degering (2007) used measurements from the same gamma spectrometer used in this study to infer radioactive disequilibria in the ^{238}U decay chain. The 186 keV line, which is a superposition of ^{226}Ra and ^{235}U, was taken as substitute for the ^{238}U concentration, assuming a natural ^{238}U/^{235}U isotope ratio. The two ^{214}Bi and ^{214}Pb lines were taken as substitute for the ^{226}Ra concentration, under the premise of radioactive equilibrium between Ra and its Bi and Pb daughters. The same approach is used in this study.

Only in a few samples a distinctly different activity of ^{238}U and ^{226}Ra was noticed. As mentioned above, other studies have shown that dune sands are not likely to be

susceptible to radioactive disequilibria (Krbetschek et al. 1994, Prescott and Hutton 1995). However, it has been demonstrated that carbonate-rich environments may pose some problems in this respect due to post-depositional uranium mobilisation during carbonate precipitation (e.g. Olley et al. 1997, Lomax et al. 2003, Zander et al. 2007). In order to visually assess discrepancies between ^{238}U and ^{226}Ra, scatter plots were constructed, which show ^{238}U (the concentration derived from the 186 keV line) on the y-axis and ^{226}Ra (the mean of the concentration derived from the ^{214}Bi and ^{214}Pb lines) on the x-axis (Fig. 7.8). Only those sections are shown which contain samples with discrepancies between ^{238}U and ^{226}Ra of more than 20 %. Discrepancies within 20 % are considered minor and caused by analytical uncertainties.

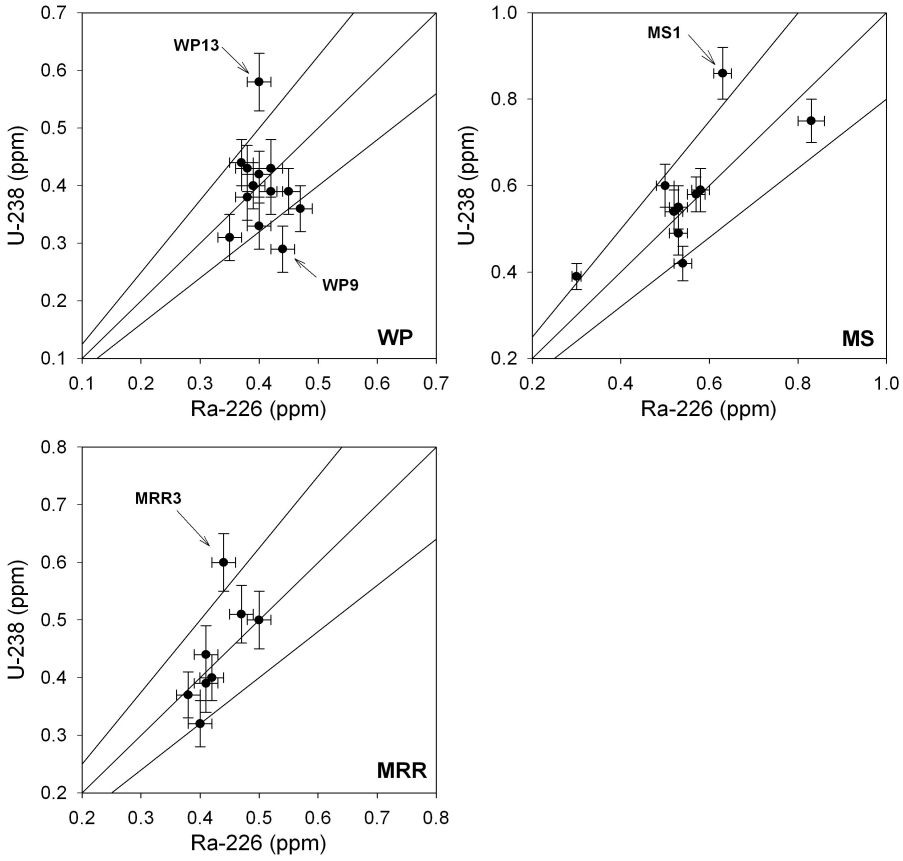

Fig. 7.8. Relation between ^{238}U and ^{226}Ra in selected sections of the western Murray Basin showing possible radioactive disequilibria. The solid lines represent the 1:1 ratio and deviation of 20 % from unity.

Samples with distinct deviation between the relevant radionuclides are WP9, WP13, MRR3 and MS1. ^{238}U/^{226}Ra ratios in these samples are 0.66, 1.45, 1.36, and 1.37, respectively. No clear association with calcretes in the sections is obvious. WP9 and WP13 are both located above calcretes, and are both carbonate-rich, but WP13 though shows a higher ^{238}U concentration compared to ^{226}Ra, whilst WP9 has lower ^{238}U

concentration compared to ^{226}Ra. MRR3 is located above a carbonate-rich layer, and MS1 is from a hardpan calcrete. The latter two samples show an excess of ^{238}U compared to ^{226}Ra. However, a lot of samples from locations near hardpan calcretes or from very carbonate-rich layers show no distinct difference between the two radionuclides. The average ^{238}U/^{226}Ra ratio of all the other samples investigated (excluding the four samples mentioned above) is 1.02, underlining the expectation that radioactive disequilibria are not a major concern in the dune sands investigated in this study, even for most of the carbonate-rich samples. For those four samples that do show radioactive disequilibria of the ^{238}U decay chain, the effect on the resulting dose rate is considered minor. As will be demonstrated in Section 7.4, the uranium concentration in the samples investigated in this study contributes only around 12 % to the total dose rate, thus even serious and long lasting disequilibria do not result in major changes of dose rates and hence luminescence ages. In order to estimate the influence of the disequilibria on the resulting dose rate for the three samples with ^{238}U excess over ^{226}Ra, two dose rates were calculated, one using the increased ^{238}U concentration and one using the lower ^{226}Ra concentration (weighted mean of ^{214}Bi and ^{214}Pb). The difference between the dose rates is 5 % in sample MS1, and 4 % in sample WP13 and MRR3, and the dose rates overlap within errors, thus, are statistically indistinguishable from each other. For calculation of the dose rate of these samples, the mean of all measured uranium daughters was used.

7.4 Environmental dose rates of the western Murray Basin samples

As outlined in Section 7.2, for the dose rate of quartz, the beta, gamma and cosmic dose have to be considered, including attenuation of the beta dose in sand-sized quartz grains and attenuation of radiation through water in sediment interstices. For all samples, dose rates were calculated using uranium, thorium and potassium concentrations derived from laboratory gamma spectrometry. The dose rate was calculated using beta doses and gamma doses calculated from conversion factors of Adamiec and Aitken (1998), a beta attenuation factor of 0.9 after Mejdahl (1979) and Aitken (1998), the cosmic dose calculated from the formula given in Prescott and Hutton (1994) and water content fluctuations ranging from 0-6 %. The water content range reflects the range of measured water contents in all samples investigated. Water contents were determined by weighing the samples with as found water contents, then drying them for 24 hours at 105°C and re-weighing them. The values measured are considered relatively representative of the

degree of climatic fluctuation, as some of the samples were taken after a prolonged dry period, whereas other samples were taken after a night of heavy rain.

Total dose rates and the contribution of the dose rate derived from each radionuclide as well as from the cosmic dose rate are given in Table 1 in the Appendix. Median values of the total dose rates and the range of the contributions to the total dose rate from uranium, thorium, potassium and the cosmic dose rate for the different dune fields and sections are summarised in Tab. 6.4. The dose rates given in Table 1 (Appendix) and Tab. 6.4. are calculated for a grain-size of 200-250 µm. This grain size spectrum was used for the single grain De-determinations carried out in the study. For the multiple grain analysis, however, grain sizes of 100-150 µm were measured to determine the equivalent dose. In this case, dose rates were recalculated with a different beta attenuation factor.

Tab. 6.4. Median total dose rates of the western Murray Basin samples for the different dune fields and geological formations and the contribution of uranium, thorium, potassium and the cosmic dose rate to the total dose rate.

Dune field or section, geological formation	total dose rate (Gy/ka)	U (%)	Th (%)	K (%)	cosmic (%)
Linear dune field, Woorinen Formation	0.94	9-14	11-22	48-63	8-23
Section BM, Bunyip Sands	1.42	12-14	18-21	54-62	7-12
Sub-parabolic dune field, Molineaux Sands	0.59	12-14	14-21	26-50	18-43
Section PSP, (Woorinen F. and Molineaux S.)	0.67	10-14	14-26	44-54	15-32

In most of the samples, potassium is the main contributor to the total dose rate with a percentage of often more than 50 %. The cosmic dose rate proportion is very variable and dependent on the concentration of radionuclides. Samples with very low radionuclide concentrations, as is the case for samples from the sub-parabolic dune field, have a relatively high contribution of the cosmic dose rate to the total dose rate. In section NG, the contribution of the cosmic dose rate to the total dose rate even exceeds the contribution of potassium. Correct assessment of the cosmic dose is hence a major concern in some of the samples investigated and will be further discussed in Section 8.2.

8. The resulting luminescence ages and their chronostratigraphic context

8.1 Age calculation

OSL ages were calculated by dividing the equivalent dose, presented in Section 6.8, by the dose rate, presented in Section 7.4. All ages were calculated using De-values from the single grain analysis. Ages of samples, for which equivalent doses were determined using the finite mixture model, were calculated only for the main De-component. It is also possible to calculate ages for components with minor proportions, but this was considered to introduce an additional source of error to the ages in respect to the dose rate. For example, little proportions of grains might be moved by bioturbation from layers with higher dose rates to layers with lower dose rates. As it is unclear when this movement occurred, it is difficult to determine a dose rate for these grains. The main De-proportion is considered to represent the host layer, into which older grains from underlying layers and younger grains from overlying layers intruded. Thus, the dose rate for grains within the main De-population should have stayed similar.

The error of the luminescence age consists of the dose rate error and the equivalent dose error, combined using gaussian error propagation. A beta source calibration uncertainty of 3.5 % was included in the total error of the equivalent dose (Murray and Funder 2003).

In the following, all OSL ages will be shown in their stratigraphic context. Correction procedures in respect to varying cosmic doses will be discussed. Furthermore, net sedimentation rates will be quoted. It has to be considered though that these net sedimentation rates do not necessarily reflect real sedimentation rates. The latter could have been much higher, but due to susceptibility of dune sands to reactivation, evidence of higher sedimentation rates might have been destroyed. Furthermore, it has to be considered that dune sands might be packed more densely with increasing overburden. Thus, sedimentation rates at basal parts of the sampling sections might appear lower than in near-surface layers.

8.2 Luminescence ages of the sub-parabolic dune field (Molineaux Sands)

Four sections in the sub-parabolic dune field of the western Murray Basin were investigated. Resulting OSL ages (in ka) are shown in Fig. 8.1, and the locations of the sections are shown in Fig. 4.9.

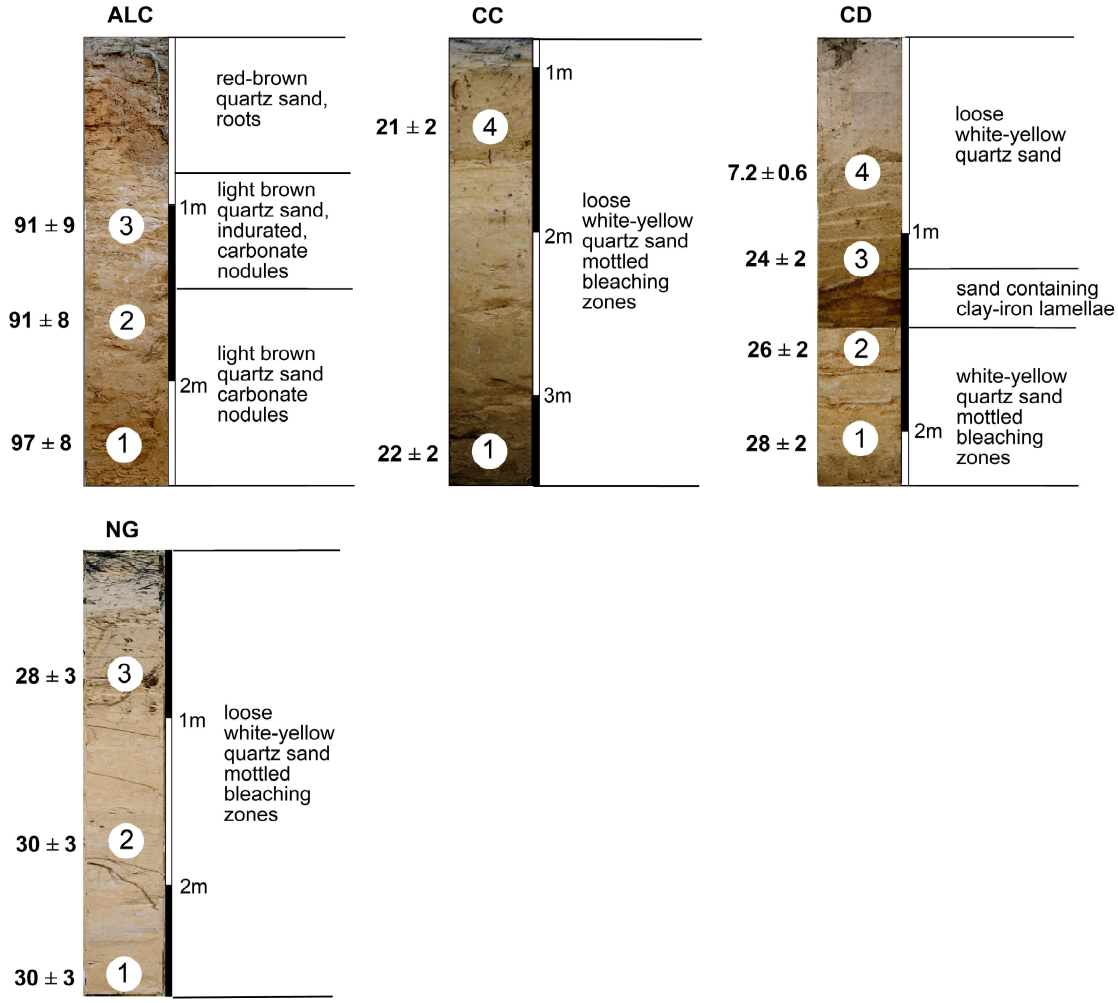

Fig. 8.1. Luminescence ages obtained for the sub-parabolic dune field (Molineaux Sands) of the southwestern Murray Basin. All ages are calculated from single grain De-values, and are given in ka.

The obtained ages in the sub-parabolic dune field range from 7.2 ± 0.6 to 97 ± 8 ka and are in correct chronostratigraphic order. Errors on the ages approximate 10 % and consist to similar proportions of uncertainties in De-determination (5-7 %) and uncertainties in dose rate determination (6-7 %).

In section ALC, CC and NG, OSL-ages for each profile are indistinguishable from each other within errors, indicating very high sedimentation rates. It thus appears likely that the as found sampling depths are similar to those at the time of deposition of the dune sands. Therefore, no corrections with respect to cosmic dose rate variations should be necessary. However, in these three sections the contribution of the cosmic dose to the

total dose rate was the highest of all investigated samples from the western Murray Basin. In order to estimate the effect of varying cosmic doses, two worst case scenarios were simulated for sample NG3. This sample has a contribution of the cosmic dose to the total dose rate of 43 % (see Table 1 in the Appendix). Calculated with the as found depth of 0.7 m, the OSL-age of this sample is 27.8 ± 2.7 ka. If it was assumed that this sample had been located only 0.2 m below the surface and was covered by additional dune sands very recently, then the resulting OSL-age would be 26.9 ± 2.6 ka (~900 years younger). This is only a deviation of 3 % and well within the error of the luminescence age itself. If it was assumed that the same layer was covered by an additional meter of dune sand at deposition, and these overlying sands were eroded very recently, this would result in an OSL-age of 29.5 ± 2.8 ka. This age is 6 % higher than the age calculated with as found sampling depth, but also indistinguishable from it within the age uncertainty. Thus, although these are worst case scenarios, the effects on the resulting age are small. A correction with respect to varying cosmic doses was thus considered unnecessary. Furthermore, it is not sure which of the two scenarios would be more likely, more overburden and later erosion, or less overburden and later coverage. Any correction procedure would therefore possibly even decrease the accuracy of the luminescence age.

For section CD, the situation is slightly different. Within the lower part of the section, net sedimentation rates are comparable to those calculated for the other three sections, with 1 m of sediment deposited within about 4 ka. The youngest sample (CD4) yields an age of 7.2 ± 0.6 ka and the underlying sample (CD3) and age of 24 ± 2 ka. This possibly reflects a break in aeolian sedimentation between ~24 and ~7 ka. Therefore, sample CD3 might have been located nearer to the surface for quite a long time (at maximum for 17 ka). If one assumes a cosmic dose found in a depth of 0.3 m for 17 ka and for further 7 ka a cosmic dose found in 1.25 m, then the OSL-age of sample CD3 decreases from 23.7 ± 2.4 ka to 23.2 ± 2.3 ka. This is a difference of only 2 %. Therefore, correcting for varying cosmic doses was considered ineffective to increase the accuracy of the luminescence ages of section CD.

8.3 Luminescence ages of the linear dune field (Woorinen Formation)

In the linear dune field of the northwestern Murray Basin, eight sections were dated. Resulting OSL ages (in ka) are shown in Fig. 8.2, and the locations of the sections are given in Fig. 4.3 and Fig. 4.9.

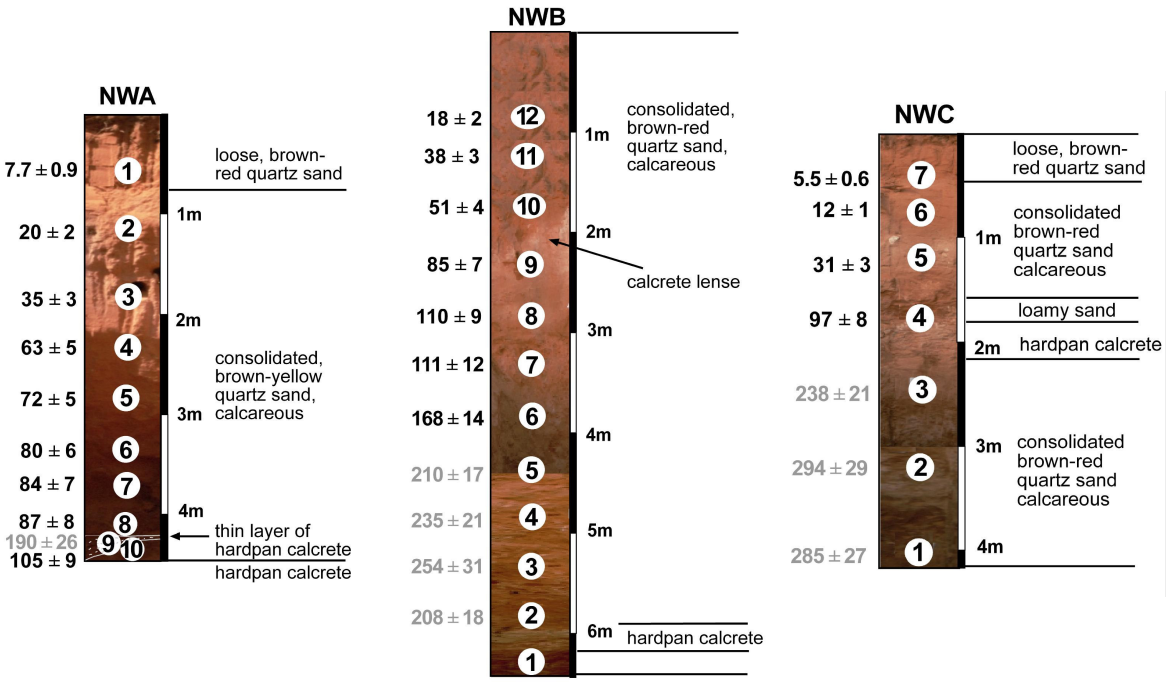

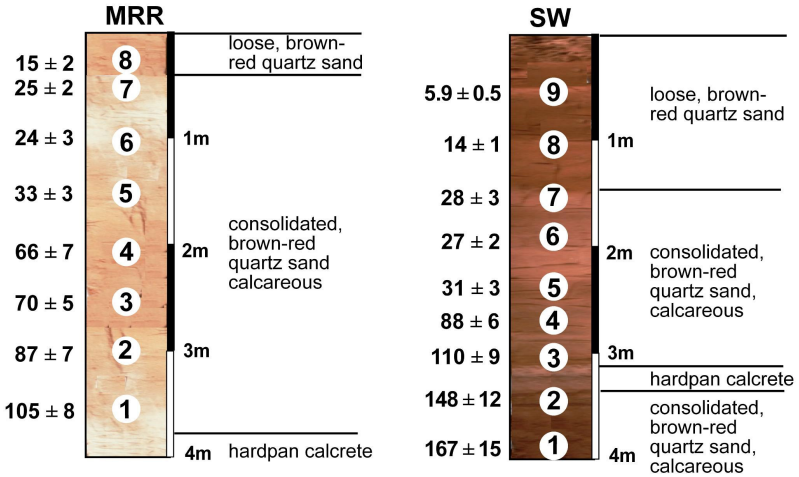

continued on the next page

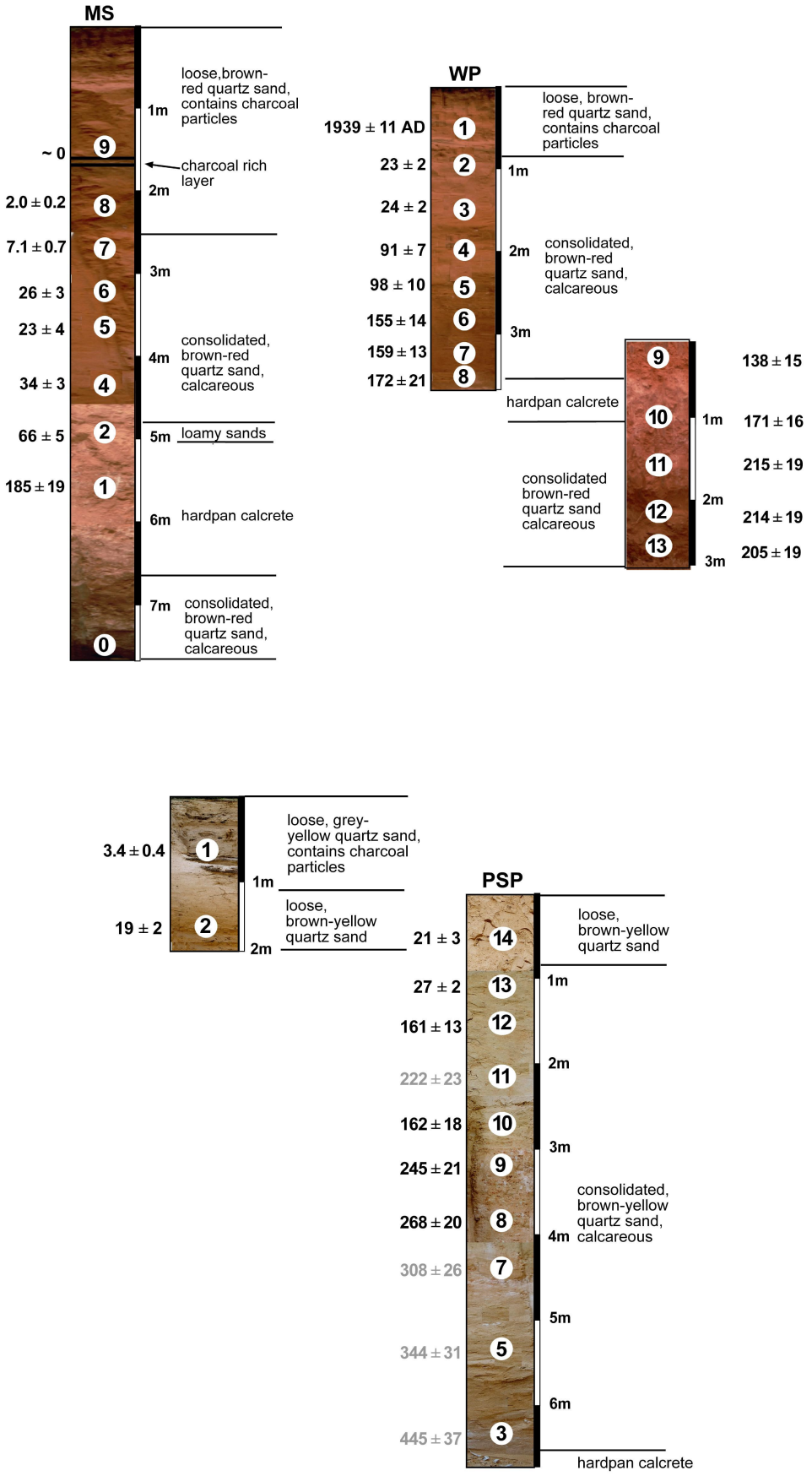

Fig. 8.2. Luminescence ages obtained for the linear dune field (Woorinen Formation) of the western Murray Basin. All ages are calculated from single grain De-values, and are given in ka, except for sample WP1. For this sample, the age is given in yrs AD. Unreliable ages are quoted as grey numbers.

In the linear dune field, luminescence ages range from ~0 ka to 445 ± 37 ka. In most of the sections, ages are in correct chronostratigraphic order. This is not the case for the sections NWA and PSP. The reason for the age inversion at the bottom of section NWA is related to problems in the De-determination and in the dose rate determination. Although these samples are located very close to each other, they have distinctively different dose rates. With an average range of 30 cm of gamma rays, a reciprocal influence of gamma radiation in the two lowest layers is expected. As sample NWA9 is located between sediment layers with higher dose rates, the measured dose rate is probably underestimated. Since the equivalent dose of sample NWA9 is higher than that of sample NWA10, even a correction of the dose rate would not produce a correct chronostratigraphic order.

Sample PSP 11 is significantly older than the overlying and the underlying samples. The dose rate of this sample is also significantly lower than in the neighbouring samples (by 13 and 19 %), causing the age inversion. Very likely, the dose rate of sample PSP 11 is underestimated, due to problems detecting the very low radionuclide concentrations in section PSP by the gamma spectrometry measurements. For further palaeoclimatic implications of the western Murray Basin dune record (Chapter 9), the ages of sample NWA9 and PSP11 are not considered.

Furthermore, all ages with De-values of >200 Gy are considered to be unreliable due to their proximity to signal saturation (see Section 6.8.5). In case these very old samples yielded (unreliable) De-values, an age is none the less shown in Fig. 8.2, given in grey numbers. These ages are in correct chronostratigraphic order, providing some confidence in their accuracy. For two samples (NWB1 and MS0), no De-value could be determined due to OSL signal saturation. Reliable ages up to ~270 ka were calculated for section PSP as dose rates in this section were very low (0.67 Gy/ka on average).

At the locations PSP and WP, two sections were exposed by backhoe trenching as creating a single section was not feasible at these locations. In order to assure that no dune layers were missed at these composite sections, layers that appeared to correlate in age - as based on field observations - were sampled twice. At section PSP, this was the sand layer that contained sample PSP2 and PSP 14 Indeed, both samples yield the same age of ~20 ka. In section WP, samples WP7 and WP9 as well as samples WP8 and WP10 yielded the same ages within errors (~150 ka and ~170 ka, respectively). In order to prevent the PDFs shown in Chapter 9 being biased by these doubled ages, weighted

mean values were calculated for these the age pairs and were used for the construction of the PDFs.

Variations in cosmic doses due to variations in overburden sediment were not considered. The contribution of the cosmic dose to the total dose rate in the linear dune field is lower than in the sub-parabolic dune field. As simulations of different overburden scenarios only resulted in small changes of the luminescence age in the sub-parabolic dune field (see discussion in Section 9.2), it follows that the effect on the luminescence ages of the linear dune samples is even smaller.

Sedimentation rates are much lower than in the sub-parabolic dune field. Average sediment rates are ~10 cm/ka, as opposed to ~80 cm/ka in the sub-parabolic dune field. Very similar ages of neighbouring samples often appear in a range of ~23-28 ka. In this age range, sedimentation rates are ~35 cm/ka on average.

8.4 Luminescence ages of the Bunyip Sands Formation

One parabolic dune of the Bunyip Sands Formation was investigated. Resulting OSL ages (in ka) are shown in Fig. 8.3, and the location of the section is given in Fig. 4.3.

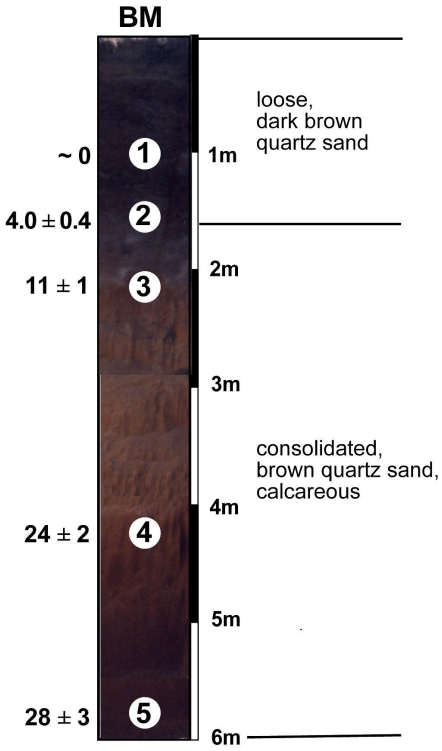

Fig. 8.3. Luminescence ages obtained for the parabolic dune of the Bunyip Sands Formation. All ages are calculated from single grain De-values and are given in ka.

In the section of the Bunyip Sands formation, luminescence ages range from ~0 ka to 28 ± 3 ka. Ages are in chronostratigraphic order. As samples of this section have the highest dose rates of all samples investigated and thus the lowest contribution of the cosmic dose rate, no correction procedures with respect to varying sediment overburden were considered. Sedimentation rates average ~17 cm/ka and are higher than in the linear dune field. Between ~24 and ~28 ka, sedimentation rates are ~44 cm/ka.

9. Discussion

In this chapter, the results of the luminescence dating of the western Murray Basin samples will be discussed with respect to the potential of the dune record to reconstruct the palaeoenvironmental history of southeastern Australia. The following questions will be considered in detail.

1. Did the deposition of dune sands take place at about the same time in the different dune fields investigated?
2. Are multiple phases of aeolian deposition recognised in the western Murray Basin dune record? Do representative gaps exist or was aeolian deposition continuous?
3. Are the results of the western Murray Basin dune record in agreement with the dune record of arid central Australia (Fitzsimmons et al. 2007), which is based on a comparable data set with respect to the number of samples and the luminescence methodology?
4. Which environmental conditions controlled the dune sand deposition in the western Murray Basin?
5. Does the dune record provide information on the onset of dune formation in the Murray Basin?

In order to display the data derived from luminescence dating, probability density functions (PDFs) are used. The method of creating PDFs and their advantages and disadvantages have already been outlined in Section 6.5. This discussion however considered the display of De-values, not the display of luminescence ages. The criticism of Galbraith (1998), namely that precise values are combined with imprecise ones and that modes in a PDF not necessarily represent discrete components, are also true for PDFs of luminescence ages (or ages of other dating methods). The first point of objection is less relevant for the presentation of luminescence ages, as the relative error of the age is much more uniform than for individual De-values. Relative errors on the luminescence ages presented in this study range from around 8 to 12 %. The risk of combining very precise values with imprecise ones therefore is relatively low. As PDFs provide good visual assessment of age groupings, and are easy to compare with other palaeoclimatic datasets, they have been widely used in the past to display luminescence

ages of aeolian sediments (e.g. Singvhi et al. 2001, Rhodes et al. 2005, Fitzsimmons et al. 2007, Telfer and Thomas 2007). For the same reasons they will be used in this study as mode of display of the OSL ages. Some aspects should be kept in mind though when interpreting PDFs. In a PDF each peak represents a cluster of luminescence ages. The peak height is a function of the number of ages within this cluster and of the precision of the luminescence ages. As younger luminescence ages are usually more precise than older ones, peaks in the younger age range of the diagram tend to be higher than those in the older age range. Thus, the mere existence of a peak is significant but not its amplitude (Geyh and Schleicher 1990).

9.1 The synchroneity of dune sand deposition in the western Murray Basin

In Fig. 9.1 and 9.2, PDFs for each dune field are shown. These are the linear dune field in the northwestern Murray Basin (Woorinen Formation), the sub-parabolic dune field in the southwestern Murray Basin (Molineaux Sands) and the Bunyip Sands on the eastern banks of the Murray River. Section PSP is considered separately as it belongs to the linear dunes of the Woorinen Formation but is located in a transitional zone to the sub-parabolic dune field. Unreliable ages (those calculated from De-values >200 ka and the ages of sample NWA9 and PSP11, see Section 8.3) are not included in the PDF. The three near zero ages are also not displayed. Furthermore, as discussed in section 8.3, some ages of section PSP and WP were combined due to doubled sampling of the dune layers. In Fig. 9.1, all ages are shown, whereas Fig. 9.2 only displays ages up to 45 ka for a better visualisation of the younger ages.

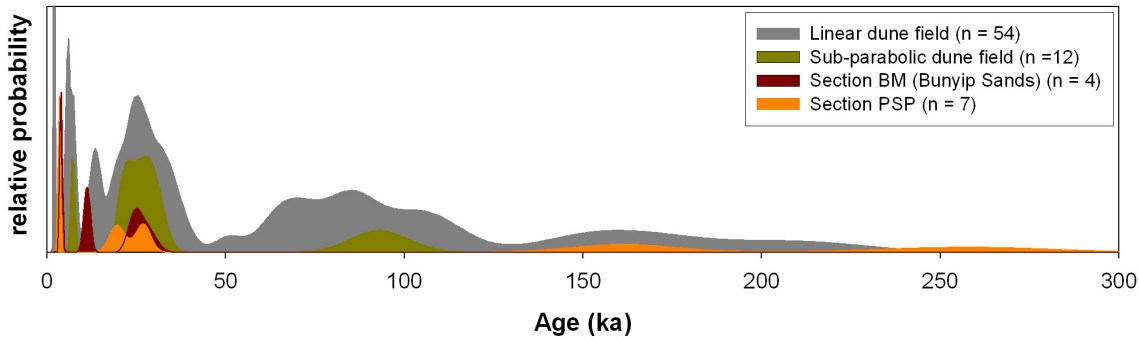

Fig. 9.1. Probability density functions of all reliable single grain luminescence ages from the individual dune fields of the western Murray Basin. The bin width is 0.5 ka.

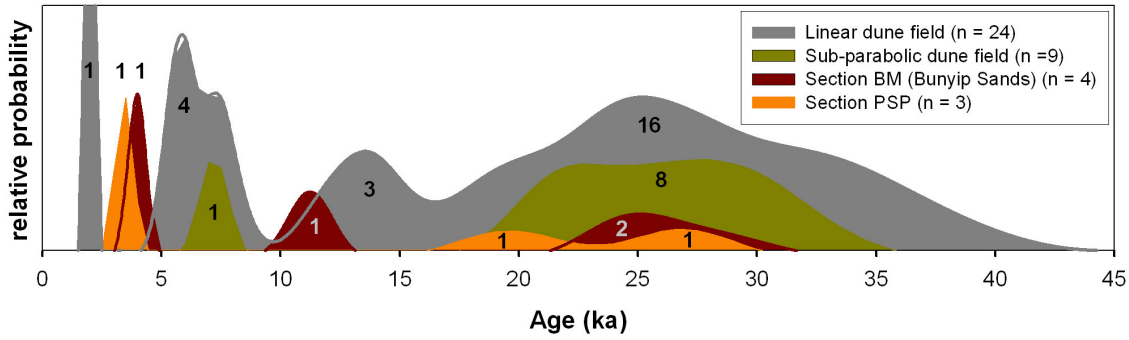

Fig. 9.2. Same data as in Fig. 9.1, but only for luminescence ages <45 ka, in order to better visualise the younger peaks. The numbers indicate of how many ages a peak consists. The bin width is 0.5 ka.

Tab. 9.1. Age clusters and single-age peaks for the three dune fields and section PSP of the western Murray Basin. The groupings are based on visual assessment of the PDFs shown in Fig. 9.1 and Fig. 9.2.

Linear dune field	Sub-parabolic dune field	Bunyip Sands (section BM)	Section PSP (Woorinen F.)
2 ka			
		~4 ka	~3.5 ka
4-9.5 ka	6-8 ka		
11-15.5 ka		10-12.5 ka	
17-37 ka	19-34 ka	22-30 ka	17-22; 24-29 ka
55-120 ka	80-105 ka		
140-190 ka			140-180 ka
			220-290 ka

The PDFs reveal the several age clusters or single-age peaks, summarised in Tab. 9.1. From the three dune fields and section PSP, the dataset from the linear dune field is surely the most representative as it contains by far the largest number of luminescence ages (n = 54) and the more detailed records per individual section. This is confirmed by the highest number of age clusters in this dune field. The peaks of dune sand deposition from the other two dune fields and section PSP are not as broad and not as numerous as those from the linear dune field. Most likely this is merely a result of the much lower number of samples taken in these dune fields. The absence of luminescence ages >97 ka in the sub-parabolic dune field does not necessarily imply that this field is younger than the linear dune field, but that older sediments were not sampled, particularly when considering the rather 'surficial' sampling strategy in this dune field (see Section 4.1.2).

Most of the peaks from the sub-parabolic dune field, the Bunyip Sands, and section PSP merge into the broader peaks from the linear dune field. This is not the case for the oldest age cluster (220-290 ka) in section PSP. However, dune sands older than 190 ka also exist in the linear dune field, but these ages are not listed in Tab. 9.1 due to their unreliability. Furthermore, two young ages at ~3.5 ka (PSP1) and ~4 ka (BM2) are not represented in the linear dune field. However, besides these two ages, dune sand deposition seems to have taken place at about the same time throughout the dune fields investigated in this study.

Therefore, it is concluded that the different dune morphologies in the linear and in the sub-parabolic dune field are not a result of significantly different climate conditions. In contrast, similar climatic conditions seem to have prevailed throughout the last ~200 ka in the entire western Murray Basin, leading to aeolian activity during defined periods. If the different morphologies are not caused by different climate conditions such as a different degree of vegetation cover, the major controls on the dune morphology in the western Murray Basin are probably differences in sand supply and the grain size distribution of the dune sands. As outlined in Section 2.3, sand supply in the sub-parabolic dune field is higher than in the linear dune field. Furthermore, dunes of the sub-parabolic dune field lack binding clays and carbonates. Due to the latter factor, Bowler and Magee (1978) and Pell et al. (2001) ascribed the sub-parabolic dunes a much higher mobility than the linear dunes. The luminescence ages clearly support this statement, confirmed by the very high sedimentation rates in the sub-parabolic dune field (Section 8.2). Presumably much larger sand volumes were transported in the sub-parabolic dune field during phases of pronounced aeolian activity compared to the linear dune field, due to the abundant sand supply and the mobility of the dunes.

9.2 Phases of dune formation in the western Murray Basin

Based on the good agreement between the luminescence ages of the dune fields, all probability density functions can be combined to one summarising function. All further implications derived from the dune record of the western Murray Basin will be based on the total dataset. Fig. 9.3(c) shows a PDF for the last 300 ka, Fig. 9.3(b) for a period between 45-300 ka and Fig. 9.3(a) for the last 45 ka. For better assessment of the errors on the luminescence ages and of the number of ages forming a peak in the PDF, ranked individual ages with one sigma error bars are included in the graph. Furthermore, age groupings are highlighted with grey bars in Fig. 9.3(a) and Fig. 9.3(b).

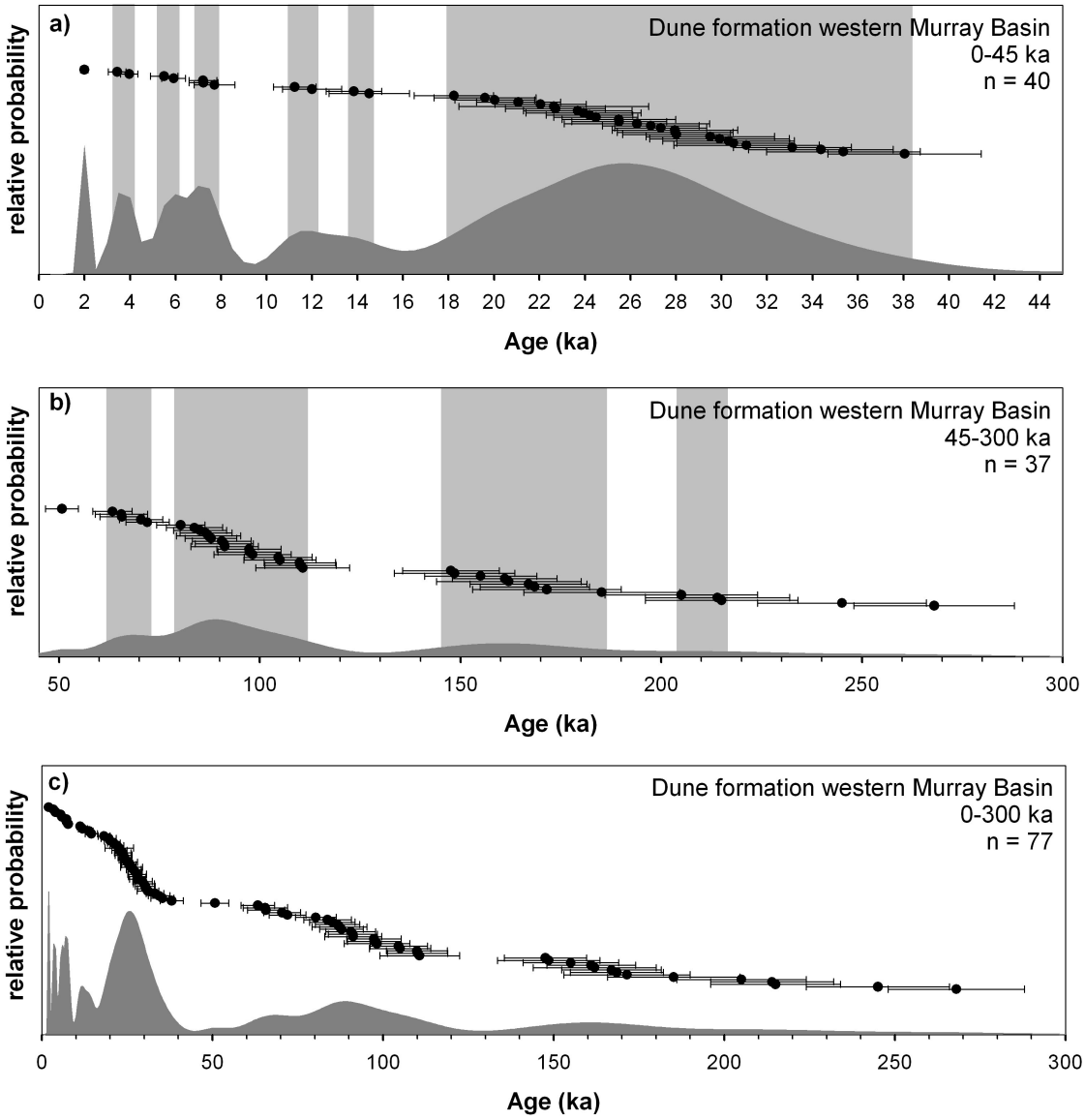

Fig. 9.3. The dune record from the western Murray Basin including all reliable luminescence ages, (a) for the period 0-45 ka, (b) for the period 45-300 ka and (c) for the period 0-300 ka. Grey bars highlight age groupings. Ranked individual luminescence ages with error bars are additionally shown. The bin width is 0.5 ka.

Age groupings were defined to consist of at least two ages that are consistent on a 0.5 sigma level. The following age groupings were inferred from the total data set: 3-4 ka, 5-6 ka, 7-8 ka, 11-12 ka, 13.5-14.5 ka, 18-38 ka, 62-73 ka, 79-112 ka, 145-185 ka and 205-215 ka. During each of these periods, extensive dune sand deposition occurred, indicating favourable environmental conditions such as dry surfaces with sparse vegetation cover, sufficient wind speed and supply of sand sized grains.

Prominent gaps in the dune record exist at ~2.5 ka, ~4.5 ka, 8.5-10.5 ka, ~16 ka, 41-47 ka, 55-58 ka and 120-140 ka. Furthermore, no dune building is evident in the record

between 1.8 ka and near-modern times. Three modern ages (not shown in the PDF) give evidence of very recent dune activity.

An important question with respect to the dune record is the representativeness of the peaks and gaps in deposition. In order to establish a dune record which is as representative as possible, many dune sections were investigated and high resolution sampling was applied. Nevertheless, the possibility always remains that gaps observed in a dune record might be filled if more samples are dated. This was exemplarily shown by Stone and Thomas (2008) for the Kalahari Dunes. When switching from a 1 m to a 0.5 m sampling resolution, the dune record changed from one with prominent peaks and gaps to one of continuous deposition when considering the errors on the luminescence ages. Thus, the significance of a dune record is always to some degree dependent on the sampling strategy applied.

When interpreting the dune record of the western Murray Basin, several aspects need to be taken into consideration. First, basal samples of the sections investigated were of different age. In the linear dune field, two out of the eight investigated sections yielded ages of <110 ka. The number of samples with ages >110 is therefore comparatively low. A further concern is that dune sands might be more densely packed in deeper layers. Therefore, the risk of missing phases of dune sand deposition might be higher than in upper layers, when a uniform sampling resolution is applied throughout the section. As a consequence, gaps in the record older than 110 ka need to be interpreted with caution.

Another problem, when discussing phases and gaps of dune sand deposition derived from luminescence chronologies, is associated with the different absolute errors of the ages. Young ages have small absolute errors. Thus, multiple phases of dune sand deposition in younger age ranges can be distinguished much better. For example, 15 samples of the western Murray Basin yielded ages of <18 ka. Approximately the same amount of samples falls into an age range of 80-100 ka. The latter phase appears as continuous deposition due to the large errors, whereas five individual short phases of dune sand deposition were identified for the younger period. Yet, aeolian deposition between 80-100 ka might just as well have occurred in short activity phases interrupted by short stability phases. For older phases of deposition, even large gaps in the dune record, lasting a few tens of thousands of years, might be masked by the relatively large errors on the luminescence ages.

In order to reconstruct palaeoclimates it further needs to be established if the depositional phases are climatically driven. Human occupation in the Murray Basin dates back to at least 46 ka (Bowler et al. 2003). Therefore, the possibility remains that some of the aeolian depositional phases <40 ka were induced, for instance, by clearing of the protecting vegetation cover through aboriginal burning practices. Evidence of extensive burning during the early human settlement in northeastern Australia was demonstrated by Turney et al. (2001) and Kershaw et al. (2003). In order to detect if dune sand deposition was triggered climatically or by human impact on the landscape, PDFs for each individual section were constructed. By this, the regional occurrence of certain depositional events is investigated. Widespread occurrence of dune sand layers of the same age throughout the study area are most likely induced by favourable climatic conditions. The singular occurrence of dune sand layers of a certain age might result from local removal of vegetation, leading to local dune sand reactivation (Hilgers 2007). The latter potentially indicates human interference on the landscape. It has to be noted though that such observations can be biased by the sampling strategy and a substantial number of sites is necessary for this kind of comparison. A further limitation is that natural bushfires, induced by drought periods, also frequently occur in semi-arid Australia, therefore, this approach is not very straightforward. Furthermore, by comparing the depositional phases in each section, it will be investigated how susceptible the dunes of the western Murray Basin are to aeolian reactivation. The PDFs of the individual sampling sections are shown in Fig. 9.4. Only ages <120 ka are displayed.

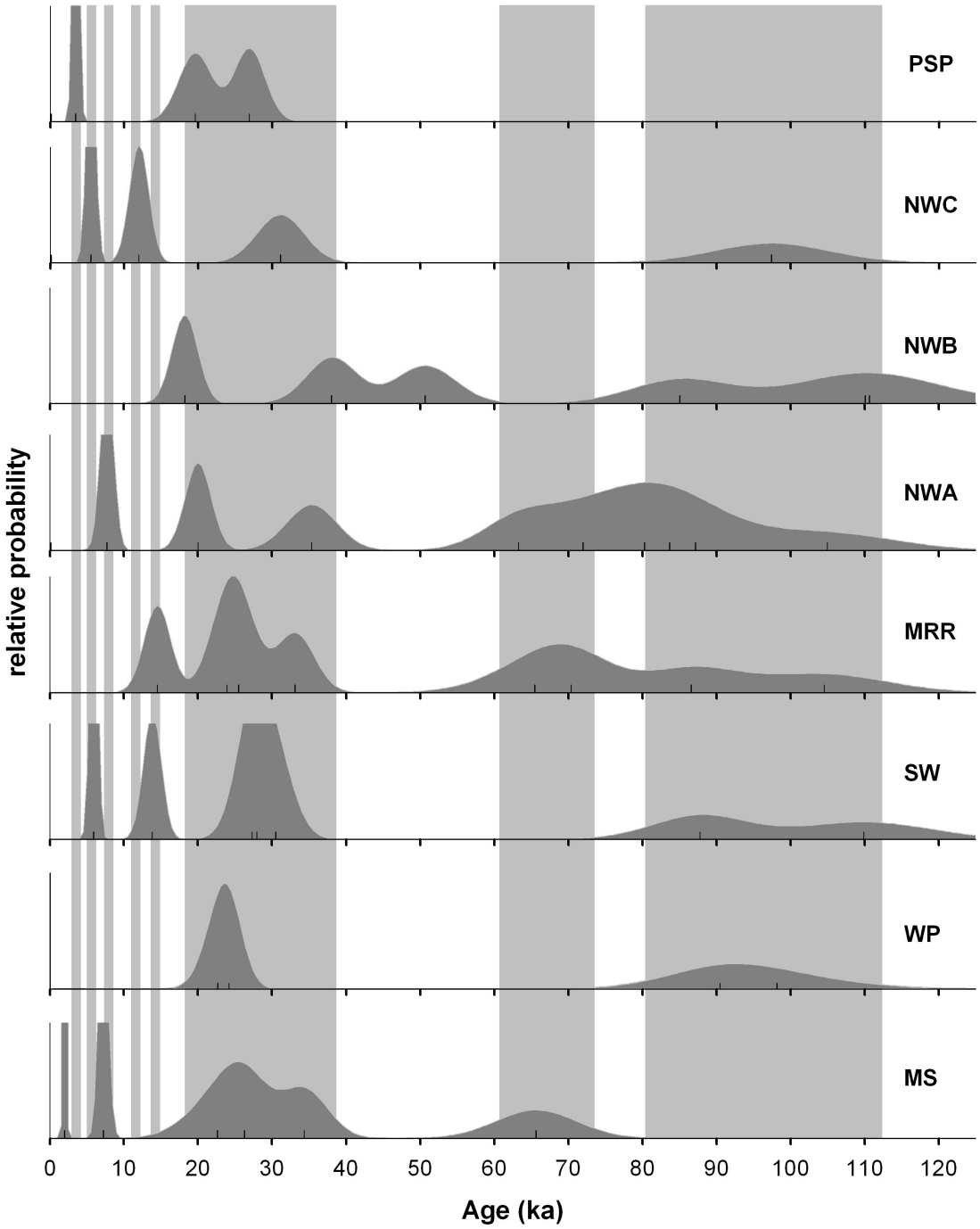

Fig. 9.4. Probability density functions of each section from the linear dune field. The grey bars highlight the aeolian depositional phases identified in the study area. Locations of the sections are shown in Fig. 4.3 and Fig. 4.9.

Depositional phases: 18-38 ka, 62-73 ka and 80-112 ka

The only two sections, in which all of the three depositional phases between 18 and 112 ka are represented, are NWA and MRR. In all other sections, at least one of these phases is not represented by luminescence ages. It is difficult to ascertain if these layers were missed by the sampling procedure. Most likely though, each depositional phase is

preserved as a dune sand layer of different thickness in each section due to a different degree of aeolian morphodynamics. This scenario was illustrated for linear dunes that were formed under a bi-directional wind regime (Munyikwa 2005a). The depositional phase from 18-38 ka is preserved in each section in the linear dune field of the western Murray Basin. This extensive phase of aeolian activity might have been responsible for the partial or complete destruction of older dune sand layers. Furthermore, the widespread occurrence of this depositional phase might indicate that after 18 ka, no large scale dune sand reactivation occurred in the western Murray Basin.

Depositional phases: 3-4 ka, 5-6 ka, 7-8 ka, 11-12 ka and 13.5-14.5 ka

For the period from 3 to 18 ka, five short depositional phases were identified, but only a maximum of two of these phases are recorded in any section. However, it needs to be taken into account that most of these depositional phases would be approximately represented by ages calculated from minor De-components identified through the finite mixture model (Section 6.8.8). For example, evidence of aeolian deposition between 6-8 ka can also be found in section PSP and MRR (if tentative ages are calculated from minor De-components). This is also the case for a time slice of ~2 ka, which is only recorded in section MS, but also appears as minor component age in section BM, NWC and SW. It is therefore very likely that most of the sections did preserve multiple young depositional phases, but these were missed by the sampling procedure.

In conclusion, some of the depositional phases identified in the western Murray Basin are potentially not fully preserved in every section investigated (or were missed by the sampling procedure). Yet, all depositional phases are represented in at least three of the seven sections from the linear dune field. The only explanation for such widespread aeolian activity is climate as a main trigger. This is also valid for the depositional phases <45 ka, since human colonisation of southeastern Australia (e.g. Bowler et al. 2003). It is thus proposed that the aeolian depositional phases detected in the dune record from the western Murray Basin represent phases of increased aridity, leading to dry surfaces with sparse vegetation cover which in turn enabled aeolian deposition. Whether the aeolian depositional phases indeed represent arid phases will be investigated in Section 9.5, by comparison with other Australian records of past climate change. From this comparison it will also be seen whether the gaps in the dune record represent dune stability phases induced by more humid conditions, or if they are an

artefact of the sampling procedure or intensive aeolian reworking. However, considering the large dataset of 77 luminescence ages and the high sampling resolution it appears very likely that at least the gaps <110 ka represent phases in which no aeolian deposition occurred and thus that the dunes of the western Murray Basin formed under discontinuous aeolian deposition.

9.3 Comparison with other dune chronologies from the Murray Basin and the Eyre Peninsula

In the following the dune record established in this study will be compared to other dune chronologies from the Murray Basin, provided by Gardner et al. (1987), Readhead (1988), Robertson and Prescott (2006), Cupper and Duncan (2006) and Twidale et al. (2007). The location of their study areas is shown in Fig. 3.9. In these studies, dunes were dated using different luminescence techniques. Multiple grain single aliquot OSL dating, the technique most similar to that used in this study, was applied by Twidale et al. (2007), Cupper and Duncan (2006), and Robertson and Prescott (2006). In the two older studies of Readhead (1988) and Gardner et al. (1987), dunes where dated using multiple aliquot TL techniques. In none of the studies were problems of overdispersed equivalent doses or post-sedimentary mixing discussed or accounted for.

In total 41 luminescence ages from the above mentioned studies are compiled and displayed as PDF in Fig. 9.5, together with the western Murray Basin dune record. Ranked individual ages with error bars are also shown. Furthermore, only ages <180 ka are shown as no older ages were obtained in the above mentioned studies. The compiled dataset is not very representative (see discussion in Section 9.2), due to a relatively low number of samples investigated in each of these studies, and a wide variation in sampling resolution. As a consequence, the importance of gaps in the compiled dune record should not be emphasized, as they might be a result of the fragmentary sampling.

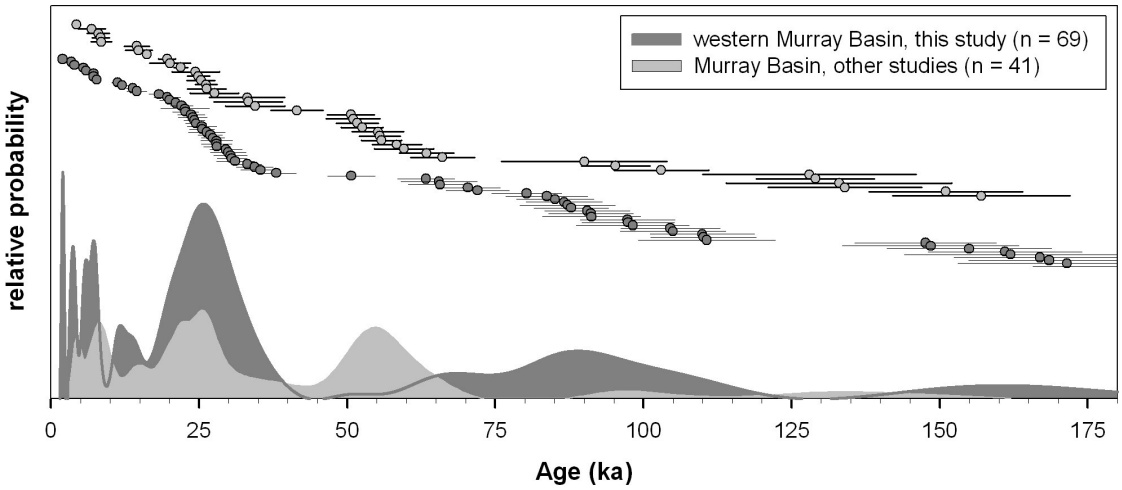

Fig. 9.5. Comparison of the dune record obtained in the present study with a compiled dune record of the Murray Basin comprising luminescence ages of Gardner et al. (1987), Readhead (1988), Cupper and Duncan (2006), Robertson and Prescott (2006) and Twidale et al.(2007). The bin width is 0.5 ka.

Despite the wide variety in locations and luminescence techniques applied, the two dune records show a lot of similarities. Broadly coincident peaks occur at ~4 ka, ~8 ka, 14 ka, and 17-42 ka. In the dune record obtained in this study, the time between 41 and 58 ka is characterised by very little dune sand deposition, with only one luminescence age at ~50 ka falling in this period. However, Robertson and Prescott (2006) and Cupper and Duncan (2006) obtained eight luminescence ages that fall into the time span from 50-58 ka. A potential explanation is that post-sedimentary mixing through bioturbation was not accounted for in these studies. In a lot of samples investigated in the present study, central mean De-values in a range of 50-60 ka are slightly lower than the main De-component identified by the finite mixture model (see Section 6.8.8 and Fig. 6.31). This is because younger grains with De-values of 20-30 Gy are often mixed into these older layers. With regard to the luminescence ages obtained by Cupper and Duncan (2006), the difference can also be explained by the fact that their study area is located approximately 400 km further to the north than the area covered by the present study and will therefore be characterised by a higher degree of aridity. A further difference occurs at around 130 ka. The dune record from this study shows a gap in this age range, whereas Readhead (1988) derived four TL ages of ~130 ka on linear dune sands from the eastern Murray Basin. This difference should not be overrated though, as the TL ages are associated with large uncertainties.

In the same project as the present study is imbedded, dune sands from the Eyre Peninsula in southwestern South Australia were dated using OSL on individual quartz grains by Melcher (2008). Hence, a very similar methodology was applied, although the luminescence data has not been treated for the effects of bioturbation. From the 18 samples dated so far, age clusters are recognised at ~185 ka, ~90 ka, 38-18 ka and 8-6 ka. These clusters generally show good correspondence to the age clusters identified for the western Murray Basin in the present study. The number of ages from the Eyre Peninsula however is too low for a comprehensive comparison of the two data sets.
In general, the good correspondence of peaks of aeolian deposition <45 ka in the Murray Basin, and of age clusters from the Eyre Peninsula suggests that dunes in southeastern Australia were active at around the same time. This supports the assumption discussed in Section 9.2 that dune formation in this area was mainly controlled by climatic factors such as aridity.

9.4 Comparison with the dune record from arid central Australia

Recently, Fitzsimmons et al. (2007) published 82 OSL ages of linear dunes from the Strzelecki and Tirari Desert, located within the Lake Eyre Basin in arid central Australia. De-determination was carried out using small multiple grain aliquots and a weighted mean was used for De-calculation. Similar to this study, they identified aeolian depositional phases by age clusters and displayed their ages as PDF. The dune records of the Strzelecki Desert and of the western Murray Basin are shown in Fig. 9.6. Fitzsimmons et al. (2007) identified five distinct periods of high aeolian sedimentation, and these periods are compiled in Tab. 9.2, together with the aeolian depositional phases detected in the western Murray Basin.

Tab. 9.2. Aeolian depositional phases detected in the Strzelecki and Tirari Desert (Fitzsimmons et al. 2007) and the western Murray Basin (this study).

Strzelecki/ Tirari Desert	0-4 ka		10-11.7 ka 12.1-14.1 ka	18-22 ka	32-35 ka	59-73 ka	
Western Murray Basin	3-4 ka	5-6 ka, 7-8 ka	11-12 ka, 13.5-14.5 ka	18-38		62-73 ka	79-112 ka, 145-185 ka, 205-215 ka

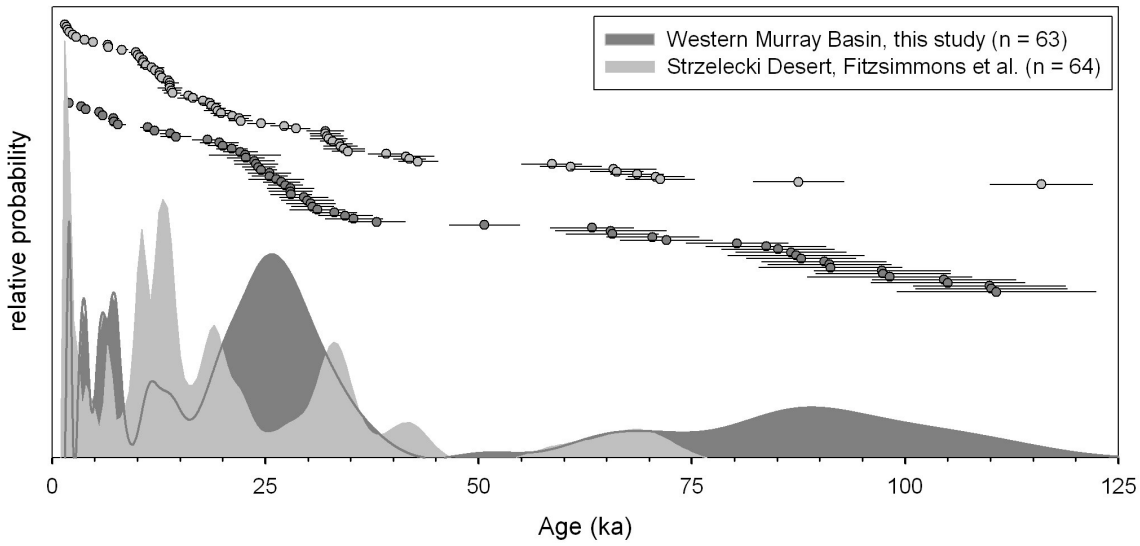

Fig. 9.6. Comparison of the dune records from the western Murray Basin and the Strzelecki and Tirari Desert (Fitzsimmons et al. 2007). The bin width is 0.5 ka.

The depositional phases identified by Fitzsimmons et al. (2007) and by the present study are strikingly similar (see Tab. 9.2). Between 4 and 10 ka, Fitzsimmons et al. (2007) did not ascertain a distinctive phases, but they obtained four luminescence ages in the range of 6-10 ka. This is also the case for the period between 22 and 32 ka, for which they obtained three luminescence ages. Furthermore, both dune records reveal a conspicuous gap between around 45 to 60 ka (although one luminescence age of 50 ka was obtained by the present study). Fitzsimmons et al. (2007) identified palaeosols in some of the investigated dunes which, from the stratigraphic context, must have formed during this period, providing evidence of dune stability.

It has to be considered though that the methodology applied by Fitzsimmons et al. (2007) differs from that used in the present study. They used multiple grain analyses for the De-determination and did not apply a finite mixture model to account for bioturbation. However, their spread in De-data was small, so no such procedures appear neccessary. Also, the dunes from the Strzelecki Desert show a clear typical cross-bedding stratification in most places (e.g. Twidale et al. 2001, Fitzsimmons et al. 2007), providing evidence that the dunes are not strongly affected by bioturbation.

One of the main differences between the two records is a stronger bias towards younger ages in the Strzelecki and Tirari Desert. This can probably be explained by a higher degree of dune sand remobilisation in the Strzelecki Desert when compared to the western Murray Basin. At least today, the Lake Eyre Basin with annual precipitation of less than 150 mm (Gentilli 1986) is more arid than the western Murray Basin (250-400

mm annual precipitation). Thus, activity of the dune crests, and even of entire linear dunes, is a common feature of the Lake Eyre Basin dune fields (Fitzsimmons et al. 2007), leading to a partial removal of previously deposited dune sands. This might also explain why no aeolian depositional phases older than 73 ka were identified by Fitzsimmons et al. (2007) whereas the western Murray Basin reveals three depositional phases >73 ka. The higher concentrations of fines and carbonates, and thus, resistence to reworking, of the dune sands of the western Murray Basin may also account for the different degree of preservation.

A further difference is noticed for the time between 17 and 45 ka. During this period, aeolian deposition in the record of Fitzsimmons et al. (2007) is centred at 19 ka, 34 ka and 42 ka. Between 23 and 30 ka, a marked drop in aeolian deposition, although still existent, can be noticed. In contrast, in the western Murray Basin, the depositional phase between 17-42 ka shows a singular peak centred at around 25 ka.

However, besides these differences, the similarity of the two dune records suggests that aeolian depositional and stability phases are controlled by the same climatic conditions in central and southeastern Australia. Fitzsimmons et al. (2007) demonstrated that the aeolian depositional phases in the Strzelecki and Tirari Desert correlate with arid conditions preserved in other palaeoclimatic records from Australia. This correlation therefore is also valid for the western Murray Basin dune record. The stable phase between around 45 and 60 ka in the Strzelecki and Tirari Desert coincides with a period of increased effectiveness of the summer monsoon in central and northern Australia (Johnson et al. 1999). This cannot explain the gap in the dune record of the western Murray Basin at around the same time, as the study area is located out of the reach of summer monsoonal influence. However, according to Ayliffe et al. (1998) and references therein, simultaneous phases of increased precipitation in northeastern, central and southeastern Australia can be caused by a strengthening of the Walker circulation.

9.5 Palaeoclimates reflected in the western Murray Basin dune record

It has been demonstrated in Section 9.2, 9.3 and 9.4 that the dune record of the western Murray Basin reflects climate conditions. This is suggested by the synchroneity of aeolian depositional phases in southeastern and central Australia, indicating that the controlling factor is one of large scale, which can only be attributed to climate. The association of aeolian depositional phases with aridity recorded elsewhere in Australian

records has already been demonstrated by Fitzsimmons et al. (2007). Nevertheless, in order to gain more information on the palaeoclimate that prevailed in the study area during phases of increased and decreased dune sand deposition, the dune record of the western Murray Basin will be compared with other proxy data from southeastern Australia. This is especially crucial for the gaps in the dune record, as it is not certain if these reflect more humid conditions, intensive aeolian reworking or an artefact of the sampling resolution. It may further be possible to investigate if the aeolian depositional phases reflect full arid conditions or waning aridity, as proposed by Nanson et al. (1992a).

Fig. 9.7 shows the comparison of the western Murray Basin dune record with the Tasman Sea dust record (Hesse 1994, Kawahata 2002) and the speleothem record (Ayliffe et al. 1998) for the last 220 ka.

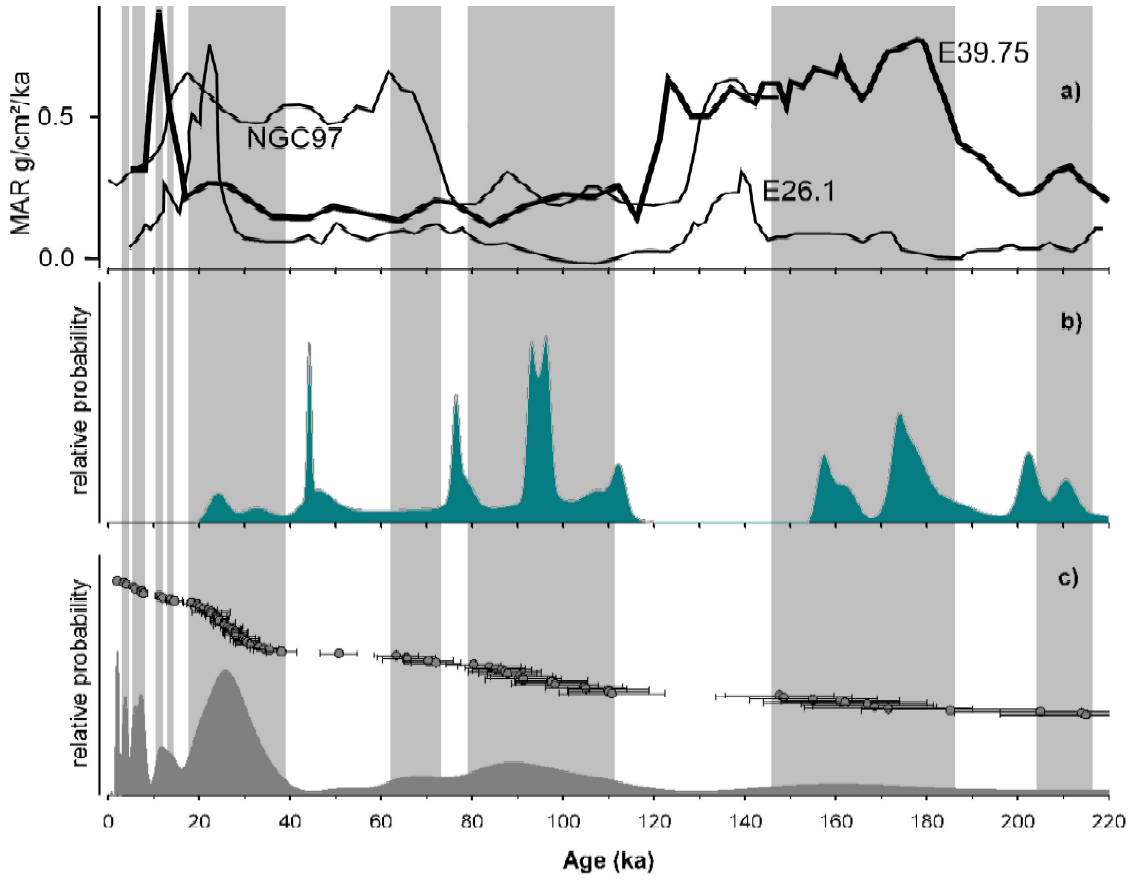

Fig. 9.7. (a) The dust record from the Tasman Sea (Hesse 1994 (core E26.1 and E39.75), Kawahata 2002 (core NGC97), redrawn from Hesse et al. 2004), (b) the speleothem record from the Naracoorte caves reflecting periods of increased effective precipitation (Ayliffe et al. 1998) and (c) the dune record of the western Murray Basin. The grey bars highlight phases of enhanced aeolian deposition.

In the following, the phases of enhanced and decreased aeolian deposition will be considered in the context of Late Quaternary palaeoclimates derived from other records across southeastern Australia. For further detailed information on southeastern Australian Late Quaternary climates, see Section 3.3. With respect to the gaps observed in the dune record, only those <150 ka will be discussed as older breaks are likely a relic of the low number of samples taken from older dune sand layers. OIS boundaries are taken from Martinson et al. (1987).

9.5.1 Depositional phase: 205-215 ka

This aeolian depositional phase falls into the interglacial OIS7 (190-244 ka). Terrestrial records of past climatic change in these age ranges are sparse. Exceptions are the speleothem record (Ayliffe et al. 1998) which reaches back to 500 ka and the dust record (Hesse 1994), reaching back to 350 ka (see Fig. 9.7). The dust record implies relatively wet conditions during this interglacial, although between 205 and 215 ka, a relatively distinct phase of increased dust deposition is recognised in core E39.75. The speleothem record indicates wet conditions between 200 and 215 ka and dry conditions at around 220 ka. However, the errors on the luminescence ages of the western Murray Basin samples are too large to allow a precise correlation of dune sand deposition with the speleothem record in this age range.

9.5.2 Depositional phase: 145-185 ka

This aeolian depositional phase covers nearly the entire glacial period of OIS6 (130-190 ka). The speleothem record indicates dry conditions between 115 and 160 ka and mainly wet conditions between 160 and 190 ka. In the dust record, the entire OIS6 is represented by very high dust deposition rates, implying arid conditions. Again, the luminescence ages are too imprecise for a more straightforward correlation with the speleothem record.

9.5.3 Gap: 120-140 ka

No luminescence ages were obtained for this time span, possibly reflecting dune stability under more humid conditions, but as discussed in Section 9.2, the dune record

may not be representative in this age range. Therefore, it is not straightforward to infer a non-depositional phase for this period from the dune record alone. The gap covers the latter part of OIS6 and the height of the last interglacial (OIS5e, 115-130 ka). Both the speleothem and the dust record imply arid conditions between 130 and 140 ka. For OIS5e, the palaeoclimatic evidence preserved in these records is conflicting. Evidence preserved in the speleothem record and in core E39.75 suggests arid conditions during this period, whereas core E26.1 and NGC97 indicate humid conditions (Fig. 9.7). Further evidence of wet conditions is provided by the pollen record from off-shore Victoria. In the dunes of the western Murray Basin, a lot of the hardpan calcrete layers are overlain by dunes sands with luminescence ages between 100 and 110 ka (section NWA, NWC, MRR, SW) (see Fig. 8.2). In section SW, the dune sand layer below the calcrete yieded an age of ~150 ka. This might indicate that some of the calcretes were formed between around 110 and 150 ka as a result of dune stability and pedogenesis.

9.5.4 Depositional phase: 79-112 ka

The aeolian depositional phase covers the OI sub-stages 5a-5d (74-115 ka). The sea surface temperature (SST) record implies cool conditions during sub-stages 5b and 5d, and relatively warm temperatures during sub-stages 5a and 5c for the Australasian region (Barrows et al. 2007) (see Fig. 3.1). In the speleothems of the Naracoorte Caves, phases of high effective precipitation are recorded at around 95 ka and 110 ka, correlating with phases of cool SSTs. For the rest of this period, relatively arid conditions are implied. Dust accumulation was relatively low during this period, implying overall humid conditions. A trend towards increasing dust deposition is noticed at the end of the period. The fluvial record of the Murrumbidgee River reflects a phase of increased channel activity between 80 and 105 ka, also suggesting relatively humid conditions (Page et al. 1996) (see Fig. 3.6). In the pollen record of off-shore western Victoria, a drying trend following the wet conditions of sub-stage 5e is recognised (Harle et al. 1997). From the comparison with these other southeastern Australian records, it can be deduced that the phase between 79 and 112 ka was probably not characterised by continuous dune sand deposition, since partially wet conditions during OI sub-stages 5a-5d are noticed in many other records from southeastern Australia. The luminescence ages of the western Murray Basin are too imprecise though to resolve non-depositional phases. However, at least during parts of OI sub-stages 5a-5d, substantial dune sand deposition took place in the Murray Basin.

9.5.5 Depositional phase: 62-73 ka

This depositional phase correlates with OIS4 (58-74 ka) and was characterised by very low SSTs in the Australasian region (Barrows et al. 2007). For the aeolian depositional phase at 62-73 ka, there is widespread evidence of arid conditions in southeastern Australia, reflected in the dust record of Kawahata (2002), the off-shore western Victorian pollen record (Harle 1997), the speleothem record (Ayliffe et al. 1998) and the Lake Mungo record (Bowler 1998, Bowler et al. 2003). However, two of Tasman Sea cores displayed in Fig. 9.7 show no increase of dust accumulation rates during this period (Hesse 1994).

9.5.6 Gap: 41-58 ka

Very limited aeolian deposition is indicated by the western Murray Basin dune record for the time between 41 and 58 ka, with only one luminescence age falling into this period. The phase correlates with the early part of the interstadial OIS3 (24-59 ka), reflecting cool to intermediate SSTs in the Australasian region (Barrows et al. 2007). Most of the records from southeastern Australia provide evidence of more humid conditions at around this time, such as the Lake Mungo record (Bowler et al. 2003), the western Victoria off-shore pollen record (Harle 1997), the speleothem record and the dust record (Fig. 9.7). In the dust core analysed by Kawahata (2002), dust deposition rates are still relatively high though, indicating more arid conditions as for example during the latter part of OIS5. In the pollen record of Lake Wangoom, no response of vegetation to this interstadial period was recognised (Harle et al. 1999).

9.5.7 Depositional phase: 18-38 ka

The depositional phase between 18 and 38 ka covers the latter part of OIS3 and the earlier part of OIS2 (12-24 ka). Low SSTs are recognised at this time, peaking in minimum temperatures at the Late Glacial Maximum (~20 ka) (Barrows et al. 2007). Widespread aridity in southeastern Australia is recognised for this period. For example, lake levels of Lake Mungo dropped markedly at around 40 ka, with lake levels remaining low until around 19 ka (Bowler 1998, Bowler et al. 2003). The western

Victoria pollen record also indicates dry conditions (Harle 1997). Further evidence of arid conditions is provided by the dust record and the speleothem record (Fig. 9.7).

9.5.8 Depositional phases and gaps between 12-18 ka

Australasian SSTs rose dramatically from around 19 ka on. A marked drop in aeolian deposition is noticed in the western Murray Basin dune record at around 16 ka. At this time, an increase in channel activity of the Murrumbidgee is recognised in the fluvial record (Page et al. 1996). Rising lake levels are recorded at Lake Mungo, though slightly earlier, at about 17.5-19 ka (Bowler 1998). Furthermore, a significant decline in dust deposition rates is evident in the Tasman Sea sediments (Hesse 1994). However, the pollen record at Tower Hill indicates dry conditions between 13.5 and 17 ka (Turney et al. 2006).

A further increase in aeolian deposition in the western Murray Basin between 11 and 14.5 ka partially coincides with the Antarctic Cold Reversal (ACR) lasting from 12.5 to 14 ka (Jouzel et al. 1995). An increase in dust deposition at this time is noticed in the Tasman Sea sediments (Hesse 1994). Lake Mungo dried out at least 15 ka ago, with only occasional floodings experienced since this date (Bowler 1998). The Tower Hill pollen record indicates wet conditions between 12.5-13.5 ka, followed by drier conditions until around 11 ka (Turney et al. 2006).

9.5.9 Depositional phases between 0-12 ka

In the early part of the Holocene, a time of very high SSTs, the dune record reveals a prominent gap between 8.5 and 10.5 ka. Holocene aeolian deposition is noticed in the dune record at ~2 ka, ~4 ka, 5-6 ka and 7-8 ka. SSTs remained high, though slightly lower than during the early Holocene. Similar to the last interglacial, evidence of Holocene climate conditions is conflicting. The pollen records at Lake Wangoom, Lake Terang and off-shore western Victoria indicate wet conditions (Edney et al. 1990, D'Costa and Kershaw 1995, Harle et al. 1999) whereas the speleothem record provides evidence of arid conditions (Ayliffe et al. 1998). As discussed in Section 3.3.7, this might be a problem of defining Holocene climates as humid or arid. The dune record shows that aeolian deposition took place in short phases or time slices throughout the Holocene, except for the time between 8.5 and 10.5 ka. Nevertheless, aeolian activity is

significantly lower than during the time between 20 and 30 ka. This is confirmed by the fact that only twelve luminescence ages date to the Holocene, whereas the period at 20-30 ka is represented by 19 luminescence ages. Three modern ages obtained in the present study (WP1: 1939 ± 11 AD, BM1: ~0 ka, MS9: ~0 ka) provide evidence of very recent aeolian activity. In section WP and MS, these young dune sand layers contain abundant charcoal particles, which points to aeolian deposition after removal of vegetation through fire. The age of sample WP1 (1939 ± 11 AD) correlates very well with a near modern age of 1933 ± 7 AD obtained by Twidale et al. (2007). Both ages fall into a period of severe drought from 1937 to 1945 that affected major parts of Australia. This drought period lead to a disastrous bushfire in January 1939 (known as the Black Friday) in southeastern South Australia and southwestern Victoria, and the year 1940 was one of the driest years of the 20th century in southeastern Australia (BOM 2008). The charcoal particles observed in section WP may thus be the remains of the Black Friday bushfires. Interestingly, the time of European settlement since the end of the 19th century, which was associated with widespread land clearing activities, does not show in the dune record as peak of high aeolian sedimentation.

9.5.10 Conclusion

It has been demonstrated that most of the depositional phases of the western Murray Basin dune record correlate well with arid conditions recorded elsewhere in southeastern Australia. No bias of dune sand deposition towards waning activity was noticed (cf. Nanson et al. 1992 a). Furthermore, the gap noticed between 40 and 60 ka is reflected by humid conditions in most of the other records. It is therefore concluded that the dune record of the western Murray Basin is a very valuable terrestrial archive for the reconstruction of palaeoclimates. From phases of enhanced aeolian deposition, aridity can be inferred, and the gaps in the dune record can be used to reconstruct relatively humid conditions. The latter only holds true though if the dune record is based on a high number of luminescence ages, otherwise gaps are too likely to represent fragmentary sampling. However, beyond ages of 70 ka, the uncertainties of the luminescence ages are too large for a precise deduction of palaeoclimatic conditions. The main palaeoclimatic implications of the western Murray Basin dune record can be summarised as follows:

- Cold conditions, such as during the LGM, the later part of OIS3, OIS4 and OIS6 are associated with substantial dune building phases under arid conditions. During OI sub-stages 5d-5a, at least partial aridity is inferred by the dune record, although the luminescence ages are too imprecise for a correlation with each sub-stage.
- From around 40-60 ka a prolonged humid period is indicated from the dune record, which seems to have been wetter than the Holocene. This humid phase coincides with the proposed initial human occupation of southeastern Australia, which was dated to around 45-50 ka (Bowler et al. 2003, Cupper and Duncan 2006), and with megafaunal extinction at around the same time (Roberts et al. 2001). Due to the synchroneity of the two events, a discussion arose whether the megafaunal extinction was the result of human impact or of a climatic deterioration (e.g. Miller et al. 1999, Roberts et al. 2001, Cupper and Duncan 2006). The dune record of the western Murray Basin provides further evidence that aridity as a cause of the extinction can be ruled out.
- Three interglacials are covered by the record (OIS1, OIS5 and OIS7). No clear association of warm periods and the degree of aridity can be inferred from the dune record. During OIS7, aeolian activity, and thus, a certain degree of aridity is noted. This interglacial is characterised by very variable global temperatures, comprising three phases of low global ice volume, interrupted by two phases of relatively high global ice-volume (Bassinot et al. 1994). However, the luminescence ages are too imprecise to be correlated with one of these sub-stages. The dune record implies dune stability and relatively humid conditions during OI sub-stage 5e. Possibly, the formation of some of the calcretes observed in the western Murray Basin dunes also date to this time, although over- and underlying sand units do not constrain the time of their formation very well. If the calcretes were formed during sub-stage 5e, this would further indicate highly seasonal climates with a temporary net water deficit (Goudie 1983). The Holocene appears to have been significantly drier than, for example, the period between around 40 and 60 ka, but less dry than the period between around 20 and 30 ka.
- Today, the dunes of the western Murray Basin are stabilised by vegetation. However, the three modern luminescence ages obtained in this study provide evidence of very recent aeolian activity in association with drought periods and bushfires. The dunes of the western Murray Basin thus appear to lie close to the threshold of reactivation at the moment, and removal of the protecting vegetation

cover can lead to renewed substantial aeolian activity. Furthermore, the dune record of the western Murray Basin provides a reliable record of Holocene climatic conditions in southeastern Australia, a period not well represented in other records from this area. For the early Holocene (until ~8 ka), more humid conditions are reflected in the record, whereas the mid and late Holocene was characterised by short periods of aridity at around 2 ka, 4 ka, 5.5 ka and 7.5 ka).

9.6 On the onset of dune formation in the western Murray Basin

It was not possible in any of the sections investigated in the western Murray Basin, to expose the base of the dunes. Therefore, the onset of dune formation cannot be assessed with certainty. However, in the linear dune field some of the sections were exposed to depths of 6 m or even 7 m. With reported average heights of the linear dunes in the Murray Basin of 2-6 m (Bowler and Magee 1978), the lowermost samples are expected to be located relatively close to the base of the dunes. And even if the base of a dune is exposed, this is not a guarantee that this would identify the oldest dune sands that exist in a given area. Dune formation is not necessarily initiated at the same time at every location in a dune field, for example due to differences in topography. Twidale et al. (2007), for instance, exposed the base of the dune in the western Murray Basin. They obtained an age of ~160 ka for the dune sands directly overlying the base. It is obvious from this study though, that dune formation reaches further back. In the study of Twidale et al. (2007), the base of the dune consisted of Tertiary sandstone, although the section is located in the former Lake Bungunnia area. As the section also lies very close to the Murray River, it is possible that fluvial activity resulted in removal of Lake Bungunnia sediments and, possibly, of older dune sand layers.

The oldest reliable luminescence age was obtained for sample PSP8, yielding an age of 269 ± 20 ka (OIS8). This age reflects a reliable minimum age for the onset of dune formation in the western Murray Basin. Ages of samples with equivalent doses >200 Gy were considered as unreliable due to the proximity of the OSL signal to saturation. Nevertheless, it is evident from these unreliable ages that dune formation reaches further back than 270 ka. Two older (unreliable) ages were obtained in section NWC (285 ± 27 ka and 294 ± 29 ka) and three in section PSP (308 ± 26 ka, 344 ± 31 ka and 445 ± 37 ka). In both sections, ages are in correct chronostratigraphic order, which provides some confidence in the ages. Dose recovery tests (see Section 6.8.4.3 and Tab. 6.2) demonstrated that when recovering high laboratory beta doses (200-385 Gy) no

tendency towards over- or underestimation is observed. In one sample, the recovered dose overestimated the given dose and in three samples, the given doses were underestimated. Two dose recovery tests (using single grains and multiple grains) on sample NWC3 even yielded dose recovery ratios of unity within errors. It is therefore not clear if the unreliable ages over- or underestimate the time of deposition of the dune sands.

Sample PSP3 yielded a mean De-value of 231 ± 11 Gy, resulting in an age of 445 ± 37 ka. Both the equivalent dose and the age are unreliable. However, a minimum age can be derived from the 2*Do-value (see Section 6.8.5 and Tab. 6.3) which was 192 Gy in sample PSP3. With a dose rate of 0.52 Gy/ka, sample PSP3 yields a reliable minimum age of 369 ka.

All the sections discussed above are located in the linear dune field. The oldest ages in the sub-parabolic dune field ranged from 91-97 ka. It cannot be definitely concluded if the onset of sub-parabolic dune formation occurred at the same time as in the linear dune field. However, the synchroneity of aeolian deposition in the linear and the sub-parabolic dune field (Section 9.2) demonstrates that, at least in younger age ranges, both dune fields were formed contemporaneously. Hence, there is no reason why this tentative onset of dune formation should not also apply to the sub-parabolic dune field.

Despite the fact that the oldest age of ~450 ka obtained for the western Murray Basin samples is an unreliable one, it agrees with previous estimates of the onset of dune formation in the Murray Basin. From palaeomagnetic measurements, Zhisheng et al. (1986) placed the onset of aridity to about 500 ka. A similar estimate was obtained by Bowler et al. (2006). They assumed that the 4-5 palaeosols observed in some of the linear dunes of the Murray Basin were deposited in insolation-forced 100 ka cycles. The Tasman Sea dust record points to younger initiation of aeolian activity at around 350 ka. In conclusion, an accurate age for the onset of dune formation can not be provided by this study. Based on the minimum age of sample PSP3, it is evident that dune formation in the western Murray Basin reaches back more than 370 ka.

10. Conclusions and future research directions

The semi-arid western Murray Basin in southeastern Australia is characterised by vast fields of palaeodunes. These dunes are today stabilised by the protective effects of vegetation, but their existence implies that this was not always the case. They thus provide evidence of different environmental conditions in the past that allowed the formation of these dunes. Specific conditions such as sparse vegetation cover and sufficient wind speed are necessary for dune formation. Every dune sand layer is therefore a key to past climatic conditions and by dating the dune sands a record of past environmental change can be established. This information is of immeasurable value with respect to predicting future climate change, particularly in areas such as semi-arid southeastern Australia, which is very prone to drought and will respond very sensitively to future global warming. Potential future increases of aridity will endanger the livelihood of many farmers in this area and will result in significant reduction of the Australian agricultural production.

The aim of this study was to apply luminescence dating on dune sands of the western Murray Basin, in order to reconstruct palaeoclimatic conditions over the last ~300 ka in southeastern Australia. The chronology of the dune record in the present study is based on 80 reliable single grain luminescence ages. The samples were collected in high resolution (~0.5 m) from linear, sub-parabolic and parabolic dunes in the western Murray Basin in southeastern South Australia.

In the following, the major outcomes will be summarised with respect to the methodology, the potential to reconstruct palaeoclimatic conditions using this terrestrial archive and the onset of dune formation in the western Murray Basin.

10.1 Single grain luminescence dating

For the first time, single grain dating has been consistently applied to a dataset as large as the one in the present study. Australian quartz grains exhibit very high luminescence sensitivities and are therefore an ideal material for this luminescence technique. For instance, dune sands from the study area yielded a valid equivalent dose for, on average, 30 % of all measured quartz grains. It has been shown that the dunes of the western

Murray Basin are severely affected by post-sedimentary mixing through bioturbation. This seems to be a very common problem when dating sediments from semi-arid environments (Bateman et al. 2007, Duller 2008). Only single grain OSL dating has the potential to explore equivalent dose distributions in detail and to fully account for this problem. By identifying dune sands from the study area which were not problematic with respect to sediment mixing, it was possible to establish a reference overdispersion value of 20 % which could be attributed to microdosimetric effects and by instrumental uncertainties. Such reference values are needed for age models such as the finite mixture model or minimum age models in order to define the spread allowed for the most appropriate De-component (Bailey and Arnold 2006). The reference value of 20 % obtained in this study for fully bleached, non-mixed samples may not be translatable to other study areas, as it depends on the various factors such as the potassium concentration of a sample (Mayya et al. 2006). However, it can be used in other single grain studies, where no such reference values are available. For older samples (in this study, samples with a De-value >85 Gy) it needs to be taken into account that the spread in data further increases due to approaching signal saturation.

Applying the finite mixture model on the western Murray Basin samples yielded reliable ages in chronostratigraphic order up to 270 ka. These ages were calculated from the main De-component identified by the mixture model. It was demonstrated that De-components identified by the finite mixture model are repeated in neighbouring samples within individual sections. In younger samples (<20 Gy), equivalent doses from multiple grain analyses severely overestimated the single grain De-values. Applying the finite mixture model on multiple grain data sets yielded similar De-components as identified from the single grain datasets. However, the smallest De-components derived from single grain analyses could not always be detected on a multiple grain scale. Due to the intensive post-sedimentary mixing and the high sensitivity of the quartz grains, a lot of previously published multiple grain luminescence ages from dune sands of semi-arid areas may be questionable, particularly if sediment mixing is not accounted for by the use of a finite mixture model.

Single grain analyses further enable the investigation of the luminescence properties of individual grains in detail. For instance, it has been demonstrated by this study that the signal intensity and signal growth of individual quartz grains can vary significantly within a sample. This allows the removal of De-values derived from grains with inappropriate luminescence properties from a data set, and furthermore, provides

valuable information for multiple grain analyses. However, exploring the luminescence properties of individual grains is very time consuming, and could therefore not be carried out routinely for each of the 97 samples investigated in this study.

10.2 The onset of dune formation

For the onset of dune formation in the western Murray Basin, only a minimum age of 370 ka could be determined. This is one of the oldest minimum ages obtained for Australian dunes by a numerical dating method so far. The dunes of the study area are relatively resistant to aeolian reworking, due to their location in the desert margin. Thus in general, the Murray Basin is a very suitable area for investigations on the onset of mid Pleistocene aridity in Australia. The dose rates of some of the samples were as low as 0.5 Gy/ka. Therefore, some of the dunes provide the potential to obtain ages up to ~400 ka with conventional OSL dating, considering the saturation level of ~200 Gy in the investigated samples. The study area therefore bears excellent opportunity to test other luminescence techniques such as thermally transferred OSL (TT-OSL) and isothermal TL (ITL), or other radiometric dating methods such as electron spin resonance (ESR) dating (cf. Beerten et al. 2006, Trauerstein 2008). These techniques exhibit higher signal saturation levels than the fast component dominated OSL signal (Choi et al. 2006c, Wang et al. 2006). However, they are still in an experimental state of research and by testing them on the western Murray Basin, new findings on their applicability to sediments could be derived, and they may also provide new valuable insights on the onset of dune formation and aridity in southeastern Australia. On one of the sections investigated in this study (MS from the linear dune field), ESR dating already has been carried out on five selected samples by Beerten et al. (2006). They used the Ti-H, Ti-Li and the total Ti centres of quartz grains to estimate the equivalent dose. For the oldest sample (MS0), for which no single grain luminescence age was determinable, they obtained a Ti-H De of ~210 Gy, a total Ti De of ~390 Gy, and a Ti-Li De of ~670 Gy. They state that the Ti-H De can be considered as minimum estimate, due to the instability of these centres, and the Ti-Li as a maximum estimate, due to a low optical sensitivity of these centres. Therefore, the two centres can provide an age window for mid Pleistocene samples for which no other dating techniques are available. It has to be noted though that this window can only serve as very broad estimate of the time of sediment deposition. Further investigations on the total Ti centre need to be

carried out in future, as this centre might yield more precise and accurate De-estimates (Beerten et al. 2006).

Furthermore, the use of feldspars as dosimetres should be tested in future on the samples investigated in this study. Besides the higher signal saturation level of feldspars they bear the further advantage of being less prone to microdosimetric heterogeneity of the surrounding sediments due to their relatively high internal dose rate. Preliminary measurements carried out on feldspars of the Murray Basin samples exhibited that they were subject to severe anomalous fading. However, determination of the fading rate (and correction of the feldspar ages) or radiofluorescence dating of the feldspars might help to gain further information on the onset of dune formation in southeastern Australia.

10.3 The potential of the western Murray Basin dune record for palaeoclimatic reconstruction

This study, for the first time, establishes a robust chronology of dune formation in the Murray Basin, based on a large data set of luminescence ages that were dated under consistent laboratory conditions. This is the only approach that allows the use of the dune record as an indicator of palaeoclimatic conditions. It has been demonstrated that not only are the dunes of the western Murray Basin of great antiquity and date back to at least 370 ka, but that the Holocene is also well represented in the record. Terrestrial archives that cover time spans as large as these are very rare, underlining the value and potential of this record.

It was shown that the linear dunes and sub-parabolic dunes were formed at the same time. A different amount of sand supply was suggested as explanation for the different morphologies of the dunes.

Phases of enhanced aeolian deposition were identified at 3-4 ka, 5-6 ka, 7-8 ka, 11-12 ka, 13.5-14.5, 18-38 ka, 62-73 ka, 79-112 ka, 145-185 ka and 205-215 ka. Some of these depositional phases correlate with well documented phases of arid conditions in southeastern Australia, such as the LGM, late OIS3 and OIS4. However, beyond around 70 ka, the uncertainties on the luminescence ages (~10 %) become too large to reconstruct climate variability precisely. For instance, climatic fluctuations during sub-stages of OIS5, as evident from other palaeoclimatic records, cannot be resolved.

A relatively high resolution of depositional phases was obtained in the Holocene part of the record. Three near-modern ages give evidence of very recent aeolian activity in the

study area, and indicate that at the moment, the dunes are close to the threshold of reactivation. One luminescence age dates to 1939 ± 11 AD, coincident with the Black Friday bushfire that disastrously affected western Victoria and southeastern Australia in January 1939. Therefore, luminescence dating of dune sands in the study area bears the potential to reconstruct historically documented and older Holocene drought periods. However, in this study, too few young samples were collected for further conclusions in this direction

Conspicuous gaps in the dune record were noticed from 8.5-10 ka, at around 16 ka, from around 40-60 ka and 120-140 ka. The period between 40 and 60 ka is recorded as humid phase in a lot of other records from southeastern and central Australia. It further coincides with the age of oldest human artefacts and the extinction of Australian megafauna in southeastern Australia (e.g. Miller et al. 1999, Roberts et al. 2001, Bowler et al. 2003, Cupper and Duncan 2006). The dune record thus provides evidence that megafauna extinction was not caused by aridity. It further implies that humid conditions prevailed in southeastern Australia at around 16 ka and during the early Holocene. The height of the last interglacial also appears to have been characterised by humid conditions and dune stability, possibly associated with calcrete formation in the western Murray Basin. However, this phase and the time of calcrete formation are not well constrained due to the large uncertainties on the luminescence ages.

Comparison of the dune record obtained in the present study with a dune record from arid central Australia (Fitzsimmons et al. 2007) showed that dunes were formed at around the same time in the two study areas. This implies that similar climatic conditions prevailed over major parts of Australia during the late Quaternary.

The study demonstrates that dunes in semi-arid areas are excellent sedimentary archives for the reconstruction of palaeoclimatic conditions. The dunes of the western Murray Basin, although subject to some degree of aeolian reworking, record multiple and also very old phases of aeolian activity over the last ~220 ka. In the younger part of the record (<70 ka), the phases and gaps in the dune record can be used to reconstruct palaeoclimatic conditions with a relatively high resolution. However, in order to better constrain older depositional phases, more samples would need to be dated with optically stimulated luminescence.

Summary

This study is concerned with the reconstruction of the palaeoenvironmental history of southeastern Australia for the last ~300 ka by establishing a luminescence chronology of dune sand deposition. For this purpose, a study area in the western Murray Basin in southeastern South Australia was chosen which today is characterised by semi-arid climate conditions. Vast fields of palaeodunes, stabilised by vegetation, provide evidence of past environmental change. By dating these dunes, past climatic changes can be deciphered, providing valuable information for predicting future climate change. In total, 97 samples were collected from dune sand layers and the time of their deposition was determined using multiple grain and single grain optically stimulated luminescence dating of the quartz fraction.

Dunes form under specific environmental conditions such as sparse vegetation cover, sufficient wind speed and sufficient supply of sand sized grains. These conditions are preserved in every deposited dune sand layer. However, like most terrestrial sedimentary archives, the dune record is discontinuous. Due to the unconsolidated nature of dune sands, evidence of past climatic change can easily be destroyed by younger phases of aeolian activity phases. To account for this problem, a large data set and good spatial coverage of investigated dunes is required.

Various studies have been concerned with luminescence dating of dunes from the Murray Basin (Gardner et al. 1987, Readhead 1988, Cupper and Duncan 2006, Robertson and Prescott 2006, Twidale et al. 2007). From these studies it is evident that dunes in this area formed since at least ~160 ka until modern times. However, only a limited number of samples has been investigated and dated using different luminescence techniques (optically stimulated luminescence (OSL) and thermoluminescence (TL), multiple aliquot and single aliquot techniques). Inter-comparison between the results of theses studies is thus difficult. Due to the limited quantity of samples investigated, it is further not known if dune formation in the Murray Basin was continuous or if the dune sands were deposited during discrete aeolian activity phases interrupted by periods of dune stabilisation. Furthermore, it is estimated that the onset of dune formation in the Murray Basin might reach back as far as 500 ka (Zhisheng et al. 1986, Bowler et al.

2006). These estimates are based on palaeomagnetic dating of the dunes and underlying lacustrine sediments and on 4-5 palaeosols which are assumed to have formed in insolation forced 100 ka cycles. By numerical dating methods, however, no ages beyond 160 ka have yet been obtained.

In order to gain more knowledge on the dune formation in the Murray Basin and on southeastern Australian palaeoclimates, deep sections were excavated by backhoe trenching and the dunes were sampled with a high resolution of ~0.5 m. These samples were dated with a consistent methodology in order to establish a representative chronology of the timing of dune formation in the western Murray Basin. Three different geological formations are covered by this study; that is, the Molineaux Sands (sub-parabolic dunes), the Woorinen Formation (linear dunes) and the Bunyip Sands (parabolic dunes).

In a first approach, several samples were dated using multiple grain aliquots, consisting of around 50-100 grains of quartz. A significant spread in equivalent doses (De) was noticed on the multiple grain scale and arose the question of the causes of this scatter. In order to analyse the De-distributions in more detail and to gain information on the sources of variations in equivalent doses, single grain measurements were carried out on all samples. Based on analysis of single grain De-distributions, field observations and laboratory bleaching tests, it was demonstrated that mainly microdosimetric effects and post-sedimentary mixing by bioturbation were responsible for the spread of the De-values. Although some of the dune sands exhibited intensive pre-depositional iron crusts, they were well bleached at the time of deposition. A further proportion of the spread in data was attributed to a non-uniform dose rate delivered by the beta source of the luminescence reader. In addition, the single grain measurements yielded interesting information on the luminescence properties of the quartz grains, demonstrating, for instance, that the investigated dune sands contained very high proportions of luminescent grains.

To account for the mixing of sediment layers of different age by bioturbation, De-values were calculated using the finite mixture model (Galbraith and Green 1990). The investigation of the De-distributions of samples not affected by bioturbation demonstrated that microdosimetric effects accounted for ~20% of the observed spread

in De-values. This value was used to define the allowed spread of the individual components identified by the finite mixture model. In older samples, this value was set to 27% to account for variations in De-values induced by approaching signal saturation. Samples with De-values >200 Gy were shown to yield unreliable equivalent dose estimates due to approaching signal saturation. This finding is based on dose recovery tests and on analysis of the saturating exponential growth curve.

Luminescence ages were calculated from the main De-component identified by the finite mixture model while dose rates were derived from radionuclide concentrations that were measured by means of laboratory gamma spectrometry. These dose rates were generally low (often <1 Gy/ka), allowing age determination of samples older than 200 ka. Furthermore, radioactive equilibrium was demonstrated for the majority of samples. Except for two samples, all ages were in correct chronostratigraphic order, providing confidence in the accuracy of the obtained luminescence ages, despite the intensive mixing of the dune sands.

Net sedimentation rates were much higher in the sub-parabolic dune field than in the linear dune field. This confirms previous findings that the sub-parabolic dunes exhibit a much higher degree of mobility compared to the linear dunes of the western Murray Basin (Bowler and Magee 1978, Pell et al. 2001). Despite their different morphology and mobility, the dunes of the sub-parabolic, the parabolic and the linear dune field were active at the same time. Therefore, the different morphology seems to be the result of non-climatic factors. A different amount of sediment supply is the most likely explanation for the dunes of the western Murray Basin.

Phases of substantial dune sand deposition were identified for the periods 11-12 ka, 13.5-14.5 ka, 18-38 ka, 62-73 ka, 79-112 ka, 145-185 ka and 205-215 ka, thus up to Oxygen Isotope Stage 7. The oldest depositional phase demonstrates that dune sand layers of great antiquity are preserved in the western Murray Basin. Holocene events of dune sand deposition, represented by at least two luminescence ages, were recognised at 3-4 ka, 5-6 ka and 7-8 ka. Furthermore, two zero ages and an age of 1939 ± 11 AD were obtained.

Comparison of the western Murray Basin dune record with a dune record of arid central Australia (Fitzsimmons et al. 2007) showed excellent agreement between the two chronologies. This implies that similar climatic conditions prevailed over major parts of Australia during the Late Quaternary

The aeolian depositional phases of the western Murray Basin broadly correlate with arid conditions recorded in other southeastern Australian sedimentary archives. Phases of very limited dune sand deposition were shown to be associated with more humid conditions. A conspicuous phase of very limited aeolian sedimentation dates to around 40-60 ka, characterised by more humid conditions than prevailing in the study area during the Holocene. This phase coincides with the age of the oldest human artefacts found in southeastern Australia and with the continent-wide megafaunal extinction (e.g. Roberts et al. 2001). The height of the last interglacial also appears to be characterised by more humid conditions. However, the relatively large errors on the luminescence ages (~10%) prevent to resolve climatic fluctuations >70 ka and the identification of older non-depositional phases in detail.
The near-modern ages provide the potential to reconstruct historically documented drought periods. For instance, the age of 1939 ± 11 AD correlates well with a disastrous drought that affected Australia in 1937-1945, and charcoal particles found in the respective dune sand layer most likely are the remains of the Black Friday bushfire of January 1939.

The oldest, but unreliable age obtained in the present study indicates that the onset of dune formation might reach back to ~450 ka. Although this estimate may not be accurate, it agrees with previous estimates of the onset of dune formation in this area. Based on a reliable minimum De-value derived from the 2*Do-value of this sample, it is demonstrated that dune formation was initiated at least 370 ka ago.

This study demonstrates that dunes in semi-arid areas are excellent sedimentary archives for the reconstruction of palaeoclimatic conditions. Single grain dating is very well suitable for establishing a sound chronology of aeolian depositional phases, and ages up to ~270 ka can be obtained with this method, provided that dose rates are low. However, the effects of bioturbation, a common problem in semi-arid areas, need to be taken into account. Although the dune record might be of discontinuous nature, multiple

phases of dune formation and dune stability are recorded in the dunes of the western Murray Basin. Not only peaks but also gaps in this dune record can be used for the reconstruction of aridity and humidity, respectively, provided that the chronology is based on a high number of samples. However, a detailed resolution of past climatic fluctuations in the study area was only provided for the last ~70 ka and the interpretation of the dune record has to be supported by comparison with other well dated proxy data of past climatic change.

Zusammenfassung

Im Fokus dieser Arbeit steht die Rekonstruktion der Klimageschichte der letzten ~300 ka des südöstlichen Australiens mittels Lumineszenzdatierung von Dünensanden. Das Untersuchungsgebiet im westlichen Murray Becken (südöstliches Südaustralien) ist momentan durch ein semi-arides Klima geprägt. Eine charakteristische Landschaftsform des Untersuchungsgebietes sind Paläodünenfelder, die durch Vegetation vor der Umlagerung geschützt sind. Sie zeugen von anderen Klimabedingungen in der Vergangenheit, die zur Dünenbildung führten. Durch die Datierung der Dünensande kann daher das Paläoklima rekonstruiert werden, wertvolle Information, die für die Abschätzung zukünftiger Klimaänderungen benötigt werden. Insgesamt wurden 97 Dünensandproben genommen und mittels optisch stimulierter Lumineszenz datiert. Hierbei kamen sowohl die Einzelkorndatierung (*single grain dating*) als auch die Mehrkorndatierung (*multiple grain dating*) von Quarzkörnern zur Anwendung. Diese Methode erlaubt es, die letzte Ablagerung von Sedimenten zu bestimmen.

Dünen entstehen nur unter spezifischen Umweltbedingungen. Diese sind z.B. eine geringe Vegetationsbedeckung, eine ausreichende Windgeschwindigkeit und Verfügbarkeit von Sand. Diese Bildungsbedingungen werden mit jeder Dünensandschicht archiviert. Typisch für dieses terrestrische Sedimentarchiv ist seine Diskontinuität. Dünensande sind in der Regel wenig verfestigt, d.h. bei äolischen Aktivitätsphasen können auch ältere Dünensande erneut umgelagert werden, so dass Hinweise auf den Verlauf des vergangen Klimawandels zerstört werden können. Mit einer hochauflösenden Beprobung und einer hohen räumlichen Abdeckung kann diesem Problem in gewissem Maße begegnet werden.

Im Rahmen verschiedener Studien wurden bereits Dünen des Murray Beckens mittels der Lumineszenz-Methode datiert (Gardner et al. 1987, Readhead 1988, Cupper and Duncan 2006, Robertson and Prescott 2006, Twidale et al. 2007). Die Untersuchungen haben gezeigt, dass die Dünengenese in dieser Gegend bis mindestens ~160 ka zurückreicht und dass sie bis heute andauert. Allerdings wurden in diesen Studien nur jeweils wenige Proben datiert, und es kamen verschiedene Lumineszenztechniken wie z.B. die optisch stimulierte Lumineszenz (OSL) und die Thermolumineszenz (TL) zur Anwendung. Die Vergleichbarkeit der Ergebnisse ist daher eingeschränkt. Aufgrund der

geringen Probendichte ist es zudem nicht klar, ob die Dünenbildung im Murray Becken kontinuierlich ablief oder nur zu bestimmten Zeiten, unterbrochen von Phasen der Dünenstabilität. Des Weiteren gibt es Schätzungen, dass die Dünenbildung im Murray Becken möglicherweise bis ca. 500 ka zurück reicht (Zhisheng et al. 1986, Bowler et al. 2006). Diese Schätzungen basieren auf paläomagnetischen Datierungen der Dünen und der darunter liegenden Seesedimente sowie das Vorkommen von 4-5 Paläoböden in einigen Dünen des Untersuchungsgebietes, die eventuell in 100 ka Zyklen gebildet wurden. Mittels numerischer Datierungsmethoden wurden allerdings bisher keine Alter erzielt, die weiter als 160 ka zurückreichen.

Mit dem Ziel, das bestehende Wissen über die Dünengenese und das Paläoklima im Murray Becken zu erweitern, wurden tiefe Baggerschurfe angelegt und die Dünen mit einer Auflösung von ca. 0.5 m beprobt. Diese Proben wurden mit einem konsistenten methodischen Ansatz datiert, um eine repräsentative Chronologie der Dünenbildungsphasen zu erzielen. Drei verschiedene geologische Formationen werden von dieser Studie abgedeckt. Diese sind die Molineaux Sands (unregelmäßige Parabeldünen), die Woorinen Formation (Lineardünen) und die Bunyip Sands (Parabeldünen).

Zunächst wurden die Proben mittels *multiple grain aliquots* datiert, welche aus etwa 50 bis 100 Quarzkörnern bestehen. Eine signifikante Streuung der Äquivalenzdosis (De) wurde hierbei festgestellt, woraufhin in einem zweiten Schritt *single grain aliquots* datiert wurden. Diese erlauben es, die De-Verteilungen in höchst möglicher Auflösung zu untersuchen und Informationen über die Ursachen der Streuung der De-Werte zu erhalten.

Auf der Grundlage der Analyse der De-Verteilungen, Feldbeobachtungen und Bleichtests konnte gezeigt werden, dass hauptsächlich eine mikrodosimetrische Heterogenität des Sediments und post-sedimentäre Umlagerung durch Bioturbation für die hohe Streuung der Äquivalenzdosen verantwortlich sind. Eine schlechte Bleichung konnte, trotz intensiver Eisenverkrustung der Quarzkörner, ausgeschlossen werden. Des Weiteren wurde belegt, dass die Dosisleistung der beta-Quelle, die zur künstlichen Bestrahlung der Proben verwendet wird, ungleichmäßig verteilt ist, was eine zusätzliche Streuung der Äquivalenzdosen verursachte.

Darüber hinaus lieferten die *single grain*-Messungen interessante Informationen über die Lumineszenzeigenschaften der Quarze im Untersuchungsgebiet. So wurde z.B. festgestellt, dass die untersuchten Proben einen außergewöhnlich hohen Anteil stark lumineszierender Quarzkörner aufweisen.

Der Problematik der Bioturbation, also der Mischung von Sedimentschichten unterschiedlichen Alters, wurde damit begegnet, dass einzelne De-Populationen in der Verteilung mittels eines *finite mixture models* separiert wurden. Die detaillierte Untersuchung der De-Verteilung zeigte, dass insgesamt 20 % der beobachteten Streuung auf mikrodosimetrische Effekte zurückgeführt werden können. Dieser Wert wurde im *finite mixture model* verwendet, um die maximal erlaubte Streuung der einzelnen Populationen zu definieren. In älteren Proben wurde dieser Wert auf 27 % festgesetzt, um einer zusätzlichen Streuung durch die einsetzende OSL-Signalsättigung gerecht zu werden.
Proben mit De-Werten >200 Gy wurden als unzuverlässig eingestuft. Dieser Grenzwert beruht auf *dose recovery tests* und der Analyse der exponentiellen Sättigungsfunktion.
Die Lumineszenz-Alter wurden anhand der Haupt-De-Population, die über das *finite mixture model* bestimmt wurde, berechnet. Die Umweltdosisleistung wurde mittels Gammaspektrometrie bestimmt. Hierbei konnte gezeigt werden, dass sich der Großteil der Proben in einem radioaktiven Gleichgewicht befindet. Aufgrund der überwiegend niedrigen Dosisleistungen von meist weniger als 1 Gy/ka, war es möglich Proben zu datieren, die älter als 200 ka sind. Mit Ausnahme von zwei Proben waren alle Alter in der korrekten chronostratigraphischen Reihenfolge. Angesichts der intensiven Durchmischung der Dünensande zeigt dies die Zuverlässigkeit der gewonnenen Lumineszenzalter. Anhand der berechneten Sedimentationsraten konnte gezeigt werden, dass die Parabeldünen im Untersuchungsgebiet eine weitaus höhere Mobilität aufweisen als die Lineardünen. Dies bestätigt frühere Untersuchungen hinsichtlich der Mobilität der beiden Dünenfelder (Bowler and Magee 1978, Pell et al. 2001).
Trotz der unterschiedlichen Morphologie und Mobilität verlief die Dünenbildung in den beiden Dünenfeldern zeitgleich. Die unterschiedliche Morphologie der Dünen im Untersuchungsgebiet ist somit nicht auf klimatische Faktoren zurückzuführen, sondern höchstwahrscheinlich bedingt durch das höhere Sandangebot im Parabeldünenfeld.

Es wurden mehrere Phasen verstärkter äolischer Ablagerung festgestellt. Diese liegen um 11-12 ka, 13.5-14.5 ka, 18-38 ka, 62-73 ka, 79-112 ka, 145-185 ka und 205-215 ka, reichen also bis in das Marine Isotopenstadium 7 zurück. Die ältesten dieser Phasen belegen das hohe Alter der Dünen im westlichen Murray Becken und somit eine gute Erhaltung der Sandlagen. Weitere holozäne Events der Dünenmobilisierung wurden auf 3-4 ka, 5-6 ka und 7-8 ka datiert. Des Weiteren wurden drei rezente Alter ermittelt.

Der Vergleich der Dünenchronologie des westlichen Murray Beckens mit der des ariden Zentralaustraliens (Fitzsimmons et al. 2007) zeigte eine sehr gute Korrelation der Dünenbildungsphasen in den beiden Untersuchungsgebieten. Dies impliziert, dass das jungquartäre Klima in weiten Teilen Australiens sehr ähnlich war.

Die Dünenbildungsphasen korrelieren mit ariden Bedingungen, wie der Vergleich mit anderen Paläoumweltarchiven SO-Australiens gezeigt hat. Phasen, in denen keine äolische Ablagerung stattfand, sind hingegen mit vergangenen humiden Klimaperioden gleichzusetzen. Eine Phase von äolischer Sedimentationsruhe datiert auf den Zeitraum zwischen 40 und 60 ka. In diesen Zeitraum fallen auch die ältesten archäologischen Funde in SO-Australien und das Aussterben der australischen Megafauna (z.B. Roberts et al. 2001). Ebenso scheint das letzte interglaziale Maximum durch humidere Bedingungen geprägt gewesen zu sein. Die relativ hohen Fehler der Lumineszenzalter (~10%) verhindern allerdings eine genauere Auflösung der Klimageschichte >70 ka.
Die rezenten Alter erlauben es, historisch dokumentierte Dürren rekonstruieren. So wurde z.B. eine Probe auf 1939 ± 11 AD datiert, welches mit einer lang anhaltenden Dürreperiode in weiten Teilen Australiens zwischen 1937 and 1945 korreliert. Diese Dürre führte im Januar 1939 zu einem der katastrophalsten Buschfeuer in der Geschichte Südaustraliens (das sogenannten Black Friday Bushfire). Holzkohlepartikel in der entsprechenden Sandlage stellen möglicherweise die Hinterlassenschaften dieses Buschfeuers dar.

Die älteste Probe des Untersuchungsgebietes wurde auf ca. 450 ka datiert. Dieses Alter wurde als unzuverlässig eingestuft, es stimmt aber mit vorherigen Abschätzungen zum Einsetzen der Dünengenese im Murray Becken überein. Es konnte zudem ein zuverlässiges Minimumalter von 370 ka für den Beginn der Dünengenese im Untersuchungsgebiet erzielt werden.

Diese Studie zeigt, dass Dünen in semi-ariden Gebieten exzellente terrestrische Klimaarchive sind. Die *single grain* OSL-Datierung erlaubte die Bestimmung zuverlässiger Alter äolischer Sedimentation bis 270 ka im Untersuchungsgebiet. Die Dünenbildung im westlichen Murray Becken im Jüngeren Quartär war geprägt durch abwechselnde Phasen äolischer Aktivität und Dünenstabilität, und die zeitliche Einordnung dieser Phasen erlaubt die Rekonstruktion jungquartärer Aridităts- und Humiditätsperioden. Dies ist nur unter der Voraussetzung eines hohen Datensatzes an zuverlässigen Lumineszenzaltern möglich. Eine ausreichende zeitliche Auflösung klimatischer Fluktuationen konnte allerdings nur für die letzten 70 ka erzielt werden. Zudem muss die Interpretation dieses Archivs durch Ergebnisse aus anderen Paläoumweltarchiven gestützt werden.

References

Adamiec, G., Aitken, M. (1998). Dose-rate conversion factors: update. Ancient TL, 16: 37-50.

Aitken, M.J. (1985). Thermoluminescence Dating. Academic Press, London, 359 p.

Aitken, M.J. (1998). An Introduction to Optical Dating - The Dating of Quaternary Sediments by the Use of Photon-stimulated Luminescence. Oxford University Press, Oxford, 267 p.

Aitken, M.J., Smith, B.W. (1988). Optical dating: recuperation after bleaching. Quaternary Science Reviews, 7: 387-393.

Aitken, M.J., Tite, M.S., Reid, J., (1964). Thermoluminescent dating of ancient ceramics. Nature, 202: 1032-1033.

Aitken, M.J., Zimmerman, D.W., Fleming, S.J. (1968). Thermoluminescent dating of ancient pottery. Nature, 219: 442-444.

Armitage, S.J., Duller, G.A.T., Wintle, A.G. (2000). Quartz from southern Africa: sensitivity changes as a result of thermal pretreatment. Radiation Measurements, 32: 571-577.

Ash, J.E., Wasson, R.J. (1983). Vegetation and sand mobility in the Australian desert dunefields. Zeitschrift für Geomorphologie, 45: 7-25.

Auclair, M., Lamothe, M., Huot, S. (2003). Measurement of anomalous fading for feldspar IRSL using SAR. Radiation Measurements, 37: 487-492.

Ayliffe, L.K., Marianelli, P.C., Moriarty, K.C., Wells, R.T., McCulloch, M.T., Mortimer, G.E., Hellstrom, J.C. (1998). 500ka precipitation record from southeastern Australia: evidence for interglacial relative aridity. Geology, 26: 147-150.

Bailey, R.M. (2000a). The interpretation of quartz optically stimulated luminescence equivalent dose versus time plots. Radiation Measurements, 32/2: 129-140.

Bailey, R.M. (2000b). Circumventing possible inaccuracies of the single aliquot regeneration method for the optical dating of quartz. Radiation Measurements, 32: 833-840.

Bailey, R.M. (2004). Paper I - simulation of dose absorption in quartz over geological timescales and its implications for the precision and accuracy of optical dating. Radiation Measurements, 38/3: 299-310.

Bailey, R.M., Arnold, L.J. (2006). Statistical modelling of single grain quartz D_e distributions and an assessment of procedures for estimating burial dose. Quaternary Science Reviews, 25/19-20: 2475-2502.

Bailey R.M., Smith B.W., Rhodes E.J. (1997). Partial bleaching and the decay form characteristics of quartz OSL. Radiation Measurements, 27: 126-126.

Bailey, R.M., Singarayer, J.S., Ward, S., Stokes, S. (2003). Identification of partial resetting using De as a function of illumination time. Radiation Measurements, 37: 511-518.

Ballarini, M., Wallinga, J., Murray, A.S., van Heteren, S., Oost, A.P., Bos, A.J.J., van Eijk, C.W.E. (2003). Optical dating of young coastal dunes on a decadal time scale. Quaternary Science Reviews, 22: 1011-1017.

Ballarini, M., Wallinga, J., Duller, G.A.T., Brouwer, J.C., Bos, A.J.J., Van Eijk, C.W.E. (2005). Optimizing detection filters for single-grain optical dating of quartz. Radiation Measurements, 40/1: 5-12.

Ballarini, M., Wintle, A.G., Wallinga, J. (2006). Spatial variation of dose rate from beta sources as measured using single grains. Ancient TL, 24/1: 1-7.

Ballarini, M., Wallinga, J., Wintle, A.G., Bos, A.J.J. (2007). A modified SAR protocol for optical dating of individual grains from young quartz samples. Radiation Measurements, 42/3: 360-369.

Banerjee, D., Hildebrand, A.N., Murray-Wallace, C.V., Bourman, R.P., Brooke, B.P., Blair, M., (2003). New quartz SAR-OSL ages from the stranded beach dune sequence in south-east South Australia. Quaternary Science Reviews, 22: 1019-1025.

Barrows, T.T., Juggins, S. (2005). Sea-surface temperatures around the Australian margin and Indian Ocean during the Last Glacial Maximum. Quaternary Science Reviews, 24/7-9: 1017-1047.

Barrows, T.T., Stone, J.O., Fifield, L.K., Cresswel, R.G. (2001). Late Pleistocene Glaciation of the Kosciuszko Massif, Snowy Mountains, Australia. Quaternary Research, 55/2: 179-189.

Barrows, T.T., Stone, J.O., Fifield, L.K., Cresswel, R.G. (2002). The timing of the Last Glacial Maximum in Australia. Quaternary Science Reviews, 2/1-3: 159-173.

Barrows, T.T., Juggins, S., De Deckker, P., Calvo, E., Pelejero, C., (2007). Long-term sea-surface temperature and climate change in the Australian–New Zealand region. Paleoceanography, 22: PA2215, (doi:10.1029).

Bassinot, F.C., Labeyrie, L.D., Vincent, E., Quidelleur, X., Shackleton, N.J., Lancelot, Y. (1994). The astronomical theory of climate and the age of the Brunhes-Matuyama magnetic reversal. Earth and Planetary Science Letters, 126/1-3: 91-108.

Bateman, M.D., Frederick, C.D., Jaiswal, M.K., Singhvi, A.K. (2003a). Investigations into the potential effects of pedoturbation on luminescence dating. Quaternary Science Reviews, 22: 1169-1176.

Bateman, M.D., Thomas, D.S.G., Singhvi, A.K. (2003b). Extending the aridity record of the Southwest Kalahari: Current problems and future perspectives. Quaternary International, 111**:** 37-49.

Bateman, M.D., Boulter, C.H., Carr, A.S., Frederick, C.D., Peter, D., Wilder, M. (2007). Preserving the palaeoenvironmental record in Drylands: Bioturbation and its significance for luminescence-derived chronologies. Sedimentary Geology, 195/1-2: 5-19.

Beerten, K., Lomax, J., Clémer, K., Stesmans, A., Radtke, U. (2006). On the use of Ti centres for estimating burial ages of Pleistocene sedimentary quartz: Multiple-grain data from Australia. Quaternary Geochronology, 1/2: 151-158.

Belperio, A.P. (1995). Quaternary. In: Drexel, J.F., Priess, W.V. (eds.). The Geology of South Australia. South Australia Geological Survey Bulletin, 54/2: 219-280.

Berger, G.W. (1990). Effectiveness of natural zeroing of the thermoluminescence in sediments. Journal of Geophysical Research, 95: 12375-12397.

Blackburn, G. (1962). Stranded coastal dunes in North-western Victoria. Australian Journal of Science, 26: 388-389.

Bøe, A.-G., Murray, A.S., Dahl, S. O. (2007). Resetting of sediments mobilised by the LGM ice-sheet in southern Norway. Quaternary Geochronology, 2: 222-228.

BOM (2006). Bureau of Meteorology. Climate data online. www.bom.gov.au. Accessed 10 October 2006.

BOM (2008). Bureau of Meteorology. The World War II droughts 1937-45. www.bom.gov.au. Accessed September 20 2008.

Bostock, H.C., Opdyke, B.N., Gagan, M.K., A. Kiss, E., Fifield L.K. (2006). Glacial/interglacial changes in the East Australian current. Climate Dynamics, 26: 645-659.

Bøtter-Jensen, L., Duller, G.A.T., Poolton, N.R.J. (1994). Excitation and emission spectrometry of stimulated luminescence from quartz and feldspars. Radiation Measurements, 23: 613-616.

Bøtter-Jensen, L., Mejdahl, V., Murray, A.S. (1999a). New light on OSL. Quaternary Gechronology, 18: 303-309.

Bøtter-Jensen, L., Duller, G.A.T., Murray, A.S., Banerjee, D. (1999b). Blue light emitting diodes for optical stimulation of quartz in retrospective dosimetry and dating. Radiation Protection Dosimetry, 84: 335-340.

Bøtter-Jensen, L., Bulur, E., Duller, G.A.T., Murray, A.S. (2000). Advances in luminescence instrument systems. Radiation Measurements, 32/5-6: 523-528.

Bøtter-Jensen, L., McKeever, S.W.S,. Wintle, A.G. (2003a). Optically Stimulated Luminescence Dosimetry. Elsevier Science B.V., Amsterdam, 355 p.

Bøtter-Jensen L., Andersen C.E., Duller G.A.T., Murray A.S. (2003b). Developments in radiation, stimulation and observation facilities in luminescence measurements. Radiation Measurements, 37: 535-541.

Boutakoff, N. (1963). The geology and geomorphology of the Portland area. Geological Survey of Victoria, 22: 52-58.

Bowler, J.M., (1973). Clay Dunes: Their occurrence, formation and environmental significance. Earth-Science Reviews, 9: 315-338.

Bowler, J. M. (1976). Aridity in Australia: age, origins and expression in aeolian landforms and sediments. Earth Science Reviews, 12/2-3: 279-310.

Bowler, J.M. (1980). Quaternary chronology and palaeohydrology in the evolution of Mallee landscapes. In: Storrier, R.R., Stannard M.E. (eds.). Aeolian Landscapes in the Semi-arid Zone of Southeastern Australia. Society of Soil Science, Riverina Branch: 17-36.

Bowler, J.M., 1998. Willandra lakes revisited: environmental framework for human occupation. Archaeology in Oceania, 33: 120-155.

Bowler, J.M. (2002). Lake Mungo: Window to Australia's Past. CD-ROM. University of Melbourne Press.

Bowler, J.M., Magee, J.W. (1978). Geomorphology of the Mallee Region in semi-arid northern Victoria and western New South Wales. Proceedings of the Royal Society of Victoria, 90: 5-21.

Bowler, J.M.; Price, D.M. (1998). Luminescence dates and stratigraphic analyses at Lake Mungo: review and new perspectives. Archaeology in Oceania, 33/3: 156-168.

Bowler, J.M., Johnston, H., Olley, J.M., Prescott, J.R., Roberts, R.G., Shawcross, W., Spooner, N.S. (2003). New ages for human occupation and climatic change at Lake Mungo,Australia. Nature, 421: 837-840.

Bowler, J.M., Kotsonis, A., Lawrence, C.R. (2006). Environmental evolution of the Mallee region, western Murray Basin. Proceedings of the Royal Society of Victoria, 118/2: 161-210.

Bray, H. E., Stokes, S. (2003). Chronologies for Late Quaternary barchan dune reactivation in the southeastern Arabian Peninsula. Quaternary Science Reviews, 22: 1027-1033.

Brennan, B.J. (2003). Beta doses to spherical grains. Radiation Measurements, 37: 299-303.

Bristow, C. S., Bailey, S.D., Lancaster, N. (2000). The sedimentary structure of linear sand Dunes. Nature, 406: 56-59.

Bristow, C.S., Lancaster, N., Duller, G.A.T. (2005). Combining ground penetrating radar surveys and optical dating to determine dune migration in Namibia. Journal of the Geological Society, 162/2: 315-322.

Bristow, C.S., Duller, G.A.T., Lancaster, N. (2007). Age and dynamics of linear dunes in the Namib desert. Geology, 35/6: 555-558.

Brown, C.M., Stephenson, A.E. (1991). Geology of the Murray Basin, southeastern Australia. Bureau of Mineral Resources Bulletin, 235, Canberra. 430 p.

Bullard, J.E.; McTainsh, G.H. (2003). Aeolian-fluvial interactions in dryland environments: examples, concepts and Australia case study. Progress in Physical Geography, 27/4: 471-501.

Bulur, E. (1996). An alternative technique for optically stimulated luminescence (OSL) experiment. Radiation Measurements, 26: 701-709.

Bulur, E., Bøtter-Jensen, L., Murray, A.S. (2000) Optically stimulated luminescence from quartz measured using the linear modulation technique. Radiation Measurements, 32: 407-411.

Bulur, E., Duller, G.A.T., Solongo, S., Bøtter-Jensen, L., Murray, A.S. (2002). LM-OSL from single grains of quartz: a preliminary study. Radiation Measurements, 35: 79-85.

Butler, B.E. (1956). Parna. An Aeolian Clay. Australian Journal of Science, 18: 145-151.

Butler, B.E., Hubble, G.D. (1978). The general distribution and character of soils in the Murray-Darling River system. Proceedings of the Royal Society of Victoria, 90/1: 149-156.

CalPal, (2007). Cologne Radiocarbon Calibration and Paleoclimate Research Package. Version 1.5. www.calpal-online.de (accessed 4 April 2008).

Chase, B.M., Thomas, D.S.G. (2007). Multiphase late Quaternary aeolian sediment accumulation in western South Africa: Timing and relationship to palaeoclimatic changes inferred from the marine record. Quaternary International, 166**:** 29-41.

Chen, X.Y., Barton., C.E. (1991). Onset of aridity and dune-building in central Australia: sedimentological and magnetostratigraphic evidence from Lake Amadeus. Palaeogeography, Palaeoclimatology, Palaeoecology, 84/1-4: 55-73.

Chen, X.Y., Lintern, M.J., Roach, I.C. (2002a). Calcrete: Characteristics, distribution and use in mineral exploration. CRC LEME, Canberra, 160 p.

Chen X.Y., Spooner N.A., Olley J.M., Questiaux D.G. (2002b). Addition of aeolian dusts to soils in southeastern Australia: red silty clay trapped in dunes bordering Murrumbidgee River in the Wagga Wagga region. – Catena, 47: 1-27.

Choi, J.H., Murray, A.S., Jain, M., Cheong, C.S., Chang, H.W. (2003a). Luminescence dating of well-sorted marine terrace sediments on the southeastern coast of Korea. Quaternary Science Reviews, 22: 407-421.

Choi, J.H., Murray, A.S., Cheong, C.S., Hong, D.G., Chang, H.W. (2003b). The resolution of stratigraphic inconsistency in the luminescence ages of marine terrace sediments from Korea. Quaternary Science Reviews, 22: 1201-1206.

Choi, J.H., Duller, G.A.T., Wintle, A.G. (2006a). Analysis of quartz LM-OSL curves. Ancient TL, 24/1: 9-20.

Choi, J.H., Duller, G.A.T., Wintle, A.G., Cheong, C.S. (2006b). Luminescence characteristics of quartz from the southern Kenyan Rift Valley: Dose estimation using LM-OSL SAR. Radiation Measurements, 41/7-8: 847-854.

Choi, J.H., Murray A.S., Cheong, C.-S., Hong, D.G.H., Chang, H.W. (2006c). Estimation of equivalent dose using quartz isothermal TL and the SAR procedure. Quaternary Geochronology, 1: 101-108.

Churchward, H.M. (1961). Soil studies at Swan Hill, Victoria, Australia. Journal of Soil Science, 12: 73-86.

Crocker, R.L. (1946). The Simpson Desert Expedition, 1939 Scientific Reports: No. 8. The soil sand vegetation of the Simpson Desert and its borders. Transactions of the Royal Society of South Australia, 70: 235-258.

Croke, J., Magee, J., Price, D. (1996). Major episodes of Quaternary activity in the lower Neales River, northwest of Lake Eyre, central Australia. Palaeogeography, Palaeoclimatology, Palaeoecology, 124/1-2: 1-15.

Cupper, M.L. (2006). Luminescence and radiocarbon chronologies of playa sedimentation in the Murray Basin, southeastern Australia. Quaternary Science Reviews, 25/19-20: 2594-2607.

Cupper, M.L., Duncan, J. (2006). Last glacial megafaunal death assemblage and early human occupation at Lake Menindee, southeastern Australia. Quaternary Research, 66/2: 332-341.

Daniels, F., Boyd, C.A., Saunders, D.F. (1953). Thermoluminescence as a research tool. Science, 117: 343-349.

Dart, R.C., Barovich, K.M., Chittleborough, D. (2005). Pedogenic carbonates, strontium isotopes and their relationship with Australian dust processes. Regolith 2005 - Ten Years of CRC LEME: 64-66.

D'Costa, D M., Kershaw, A.P. (1995). A Late Pleistocene and Holocene pollen record from Lake Terang, Western Plains of Victoria, Australia. Palaeogeography, Palaeoclimatology, Palaeoecology, 113/1: 57-67.

Debertin, K., Helmer, R.G. (1988). γ and X-ray Spectrometry with Semiconductor Detectors, Elsevier, Amsterdam, 399 p.

Degering, D., Kulig, G., Krbetschek, M. (submitted). ADELE—a novel software for Age Determination based on Luminescence and Electron spin resonance, Ancient TL.

DeVogel, S.B., Magee, J.W., Manley, W.F., Miller, G.H. (2004). A GIS-based reconstruction of late Quaternary paleohydrology: Lake Eyre, arid central Australia. Palaeogeography, Palaeoclimatology, Palaeoecology, 204/1-2: 1-13.

Duller G.A.T. (1991). Equivalent dose determination using single aliquots. Nuclear Tracks and Radiation Measurements, 18: 371-378.

Duller G.A.T. (1994a). Luminescence dating of sediments using single aliquots: new procedures. Quaternary Geochronology (Quaternary Science Reviews), 13: 149-156.

Duller G.A.T. (1994b). Luminescence dating of poorly bleached sediments from Scotland. Quaternary Geochronology (Quaternary Science Reviews), 13: 521-524.

Duller, G.A.T. (1995). Luminescence dating using single aliquots: methods and applications. Radiation Measurements, 24: 217-226.

Duller, G.A.T. (2004). Luminescence dating of Quaternary sediments: recent advances. Journal of Quaternary Science, 19: 183-192.

Duller, G.A.T. (2003). Distinguishing quartz and feldspar in single grain luminescence measurements. Radiation Measurements, 37: 161-165.

Duller, G.A.T. (2005). Luminescence Analyst, Version 3.22b (Manual).

Duller, G.A.T. (2006). Single grain optical dating of glacigenic deposits. Quaternary Geochronology, 1/4: 296-304.

Duller, G.A.T. (2007). Assessing the error on equivalent dose estimates derived from single aliquot regenerative dose measurements. Ancient TL, 25/1:15-24.

Duller,G.A.T. (2008). Single-grain optical dating of Quaternary sediments: why aliquot size matters in luminescence dating. Boreas, 37/4: 589-612.

Duller, G.A.T., Bøtter-Jensen, L. (1996). Comparison of optically stimulated luminescence signals from quartz using different stimulation wavelengths. Radiation Measurements, 26/4: 603-609.

Duller G.A.T., Bøtter-Jensen, L., Murray A.S. and Truscott A.J. (1999). Single gain laser luminescence (SGLL) measurements using a novel automated reader. Nuclear Instruments and Methods in Physics Research B, 155: 506-514.

Duller G.A.T., Bøtter-Jensen L., Murray A.S. (2000). Optical dating of single sand-sized grains of quartz: sources of variability. Radiation Measurements 32: 453-457.

Edney, P.A., Kershaw, A.P., De Deckker, P. (1990). A late Pleistocene and Holocene vegetation and environmental record from Lake Wangoom, Western Plains of Victoria, Australia. Palaeogeography, Palaeoclimatology, Palaeoecology, 80/3-4: 325-343.

Edwards, R.L., Chen, J.H., Wasserburg, G. J. (1987). ^{238}U-^{234}U-^{230}Th-^{232}Th systematics and the precise measurement of time over the past 500 000 years. Earth and Planetary Science Letters, 81: 175-192.

Eitel, B., Kadereit, A., Blümel, W.D., Hüser, K., Kromer, B. (2005). The Amspoort Silts, northern Namib desert (Namibia): formation, age and palaeoclimatic evidence of river-end deposits. Geomorphology, 64: 299-314.

Erfurt, G., Krbetschek, M.R. (2003). IRSAR – A single aliquot regenerative-dose dating protocol applied to the infrared radiofluorescence (IR-RF) of coarse-grain K-feldspar. Ancient TL, 21/1: 35-42.

Fattahi, M., Stokes, S., (2000). Extending the time range of luminescence dating using red TL (RTL) from volcanic quartz. Radiation Measurements, 32: 479–485.

Feathers, J.K. (2003). Single-grain OSL dating of sediments from the Southern High Plains, USA. Quaternary Science Reviews, 22/10-13: 1035-1042.

Fiebig, M., Preusser, F. (2007). Investigating the amount of zeroing in modern sediments of River Danube, Austria. Quaternary Geochronology, 2/1-4: 143-149.

Firman, J.B. (1965). Late Cainozoic lacustrine deposits in the Murray Basin, South Australia. Geological Survey South Australia. Quarterly Geological Notes, 16: 1-2.

Firman, J.B. (1966a). Parilla Sand showing ortstein and fossil stream patterns, Pinnaroo-Karoonda 1:250 000 map sheet, Atlas of South Australia. Geological Survey of South Australia, Special Series.

Firman, J.B. (1966b). Molineaux Sand. Pinnaroo-Karoonda map sheet, Geological Atlas of South Australia, 1:250,000 series, Geological Survey of South Australia.

Firman, J.B. (1967). Stratigraphy of late Cainozoic deposits in South Australia. Transactions of the Royal Society of South Australia, 91: 165-178.

Firman, J.B. (1971). Renmark sheet SI 54-10, South Australian Geological Atlas Series, Geological Survey of South Australia, Adelaide.

Firman, J.B. (1973). Regional stratigraphy of surficial deposits in the Murray Basin and Gambier Embayment. Geological Survey of South Australia, Report of Investigation, 39. Geological Survey of South Australia, Adelaide.

Fitzsimmons, K.E., Rhodes, E.J., Magee., J.W., Barrows, T.T. (2007). The timing of linear dune activity in the Strzelecki and Tirari Deserts, Australia. Quaternary Science Reviews, 26/19-21: 2598-2616.

Fleming S.J. (1966). Study of thermoluminescence of crystalline extracts from pottery. Archaeometry, 9: 170-173.

Fleming, S.J. (1970). Thermoluminescence dating: refinement of the quartz inclusion technique. Archaeometry, 12: 133-145.

Folz, E., Bodu, P., Bonte, P., Joron, J.-L., Mercier, N., Reyss, J.-L. (2001). OSL dating of fluvial quartz from Le Closeau, a Late Paleolithic site near Paris — comparison with ^{14}C chronology. Quaternary Science Reviews, 20/5-9: 927-933.

Franklin, A.D., Hornyak, W.F. (1990). Isolation of the rapidly bleaching peak in quartz TL glow curves. Ancient TL, 8: 29-31.

Fuchs, M., Lang, A. (2001). OSL dating of coarse-grain fluvial quartz using single-aliquot protocols on sediments from NE Peloponnese, Greece. Quaternary Science Reviews, 20: 783-787.

Galbraith, R.F. (1988). Graphical display of estimates having differing standard errors. Technometrics, 30: 271-281.

Galbraith R.F. (1990). The radial plot: graphical assessment of spread in ages. Nuclear Tracks and Radiation Measurements, 17: 207-214.

Galbraith, R.F. (1998). The trouble with "probability density" plots of fission track ages. Radiation Measurements, 29: 125-131.

Galbraith, R.F. (2002). A note on the variance of a background-corrected OSL count. Ancient TL, 20: 49-51.

Galbraith, R.F. (2003). A simple homogeneity test for estimates of dose obtained using OSL. Ancient TL, 21/2: 75-77.

Galbraith, R.F., Green, P.F. (1990). Estimating the component ages in a finite mixture. Nuclear Tracks and Radiation Measurements, 17: 197-206.

Galbraith, R.F., Roberts, R.G., Laslett, G.M., Yoshida, H., Olley, J.M. (1999). Optical dating of single and multiple grains of quartz from Jinmium rock shelter, northern Australia: Part I, experimental design and statistical models. Archaeometry, 41: 339-364.

Galbraith, R. F., Roberts, R.G., Yoshida, H. (2005). Error variation in OSL palaeodose estimates from single aliquots of quartz: a factorial experiment. Radiation Measurements, 39: 289-307.

Gardner, G.J., Mortlock, A.J., Price, D.M., Readhead, M.L., Wasson, R.J. (1987). Thermoluminescence and radiocarbon dating of Australian desert dunes. Australian Journal of Earth Sciences, 34: 343-357.

Gentilli, J. (1986). Climate. In: Jeans, D.N. (ed.). Australia, geography. The natural environment. Sydney University Press, Sydney: 14–48.

Geyh, M.A. (2005). Handbuch der physikalischen und chemischen Altersbestimmung. Wissenschaftliche Buchgesellschaft, Darmstadt, 224 p.

Geyh, M.A., Schleicher, H. (1990). Absolute Age Determination – Physical and Chemical Dating Methods and their Application. Springer, Berlin-Heidelberg-New York, 503 p.

Gill, E.D. (1978). The Murray Darling River system. Royal Society of Victoria. Proceedings, 90/1: 1-4.

Godfrey-Smith, D.I., Huntley, D.J., Chen, W.H. (1988). Optical dating studies of quartz and feldspar sediment extracts. Quaternary Science Reviews, 7: 373-380.

Goudie, A.S. (1983). Calcrete. In: Goudie, A.S., Pye, K. (eds.). Chemical Sediments and Geomorphology. Academic Press, London: 93-131.

Grevenitz, P. (2006). The Character and Genesis of Pedogenic Calcrete in Southern Australia. PhD Thesis, University of Wollongong, 222 p.

Grün, R. (1989). Die ESR-Altersbestimmungsmethode. Reihe: Hochschultext, Berlin-Heidelberg, 132 p.

Hack, J. T. (1941). Dunes of the western Navajo Country. Geographical Review, 31: 240-263.

Harle, K.J. (1997). Late Quaternary vegetation and climate change in southeastern Australia: palynological evidence from marine core E55-6. Palaeogeography, Palaeoclimatology, Palaeoecology, 131/3-4: 465-483.

Harle, K.J., Kershaw, A.P., Heijnis, H. (1999). The contributions of uranium/thorium and marine palynology to the dating of the Lake Wangoom pollen record, western plains of Victoria, Australia. Quaternary International, 57-58: 25-34.

Hesse, P.P. (1994). The record of continental dust from Australia in Tasman Sea Sediments. Quaternary Science Reviews, 13/3: 257-272.

Hesse, P.P., McTainsh, G.H. (1999). Last Glacial Maximum to Early Holocene Wind Strength in the Mid-latitudes of the Southern Hemisphere from Aeolian Dust in the Tasman Sea. Quaternary Research, 52/3: 343-349.

Hesse, P.P., McTainsh, G.H. (2003). Australian dust deposits: modern processes and the quaternary record. Quaternary Science Reviews, 22: 2007-2035.

Hesse, P.P., Magee, J.W., van der Kaars, S. (2004). Late Quaternary climates of the Australian arid zone: A review. Quaternary International, 118/119: 87-102.

Hilgers, A. (2007). The chronology of Late Glacial and Holocene dune development in the northern Central European lowland reconstructed by optically stimulated luminescence (OSL) dating. PhD Thesis, University of Cologne, 353 p.

Hilgers, A., Murray, A.S., Schlaak, N., Radtke, U. (2001). Comparison of quartz OSL protocols using Lateglacial and Holocene dune sands from Brandenburg. Germany Quaternary Science Reviews, 20/5-9: 731-736.

Hills, E.S. (1975). The Physiography of Victoria. An Introduction to Geomorphology. Whitcombe & Tombs, Melbourne. 373 p.

Hollands, C.B., Nanson, G.C., Jones, B.G., Bristow, C.S., Price, D.M., Pietsch, T.J. (2006). Aeolian–fluvial interaction: evidence for Late Quaternary channel change and wind-rift linear dune formation in the northwestern Simpson Desert, Australia. Quaternary Science Reviews, 25: 142-162.

Hope, P. (2005). The Weather and Climate of Australia at the Last Glacial Maximum. PhD Thesis, The University of Melbourne, 266 p.

Huntley, D.J., Godfrey-Smith, D.I., Thewalt, M.L.W. (1985). Optical dating of sediments. Nature, 313: 105-107.

Huntley, D.J., Godfrey-Smith, D.I., Haskell, E.H. (1991). Light-induced emission spectra from some quartz and feldspars. Nuclear Tracks and Radiation Measurements, 18: 127-131.

Huntley, D.J., Hutton, J.T., Prescott, J.R. (1993). The stranded beach-dune sequence of south-east South Australia: A test of thermoluminescence dating, 0–800 ka. Quaternary Science Reviews, 12/1: 1-20.

Hütt, G., Jaek, I., Tchonka, J. (1988). Optical dating: K-feldspars optical response stimulation spectra. Quaternary Science Reviews, 7: 381-385.

Hutton, J.T., Dixon, J.C. (1981). The chemistry and mineralogy of some South Australian calcretes and associated soft carbonates and their dolomitization. Journal of the Geological Society of Australia, 28: 71-79.

Idnurm, M., Cook, P.J. (1980). Palaeomagnetism of beach ridges in South Australia and the Milankovitch theory of ice ages. Nature, 286: 669-702.

Iriondo, M. (1999). Last Glacial Maximum and Hypsithermal in the Southern Hemisphere. Quaternary International, 62/1: 11-19.

Jacobs, Z., Duller, G.A.T., Wintle, A.G. (2003a). Optical dating of dune sand from Blombos Cave, South Africa: II – Single grain data. Journal of Human Evolution, 44: 613-625.

Jacobs, Z., Duller, G.A.T., Wintle, A.G. (2003b). Optical dating of dune sand from Blombos Cave, South Africa: I—multiple grain data. Journal of Human Evolution, 44/5: 599-612.

Jacobs, Z., Wintle, A.G., Duller, G.A.T. (2006a). Evaluation of SAR procedures for D_e determination using single aliquots of quartz from two archaeological sites in South Africa. Radiation Measurements, 41/5: 520-533.

Jacobs, Z., Duller, G.A.T., Wintle, A.G., (2006b). Interpretation of single grain De distributions and calculation of De. Radiation Measurements, 41: 264-277.

Jacobs, Z., Wintle, A.G., Roberts, R.G., Duller, G.A.T. (2008). Equivalent dose distributions from single grains of quartz at Sibudu, South Africa: context causes and consequences for optical dating of archaeological deposits. Journal of Archaeological Science, 35/7: 1808-1820.

Jain, M., Murray, A.S., Bøtter-Jensen, L. (2003). Characterisation of blue-light stimulated luminescence components in different quartz samples: implications for dose measurement. Radiation Measurements, 37: 441-449.

Jain, M., Murray, A.S., Bøtter-Jensen, L. (2004). Optically stimulated luminescence dating: How significant is incomplete light exposure in fluvial environments? Quaternaire, 15: 143-157.

Jain, M., Murray, A.S., Bøtter-Jensen, L., Wintle, A.G. (2005). A single-aliquot regenerative-dose method based on IR (1.49 eV) bleaching of the fast OSL component in quartz. Radiation Measurements, 39: 309-318.

Johnson, B.J., Miller, G.H., Fogel, M.L., Magee, J.W., Gagan, M.K., Chivas, A.R. (1999). 65,000 Years of Vegetation Change in Central Australia and the Australian Summer Monsoon. Sciene, 284: 1150-1152.

Jouzel, J., Lorius, C., Petit, J.R., Genthon, C., Barkov, N.I., Kotlyakov, V.M., Petrov, V.M. (1987). Vostok ice core: a continuous isotope temperature record over the last climatic cycle (160,000 years). Nature, 329: 403-408.

Jouzel, J., Vaikmae, R., Petit, J.R., Martin, M., Duclos, Y., Stievenard, M., Lorius, C., Toots, M., Melieres, M.A., Burckle, L.H., Barkov, N.I., Kotlyakov, V.M. (1995). The two-step shape and timing of the last deglaciation in Antarctica. Climate Dynamics, 11: 151-161.

Kalchgruber, R., Fuchs, M., Murray, A.S., Wagner, G.A. (2003). Evaluating dose-rate distributions in natural sediments using α-Al2O3:C grains. Radiation Measurements, 37/4-5: 293-297.

Karelsky, S. (1956). Classification of the surface circulation in the Australian region. Meteorological Study No. 8, AGPS, Canberra, 68 p.

Kawahata, H. (2002). Shifts in oceanic and atmospheric boundaries in the Tasman Sea (Southwest Pacific) during the Late Pleistocene: evidence from organic carbon and lithogenic fluxes. Palaeogeography, Palaeoclimatology, Palaeoecology, 184/3-4: 225-249.

Kershaw, A.P., van der Kaars, S., Moss, P.T. (2003). Late Quaternary Milankovitch-scale climatic change and variability and its impact on monsoonal Australasia. Marine Geology, 20: 81-95.

Klasen, N. (2008). Lumineszenzdatierung glazifluvialer Sedimente im nördlichen Alpenvorland. PhD Thesis, University of Cologne, 209 p.

Klasen, N., Fiebig, M., Preusser, F., Radtke, U. (2006). Luminescence properties of glaciofluvial sediments from the Bavarian Alpine Foreland. Radiation Measurements, 41: 866-870.

Klasen, N., Fiebig, M., Preusser, F., Reitner, J.M., Radtke, U. (2007). Luminescence dating of proglacial sediments from the Eastern Alps. Quaternary International, 164-165: 21-32.

Kocurek, G. (1998). Aeolian system response to external forcing factors - A sequence stratigraphic view of the Saharan region. In: Alsharan, A. Glennie, K.W., Wintle, A.G., Kendell, C.G.S.C. (eds.). Quaternary Deserts and Climate Change. Rotterdam, Balkema: 327-337.

Kotsonis, A. (1999). Tertiary shorelines of the western Murray Basin: weathering, sedimentology and exploration potential. –In: Stewart, R. (ed.). Murray Basin Mineral Sands Conference, April 1999, Mildura, Australian Institute of Geoscientists Bulletin, 26, Extended Abstracts: 57-63.

Krbetschek, M.R., Rieser, U., Zöller, L., Heinicke, J. (1994). Radioactive disequilibria in palaeodosimetric dating of sediments. Radiation Measurements, 23: 485-489.

Krbetschek, M.R., Götze, J., Dietrich, A., Trautmann, T. (1997). Spectral information from minerals relevant for luminescence dating. Radiation Measurements, 27: 695-748.

Kuhns, C.K., Agersnap Larsen, N., McKeever, S.W.S. (2000). Characteristics of LM-OSL from several different types of quartz. Radiation Measurements, 32: 413-418.

Lamothe, M., Balescu, S., Auclair, M. (1994). Natural IRSL intensities and apparent luminescence ages of single feldspar grains extracted from partially bleached sediments. Radiation Measurements, 23/2-3: 555-561.

Lamothe, M., Auclair, M., Hamzaoui, C., Huot, S. (2003). Towards a prediction of long-term anomalous fading of feldspar IRSL. Radiation Measurements, 37: 493-498.

Lancaster, N. (1990). Palaeoclimatic evidence from sand seas. Palaeogeography, Palaeoclimatology, Palaeoecology, 76/3-4: 279-290.

Lancaster, N. (1995). Geomorphology of desert dunes. Routledge, London, 290 p.

Lawrence, C.R. (1966). Cainozoic Stratigraphy and Structure of the Mallee Region, Victoria. Proceedings of the Royal Society of Victoria, 79: 517-554.

Lawrence, C.R. (1975). Geology, hydrodynamics and hydrochemistry of the southern Murray Basin. Geological Survey of Victoria, Memoir, 30/1.

Lepper K., Agersnap Larsen N., McKeever, S.W.S. (2000). Equivalent dose distribution analysis of Holocene Aeolian and fluvial quartz sands from Central Oklahoma. Radiation Measurements, 32: 603-608.

Lian, O.B., Roberts, R.G. (2006). Dating the Quaternary: progress in Luminescence dating of sediments. Quaternary Science Reviews, 25: 2449-2468.

Lomax, J., Hilgers, A., Wopfner, H., Gruen, R., Twidale, C.R., Radtke, U. (2003). The onset of dune formation in the Strzelecki Desert, South Australia. Quaternary Science Reviews, 22**:** 1067-1076.

Lomax, J., Hilgers, A. Twidale, C.R., Bourne, J.A., Radtke, U. (2007). Treatment of broad equivalent dose distributions in OSL dating of dune sands from the western Murray Basin, South Australia. Quaternary Geochronology, 2/1-4: 51-56.

Lowe, J.J., Walker, M.J.C. (1997). Reconstructing Quaternary Environments. Prentice Hall, London, 446 p.

Lukas, S., Spencer, J.Q.C., Robinson, R.A.J., Benn, D.I. (2007). Problems associated with luminescence dating of Late Quaternary glacial sediments in the NW Scottish Highlands. Quaternary Geochronology, 2/1-4: 243-248.

Madsen, A.T., Murray, A.S., Andersen, T.J., Pejrup, M., Breuning-Madsen, H. (2005). Optically stimulated luminescence dating of young estuarine sediments: a comparison with ^{210}Pb and ^{137}Cs dating. Marine Geology, 214/1-3: 251-268.

Magee, J.W., Bowler, J.M., Miller, G.H., William, D.L.G. (1995). Stratigraphy, sedimentology, chronology and palaeohydrology of Quaternary lacustrine deposits at Madigan Gulf, Lake Eyre, south Australia. Palaeogeography, Palaeoclimatology, Palaeoecology, 113/1: 3-42.

Magee, J.W., Miller, G.H., Spooner, N.A., Questiaux, D. (2004). Continuous 150 k.y. monsoon record from Lake Eyre, Australia: insolation-forcing implications and unexpected Holocene failure. Geology, 32: 885-888.

Martinson, D.G., Pisias, N.G., Hays, J.D., Imbrie, J., Moore T. C. Jr., Shackleton, N. J. (1987). Age dating and the orbital theory of the ice ages: Development of a high-resolution 0 to 300,000-year chronostratigraphy. Quaternary Research, 27/1: 1-29.

Mayya, Y.S., Morthekai, P., Murari, M.K., Singhvi, A.K. (2006). Towards quantifying beta microdosimetric effects in single-grain quartz dose distribution. Radiation Measurements, 41: 1032-1039.

McCoy D.G., Prescott J.R., Nation, R.J. (2000). Some aspects of single-grain luminescence dating. Radiation Measurements, 32: 859-864.

McFee, C.J., Tite, M.S. (1994). Investigations into the thermoluminescence properties of single quartz grains using an imagining photon detector. Radiation Measurements, 23: 355-360.

McKenzie, K.G., Gill, E.D. (1968). Ostracoda from the Murray River valley west of Wentworth, N.S.W. Australian Journal of. Science, 30: 463-464.

McQueen, K.M. (2006). Calcrete geochemistry in the Cobar-Girilambone Region, New South Wales. CRC LEME Open File Report 200, 27 p.

Mejdahl V. (1969). Thermoluminescence dating of ancient Danish ceramics. Archaeometry, 11: 99-104.

Mejdahl, V. (1979). Thermoluminescence dating: beta-dose attenuation in quartz grains. Archaeometry, 21: 61-72.

Melcher, M. (2008). Ein Beitrag zur quartären Klimarekonstruktion anhand von Einzelkorn-Lumineszenzdatierungen (SG-OSL) und sedimentologischen Untersuchungen an Dünensanden der Eyre Peninsula, Südaustralien. Unpublished diploma thesis, University of Cologne.

Miller, G.H., Magee, J.W., Jull, A.J.T. (1997). Low-latitude glacial cooling in the Southern Hemisphere from amino acids in emu eggshells. Nature, 385: 241-244.

Miller, G.H., Magee, J.W., Johnson, B.J., Fogel, M.L., Spooner, N.A., McCulloch, M.T., Ayliffe, L.K. (1999). Pleistocene extinction of Genyornis newtoni: human impact on Australian megafauna. Science, 283: 205–208.

Munyikwa, K. (2000). Cosmic ray contribution to environmental dose rates with varying overburden thickness. Ancient TL, 18: 27-34.

Munyikwa, K. (2005a). The role of dune morphogenetic history in the interpretation of linear dune luminescence chronologies: A review of linear dune dynamics. Progress in Physical Geography, 29: 317-336.

Munyikwa, K. (2005b). Synchrony of Southern Hemisphere Late Pleistocene arid episodes: A review of luminescence chronologies from arid aeolian landscapes south of the Equator. Quaternary Science Reviews, 24**:** 2555-2583.

Murray, A.S., Clemmensen, L.B. (2001). Luminescence dating of Holocene aeolian sand movement, Thy, Denmark. Quaternary Science Reviews, 20/5-9: 751-754.

Murray, A.S., Funder, S. (2003). Optically stimulated luminescence dating of a Danish Eemian coastal marine deposit: a test of accuracy. Quaternary Science Reviews, 22: 1177-1183.

Murray, A.S., Olley, J.M. (2002). Precision and accuracy in the optically stimulated luminescence dating of sedimentary quartz: a status review. - Geochronometria, 21: 1-15.

Murray, A.S., Roberts, R.G. (1997). Determining the burial time of single grains of quartz using optically stimulated luminescence. Earth and Planetary Science Letters, 152/1-4: 163-180.

Murray, A.S., Roberts, R.G. (1998). Measurement of the equivalent dose in quartz using a regenerative-dose single-aliquot protocol. Radiation Measurements, 29: 503-515.

Murray, A.S., Wintle, A.G. (1999). Isothermal decay of optically stimulated luminescence in quartz. Radiation Measurements, 30: 119-125.

Murray A.S., Wintle, A.G. (2000). Luminescence dating using an improved single-aliquot regenerative-dose protocol. Radiation measurements, 32: 57-73.

Murray, A.S., Wintle, A.G. (2003). The single aliquot regenerative dose protocol: potential for improvements in reliability. Radiation Measurements, 37: 377-381.

Murray, A.S., Wintle, A.G., Wallinga, J., (2002). Dose estimation using quartz OSL in the non-linear region of the growth curve. Radiation Protection Dosimetry, 101: 371-374.

Murray-Wallace, C.V., Brooke, B.P., Cann, J.H., Belperio, A.P., Bourman, R.P. (2001). Whole-rock aminostratigraphy of the Coorong Coastal Plain, South Australia: towards a million year record of sea-level highstands. Journal of the Geological Society of London, 158: 111-124.

Nanson, G.C, Chen, X.Y, Price, D.M. (1992a). Lateral migration, thermoluminescence chronology and colour variation of longitudinal dunes near Birdsville in the Simpson Desert, central Australia. Earth Surface Processes and Landforms, 17: 801-819.

Nanson, G.C., Price, D.M., Short, S.A. (1992b). Wetting and drying of Australia over the past 300 ka. Geology, 20: 791-794.

Nanson, G.C., Chen, X.Y., Price, M. (1995). Aeolian and fluvial evidence of changing climate and wind patterns during the past 100 ka in the western Simpson Desert, Australia. Palaeogeography, Palaeoclimatology, Palaeoecology, 113/1: 87-102.

Nathan, R.P., Thomas, P.J., Jain, M., Murray, A.S., Rhodes, E.J. (2003). Environmental dose rate heterogeneity of beta radiation and its implications for luminescence dating: Monte Carlo modelling and experimental validation. Radiation Measurements, 37: 305-313.

Olley, J.M., Murray, A.S. Roberts R.G. (1996). The effects of disequilibria in the uranium and thorium decay chains on burial dose rates in fluvial sediments. Quaternary Science Reviews (Quaternary Geochronology), 15: 751-760.

Olley, J.M., Roberts, R.G., Murray, A.S. (1997). Disequilibria in the Uranium decay series in sedimentary deposits at Allen's Cave, Nularbor Plain, Australia: implications for dose rate determinations. Radiation Measurements, 27: 433-443.

Olley, J., Caitcheon, G., Murray, A.S. (1998). The distribution of apparent dose as determined by optically stimulated luminescence in small aliquots of fluvial quartz: implications for dating young sediments. Quaternary Geochronology, 17: 1033-1040.

Olley, J.M., Caitcheon, G.G., Roberts, R.G. (1999). The origin of dose distributions in fluvial sediments, and the prospect of dating single grains from fluvial deposits using optically stimulated luminescence. Radiation Measurements, 30: 207-217.

Olley, J.M., de Deckker, P., Roberts, R.G., Fifield, L.K., Yoshida, H., Hancock, G. (2004a). Optical dating of deep-sea sediments using single grains of quartz: A comparison with radiocarbon. Sedimentary Geology, 169: 175-189.

Olley, J.M., Pietsch, T., Roberts, R.G. (2004b). Optical dating of Holocene sediments from a variety of geomorphic settings using single grains of quartz. Geomorphology, 60: 337-358.

Olley, J.M., Roberts, R.G., Yoshida, H., Bowler, J.M. (2006). Single-grain optical dating of grave-infill associated with human burials at Lake Mungo, Australia. Quaternary Science Reviews, 25: 2469-2474.

Page, K., Nanson, G., Price, D. (1996). Chronology of Murrumbidgee River palaeochannels on the Riverine Plain, southeastern Australia. Journal of Quaternary Science, 11/4: 311-326.

Page, K.J., Dare-Edwards, A.J., Owens, J.W., Frazier, P.S., Kellett, J., Price, D.M. (2001). TL chronology and stratigraphy of riverine source bordering sand dunes near Wagga Wagga, New South Wales, Australia. Quaternary International, 83/85: 187-194.

Passlow, V., Pinxian, W., Chivas, A.R. (1997). Late Quaternary palaeoceanography near Tasmania, southern Australia. Palaeogeography, Palaeoclimatology, Palaeoecology, 131/3-4: 433-463.

Pell, S.D., Chivas, A.R., Williams, I.S. (2001). The Mallee Dunefield: development and sand provenance. Journal of Arid Environments, 48: 149-170.

Pietsch, T.J., Olley, J.M., Nanson, G.C. (2008). Fluvial transport as a natural luminescence sensitiser of quartz. Quaternary Geochronology, 3/4: 365-376.

Prescott, J.R., Stephan, L.G. (1982). The contribution of cosmic radiation to the environmental dose for thermoluminescent dating. Latitude, altitude and depth dependences. PACT, 6: 17-25.

Prescott, J.R., Hutton, J.T. (1988). Cosmic ray and gamma ray dosimetry for TL and ESR. Nuclear Tracks and Radiation Measurements, 14: 223-227.

Prescott, J.R., Hutton, J.T. (1994). Cosmic ray contributions to dose rates for luminescence and ESR dating: large depths and long-term time variations. Radiation Measurements, 23: 497-500.

Prescott, J.R., Hutton, J.T. (1995). Environmental dose rates and radioactive disequilibrium from some Australian luminescence dating sites. Quaternary Science Reviews (Quaternary Geochronology), 14: 439-448.

Prescott, J.R., Robertson, G.B. (1997). Sediment dating by luminescence: a review. Radiation Measurements, 27: 893-922.

Preusser, F., Kasper, H.U. (2001). Comparison of dose rate determination using high resolution gamma spectrometry and inductively coupled plasma - mass spectrometry. Ancient TL, 19/1: 19-23.

Preusser, F., Geyh, M.A., Schlüchter, C. (2003). Timing of Late Pleistocene climate change in lowland Switzerland. Quaternary Science Reviews, 22/14: 1435-1445.

Preusser, F., Ramseyer, K., Schlüchter, C. (2006). Characterisation of low OSL intensity quartz from the New Zealand Alps. Radiation Measurements, 41/7-8: 871-877.

Preusser, F., Degering, D., Fuchs, M., Hilgers, A., Kadereit, A., Klasen, N., Krbetschek, M., Richter, D., Spencer, J. (2008). Luminescence dating: Basics, methods and applications. Quaternary Science Journal (Eiszeitalter und Gegenwart), 57: 95-149.

Rasmussen, S.O., Andersen. K.K., Svensson. A.M., Steffensen. J.P., Vinther. B.M., Clausen, H.B., Siggaard-Andersen, M.-L., Johnsen, S.J., Larsen, L.B., Dahl-Jensen, D., Bigler, M., Röthlisberger, R., Fischer, H., Goto-Azuma, K., Hansson, M.E., Ruth, U. (2006). A new

Greenland ice core chronology for the last glacial termination. Journal of Geophysical Research 111:D06102, doi:06110.01029/02005JD006079

Readhead, M.L. (1988). TL dating study of quartz in aeolian sediments from southeastern Australia. Quaternary Science Reviews, 7: 257-264.

Rhodes E.J. (1988). Methodological considerations in the optical dating of quartz. Quaternary Science Reviews, 7: 395-400.

Rhodes, E.J., Pownall, L. (1994). Zeroing of the OSL signal in quartz from young glaciofluvial sediments. Radiation Measurements, 23: 581-585.

Rhodes, E., Chappell, J., Fujioka, T., Fitzsimmons, K., Magee, J., Aubert, M., Hewitt, D., (2005). The history of aridity in Australia: chronological developments. Regolith 2005 - Ten years of CRC LEME: 265-268.

Rhodes, E.J., Singarayer, J.S., Raynal, J.-P., Westaway, K.E., Sbihi-Alaoui, F.Z. (2006). New age estimates for the Palaeolithic assemblages and Pleistocene succession of Casablanca, Morocco. Quaternary Science Reviews, 25/19-20: 2569-2585.

Richardson, C.A. (2001). Residual luminescence signals in modern coastal sediments. Quaternary Science Reviews, 20/5-9: 887-892.

Risø (2008). The Risø TL/OSL reader. www.risoe.dk. Accessed 6 September 2008.

Rittenour, T.M., Goble, R.J., Blum, M.D. (2003). An optical age chronology of Late Pleistocene fluvial deposits in the northern lower Mississippi valley. Quaternary Science Reviews, 22: 1105-1110.

Roberts, H.M. (2006). Optical dating of coarse-silt sized quartz from loess: Evaluation of equivalent dose determinations and SAR procedural checks. Radiation Measurements, 41/7-8: 923-929.

Roberts, H.M., Duller, G.A.T. (2004). Standardised growth curves for optical dating of sediment using multiple-grain aliquots. Radiation Measurements, 38/2: 241-252.

Roberts, R.G., Galbraith, R.F., Olley, J.M., Yoshida, H. and Laslett, G.M. (1999). Optical dating of single and multiple grains of quartz from Jinmium rock shelter, northern Australia: Part II, results and implications. Archaeometry, 41: 365-395.

Roberts, R.G., Galbraith, R.F., Yoshida, H., Laslett, G.M., Olley, J.M. (2000). Distinguishing dose populations in sediment mixtures: a test of single-grain optical dating procedures using mixtures of laboratory-dosed quartz. Radiation Measurement, 32: 459-465.

Roberts, R.G., Flannery, T.F., Ayliffe, L.K., Yoshida, H., Olley, J.M., Prideaux, G.J., Laslett, G.M., Baynes, A., Smith, M.A., Jones, R., Smith, B.L. (2001). New ages for the last Australian megafauna: continent-wide extinction about 46,000 years ago. Science, 292: 1888-1892.

Robertson, G.B., Prescott, J.R. (2006). Luminescence dating at the archaeological and human burial site at Roonka, South Australia. Quaternary Science Reviews, 25/19-20: 2586-2593.

Rodnight, H. (2006). Developing a luminescence chronology for late Quaternary fluvial change in South African floodplain wetlands. PhD Thesis, University of Wales, Aberystwyth, 329 p.

Rodnight, H., Duller, G.A.T., Wintle, A.G., Tooth, S. (2006). Assessing the reproducibility and accuracy of optical dating of fluvial deposits. Quaternary Geochronology, 1/2: 109-120.

Schaetzl, R, Anderson, S. (2005). Soils: Genesis and Geomorphology. Cambridge University Press, New York, 832 p.

Schönwiese, C.-D. (2000). Praktische Statistik für Meteorologen und Geowissenschaftler. Borntraeger, Stuttgart, 298 p.

Scholefield, R.B., Prescott, J.R., Franklin, A.D., Fox, P.J. (1994). Observations on some thermoluminescence emission centres in geological quartz. Radiation Measurements, 23/2-3: 409-412.

Shulmeister, J., Goodwin, I., Renwick, J., Harle, K., Armand, L., McGlone, M.S., Cook, E., Dodson, J., Hesse, P.P., Mayewski, P., Curran, M. (2004). The Southern Hemisphere westerlies in the Australasian sector over the last glacial cycle: a synthesis. Quaternary International, 118-119: 23-53.

Singarayer, J.S., Bailey, R.M. (2003). Further investigations of the quartz optically stimulated luminescence components using linear modulation. Radiation Measurements, 37: 451-458.

Singarayer, J.S., Bailey, R.M. (2004). Component-resolved bleaching spectra of quartz optically stimulated luminescence: preliminary results and implications for dating. Radiation Measurements, 38: 111-118.

Singarayer, J.S., Bailey R.M., Rhodes, E.J. (2000). Potential of the slow component of quartz OSL for age determination of sedimentary samples. Radiation Measurements, 32/5-6: 873-880.

Singarayer, J.S., Bailey, R.M., Ward, S., Stokes, S. (2005). Assessing the completeness of optical resetting of quartz OSL in the natural environment. Radiation Measurements, 40/1: 13-25.

Singhvi, A.K., Banerjee, D., Ramesh, R., Rajaguru, S.N., Gogte, V. (1996). A luminescence method for dating 'dirty' pedogenic carbonates for paleoenvironmental reconstruction. Earth and Planetary Science Letters, 139/1-2: 321-332.

Singhvi, A. K., Bluszcz, A., Bateman, M. D., Someshwar Rao, M. (2001). Luminescence dating of loess-palaeosol sequences and coversands: methodologicall aspects and palaeoclimatic implications. Earth-Science Reviews, 54: 193-211.

Smith B.W., Rhodes E.J. (1994). Charge movements in quartz and their relevance to optical dating. Radiation Measurements, 23: 329-33.

Smith, B.W., Aitken, M.J., Rhodes, E.J., Robinson, P.D., Geldard, D.M. (1986). Optical dating: methodological aspects. Radiation Protection Dosimetry, 17: 229-233.

Smith, B.W., Rhodes, E.J., Stokes, S., Spooner, N.A. (1990). The optical dating of sediments using quartz. Radiation Protection Dosimetry, 34: 75-78.

Spooner, N. A. (1992). Optical dating: Preliminary results on the anomalous fading of luminescence from feldspars. Quaternary Science Reviews, 11: 139-145.

Spooner, N. A. (1994a). The anomalous fading of infrared-stimulated luminescence from feldspars. Radiation Measurements, 23: 625-632.

Spooner N.A. (1994b). On the optical dating signal from quartz. Radiation Measurements, 23: 593-600.

Spooner N.A., Questiaux, D.G. (2000). Kinetics of red, blue and UV thermoluminescence and optically-stimulated luminescence from quartz. Radiation Measurements, 32: 659-666.

Spooner, N.A., Prescott, J.R., Hutton, J.T. (1988). The effect of illumination wavelength on the bleaching of the thermoluminescence (TL) of quartz. Quaternary Science Reviews, 7: 325-329.

Sprigg, R.C. (1952). The Geology of the South-East Province, South Australia, with Special Reference to Quaternary Coast-line Migrations and Modern Beach Developments. South Australia Geological Survey Bulletin, 54: 219-280.

Sprigg, R.C. (1959). Stranded sea beaches and associated sand accumulations of the Upper Southeast. Royal Society of South Australia Transactions, 82: 183-193.

Sprigg, R.C. (1979). Stranded and submerged seabeach systems of southeast South Australia and the aeolian desert cycle. Sedimentary Geology, 22: 53-96.

Stace, H.C.T., Hubble, G.D., Brewer, R., Northcote, K.H., Sleeman, J.R., Mullahy, M.J., Hallsworth, E.G. (1968). A handbook of Australian soils. Rellim Technical Publications, Adelaide, 435 p.

Stephenson, A.E. (1986). Lake Bungunnia – a Plio-Pleistocene Megalake in southern Australia. Palaeogeography, Palaeoclimatology, Palaeoecology, 57: 137-156.

Stokes, S. (1992). Optical dating of young (modern) sediments using quartz: Results from a selection of depositional environments. Quaternary Science Reviews, 11/1-2: 153-159.

Stokes S. (1994). The timing of OSL sensitivity changes in a natural quartz. Radiation Measurements, 23: 601-605.

Stokes, S., Bray, H.E., Blum, M.D. (2001). Optical resetting in large drainage basins: tests of zeroing assumptions using single-aliquot procedures. Quaternary Science Reviews, 20: 879-885.

Stone, A.E.C., Thomas, D.S.G. (2008). Linear dune accumulation chronologies from the southwest Kalahari, Namibia: challenges of reconstructing late Quaternary palaeoenvironments from aeolian landforms. Quaternary Science Reviews, 27/17-18: 1667-1681.

Stuut, J.-B.W., Prins, M.A., Schneider, R.R., Weltje, G.J., Jansen, J.H.F., Postma, G. (2002). A 300 kyr record of aridity and wind strength in southwestern Africa: inferences from grain-size distributions of sediments on Walvis Ridge, SE Atlantic. Marine Geology, 180: 221–233.

Stuut, J.-B.W., Crosta, X., Van der Borg, K., Schneider, R.R. (2004). Relationship between Antarctic sea ice and southwestern African climate during the late Quaternary. Geology, 32/10: 909–912.

Telfer, M.W., Thomas, D.S.G. (2007). Late Quaternary linear dune accumulation and chronostratigraphy of the southwestern Kalahari: implications for aeolian palaeoclimatic reconstructions and predictions of future dynamics. Quaternary Science Reviews, 26: 2617-2630.

Thomas P.J., Jain, M., Juyal, N., Singhvi, A.K., (2005). Comparison of single-grain and small-aliquot OSL dose estimates in <3000 years old river sediments from South India. Radiation Measurements, 39/5: 457-469.

Thomsen, K.J., Jain, M., Bøtter-Jensen, L., Murray, A.S., Jungner, H. (2003). Variation with depth of dose distributions in single grains of quartz extracted from an irradiated concrete block. Radiation Measurements, 37: 315-321.

Thomsen, K.J., Murray, A.S., Bøtter-Jensen, L. (2005). Sources of variability in OSL dose measurements using single grains of quartz. Radiation Measurements, 39: 47-61.

Thomsen, K.J., Bøtter-Jensen, L., Denby, P.M., Moska, P., Murray, A.S. (2006). Developments in luminescence measurement techniques. Radiation Measurements, 41/7-8: 768-773.

Thomsen, K.J., Bøtter-Jensen, L., Jain, M., Denby, P.M., Murray, A.S. (2008). Recent instrumental developments for trapped electron dosimetry. Radiation Measurements, 43/2-6: 414-421.

Trauerstein, M. (2008). Datierung der ältesten (?), quartären Dünengeneration auf der Eyre Peninsula (Südaustralien) unter Anwendung verschiedener Lumineszenzverfahren – ein methodischer Vergleich. Unpublished diploma thesis, University of Cologne.

Truscott, A.J., Duller, G.A.T., Bøtter-Jensen, L., Murray, A.S. and Wintle, A.G. (2000). Reproducibility of optically stimulated luminescence measurements from single grains of Al2O3:C and annealed quartz. Radiation Measurements, 32: 447-451.

Tseo, G. (1993). Two types of longitudinal dune fields and possible mechanisms for their development. Earth Surface Processes and Landforms, 18: 627-643.

Tsoar, H., Blumberg, D.G., Stoler, Y. (2004). Elongation and migration of sand dunes. Geomorphology, 57: 293-302.

Turney, C.S.M., Kershaw, A.P., Moss, P., Bird, M.I., Fifield, L.K., Cresswell, R.G., Santos, G.M., Tada, M.L., Hausladen, P.A., Zhou, Y. (2001). Redating the onset of burning at Lynch's Crater (North Queensland): Implications for human settlement in Australia. Journal of Quaternary Science, 16: 767–771.

Turney, C.S.M., Kershaw, A.P., John Lowe, J.J., van der Kaars, S., Johnston, R., Rule, S., Moss, P., Radke, L., Tibby, J., McGlone, M.S., Wilmshurst, J.M., Vandergoes, M.J., Fitzsimons, S.J., Bryant, C., James, S., Branch, N.P., Cowley, J., Kalin, R.M., Ogle, N., Jacobsen,G., Fifield, L.K. (2006). Climatic variability in the southwest Pacific during the Last Termination (20–10 kyr BP). Quaternary Science Reviews, 25/9-10: 886-903.

Twidale, C.R. (1981). Age and origin of longitudinal dunes in the Simpson and other sand ridge deserts. Die Erde, 112: 231-247.

Twidale, C.R., Prescott, J.R., . Bourne, J.A, Williams, F.M. (2001). Age of desert dunes near Birdsville, southwest Queensland. Quaternary Science Reviews, 20/12: 1355-1364.

Twidale, C.R., Bourne, J.A., Spooner, N.A., Rhodes, E.J. (2007). The age of the palaeodunefield of the northern Murray Basin in South Australia – preliminary results. Quaternary International, 166/1: 42-48.

Vandenberghe, D. (2003). Investigation of the optically stimulated luminescence dating method for application to young geological sediments. PhD thesis, University of Gent, 298 p.

Vandenberghe, D., Hossain, S.M., De Corte, F., van den Haute, P. (2003). Investigation on the origin of the equivalent dose distribution in a Dutch coversand. -Radiation Measurements, 37: 433-439.

Wagner, G.A. (1995). Altersbestimmung von jungen Gesteinen und Artefakten. Enke, Stuttgart, 277 p.

Wallinga, J. (2002). On the detection of OSL age overestimation using single-aliquot techniques. Geochronometria, 21: 17-26.

Wallinga, J., Murray, A.S., Wintle, A.G. (2000). The single-aliquot regenerative-dose (SAR) protocol applied to coarse-grain feldspar. Radiation Measurements, 32: 529-533.

Wang, X.L., Lu, Y.C., Wintle, A.G. (2006). Recuperated OSL dating of fine-grained quartz in Chinese loess. Quaternary Geochronology, 1/2: 89-100.

Wasson, R.J. (1986). Geomorphology and Quaternary history of the Australian continental dunefields. Geographical Review of Japan, 59: 55-67.

Wasson, R.J., Rajaguru, S.N., Misra, V.N., Agrawal, D.P., Dhir, R.P., Singhvi, A.K., Kameswara Rao, K. (1983). Geomorphology, late Quaternary stratigraphy and palaeoclimatology of the Thar dunefield. Zeitschrift für Geomorphologie, 45: 117-151.

Watanabe, O., Jouzel, J., Johnsen, S., Parrenin, F., Shoji, H., Yoshida, N. (2003). Homogeneous climate variability across East Antarctica over the past three glacial cycles. Nature, 422: 509-512.

Watanuki, T., Murray, A.S., Tsukamoto S. (2005). Quartz and polymineral luminescence dating of Japanese loess over the last 0.6 Ma: Comparison with an independent chronology. Earth and Planetary Science Letters, 240/3-4: 774-789.

Weninger, B., Jöris, O. (2008). A ^{14}C age calibration curve for the last 60 ka: the Greenland-Hulu U/Th timescale and its impact on understanding the Middle to Upper Paleolithic transition in Western Eurasia. Journal of Human Evolution, 55/5: 772-781.

Wiggs, G.F.S. (2001). Desert dune processes and dynamics. Progress in Physical Geography, 25: 53-79.

Wiggs, G.F.S., Livingstone, I., Thomas, D.S.G., Bullard, J.E. (1995). Dune mobility and vegetation cover in the southwest Kalahari desert. Earth Surface Processes and Landforms, 20/6: 515-529.

Williams, M., Dunkerley, D., De Dekker, P., Kershaw, P., Chappell, J. (1998). Quaternary Environments. Arnolds, London, 352 p.

Wintle, A.G. (1973). Anomalous fading of thermoluminescence in mineral samples. Nature, 245: 143–144.

Wintle, A.G. (1975). Thermal quenching of thermoluminescence in quartz. Geophysical Journal of the Royal Astronomical Society, 41: 107-113.

Wintle A.G. (1997). Luminescence dating: laboratory procedures and protocols. Radiation Measurements, 27: 769-817.

Wintle, A.G., Huntley, D.J. (1979). Thermoluminescence dating of a deep-sea sediment core. Nature, 279: 710-712.

Wintle, A.G., Huntley, D.J. (1980). Thermoluminescence dating of ocean sediments. Canadian Journal of Earth Sciences, 17: 348-360.

Wintle, A.G., Murray, A.S. (1997). The relationship between quartz thermoluminescence, photo-transferred thermoluminescence, and optically stimulated luminescence. Radiation Measurements, 27: 611-624.

Wintle, A.G., Murray, A.S. (1998). Towards the development of a preheat procedure for OSL dating of quartz. Radiation Measurements, 29: 81-94.

Wintle, A.G., Murray, A.S. (2006). A review of quartz optically stimulated luminescence characteristics and their relevance in single-aliquot regeneration dating protocols. Radiation Measurements, 41/4: 369-391.

Wopfner, H., Twidale, C.R. (1988). Formation and age of desert dunes in the Lake Eyre depocentres in central Australia. Geologische Rundschau, 77: 815-834.

Wopfner, H., Twidale, C.R., (2001). Australian desert dunes: wind rift or depositional in origin? Australian Journal of Earth Sciences, 48: 239–244.

Wright, V.P., Tucker, M.E. (1991). Calcretes: an introduction. In: Wright, V. P.,Tucker, M. E. (eds.). Calcretes. Blackwell Scientific, Oxford: 1-22.

Wyrwoll, K.-H., Dong, B., Valdes, P. (2000). On the position of southern hemisphere westerlies at the Last Glacial Maximum: an outline of AGCM simulation results and evaluation of their implications. Quaternary Science Reviews, 19/9: 881-898.

Yoshida, H., Roberts, R.G., Olley, J.M., Laslett, G.M., Galbraith, R.F. (2000). Extending the age range of optical dating using single 'supergrains' of quartz. Radiation Measurements, 32: 439-446.

Yoshida H., Roberts R.G., Olley J.M. (2003). Progress towards single-grain optical dating of fossil mud-wasp nests and associated rock art in northern Australia. Quaternary Science Reviews, 22: 1273-1278.

Zander, A., Degering, D., Preusser, F., Kasper, H.U., Brückner, H. (2007). Optically stimulated luminescence dating of sublittoral and intertidal sediments from Dubai, UAE: Radioactive disequilibria in the uranium decay series. Quaternary Geochronology, 2/1-4: 123-128.

Zhisheng, A., Bowler, J.M., Opdyke, N.D., Macumber P.G., Firman, J.B. (1986). Palaeomagnetic stratigraphy of Lake Bungunnia; Plio-Pleistocene precursor of aridity in the Murray Basin, southeastern Australia. Palaeogeography, Palaeoclimatology, Palaeoecology, 54: 219-239.

Zimmerman D.W. (1967). Thermoluminescence from fine grains from ancient pottery. Archaeometry, 10: 26-28.

Zimmerman, D.W. (1971). Thermoluminescence dating using fine grains from pottery. Archaeometry, 13: 29-52.

Appendix

Table 1: Dose rate data. U, Th and K concentrations are obtained from laboratory gamma spectrometry, and the contribution of these radionuclides to the total dose rate is given in %. The cosmic dose rate is calculated after Prescott and Hutton (1988, 1994), and the contribution of the cosmic dose rate to the total dose rate is given in %. Total dose rates include assumed water content fluctuations ranging from 0-6 %, and dose rates are calculated for a grain size of 200-250 µm, which were used for the single grain De-analysis.

Dune-field	Sample	$CaCO_3$-rich	Depth (m)	U (ppm)	U (%)	Th (ppm)	Th (%)	K (%)	K (%)	Cosmic dose r. (Gy/ka)	Cosmic dose (%)	Dose rate (Gy/ka)
W	MRR8		0.35	0.41 ± 0.03	10	1.94 ± 0.16	15	0.55 ± 0.02	54	0.20	21	0.94 ± 0.05
W	MRR7		0.45	0.41 ± 0.04	11	1.87 ± 0.22	14	0.55 ± 0.02	55	0.20	21	0.94 ± 0.05
W	MRR6		1.00	0.38 ± 0.02	10	1.80 ± 0.12	14	0.53 ± 0.02	55	0.18	20	0.88 ± 0.04
W	MRR5		1.50	0.42 ± 0.04	11	1.76 ± 0.21	14	0.56 ± 0.02	57	0.17	18	0.92 ± 0.05
W	MRR4		2.00	0.40 ± 0.04	10	1.90 ± 0.19	15	0.58 ± 0.02	58	0.16	17	0.93 ± 0.05
W	MRR3		2.50	0.44 ± 0.08	11	2.13 ± 0.24	15	0.63 ± 0.02	59	0.15	15	0.99 ± 0.06
W	MRR2		3.00	0.47 ± 0.04	11	2.12 ± 0.19	15	0.63 ± 0.02	59	0.14	14	0.98 ± 0.05
W	MRR1	X	3.50	0.50 ± 0.02	12	2.34 ± 0.22	16	0.64 ± 0.02	59	0.13	13	1.00 ± 0.05
W	MS9		1.55	0.31 ± 0.04	9	1.29 ± 0.13	12	0.49 ± 0.02	58	0.17	21	0.78 ± 0.04
W	MS8		2.20	0.53 ± 0.06	13	2.35 ± 0.19	18	0.54 ± 0.02	53	0.16	16	0.93 ± 0.05
W	MS7		2.65	0.52 ± 0.03	13	2.51 ± 0.20	19	0.53 ± 0.02	53	0.15	15	0.93 ± 0.04
W	MS6		3.15	0.53 ± 0.03	14	2.44 ± 0.31	18	0.54 ± 0.02	54	0.14	14	0.92 ± 0.05
W	MS5		3.65	0.53 ± 0.04	13	2.58 ± 0.15	19	0.56 ± 0.02	54	0.13	13	0.94 ± 0.05
W	MS4		4.30	0.55 ± 0.04	14	2.39 ± 0.27	18	0.57 ± 0.02	56	0.12	12	0.93 ± 0.05
W	MS2		4.90	0.82 ± 0.05	14	4.16 ± 0.26	22	0.82 ± 0.02	56	0.11	8	1.33 ± 0.07
W	MS1	XX	5.55	0.63 ± 0.10	14	2.98 ± 0.25	19	0.67 ± 0.02	57	0.10	9	1.06 ± 0.06
W	MS0	X	7.45	0.57 ± 0.04	14	2.59 ± 0.25	19	0.63 ± 0.02	59	0.08	8	0.95 ± 0.06
W	NWA1		0.65	0.38 ± 0.05	9	1.80 ± 0.21	13	0.60 ± 0.02	58	0.19	20	0.95 ± 0.05
W	NWA2		1.20	0.38 ± 0.03	10	1.69 ± 0.24	13	0.59 ± 0.02	59	0.18	19	0.92 ± 0.05
W	NWA3		1.80	0.38 ± 0.04	10	1.60 ± 0.21	12	0.59 ± 0.02	60	0.16	18	0.90 ± 0.05
W	NWA4		2.30	0.35 ± 0.06	9	1.45 ± 0.27	11	0.60 ± 0.02	62	0.15	17	0.88 ± 0.05
W	NWA5		2.80	0.39 ± 0.02	10	1.92 ± 0.09	14	0.62 ± 0.02	61	0.14	15	0.93 ± 0.05
W	NWA6		3.30	0.41 ± 0.03	10	1.90 ± 0.23	14	0.67 ± 0.02	63	0.13	13	0.97 ± 0.05
W	NWA7		3.75	0.37 ± 0.03	10	1.70 ± 0.20	13	0.61 ± 0.02	63	0.13	14	0.89 ± 0.05
W	NWA8		4.15	0.41 ± 0.04	10	2.03 ± 0.14	15	0.62 ± 0.02	62	0.12	13	0.92 ± 0.05
W	NWA9	XX	4.30	0.37 ± 0.04	12	1.77 ± 0.18	17	0.45 ± 0.01	56	0.12	16	0.74 ± 0.04
W	NWA10	X	4.45	0.43 ± 0.03	10	2.62 ± 0.19	18	0.69 ± 0.02	61	0.12	11	1.03 ± 0.05

Dune-field	Sample	$CaCO_3$-rich	Depth (m)	U (ppm)	U (%)	Th (ppm)	Th (%)	K (%)	K (%)	Cosmic dose r. (Gy/ka)	Cosmic dose (%)	Dose rate (Gy/ka)
W	NWB12		0.80	0.45 ± 0.03	11	1.91 ± 0.26	14	0.57 ± 0.02	55	0.19	19	0.94 ± 0.05
W	NWB11		1.25	0.44 ± 0.03	10	2.13 ± 0.19	15	0.62 ± 0.02	57	0.18	17	0.99 ± 0.05
W	NWB10		1.75	0.45 ± 0.03	11	2.02 ± 0.19	14	0.64 ± 0.02	59	0.16	16	0.99 ± 0.05
W	NWB9	X	2.35	0.45 ± 0.05	11	2.12 ± 0.20	15	0.63 ± 0.02	59	0.15	15	0.98 ± 0.05
W	NWB8		2.80	0.48 ± 0.06	11	2.37 ± 0.30	16	0.64 ± 0.02	58	0.14	14	1.00 ± 0.06
W	NWB7		3.30	0.53 ± 0.04	12	2.61 ± 0.22	18	0.64 ± 0.02	57	0.13	13	1.02 ± 0.05
W	NWB6		3.80	0.50 ± 0.03	11	2.70 ± 0.19	18	0.68 ± 0.02	59	0.13	12	1.05 ± 0.05
W	NWB5		4.30	0.48 ± 0.02	10	2.85 ± 0.20	18	0.74 ± 0.02	61	0.12	10	1.10 ± 0.06
W	NWB4		4.80	0.51 ± 0.02	11	3.01 ± 0.26	18	0.77 ± 0.02	62	0.11	9	1.14 ± 0.06
W	NWB3		5.30	0.50 ± 0.04	10	3.14 ± 0.28	19	0.79 ± 0.02	62	0.11	9	1.16 ± 0.06
W	NWB2	X	5.80	0.51 ± 0.04	11	3.21 ± 0.20	20	0.74 ± 0.02	61	0.10	9	1.11 ± 0.06
W	NWB1	X	6.40	0.54 ± 0.03	12	3.30 ± 0.23	21	0.71 ± 0.02	59	0.09	8	1.09 ± 0.06
W	NWC7		0.30	0.53 ± 0.03	12	2.55 ± 0.26	16	0.64 ± 0.02	54	0.20	18	1.09 ± 0.05
W	NWC6		0.85	0.49 ± 0.05	11	2.35 ± 0.16	16	0.60 ± 0.02	54	0.19	18	1.00 ± 0.05
W	NWC5		1.25	0.46 ± 0.02	11	2.32 ± 0.22	16	0.63 ± 0.02	57	0.18	17	1.01 ± 0.05
W	NWC4		1.75	0.52 ± 0.04	10	2.92 ± 0.22	17	0.75 ± 0.02	59	0.16	14	1.17 ± 0.06
W	NWC3	X	2.40	0.47 ± 0.04	10	2.76 ± 0.19	18	0.68 ± 0.02	58	0.15	14	1.07 ± 0.05
W	NWC2		3.15	0.41 ± 0.04	10	2.41 ± 0.29	18	0.60 ± 0.02	58	0.14	14	0.94 ± 0.05
W	NWC1		4.00	0.46 ± 0.04	10	2.51 ± 0.13	16	0.72 ± 0.02	62	0.12	11	1.06 ± 0.05
W	SW9		0.60	0.45 ± 0.03	12	2.00 ± 0.27	16	0.50 ± 0.02	51	0.19	21	0.89 ± 0.05
W	SW8		1.05	0.42 ± 0.03	12	1.83 ± 0.24	15	0.48 ± 0.02	52	0.18	21	0.84 ± 0.05
W	SW7		1.50	0.45 ± 0.06	12	2.22 ± 0.21	17	0.53 ± 0.02	53	0.17	18	0.91 ± 0.05
W	SW6		1.85	0.45 ± 0.03	12	2.07 ± 0.15	17	0.49 ± 0.02	52	0.16	18	0.86 ± 0.05
W	SW5		2.30	0.47 ± 0.03	12	2.26 ± 0.28	17	0.57 ± 0.02	56	0.15	16	0.94 ± 0.05
W	SW4		2.65	0.47 ± 0.03	12	2.08 ± 0.21	15	0.59 ± 0.02	58	0.15	15	0.94 ± 0.05
W	SW3	X	3.00	0.50 ± 0.06	13	2.38 ± 0.16	18	0.55 ± 0.02	55	0.14	15	0.92 ± 0.05
W	SW2	X	3.40	0.55 ± 0.06	13	2.79 ± 0.27	19	0.61 ± 0.02	55	0.13	13	1.01 ± 0.06
W	SW1		3.95	0.50 ± 0.04	12	2.75 ± 0.16	19	0.62 ± 0.02	57	0.12	12	0.99 ± 0.05

Dune-field	Sample	$CaCO_3$-rich	Depth (m)	U (ppm)	U (%)	Th (ppm)	Th (%)	K (%)	K (%)	Cosmic dose r. (Gy/ka)	Cosmic dose (%)	Dose rate (Gy/ka)
W	WP1		0.40	0.40 ± 0.03	11	1.89 ± 0.17	16	0.45 ± 0.02	50	0.20	23	0.83 ± 0.04
W	WP2		0.95	0.37 ± 0.04	11	1.82 ± 0.18	16	0.42 ± 0.02	50	0.18	23	0.78 ± 0.04
W	WP3		1.55	0.35 ± 0.04	11	1.65 ± 0.20	15	0.43 ± 0.02	52	0.17	22	0.76 ± 0.04
W	WP4		2.00	0.38 ± 0.02	11	1.91 ± 0.23	17	0.45 ± 0.02	52	0.16	20	0.79 ± 0.04
W	WP5		2.45	0.40 ± 0.03	12	1.86 ± 0.18	17	0.44 ± 0.02	52	0.15	19	0.77 ± 0.04
W	WP6		2.80	0.42 ± 0.03	12	2.33 ± 0.20	19	0.50 ± 0.02	53	0.14	16	0.86 ± 0.05
W	WP7	X	3.20	0.46 ± 0.07	13	2.38 ± 0.21	19	0.49 ± 0.02	53	0.14	15	0.85 ± 0.05
W	WP8	X	3.65	0.45 ± 0.03	12	2.32 ± 0.25	19	0.51 ± 0.02	54	0.13	14	0.86 ± 0.05
W	WP9	X	0.25	0.44 ± 0.07	12	2.22 ± 0.16	18	0.46 ± 0.02	48	0.20	22	0.88 ± 0.05
W	WP10	XX	1.00	0.42 ± 0.03	12	2.23 ± 0.25	18	0.45 ± 0.02	49	0.18	21	0.84 ± 0.05
W	WP11		1.60	0.38 ± 0.03	11	1.86 ± 0.16	17	0.44 ± 0.02	51	0.17	21	0.79 ± 0.04
W	WP12		2.15	0.39 ± 0.05	12	1.91 ± 0.20	17	0.43 ± 0.02	51	0.16	20	0.77 ± 0.04
W	WP13		2.55	0.41 ± 0.08	10	2.64 ± 0.19	19	0.58 ± 0.02	56	0.15	15	0.95 ± 0.05
B	BM1		1.00	0.82 ± 0.04	14	4.08 ± 0.30	20	0.85 ± 0.02	54	0.18	12	1.43 ± 0.07
B	BM2		1.60	0.82 ± 0.04	14	3.98 ± 0.22	20	0.80 ± 0.02	54	0.17	12	1.36 ± 0.07
B	BM3		2.10	0.82 ± 0.04	14	4.35 ± 0.28	21	0.84 ± 0.02	54	0.16	11	1.42 ± 0.07
B	BM4		4.20	0.75 ± 0.03	12	3.68 ± 0.26	18	0.98 ± 0.02	62	0.12	8	1.45 ± 0.08
B	BM5		5.80	0.73 ± 0.03	13	3.47 ± 0.33	18	0.92 ± 0.02	62	0.10	7	1.35 ± 0.07
M	ALC3		1.10	0.36 ± 0.03	13	1.95 ± 0.27	21	0.26 ± 0.02	38	0.18	28	0.63 ± 0.04
M	ALC2		1.60	0.33 ± 0.04	13	1.88 ± 0.17	22	0.25 ± 0.02	38	0.17	27	0.60 ± 0.04
M	ALC1		2.20	0.33 ± 0.03	14	1.80 ± 0.19	22	0.24 ± 0.02	38	0.16	26	0.57 ± 0.04
M	CC4		1.70	0.29 ± 0.04	12	1.30 ± 0.34	16	0.25 ± 0.02	42	0.17	29	0.56 ± 0.04
M	CC1		3.85	0.27 ± 0.02	13	1.09 ± 0.21	15	0.26 ± 0.02	48	0.13	24	0.51 ± 0.03
M	CD4		0.75	0.42 ± 0.04	13	1.46 ± 0.19	14	0.39 ± 0.02	48	0.19	25	0.74 ± 0.04
M	CD3		1.25	0.46 ± 0.09	13	1.80 ± 0.17	15	0.45 ± 0.02	50	0.18	21	0.82 ± 0.05
M	CD2		1.55	0.49 ± 0.05	13	2.48 ± 0.27	20	0.47 ± 0.02	49	0.17	19	0.88 ± 0.05
M	CD1		2.10	0.51 ± 0.03	14	2.56 ± 0.21	21	0.45 ± 0.02	48	0.16	18	0.86 ± 0.05
M	NG3		0.70	0.22 ± 0.04	12	0.98 ± 0.13	16	0.13 ± 0.02	28	0.19	43	0.43 ± 0.03
M	NG2		1.70	0.20 ± 0.01	13	0.91 ± 0.14	17	0.11 ± 0.02	27	0.17	43	0.37 ± 0.03
M	NG1		2.55	0.21 ± 0.02	14	0.90 ± 0.20	18	0.10 ± 0.02	26	0.15	41	0.35 ± 0.03

Dune-field	Sample	$CaCO_3$ -rich	Depth (m)	U (ppm)	U (%)	Th (ppm)	Th (%)	K (%)	K (%)	Cosmic dose r. (Gy/ka)	Cosmic dose (%)	Dose rate (Gy/ka)
M/W	PSP1		0.75	0.28 ± 0.02	12	1.12 ± 0.09	14	0.27 ± 0.02	44	0.19	32	0.58 ± 0.04
M/W	PSP2		1.50	0.32 ± 0.02	12	1.68 ± 0.11	18	0.33 ± 0.02	47	0.17	25	0.66 ± 0.04
M/W	PSP14		0.65	0.33 ± 0.02	12	1.54 ± 0.11	16	0.33 ± 0.01	46	0.19	28	0.68 ± 0.04
M/W	PSP13		1.10	0.33 ± 0.02	10	2.23 ± 0.14	21	0.39 ± 0.01	48	0.18	23	0.76 ± 0.04
M/W	PSP12		1.55	0.35 ± 0.02	12	1.63 ± 0.11	17	0.35 ± 0.01	48	0.17	25	0.68 ± 0.04
M/W	PSP11		2.10	0.31 ± 0.02	12	1.50 ± 0.17	18	0.28 ± 0.02	44	0.16	26	0.60 ± 0.03
M/W	PSP10		2.70	0.38 ± 0.02	13	2.05 ± 0.13	21	0.37 ± 0.01	49	0.14	20	0.71 ± 0.04
M/W	PSP9		3.20	0.43 ± 0.04	12	3.20 ± 0.34	26	0.43 ± 0.02	46	0.14	15	0.86 ± 0.05
M/W	PSP8		3.80	0.40 ± 0.02	14	2.08 ± 0.20	21	0.35 ± 0.02	47	0.13	18	0.69 ± 0.04
M/W	PSP7		4.35	0.36 ± 0.04	12	2.33 ± 0.19	23	0.39 ± 0.02	50	0.12	16	0.72 ± 0.04
M/W	PSP5		5.35	0.33 ± 0.02	12	1.81 ± 0.15	20	0.35 ± 0.02	51	0.10	16	0.63 ± 0.03
M/W	PSP3	X	6.35	0.22 ± 0.03	10	1.36 ± 0.20	19	0.30 ± 0.02	54	0.09	18	0.52 ± 0.03

Abbreviations: W: Woorinen Formation, B: Bunyip Sands, M: Molineaux Sands, M/W: Woorinen Formation, transitional zone to Molineaux Sands, X: very carbonate-rich samples, XX: samples from hardpan calcrete layers.

Table 2: Sampling depth, dose rate (including variations in water content from 0-6%), equivalent doses (De), number of valid De-values derived from single grain measurements (n), overdispersion values (OD) of the total data set, number of components derived from the finite mixture model (Galbraith and Green, 1990) including proportion of grains in main component, and luminescence age. The luminescence ages incorporates an error of 3.5 % on the De-values to account for uncertainties of the beta source calibration of the luminescence reader. For datasets with negative De-values (very young samples), the median was used for mean De-calculation. For datasets which yielded main component De-values of <85 Gy, sigma value of 20 % was used in the finite mixture model. For samples with main component De-values of >85 Gy, a sigma value of 27 % was used in the finite mixture model. The central age model (CAM) was used for the mean De-calculation of samples with mean De-values >200 Gy. If samples yielded unreliable ages this indicated in the last column. Samples with De-values >200 Gy were considered as unreliable due to proximity to signal saturation.

Dune field	Sample	depth (m)	dose rate (Gy/ka)	De (Gy)	n	OD (%)	No. of components (proportion in main component)	OSL age (ka)	comment
W	MRR8	0.35	0.94 ± 0.05	13.7 ± 1.4	66	62	4 (44)	14.5 ± 1.8	
W	MRR7	0.45	0.92 ± 0.05	23.9 ± 1.8	60	52	3 (44)	25.5 ± 2.5	
W	MRR6	1.00	0.87 ± 0.04	21.1 ± 1.8	51	36	2 (56)	23.9 ± 2.5	
W	MRR5	1.50	0.90 ± 0.05	30.4 ± 1.3	56	33	2 (91)	33.1 ± 2.6	
W	MRR4	2.00	0.91 ± 0.05	60.7 ± 4.6	50	34	2 (74)	65.5 ± 6.5	
W	MRR3	2.50	0.97 ± 0.06	69.6 ± 2.7	58	38	2 (93)	70.4 ± 5.4	
W	MRR2	3.00	0.97 ± 0.05	85.1 ± 3.4	62	29	2 (93)	86.6 ± 6.5	
W	MRR1	3.50	0.99 ± 0.05	105 ± 5	82	40	1 (100)	105 ± 8	
W	MS9	1.55	0.78 ± 0.04	0.0	50		Median	0	
W	MS8	2.20	0.93 ± 0.05	1.9 ± 0.1	60	74	4 (54)	2.0 ± 0.2	
W	MS7	2.65	0.92 ± 0.04	6.5 ± 0.5	50	81	4 (54)	7.1 ± 0.7	
W	MS6	3.15	0.91 ± 0.05	24.2 ± 2.5	70	70	4 (37)	26.3 ± 3.2	
W	MS5	3.65	0.93 ± 0.05	21.3 ± 3.7	75	46	3 (41)	22.6 ± 4.2	
W	MS4	4.30	0.93 ± 0.05	32.0 ± 2.1	73	34	3 (76)	34.4 ± 3.2	
W	MS2	4.90	1.32 ± 0.07	87.5 ± 4.8	89	49	2 (81)	65.7 ± 5.4	
W	MS1	5.55	1.06 ± 0.06	197 ± 16	60	38	2 (78)	185 ± 19	
W	MS0	7.45	0.97 ± 0.06						In saturation

Dune field	Sample	depth (m)	dose rate (Gy/ka)	De (Gy)	n	OD (%)	No. of components (proportion in main component)	OSL age (ka)	comment
W	NWA1	0.65	0.95 ± 0.05	7.4 ± 0.7	49	84	4 (40)	7.7 ± 0.9	
W	NWA2	1.20	0.92 ± 0.05	18.5 ± 1.0	43	56	3 (66)	20.0 ± 1.8	
W	NWA3	1.80	0.90 ± 0.05	31.9 ± 2.2	51	61	3 (52)	35.4 ± 3.4	
W	NWA4	2.30	0.88 ± 0.05	56.4 ± 2.0	54	30	2 (94)	63.3 ± 4.9	
W	NWA5	2.80	0.93 ± 0.05	67.2 ± 2.6	55	37	2 (90)	72.0 ± 5.4	
W	NWA6	3.30	0.97 ± 0.05	78.3 ± 2.8	60	37	2 (95)	80.3 ± 6.0	
W	NWA7	3.75	0.89 ± 0.05	74.4 ± 3.7	51	30	1 (100)	83.7 ± 7.0	
W	NWA8	4.15	0.92 ± 0.05	80.5 ± 5.2	53	39	2 (67)	87.2 ± 8.0	
W	NWA9	4.30	0.73 ± 0.04	140 ± 17	49	40	2 (78)	190 ± 26	Age inversion
W	NWA10	4.45	1.02 ± 0.06	108 ± 7	62	52	2 (76)	105 ± 9	
W	NWB12	0.80	0.94 ± 0.05	17.2 ± 1.2	62	57	3 (41)	18.2 ± 1.7	
W	NWB11	1.25	0.99 ± 0.05	37.7 ± 2.3	55	50	3 (69)	38.0 ± 3.4	
W	NWB10	1.75	0.99 ± 0.05	50.6 ± 2.4	70	32	2 (74)	50.7 ± 4.1	
W	NWB9	2.35	0.98 ± 0.05	83.2 ± 3.5	47	33	2 (90)	85.1 ± 6.6	
W	NWB8	2.80	1.00 ± 0.06	111 ± 5	58	29	1 (100)	110 ± 9	
W	NWB7	3.30	1.02 ± 0.05	113 ± 10	54	48	2 (60)	111 ± 12	
W	NWB6	3.80	1.05 ± 0.05	177 ± 9	50	27	1(100)	168 ± 14	
W	NWB5	4.30	1.10 ± 0.06	232 ± 12	61	32	CAM	210 ± 17	Near saturation
W	NWB4	4.80	1.14 ± 0.06	268 ± 17	40	32	CAM	235 ± 21	Near saturation
W	NWB3	5.30	1.16 ± 0.06	295 ± 20	44	37	CAM	254 ± 24	Near saturation
W	NWB2	5.80	1.11 ± 0.06	231 ± 13	49	32	CAM	208 ± 18	Near saturation
W	NWB1	6.40	1.09 ± 0.06						i. S.
W	NWC7	0.30	1.09 ± 0.05	5.9 ± 0.6	47	56	3 (59)	5.5 ± 0.6	
W	NWC6	0.85	1.00 ± 0.05	12.1 ± 1.1	62	84	4 (39)	12.0 ± 1.3	
W	NWC5	1.25	1.01 ± 0.05	31.7 ± 2.5	63	32	2 (68)	31.1 ± 3.2	
W	NWC4	1.75	1.17 ± 0.06	114 ± 6	52	37	2 (94)	97.4 ± 7.9	
W	NWC3	2.40	1.07 ± 0.05	255 ± 15	59	40	CAM	238 ± 21	Near saturation
W	NWC2	3.15	0.94 ± 0.05	279 ± 20	61	49	CAM	294 ± 29	Near saturation
W	NWC1	4.00	1.06 ± 0.05	303 ± 21	65	49	CAM	285 ± 27	Near saturation

Dune field	Sample	depth (m)	dose rate (Gy/ka)	De (Gy)	n	OD (%)	No. of components (proportion in main component)	OSL age (ka)	comment
W	SW9	0.60	0.89 ± 0.05	5.3 ± 0.3	53	70	3 (58)	5.9 ± 0.5	
W	SW8	1.05	0.84 ± 0.05	11.7 ± 0.7	75	41	3 (69)	13.8 ± 1.2	
W	SW7	1.50	0.91 ± 0.05	25.5 ± 1.9	67	37	2 (56)	27.9 ± 2.8	
W	SW6	1.85	0.85 ± 0.05	23.4 ± 0.9	64	32	2 (87)	27.3 ± 2.0	
W	SW5	2.30	0.94 ± 0.05	28.6 ± 1.4	69	54	3 (57)	31.0 ± 2.5	
W	SW4	2.65	0.93 ± 0.05	84.2 ± 2.9	67	57	2 (86)	87.8 ± 6.4	
W	SW3	3.00	0.92 ± 0.05	101 ± 5	49	30	1 (100)	110 ± 9	
W	SW2	3.40	1.00 ± 0.06	152 ± 8	60	38	2 (93)	148 ± 12	
W	SW1	3.95	0.99 ± 0.05	170 ± 10	62	41	2 (83)	167 ± 15	
W	MRR8	0.35	0.94 ± 0.05	13.7 ± 1.4	66	62	4 (44)	14.5 ± 1.8	
W	MRR7	0.45	0.92 ± 0.05	23.9 ± 1.8	60	52	3 (44)	25.5 ± 2.5	
W	MRR6	1.00	0.87 ± 0.04	21.1 ± 1.8	51	36	2 (56)	23.9 ± 2.5	
W	MRR5	1.50	0.90 ± 0.05	30.4 ± 1.3	56	33	2 (91)	33.1 ± 2.6	
W	MRR4	2.00	0.91 ± 0.05	60.7 ± 4.6	50	34	2 (74)	65.5 ± 6.5	
W	MRR3	2.50	0.97 ± 0.06	69.6 ± 2.7	58	38	2 (93)	70.4 ± 5.4	
W	MRR2	3.00	0.97 ± 0.05	85.1 ± 3.4	62	29	2 (93)	86.6 ± 6.5	
W	MRR1	3.50	0.99 ± 0.05	105 ± 5	82	40	1 (100)	105 ± 8	
W	MS9	1.55	0.78 ± 0.04	0.0	50		Median	0	
W	MS8	2.20	0.93 ± 0.05	1.9 ± 0.1	60	74	4 (54)	2.0 ± 0.2	
W	MS7	2.65	0.92 ± 0.04	6.5 ± 0.5	50	81	4 (54)	7.1 ± 0.7	
W	MS6	3.15	0.91 ± 0.05	24.2 ± 2.5	70	70	4 (37)	26.3 ± 3.2	
W	MS5	3.65	0.93 ± 0.05	21.3 ± 3.7	75	46	3 (41)	22.6 ± 4.2	
W	MS4	4.30	0.93 ± 0.05	32.0 ± 2.1	73	34	3 (76)	34.4 ± 3.2	
W	MS2	4.90	1.32 ± 0.07	87.5 ± 4.8	89	49	2 (81)	65.7 ± 5.4	
W	MS1	5.55	1.06 ± 0.06	197 ± 16	60	38	2 (78)	185 ± 19	
W	MS0	7.45	0.97 ± 0.06						In saturation

Dune field	Sample	depth (m)	dose rate (Gy/ka)	De (Gy)	n	OD (%)	No. of components (proportion in main component)	OSL age (ka)	comment
W	WP1	0.40	0.83 ± 0.04	0.056 ± 0.011	38		Median	0.067 ± 0.014	
W	WP2	0.95	0.78 ± 0.04	17.6 ± 1.3	58	67	4 (43)	22.7 ± 2.2	
W	WP3	1.55	0.76 ± 0.04	18.3 ± 2.0	52	66	3 (60)	24.2 ± 1.9	
W	WP4	2.00	0.79 ± 0.04	71.4 ± 3.4	53	49	2 (81)	90.5 ± 7.3	
W	WP5	2.45	0.77 ± 0.04	75.7 ± 5.5	95	47	3 (64)	98.2 ± 9.6	
W	WP6	2.80	0.86 ± 0.05	133 ± 9	77	41	2 (75)	155 ± 14	
W	WP7	3.20	0.85 ± 0.05	136 ± 6	76	50	2 (89)	159 ± 13	
W	WP8	3.65	0.86 ± 0.05	147 ± 15	87	38	3 (69)	172 ± 21	
W	WP9	0.25	0.88 ± 0.05	121 ± 10	78	46	3 (67)	138 ± 15	
W	WP10	1.00	0.84 ± 0.05	144 ± 9	65	36	2 (86)	171 ± 16	
W	WP11	1.60	0.79 ± 0.04	169 ± 10	52	37	1 (100)	215 ± 19	
W	WP12	2.15	0.77 ± 0.04	165 ± 10	47	31	1 (100)	214 ± 18	
W	WP13	2.55	0.95 ± 0.05	195 ± 13	63	50	1 (100)	205 ± 19	
B	BM1	1.00	1.43 ± 0.07	0	76			0	
B	BM2	1.60	1.36 ± 0.07	5.4 ± 0.4	54	93	4 (36)	4.0 ± 0.4	
B	BM3	2.10	1.42 ± 0.07	15.9 ± 0.9	47	47	2 (68)	11.2 ± 0.9	
B	BM4	4.20	1.45 ± 0.08	35.4 ± 1.5	24	24	1 (100)	24.5 ± 1.9	
B	BM5	5.80	1.35 ± 0.07	38 ± 2.5	29	29	2 (81)	28.1 ± 2.6	
M	ALC3	1.10	0.63 ± 0.04	57.1 ± 3.1	44	15	1 (100)	91.2 ± 8.4	
M	ALC2	1.60	0.60 ± 0.04	54.6 ± 1.8	47	15	1 (100)	91.1 ± 7.2	
M	ALC1	2.20	0.57 ± 0.04	55.6 ± 2.1	45	31	1 (100)	97.3 ± 8.0	
M	CC4	1.70	0.56 ± 0.04	12.3 ± 0.5	50	21	1 (100)	22.0 ± 2.0	
M	CC1	3.85	0.51 ± 0.03	10.7 ± 0.4	47	23	1 (100)	21.1 ± 1.8	
M	CD4	0.75	0.74 ± 0.04	5.4 ± 0.3	46	53	3 (82)	7.2 ± 0.6	
M	CD3	1.25	0.82 ± 0.05	19.4 ± 1.4	59	56	2 (54)	23.7 ± 2.4	
M	CD2	1.55	0.88 ± 0.05	22.5 ± 1.1	71	54	3 (72)	25.5 ± 2.1	
M	CD1	2.10	0.86 ± 0.05	24.1 ± 1.3	66	44	2 (58)	28.0 ± 2.4	

Dune field	Sample	depth (m)	dose rate (Gy/ka)	De (Gy)	n	OD (%)	No. of components (proportion in main component)	OSL age (ka)	comment
M	NG3	0.70	0.43 ± 0.03	11.8 ± 0.4	60	23	1 (100)	29.5 ± 2.8	
M	NG2	1.70	0.37 ± 0.03	11.3 ± 0.3	68	20	1 (100)	30.3 ± 2.9	
M	NG1	2.55	0.35 ± 0.03	10.4 ± 0.3	58	20	1 (100)	29.9 ± 10.3	
M/W	PSP1	0.75	0.58 ± 0.04	2.0 ± 0.2	46	31	2 (83)	3.4 ± 0.4	
M/W	PSP2	1.50	0.66 ± 0.04	12.4 ± 0.9	64	34	2 (61)	18.7 ± 1.8	
M/W	PSP14	0.65	0.68 ± 0.04	13.9 ± 1.6	62	35	2 (65)	20.5 ± 22.7	
M/W	PSP13	1.10	0.76 ± 0.04	20.6 ± 2.0	86	58	3 (62)	26.9 ± 2.1	
M/W	PSP12	1.55	0.68 ± 0.04	109 ± 5	55	57	2 (83)	161 ± 13	
M/W	PSP11	2.10	0.60 ± 0.03	133 ± 11	84	53	3 (48)	222 ± 23	Age inversion
M/W	PSP10	2.70	0.71 ± 0.04	115 ± 11	43	64	3 (56)	162 ± 18	
M/W	PSP9	3.20	0.86 ± 0.05	210 ± 12	46	28	CAM	245 ± 21	Near saturation
M/W	PSP8	3.80	0.69 ± 0.04	185 ± 7	74	26	1 (100)	268 ± 20	
M/W	PSP7	4.35	0.72 ± 0.04	221 ± 12	104	36	CAM	308 ± 26	Near saturation
M/W	PSP5	5.35	0.63 ± 0.03	218 ± 14	50	50	CAM	344 ± 31	Near saturation
M/W	PSP3	6.35	0.52 ± 0.03	231 ± 11	86	86	CAM	445 ± 37	Near saturation

Abbreviations: W: Woorinen Formation, B: Bunyip Sands, M: Molineaux Sands, M/W: Woorinen Formation, transitional zone to Molineaux Sands

Acknowledgements

I am indebted to my supervisors Prof. Ulrich Radtke and Dr. Alexandra Hilgers. They enthused me for luminescence dating, encouraged me to write this PhD thesis, guided and supported me in every possible way. I thank the German Research Council (DFG) for funding this project (Ra 383-14-1, 14-2, 14-3) and PD Dr. Reinhardt Zeese for agreeing to review this thesis.

Furthermore, I owe a great deal of thanks to Dr. Matt Telfer for helping me whenever possible, for inspiring scientific discussions, for English and scientific proofreading, for motivating emails and support during a lot of conferences.
Without the scientific and organisational assistance provided by Dr. Jennie Bourne and Dr. Rowl Twidale, this research project would not have been possible. They also taught me that enjoying one or two glasses of good Australian wine is very important after a day of field work. I further thank various farmers in the Murray Basin for enabling us to excavate the dunes on their properties, and various backhoe drivers, who not only exposed the dune sections for us, but also helped with sampling.

I would like to thank my colleague and former office companion Dr. Nicole Klasen for valuable discussions and moral support. Assistance in the laboratory was provided by Max Melcher, Marcel Scheider, Mareike Trauerstein and Nina Löhr. Daniela Hülle, Mareike Trauerstein, Urs Maier and Andreas Schwen helped with proof reading, and Katja Mehlis and Inge Lomax with formatting. For this support I am extremely grateful. I would like to thank Prof. Olaf Bubenzer and Dr. Oliver Bödeker for supporting this project, during the field trips as well as during the time in Cologne. Thanks also to Dr. Oliver Bödeker and Benjamin Hennig for providing a lot of coffee, chocolate and Gummibärchen during work, and special thanks to Max Melcher and Mareike Trauerstein for keeping me sane during the fieldtrip to Australia in 2007.

I thank Dr. Jakob Wallinga and Dr. Mirko Ballarini for introducing me to the method of single grain luminescence dating, Prof. Rex Galbraith for providing the algorithms for the finite mixture model, Prof. Jon Olley for providing the radial plot programme, and Damian Steffen for help with OSL signal component fitting and the use of R and Tinn-R programmes.

Udo Beha and Dr. Bettina Schenk helped with some illustrations of this thesis. Prof. Heli Wopfner, Dr. Frank Preusser and Dr. Koen Beerten I would like to thank for inspiring scientific discussions from which I learned a lot. I am also very appreciative of Prof. Markus Fiebig, for letting me finish my PhD thesis in Vienna.

Finally, I am indebted to my parents for their support in every way during my graduate and postgraduate studies.

Erklärung gem. § 3, Abs.10 der Promotionsordnung

Ich versichere, dass ich die von mir vorgelegte Dissertation selbständig angefertigt, die benutzten Quellen und Hilfsmittel vollständig angegeben und die Stellen der Arbeit - einschließlich Tabellen, Karten und Abbildungen -, die anderen Werken im Wortlaut oder dem Sinn nach entnommen sind, in jedem Einzelfall als Entlehnung kenntlich gemacht habe; dass diese Dissertation noch keiner anderen Fakultät oder Universität zur Prüfung vorgelegen hat; dass sie - abgesehen von unten angegebenen Teilpublikationen - noch nicht veröffentlicht worden ist sowie, dass ich eine solche Veröffentlichung vor Abschluss des Promotionsverfahrens nicht vornehmen werde. Die Bestimmungen dieser Promotionsordnung sind mir bekannt. Die von mir vorgelegte Dissertation ist von Univ.-Prof. Dr. U. Radtke betreut worden.

Johanna Lomax

Teilpublikationen:

Lomax, J., Hilgers, A. Twidale, C.R., Bourne, J.A., Radtke, U. (2007). Treatment of broad equivalent dose distributions in OSL dating of dune sands from the western Murray Basin, South Australia. Quaternary Geochronology 2 (1-4): 51-56.

Beerten, K., Lomax, J., Clémer, K., Stesmans, A., Radtke, U. (2006). On the use of Ti centres for estimating burial ages of Pleistocene sedimentary quartz: Multiple-grain data from Australia. Quaternary Geochronology 1(2): 151-158.